GEOTECHNICAL CHARACTERIZATION AND ROCK MASS CLASSIFICATION OF THE ANTALYA KARSTIC ROCK MASSES

A THESIS SUBMITTED TO
THE GRADUATE SCHOOL OF NATURAL AND APPLIED SCIENCES
OF
MIDDLE EAST TECHNICAL UNIVERSITY

BY

EVRİM SOPACI

IN PARTIAL FULFILLMENT OF THE REQUIREMENTS
FOR
THE DEGREE OF DOCTOR OF PHILOSOPHY
IN
GEOLOGICAL ENGINEERING

OCTOBER 2012

Approval of the thesis:

GEOTECHNICAL CHARACTERIZATION AND ROCK MASS CLASSIFICATION OF THE ANTALYA KARSTIC ROCK MASSES

submitted by **EVRİM SOPACI** in partial fulfillment of the requirements for the degree of **Doctor of Philosophy in Geological Engineering Department, Middle East Technical University** by,

Prof. Dr. Canan ÖZGEN
Dean, Graduate School of **Natural and Applied Sciences** ______________

Prof. Dr. Erdin BOZKURT
Head of Department, **Geological Engineering** ______________

Prof. Dr. Haluk AKGÜN
Supervisor, **Geological Engineering Dept., METU** ______________

Examining Committee Members:

Prof. Dr. Asuman G. TÜRKMENOĞLU
Geological Engineering Dept., METU ______________

Prof. Dr. Haluk AKGÜN
Geological Engineering Dept., METU ______________

Prof. Dr. Ahmet Orhan EROL
Civil Engineering Dept., METU ______________

Prof. Dr. Kemal Önder ÇETİN
Civil Engineering Dept., METU ______________

Assoc. Prof. Dr. Sami Oğuzhan AKBAŞ
Civil Engineering Dept., Gazi University ______________

Date: 03 / 10 / 2012

I hereby declare that all information in this document has been obtained and presented in accordance with academic rules and ethical conduct. I also declare that, as required by these rules and conduct, I have fully cited and referenced all material and results that are not original to this work.

Name, Last name : Evrim SOPACI

Signature :

ABSTRACT

GEOTECHNICAL CHARACTERIZATION AND ROCK MASS CLASSIFICATION OF THE ANTALYA KARSTIC ROCK MASSES

Sopacı, Evrim

Ph. D., Department of Geological Engineering

Supervisor : Prof. Dr. Haluk AKGÜN

October 2012, 355 pages

This thesis identifies the geotechnical parameters of the Antalya karstic foundation rocks (travertine/tufa), which are highly variable in nature, by means of geological observations, geotechnical site investigations, and field and laboratory geomechanics tests to examine karstic (mainly tufa) rock mass behavior. Several geotechnical parameters such as porosity, seismic wave velocity, uniaxial compressive strength, Young's modulus, tensile strength, etc. that are thought to have significant influence on rock mass behavior have been tested and statistically analyzed. Principal component analysis and multiple linear and non-linear regression analyses have been carried out in order to reveal correlations between the geotechnical parameters tested. Porosity has been statistically determined to be one of the major parameters governing the strength of the Antalya tufa rock mass. Intact rock failure criteria, among which Bieniawski's criterion has been proven to be more appropriate for each tufa type (phytoherm framestone, phytoherm boundstone, microcrystalline tufa, phytoclast tufa and intraclast tufa) along with the Antalya tufa rock mass have been determined from the experiments. GSI rock mass classification of the Antalya tufa rock mass, whose GSI value was recommended between 20±5 and 75±5, has been attempted to be used in engineering design. Furthermore, the depth and dimension of the karstic cavities and fractures have been investigated by the geophysical tests, surface geological survey and subsurface investigations (borings and observation pits).

Keywords: Antalya, karst, travertine, tufa, geotechnical characterization, rock mass.

ÖZ

ANTALYA KARSTİK ZEMİNLERİNİN JEOTEKNİK KARAKTERİZASYONUN VE KAYA KÜTLESİ SINIFLAMASININ YAPILMASI

Sopacı, Evrim
Doktora, Jeoloji Mühendisliği Bölümü
Tez Yöneticisi : Prof. Dr. Haluk AKGÜN

Ekim 2012, 355 sayfa

Bu çalışmada; çok değişkenlik gösteren Antalya karstik kaya kütlesinin davranışını incelemek için jeolojik yüzey gözlemleri, arazi jeoteknik incelemeleri ve, arazi ve laboratuvar jeomekanik deneyleri sonucu belirlenen Antalya karstik zeminlerinin (genellikle tufa) jeoteknik parametreleri belirlenmiştir. Kaya kütlesi davranışını etkileyeceği düşünülen birçok jeomekanik parametre (örneğin; boşluk oranı, ses dalgası hızı, tek eksenli basınç dayanımı, Elastisite modülü, çekme dayanımı, vb.) için deneyler yapılmış ve sonuçlar istatistiksel olarak değerlendirilmiştir. Incelenen jeomekanik parametrelerin birbirleri ile olan ilişkilerinin belirlenmesi için Temel Bileşenler Analizi ve Çok Değişkenli Doğrusal ve Doğrusal Olmayan Regresyon Analizi yöntemleri kullanılmıştır. İncelenen her tufa türü (fitoherm çatıtaşı, fitoherm bağlamtaşı, mikrokristalin tufa, fitoklastik tufa and intraklastik tufa) için deney sonuçları kullanılarak som kaya yenilme ölçütü belirlenmiştir. Bu ölçütler içinden Antalya tufa birimi için en uygun olanı Bieniawski'nin yenilme ölçütü olarak belirlenmiştir. Mühendislik tasarımlarında kullanılmak üzere Antalya tufa birimi için GSI kaya kütlesi sınıflaması uygulanmış ve bu kaya için GSI değer aralığı 20-75 olarak önerilmiştir. Ayrıca, karstik boşlukların boyutlarının ve konumlarının belirlenebilmesi için arazi jeofizik yöntemleri, yüzey jeolojik gözlemleri ve yeraltı jeoteknik inceleme yöntemleri (sondaj ve araştırma çukuru) uygulanmıştır.

Anahtar Kelimeler: Antalya, karst, traverten, tufa, jeoteknik karakterizasyon, kaya kütlesi.

To my family and my grandmother

ACKNOWLEDGMENTS

I would like to express my gratitude to those who have contributed directly or indirectly to the development of this thesis. I profoundly appreciate those people who have lent me a helping hand.

I am thankful to all my instructors who have supported me through my thesis studies. I especially appreciate the assistance and support of my supervisor Prof. Dr. Haluk AKGÜN, P.E.

I also would like to thank my all thesis committee members.

I would like to thank all the staff at Technical Research Department of DLH, especially to thank Mehmet ALTINTAŞ.

The assistance of Dr. Mustafa Kerem KOÇKAR, Kıvanç OKALP, Arif Mert EKER and Selim CAMBAZOĞLU are gratefully acknowledged.

The assistance of Ferit ÖGE in rock mechanics tests is gratefully appreciated. Cengiz TAN is gratefully acknowledged due to his assistance in SEM analyses. The assistance of Ebru DENİZ in DTA+TGA analyses is appreciated.

In the name of TEMELSU International Engineering Services Inc., I would like to thank Mustafa AKINCI for sharing his vast experience and his guidance at every stage of my engineering career and my thesis. In addition, I appreciate the support of Hakan TANYAŞ. I want to thank him for all his help, support, interest and valuable hints.

Furthermore, technical and moral support of Uğur KURAN, Mustafa GÜRBÜZ, Süha AYKURT, Ersin BARBOROS, Serdar ÖZÜŞ, Özlem ALPASLAN, Oğuz TÜFENKÇİ, Onur SÜMER, Ahmet BENLİAY, Mustafa Yücel KAYA, Serkan and Burak SOPACI are gratefully acknowledged.

Especially, I would like to give my special thanks to my beloved Seda ÖZKAN for her support and presence at any time.

Finally, I am deeply grateful to my family and my friends for their endless assistance and support regarding my life.

TABLE OF CONTENTS

LIST OF TABLES

TABLES

LIST OF FIGURES

FIGURES

LIST OF SYMBOLS

A	area (mm^2)
a.m.s.l	above mean sea level
ASTM	American society for testing and materials
c	cohesion (MPa)
c.	circa (from Latin, meaning “around”)
D	diameter (mm)
D_e	equivalent core diameter (mm)
df	degree of freedom
DLH	Demiryollar, Limanlar Ve Hava Meydanları Inşaatı Genel Müdürlüğü
DSİ TAKK	Devlet Su Işleri Teknik Araştırma Ve Kalite Kontrol Dairesi Başkanlığı
DTA	differential thermal analyses
E	elasticity modulus
EDS	energy-dispersive x-ray spectroscopy
E_i	intact rock elasticity modulus
ESR	excavation support ratio
E_v	static modulus of deformation
F	force (N)
F	size correction factor
GIS	geographical information system
GPa	gigapascal
GSI	geological strength index
h_1	thickness of first layer (m)
h_2	thickness of second layer (m)
I_1	first invariant of stress
Id_n	slake durability index (%) (n represent the number of cycles employed during testing)
Is_{50}	point load strength index
ISRM	International society for rock mechanics
J_2	second invariant of stress deviation
Ja	joint alteration number

Jn	joint set number
Jr	joint roughness number
Jw	joint water reduction number
ka	thousand years ago
L	length (mm)
LOI	loss on ignition
LVDT	linear variable differential transformer
Ma	million years ago
METU	Middle East Technical University
m_i	modulus of intact rock
MPa	megapascal
MSA	measure of sampling adequacy
MTS	material testing system
N	number of samples
n	porosity of rock mass
P	maximum load at failure (kgf)
PCA	principal component analysis
PCs	principal components
P-wave	primary wave
Q	rock mass quality
r	load plate radius
R	coefficient of correlation
R^2	coefficient of determination
RMi	rock mass index
RMR	rock mass rating
RQD	rock quality designation
SEM	scanning electron microscope
Sig.	significance
SRF	stress reduction factor
SRF	stress reduction factor
SRT	seismic refraction tomography
Std. Dev.	standard deviation

Std. error	standard error
S-wave	secondary wave
T	tensile strength (MPa)
t	thickness of sample (mm)
t	t-test
TGA	thermo gravimetric analysis
To	natural period
TPAO	Türkiye Petrolleri Anonim Ortaklığı
UCS	uniaxial compressive strength
v_1	shear wave velocity of first layer (m/s)
v_2	shear wave velocity of second layer (m/s)
VES	vertical electrical resistivity
Vp	primary wave velocity
Vs	shear wave velocity
NX	2-inch diameter
JCB	Joseph Cyril Bamford Excavators Limited

<u>SYMBOLS</u>

γ	unit weight of rock mass
ν	Poisson's ratio
ϕ	internal friction angle (^{o})
σ_1	major principle stress (MPa)
σ_2	intermediate principle stress (MPa)
σ_3	minor principle stress (MPa)
σ_c	uniaxial compressive strength (MPa)
σ_{ci}	uniaxial compressive strength of intact rock (MPa)
σ_m	mean normal stress (MPa)

CHAPTER I

INTRODUCTION

I.1 Purpose and scope

Tufa/travertine deposits of Antalya located on the Mediterranean coast in southern part of Turkey form one of the world's largest tufa depositional environments. Antalya is one of the largest cities of Turkey with its population of one and a half million. The city has been the centre of culture, art, architecture and mythology throughout its history. Its spectacular nature and world known holiday villages make Antalya the capital of tourism. Most populated areas are settled on karstic rocks, namely, tufa and city planners are looking for new settlement areas of which most are founded on tufa deposits as well.

The purpose of this study is to identify the geotechnical parameters of the Antalya karstic foundation rocks (travertine/tufa), whose mechanical behavior is highly variable due to its natural variability and structure, by means of geological observations, site investigations, field and laboratory tests and, to examine the rock mass behavior. Antalya tufa rock mass is a different rock type, which has no well developed joint systems. It is variably porous and composing of different rock types with different structures. The scarce geotechnical characterizations and geomechanical evaluations exisiting in literature for the Antalya tufa are at preliminary stage and far away from providing a reliable geotechnical assessment. Therefore, an appropriate rock mass classification, which could be utilized during selecting suitable sites and engineering design for the rapidly growing urbanization in the area, has been attempted.

In order to reveal controlling geotechnical parameters for mechanical behavior of the Antalya tufa rock mass and to develop a comprehensive geotechnical database, which was missing in literature, for the Antalya tufa, numerous field and laboratory geomechanics tests have been carried out. Accordingly, the geological and geotechnical parameters of the rock material and rock mass underlying the City of Antalya have been attempted to identify. The depth and dimension of the karstic cavities and fractures have been investigated by the geophysical tests, surface geological survey and subsurface investigations (borings and observation pits).

Statistical methods, such as principal component analysis and multiple linear regression analysis, have been utilized during the assessment of geotechnical parameters. Useful relations or equations for the Antalya tufa rock mass and rock types have been proposed from a geotechnical point of view.

I.2 Study area

The study area of this dissertation is located in Antalya, a city on the Mediterranean coast of southwestern Turkey (Figure 1). Situated on coastal cliffs, which are 30 m above mean sea level (a.m.s.l.), Antalya is surrounded by Taurus Mountains,which runs parallel to the Mediterranean in an east-west direction. Narrow coastal plains, small natural bays and peninsulas are the most common morphological features resulting from the orientation of mountain range.

The area has a characteristic Mediterranean climate with hot and dry summers and mild and rainy winters. Around 300 days of the year are sunny; the sea water temperature ranges between 15 °C (59 °F) during winter and 28 °C (82 °F) during summer, the air temperature can climb as high as 40 °C (104 °F) in July and August, however the typical air temperature ranges between the low-to-mid 30 °C (86 F) (Turkish State Meteorological Service, 2012).

The geological observations and geotechnical investigations have been carried out mostly in Konyaaltı and Muratpaşa districts of Antalya (Figure 1). These areas have been densely populated and settled mainly on tufa deposits. The locations of the investigations have been scarce in urban area most of the time.

Figure 1. Sketch location map of study area.

I.3 Methodology

For the purpose of geotechnical characterization of Antalya tufa deposits, the first thing to investigate was the mode of formation and the composition of these deposits. In this regard, literature on tufa in general and on Antalya tufa deposits has been searched thoroughly. Among the studies on Antalya tufa deposits, the paper by Glover and Robertson (2003), which discusses mode of formation, composition and types of tufa in the Antalya area, was utilized to form a starting point for the geotechnical characterization of the tufa deposits.

Following the literature study, several site visits were carried out to observe and capture tufa types and their characteristics in the field. Upon recognizing and getting familiar with them, a preliminary site investigation program for the areas observed to be underlain by different tufa types was planned in August, 2009. In this preliminary site investigation program, geophysical exploration methods, namely, seismic refraction tomography (SRT) and vertical electrical resistivity (VES), were utilized in order to:

(1) detect karstic cavities beneath the ground surface,
(2) choose possible areas for further examination,
(3) determine the range for shear wave velocity (Vs), primary wave velocity (Vp) and electrical resistivity values of tufa types.

The assessment of the results of the preliminary site investigation program directed and shaped the second stage site investigation program comprising of borehole drilling, trial pitting, geotechnical field testing and sampling carried out in October, 2009. In the same site investigation program, pressuremeter tests and plate load tests were carried out in some circumstances where sampling was difficult.

During the evaluation of the field findings and the observed characteristics of tufa types, laboratory testing of tufa samples were carried out to determine mostly the geotechnical strength parameters. Laboratory testing involved uniaxial compressive strength testing (UCS), triaxial compressive strength testing, point load strength index testing, indirect tensile strength (Brazilian) testing, slake durability testing, ultrasonic velocity determination testing, porosity determination and loss on ignition (LOI).

The results of the laboratory tests for each geotechnical parameter of the tufa types were grouped and statistically studied via principal component analysis and regression analysis. By utilizing especially the results of the strength tests, the well-known failure criteria were applied to tufa types and some modifications were made for the purpose of rock mass characterization.

Empirical rock mass classification systems, which are powerful tools for determining rock mass shear strength parameters, have been attempted for tufa deposits.

At the end, geotechnical characterization and rock mass classification of the tufa rock masses in the Antalya area was attempted based on numerous geotechnical parameters.

I.4 Organization and investigation team members

The following technical staff carried out the geological and geotechnical works:

<u>Drilling works</u>

M. Süha AYKURT	(Geological Engineer/TOROS Geotechnical Eng. Inc.)
İsmet TURAN	(Geological Engineer/TOROS Geotechnical Eng. Inc.)
Evrim SOPACI	(Author, Geological Engineer)

<u>Field Geophysical Studies</u>

Ersin Barboros	(Geophysical Engineer/ TOROS Geotechnical Eng. Inc.)
Evrim SOPACI	(Author, Geological Engineer)

<u>Field Geotechnical Studies</u>

Halil KÖSE	(Plate load technician/AKADEMİ Geotech. Eng. Inc.)
Yaşar DURAK	(Pressuremeter technician/AKADEMİ Geotech. Eng.Inc.)
Evrim SOPACI	(Author, Geological Engineer)

Lab Testing

The rock mechanics laboratory testing of the recovered samples have been tested at five different institutions as follows:

Rock block samples recovered from the field were tested at the Geotechnical Laboratory of Technical Investigation Department of DLH (Railways, Ports and Airports Construction General Directorate), at the Rock Mechanics Laboratory of Mining Engineering Department of Middle East Technical University and at the Engineering Geological Laboratory of Geological Engineering Department of Middle East Technical University and at the Laboratory of The General Directorate of State Highways.

CHAPTER II

PREVIOUS WORKS

II.1 Introduction

Tufa deposits in general have mostly been the subject of researches in sedimentary geology all over the world due to its mode of occurrence. However, the researches on tufa deposits mainly focused on chemical and biological composition, mode of formation and formation environments rather than its geotechnical and engineering geological properties.

Accordingly, previous studies based on geology and engineering geology are presented in this chapter.

II.2 Previous studies on geology

II.2.1 Tufa deposits in general

Tufa and travertine, other than their identical chemical composition and similar characteristics, are different in their lithofacies and depositional environments. Both deposits are composed of calcium carbonate ($CaCO_3$) precipitations both from organic and inorganic processes. Many geologists simply refer to all carbonate incrustation on plant remains as travertine in an effort to avoid confusion (Julia, 1983). Nevertheless, there are differences in the basic characteristics of travertine and tufa.

Pedley (1990) used the term tufa to describe all cool water deposits, which are highly porous or spongy freshwater carbonate rich in microphytic and macrophytic growths, leaves and woody tissue. On the contrary, travertine is commonly deposited in warm water, and is well lithified. Before Pedley (1990), many attempts had been made for tufa classification based on physicochemical, biochemical and petrographical parameters. Buccino et al. (1978), Chafetz and Folk (1984) and Ordonez and Garcia del Cura (1983) made an appreciable achievement in classifying a range of tufa fabrics. Pedley (1990) re-defined and expanded their observations to provide a coherent scheme for application to both ancient and modern deposits. Accordingly, tufa deposits were grouped into two main divisions as autochthonous and clastic tufa deposits. While phytoherm framestone (phytoherm tufa of Buccino et al, 1978) and phytoherm boundstone (stromatolitic tufa of Buccino et al, 1978) types were included in autochthonous group; phytoclast tufa (phytoclast tufa of Buccino et al, 1978; crossed tube facies of Ordonez and Garcia del Cura, 1983), cyanolith "oncoidal" tufa (oncolites of Ordonez and Garcia del Cura, 1983), intraclast tufa (detrital tufa facies of Ordonez and Garcia del Cura, 1983), microdetrital tufa and palaeosols were included in the allochthonous tufa group.

The environmental models of tufa formation described by Pedley (1990) formed a base for almost every research on tufa deposits. Five types of environmental models, namely, perched spring line, cascade, fluviatile, paludal and lacustrine facies, were differentiated in his study. Pedley (1990) has benefited greatly from the published data of Golubic (1969), Buccino et al. (1978) and Ordonez and Garica del Cura (1983).

Golubic (1969) mentioned the principles relating to the growth, morphology and contemporaneous diagenesis of tufa but fitted them into the concept of a water table fluctuation. Buccino et al. (1978) provided a further step to Golubic (1969)'s idea by recognizing the significance of phytoherm as the basic tufa building structure and as a factory site for allochthonous tufa generation. Ordonez and Garcia del Cura (1983) studied Spanish fluvial carbonate deposition to produce models by applying modern concepts of sedimentology.

Afterwards, Ford and Pedley (1996) summarized the available literature to present a general view of tufa nature and classification world-wide. Standardization of terminology currently in use was attempted to distinguish between ambient temperature deposits, thermal deposits and speleothems, which deals with cave formation and cave deposits. It is mentioned in this study that the tufa generation process appears to be climatically controlled, hence tufa deposits could be valuable in palaeo-environmental reconstruction. It is also stated that most of the tufa deposits are of post-glacial age.

In the meantime, Pentecost (2005) has conducted an extensive study of more than four hundred pages on travertine. Starting from its definition to origin of components, fabric, morphology, facies, chemical and biological composition; so much valuable and elaborate information is presented in this study.

Most recently, Pedley and Carannante (2006) prepared a special publication by collecting several articles from various authors on cool-water carbonates; depositional systems and palaeo-environmental controls.

II.2.2 Tufa deposits in the Antalya area

Over the past two decades, the tectonics and origin of the Antalya basin has been the subject of several works (Flecker, 1995; Flecker et al., 1995, 1998, 2005; Glover, 1995; Glover and Robertson, 1998; Karabıyıkoğlu et al., 2000, 2004, 2005; Poisson et al., 2003; Deynoux et al., 2005), in which the formation, evolution and deformation of the Late Cenozoic Antalya basin was investigated.

The present configuration of the Antalya basin is formed by three distinct regions, divided and bounded by the NS-trending Kırkkavak fault and Late Miocene Aksu thrust (Dumont and Kerey, 1975; Poisson, 1977; Akay et al., 1985), which were referred from east to west as the Manavgat, Köprüçay and Aksu sub-basins in Çiner et al. (2008).

One of the first studies on tufa deposits in the Antalya area was documented by Planhol (1956), where plant remnants recognized in tufa deposits were interpreted as a sign for fresh-water deposition.

Poisson et al. (1983, 1984) and Akay et al. (1985) provided comprehensive information on the foraminiferal and nannoplankton biostratigraphy as well as lithostratigraphic considerations of the Antalya basin.

Later on, İnan (1985) studied the modes of formation for the “Antalya travertine” and distinguished four basic facies, namely, massive, spongy, plant fabric and oolitic. He interpreted that the spring water causing tufa precipitation might be coming out of the surface through geological structures such as NW-SE oriented faults and thrusts. The cavities observed in travertine deposits were assumed to be of non-karstic origin.

Glover and Robertson (2003) carried out an elaborate study on the origin of tufa and related terraces in the Antalya area. According to this study, the two main levels where tufa is exposed were distinguished; one was the upper terrace, 300 m a.m.s.l. (above mean sea level) and the other was the lower terrace, 100-200 m a.m.s.l. Furthermore, it was mentioned that much of the tufa has formed in the lacustrine to paludal depositional environments in the Antalya area. Two new facies, namely, pisolith and tufa breccias, in addition to the facies cited in literature were recognized in the Antalya tufa. Tectonic controls on the tufa depositional basins were identified as a N-S half graben in the area. Accordingly, the origin of the upper terrace was related to the tectonic uplift of the lithified tufa lake or swamp environment, whereas the origin of lower terrace was related to a combination of Early to mid-Quaternary glacio-eustatic sea level change, coupled with fluvial processes.

Koşun et al. (2005) carried out a similar study to that of Glover and Robertson (2003). A total of twelve platos, three of which are relatively large, were identified through Geographical Information System (GIS) investigations. The modern and ancient tufa depositional environments of the Antalya area were compared, thereupon the origin of terraces and tufa deposition were related. A total number of ten litho-facies, three of which was an addition to facies defined by Pedley (1990), was identified. These new facies were named as pisolith tufa, micrite tufa and formational conglomerate.

Karabıyıkoğlu et al. (2005) and Çiner et al. (2008) made a similar attempt to characterize the Late Cenozoic evolution of the Antalya basin where they tried to model the depositional environments of not only tufa but also the fluvial deposits as related to the recent tectonics of the Antalya basin. They also related sea level changes as a controlling factor for deposition with facies distribution.

II.3 Previous studies on engineering geology

II.3.1 Tufa deposits in general

Tufa deposits are very interesting rock masses in the sense of their engineering properties yet they have not been studied much from an engineering point of view. Very limited geotechnical information is available on tufa in the literature. This situation might be explained by very limited exposures of tufa deposits over which engineering structures or settlements are founded. Further, the variety of fabrics ranging from porous to massive for tufa deposits makes the situation challenging. In these cases, many engineers attempt to use some analogies to determine the geotechnical parameters for tufa for their geotechnical designs and calculations. Since the depositional environments and the fabrics of tufa are similar to those observed in karstic areas, similar circumstances and problems encountered in karstic areas might be expected to occur in tufa rock masses as well. Accordingly, engineers refer to the literature on structures situated on karstic formations.

One of the most popular and principal reference about karst terrains is Sowers (1996), the author of the book “Building on Sinkholes”. Sowers (1996) summarized his observations and research into the mechanisms of sinkhole formation in limestone or karst terrain and also discussed site investigation as well as the design and construction methods for building foundations in areas where sinkholes are likely to develop. He emphasized that though engineering problems arise largely from rock dissolution in karstic terrains, most of the engineering problems develop in the overlying residual or deposited soils which might mask the rock solution features. He illustrated rock cavity collapse mechanisms and types together with possible remediation measures. For the porous tufa deposits having similar fabric with limestone containing cavities, this reference might be of value for designers and engineers.

Waltham and Fookes (2005) reviewed and modified the karst terminology for the engineering classification of karst. The authors mostly dealt with cave or sinkhole stability in limestone. They grouped sinkholes into six categories and classified rockhead profiles at various karst terrains. By combining karst morphology and their classifications, they produced an engineering classification of karst as the progressive series of five classes. In their classification, karst class, sinkhole density, cave size and rockhead relief characteristics were used as key parameters. They also suggested some geophysical investigation methods such as microgravity and resistivity measurements.

Waltham et al. (2005) aimed to provide information for engineers and designers about cavernous karst in their publications. They presented both elaborate geotechnical and geological considerations on ground cavities, subsurface processes, sinkhole collapses and ground subsidence. They studied rock cavity collapse mechanisms, which included the overlying residual or deposited soils, and types together with possible remediation measures. Geophysical investigation techniques such as surface seismic waves, electrical resistivity surveys and ground penetrating radar were mentioned.

Tokashiki et al. (1993) proposed two averaging techniques for modeling the mechanical behavior of porous media, which is very often the case for karst terrains or in tufa deposits. In order to evaluate elastic constants, yield strength and failure strength of Ryukyu limestone, which is a Pleistocene limestone that is associated with numerous cavities, these averaging techniques were applied. They found almost the same results from the series model and the homogenization techniques and concluded that the average techniques were more effective for determining the mechanical behavior of constituents as they are relatively simple.

II.3.2 Tufa deposits in the Antalya area

Although one of the largest cities of Turkey has settled directly on tufa deposits, very little and insufficient studies have been carried out to understand and describe these rock masses from an engineering point of view. However, the Antalya area has mostly been studied by several authors in hydrological and hydrogeological point of view since it is situated in a karst terrain (Gürer et al., 1980; Günay, 1981; UNDP, 1983; Arıkan and Ekmekçi, 1985; Sipahi, 1985; Ekmekçi, 1987; Değirmenci, 1989; Denizman, 1989; Özüş, 1992; Koyuncu, 2003).

One of the earliest studies regarding the engineering geological properties of the Antalya tufa was carried out by Kılıç and Yavuz (1994) where travertine deposits of the Lara district that belong to the Düden Plateau were examined in regards to porosity, permeability, unit weight, uniaxial compressive strength and elasticity modulus in association with their fabrics. It was concluded that massive types have relatively low porosity and permeability, and relatively high unit weight and elastic constants. In addition, they mentioned that the porous type among the other types, namely, massive and spongy, has the lowest unit weight and strength values.

Dipova (2002) carried out some field and laboratory tests, particularly of single-ring consolidation (oedometer) test, on tufa deposits as part of his Ph.D. dissertation. Naturally, these oedometer tests were carried out on lithoclastic or microdetrital (named as intraclast and phytoclast tufa in this study) tufa types only. He concluded his studies with collapse potential, which is the function of initial void ratio, volume of compressibility and percentages of fine after wetting of these tufa types. The same author, in the following years, has worked on various characteristics and problems of Antalya tufa, namely, cliff stability, origin and geomorphological properties, physical and index properties, engineering properties such as unit weight, porosity and uniaxial compressive strength (Dipova, 2008, 2011). These studies were helpful to comprehend the general condition and the concerns on Antalya tufa but were almost at the preliminary assessment stage, which did not contain solutions and practical approach to the geotechnical characterization and rock mass classification in order to find solutions to the foundation problems of the Antalya tufa rock masses.

Yağız and Akyol (2005) also studied the physical and mechanical properties of travertine as a natural building stone. They carried out freezing-thawing cycles and uniaxial compressive strength tests on several samples of mostly massive type of travertine and concluded that travertines should not be used for building stone especially in contact with water since the high water absorption rate and the low rock unit weight makes the travertine susceptible to deterioration.

Temelsu (1997) and Yüksel Proje Uluslararası A.Ş. (2000 a,b,c) have carried out highway tunnel projects in karstic limestone in the Antalya region. Several boreholes were drilled in rock masses and several samples were recovered from boreholes for laboratory testing. Even though the samples recovered were limestone, they resembled the massive type of tufa deposits from an engineering geological point of view. Accordingly, the laboratory test results of karstic limestone might be of a value since, the cavities encountered in the drillings resembled massive tufa as far as the fabric and cavity distribution within the rock mass was concerned.

Koçkar and Akgün (2003 a,b) investigated the preliminary tunnel and portal support through presenting methodology along the Alanya Ilısu tunnels. The data gathered from numerous boreholes drilled along the tunnel axes were interpreted. In their studies, the tunnel alignments in their study were partly in karstic (cavernous) limestone and partly in metamorphic rocks such as pelitic schist, calc shist and phyllite.

Besides these studies mentioned above, a number of geotechnical investigations in private sector for the purpose of foundation design of structures, such as buildings, under-pass, stadium, airport, municipal solid waste landfill and light railway were carried out through the Antalya settlement area. Numerous boreholes were drilled together with geophysical investigations comprising mostly seismic refraction. A number of tufa samples were tested at the rock mechanics laboratories. The main and comprehensive investigations among them are as follows: (1) first stage light railway transportation project (Yüksel Proje Uluslararası A.Ş., 2006) with 37 boreholes, (2) 100. Yıl stadium and sport saloon project (Harzem, 2008) with 33 boreholes and seismic refraction exploration, (3) Antalya Varsak Municipality geological study (Antalya Varsak Municipality, 2004) with 15 boreholes, (4) Kepez Municipality Yaşankent project (Zemartem, 2002) with 39 boreholes and seismic refraction exploration, (5) 100. Yıl boulevard and Güllük Street under-pass project (Emay, 2004) with 20 boreholes, (6) Kızıllı municipal solid waste landfill project (Toros, 2007) with 23 boreholes and seismic refraction exploration, (7) Minicity project (Toros, 2007) with 15 boreholes, (8) Kepez Municipality lot 1242 project (Toros, 2006) with 53 boreholes and seismic refraction exploration and (9) Antalya Airport taxi road project (Toker, 2010) with 7 boreholes and pressuremeter tests.

CHAPTER III

GEOLOGICAL CHARACTERISTICS OF THE PROJECT AREA

III.1 Introduction

The city of Antalya is located in one of the Cenozoic sedimentary basins, namely Antalya basin, of southern Turkey (Figure 2). The Antalya basin has been formed by extension-compression related late post-orogeny and recently located in “Isparta Angle”, which bears the story of opening and partial closure of Neotethyan ocean basin during Mesozoic-Early Tertiary and Neotectonic (Plio-Quaternary) compressional and extensional events (Karabıyıkoğlu et al., 2005). Antalya basin has three distinctive parts divided by north-south trending structures, which, from east to west, are Lycian Nappes, Aksu Thrust and Kırkkavak Fault.

III.2 Geological setting of the Antalya basin

The Antalya basin developed unconformably on a Mesozoic autochthonous carbonate platform (the Beydağları platform to the west and the Anamas-Akseki platform to the east) and on an imbricated basement, which were overthrust by allochthonous units (Lycian Nappes, Antalya Nappes and Alanya Massif) during the time interval between Late Cretaceous and Pliocene, within the Isparta Angle in the western Taurides (Karabıyıkoğlu, 2005). Presently the Antalya basin has three distinct components, which are namely the Manavgat, Köprüçay and Aksu sub-basins (Dumont and Kerey, 1975; Poisson, 1977; Akay et al., 1985) (Figure 3).

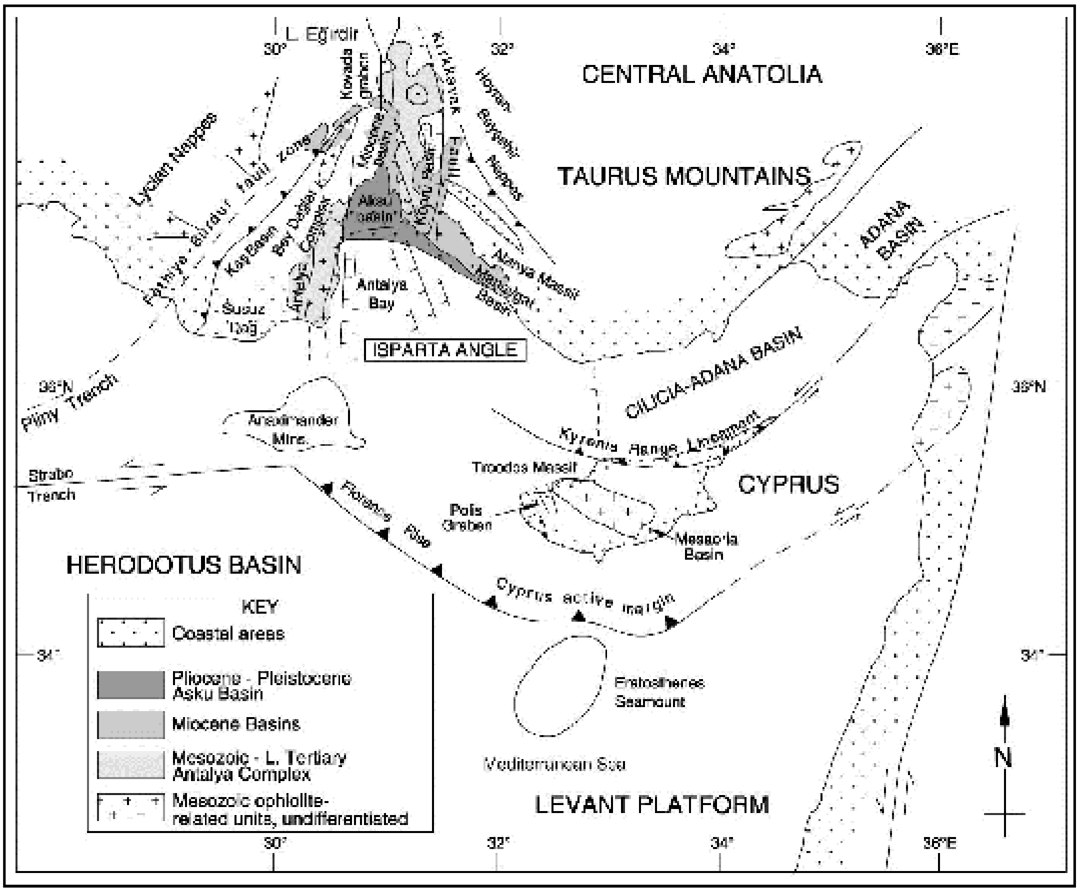

Figure 2. General layout of the basins of southern Turkey (Glover and Robertson, 2003).

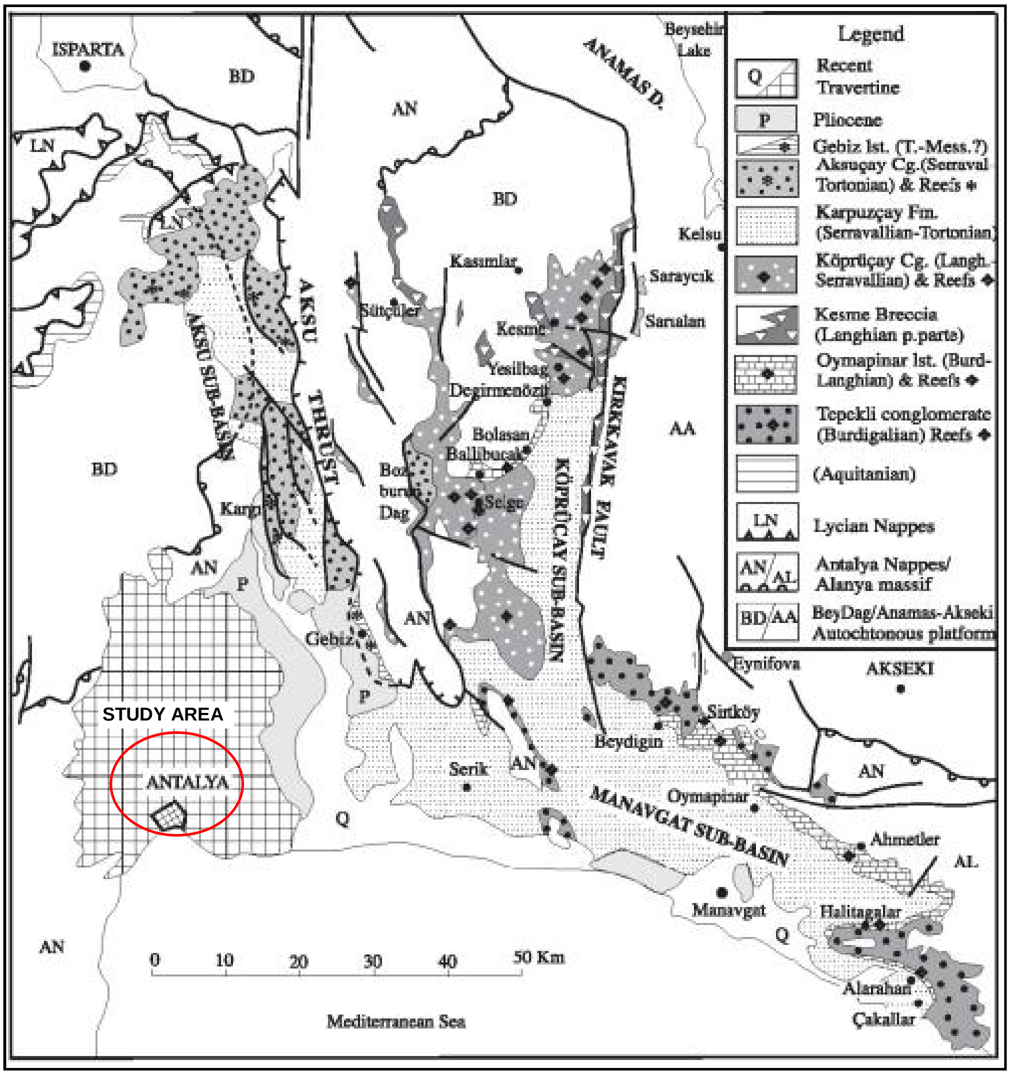

Figure 3. Layout of the basins of Antalya (Karabıyıkoğlu et al., 2005).

The Late Cenozoic sedimentary deposits of the Antalya basin include a relatively thick succession of Miocene and Pliocene clastics, coralgal reefs, reefal shelf carbonates and extensive travertine deposits (Çiner et al., 2008). Based on the foraminiferal and nannoplankton biostratigraphy as well as lithostratigraphic considerations, the Late Cenozoic deposits of the Antalya basin have been divided broadly into ten formations (Akay et al., 1985):

- Aksu formation (Upper Oligocene–Tortonian conglomerates),
- Oymapınar limestone (Langhian shelf carbonates),
- Çakallar formation (Langhian limestone breccias and marls),
- Geceleme formation (Serravalian marls),
- Karpuzçay formation (Tortonian shales, sandstones and conglomerates),
- Taşlık formation (Lower Messinian clayey limestone with limestone and conglomerate blocks),
- Eskiköy formation (Messinian sandstones and conglomerates),
- Gebiz limestone (Messinian reefal carbonates),
- Yenimahalle formation (Pliocene limely claystone and sandstone),
- Alakilise formation (Upper Pliocene sandstone with volcanic tuffs and conglomerate).

The younger sediments mentioned above were succeeded lately by alluvial deposits and extraordinarily extensive tufa deposits (Figure 4).

STANDARD CHRONO-STRATIGRAPHY			**Age (mya)**	**FORMATION**	
PLEISTOCENE	LATE			BELKIS CONGLOMERATE	
	MIDDLE		0.8		
	EARLY	CALABRIAN	1.65	ANTALYA TUFA	
PLIOCENE	LATE	GELASIAN	2.6		
		PIACENZIAN	3.5	KEMER FAN-GLOMERATE	ÇALKAYA FORMATION
	EARLY	ZANCLEAN	5.2		YENİMAHALLE FORMATION
MIOCENE	LATE	MESSINIAN	6.3	EVAPORITE	
		TORTONIAN		GEBIZ LIMESTONE KARPUZÇAY FORMATION	

Figure 4. Stratigraphical columnar section of the Antalya region (Glover and Robertson, 1998).

Apart from the tufa deposits, none of the above mentioned formations will be explained elaborately in this study since they were not encountered or observed in the vicinity of the study area. Detailed information on the tufa deposits will be provided in the following sections of this report as a separate chapter.

III.3 Tectonics

The regional geology of the project area has complex tectono-stratigraphic relations. Basically, the project area can be grouped into two units, namely, autochthonous and allocthonous units in regional scale. While the autochthonous units include Beydağları and Anamas-Akseki units, allocthonous units consist of the Antalya nappe, Beyşehir-Hoyran-Hadim nappes and Lycian nappes. Regionally, the study area with its Palaeozoic to Quaternary lithological units forms a reverse V, which is known as the Isparta Angle, with a shape parallel to the Antalya bay. According to the studies carried out in this region, these lithological units were the allocthonous nappes emplaced over Beydağları and Anamas-Akseki autochthonous units (Şenel, 1997a, b).

The emplacement order of allocthonous nappes over the autochthonous ones in the region is as follows:

- Antalya nappes was emplaced over Beydağı autochthon during Upper Cretaceous,
- Beyşehir-Hoyran-Hadim nappes were emplaced over Akseki-Anamas autochthon during Upper Eocene,
- Lycian nappes, situated at the W and NW of Beydağı autochthon, were emplaced over Beydağı autochthon after Lower Miocene.

Para-allocthonous and neo-autochthonous units are also observed in the region. Para-allocthonous units over the Antalya nappe, Paleocene-Lower Miocene aged rock units over the Lycian nappes of Middle Eocene age and neo-autochthonous units of the Middle Miocene-Quaternary age outcrop extensively in the study area.

The Beydağları autochthon representing the autochthonous rocks of the western Taurides and the Anamas-Akseki autochthon representing the autochthonous rocks of the Middle Taurides generally includes platform type carbonates and sediments. The Beydağları autochthonous unit was faulted and thrusted within itself from north to south due to the compressive tectonic regime in the Danian-Middle-Upper Eocene and the Lower Ladinian. The Anamas-Akseki autochthon representing the autochthonous rocks of the Middle Taurides is observed towards the E-NE of the study area. This unit including platform type rock units deposited discontinuously from Cambrian to Quaternary was faulted and thrusted within itself due to the dominant N-S compressive tectonic regime in Upper Eocene (Şenel, 1997a, b).

The Antalya nappes, Beyşehir-Hoyran-Nadim nappes and Lycia nappes represent allochthonous units developed at different environments from ocean to platform. The Antalya nappes include, from bottom to top, the Çataltepe nappe, the Alakırçay nappe, the Tahtalıdağ nappe and the Tekirova ophiolite, all of which are covered by the Campanian-Maastrichtian blocky flysch.

The Lycia nappes, being emplaced over Beydağları during Lower Miocene, are represented by the Tavas nappe, Bodrum nappe, Marmaris ophiolitic nappe, Gülbahar nappe and Domuzdağ nappe. Similar to the Lycian nappes, the Beyşehir-Hoyran-Nadim nappes, which were thrusted over the Anamas-Akseki autochthonous unit during Upper Eocene due to the N-S tectonic compression regime, have a close relation with the Marmaris ophiolitic nappe and Domuzdağ nappe.

The E-NE and W-SW directed compressional regime at the northern section of the Antalya bay during the Upper Tortonian, the Aksu thrust and the Kırkkavak oblique reverse fault have been developed. Following Lower Miocene, large faults and modern horst and graben structures have been formed (Akay et al., 1985).

CHAPTER IV

TUFA: FRESHWATER CARBONATES

IV.1 Introduction

Tufa is a general name that covers a wide variety of calcareous freshwater deposits that are especially common in Late Quaternary and recent successions (Pedley, 1996). The term tufa, which is derived from tophus, was extensively used in the Roman times to describe crumbly whitish deposits. Tufa has been defined by Pedley (1996) as the product of calcium carbonate precipitation under a cool water (near ambient temperature) regime and typically contains the remains of micro- and macrophytes, invertebrates and bacteria.

According to Pedley (1996), a rival term preferred especially in the United States, Spanish speaking countries and some parts of Europe, is travertine, which is derived from lapis tiburtinus or Tibur stone, from the river upon which Rome stands. Travertines are of hydrothermal origin and do not contain macrophytes or invertebrates. Travertines are dominantly hard, crystalline precipitates, frequently with thin laminations and with shrub-like bacterial growth.

Ford et al. (1996) state that calcium carbonate is believed to be absorbed by percolating water passing through soil horizons which often have high CO_2 levels due to biogenic activity. CO_2 moves much of the calcium carbonate into solution, which may travel some distance together with the water in the subsurface until it daylights at an outlet or spring.

As soon as the water reaches a certain level of oversaturation of $CaCO_3$ relative to CO_2, precipitation could be possible. Physical aspects such as temperature, pressure, and turbulence and by biochemical means, especially photosynthesis could be responsible for the change in CO_2 levels. As a result, calcium carbonate could be driven out of solution. When the CO_2 levels drop, the water becomes supersaturated with calcium carbonate and any sort of perturbation will cause the calcium carbonate to precipitate (Merz-Preib et al., 1999).

According to Julia (1983), there are two main trends in the deposition of travertine and tufa which are regulated by physio-chemical and biochemical parameters. The first trend is the predominance of the physio-chemical processes over the biochemical processes. This occurs when water turbulence, temperature, and/or pressure changes are the dominant agents in releasing CO_2. The second trend is the dominance of biochemical processes over physio-chemical processes. This occurs in calmer waters where photosynthesis is foremost in regulating the amount of CO_2 in the water, thus indirectly regulating the rate of calcium carbonate precipitation. In light of these physio-chemical and biochemical processes as well as the unique characteristics of travertine and tufa, one can better understand the settings in which either one is generally precipitated.

IV.2 Tufa systems

Tufa deposits, whose systems tend to be aggradational rather than degradational develop under the influence of flowing freshwaters. They are self-regulating systems in which they generate their own carbonate sediments and exclude virtually all other siliciclastic materials. Tufa systems contain carbonate clasts composed of cyanoliths or oncoids, which are biogenic entities. The clast size is inversely proportional to flow rate. Smaller detrital material also occurs but generally is derived from local tufa degradation.

In addition, tufa systems commonly develop reefs (phytoherms) which range from small patches or cushion especially near pool margins to major barrage constructions (Pedley, 1996).

Tufa paleoenvironmental models developed by Golubic (1969), Buccino et al. (1978) and Ordonez and Garica del Cura (1983) are accepted to be groundwork for tufa in the literature. These models well explain the basic ideas relating to growth, tufa morphology and diagenesis. These models have also been modified by Pedley (1990) and the following has been proposed for most of the tufa deposits:

1. Perched springline model
2. Cascade model
3. Fluviatile model
4. Lacustrine model
5. Paludal model

Each model mentioned above has its unique combinations of geometry, bedform characteristics, facies grouping and biotal associations (Table 1). Almost all tufa model identified by Pedley (1990) are present in the Antalya tufa basin

Modes of tufa classification are diverse. Some authors apply a botanical approach to the tufa classification in which associated vegetation is used, and some others apply physicochemical and biochemical parameters. More recently, even a petrographical approach is used for the classification purposes. However, in order to be more effective in differentiating the types and to be applicable to both ancient and modern deposits, all of the classification attempts were combined as follows (Table 1). Brief descriptions of these types mentioned in Table 2 are introduced below as given by Pedley (1990).

A. Authochthonous deposits

A.1 Phytoherm framestone

Phytoherm framestone delineates a living, anchored framework of erect or recumbent hydrophytal and semi aquatic macrophytes, frequently colonized by a dense and often felted micro-film of cyano-bacteria, coccoid bacteria, fungae and diatoms. These are cemented by thick fringes of low-Mg calcite isopachous cements. Disappearing of the carbonaceous framework by decaying leaves a highly porous and permeable fabric.

Table 1. General characteristics of the tufa facies (Ford and Pedley, 1996).

	Tufa paleoenvironmental models					
	Perched springline	Cascade	Fluviatile		Lacustrine	Paludal
			Braided	Barrage		
Geometry	Fan shaped in plan; wedge-like in profile, thickest deposit proximal to source	High angle cone and chute	Current alignment with long axis parallel to flow	Vertical walled tufa dams	Cone shaped	Broad flat
Bedform	Lines of springs coalesce to form sheet-like slope deposits	Steeply inclined sheets of carbonate precipitation behind which blind caves develop	Erosion surface, grading, local climbing ripple	Barrier-like one or more vertical walled, bryophyte-dominated tufa dams	Colonization of micro and macrophytes	Thin sheet-like spreads
Biotal association	Freshwater gastropods, insect larvae, vorms, ostracodes	No biotal association	Cyanolith (oncoid)	Cyanolith (oncoid)	Oncoids, algal bioherms, stromatolite, several gastropod families, bivalves, beetles, insect larvae ostracoda and fish	Marsh and terrestrial gastropod

Table 2. Classification of tufa facies (Ford and Pedley, 1996).

<table>
<tr><td colspan="3">ALLOCHTHONOUS</td><td>AUTOCHTHONOUS</td></tr>
<tr><td>MICRO DETRITAL TUFA</td><td colspan="2">MACRO DETRITAL TUFA</td><td>PHYTOHERM TUFA</td></tr>
<tr><td colspan="2">MATRIX SUPPORT</td><td>GRAIN SUPPORT</td><td rowspan="5">a. Boundstone sheets of micrite and paleosols
b. Microherm shrubby framework of bacterial colonies
c. Framestone true reef framework of macrophytes coated with mixed micritic and sparry fringe cements</td></tr>
<tr><td>Micrite tufa</td><td colspan="2" rowspan="2">Oncoidal and cyanolith tufa
Intraclast tufa</td></tr>
<tr><td>Peloidal tufa</td></tr>
<tr><td>Sapropelitic tufa</td><td colspan="2">Phytoclast tufa</td></tr>
<tr><td>Lithoclast tufa</td><td colspan="2">Lithoclast tufa</td></tr>
<tr><td>Lime mudstone</td><td>Wackestone/packstone</td><td>Grainstone</td><td>Boundstone</td></tr>
</table>

A.2 Phytoherm boundstone

Phytoherm boundstone is a tufa type dominated by heads of skeletal stromatolite, which are several centimeters up to 1 m in diameter and consisting of cement fringes formed in intimate associated with Oscillatoriacean cyanobacteria.

B. Allochthonous (Clastic) deposits

B.1 Phytoclast tufa

Phytoclast tufa consists of allochthonous cement-encrusted plant fragments which are cemented together after deposition, though some earlier cement development around phytoclasts may have occurred prior to or during transport.

B.2 Cyanolith (oncoidal) tufa

Oblate to sub-spherical stromatolites composing of cyanobacterial/cement fringe associations form this type of tufa. Generally the highly spheroidal forms dominate rivers but strongly oblate ones are typical of sluggish flow regimes and free-form growth-forms of static conditions. They mostly form a grain-supported fabric associated with smaller clasts.

B.3 Intraclast tufa

Intraclast tufa type mainly consists of silt and sand size detrital tufa fragments produced from the break up of older cements and phytoherm frameworks. These fragments are transported during flood to be deposited as calciclastic grain-support fabrics in fluvial channels. They also occur around phytoherm frameworks in static water conditions where supporting frameworks have decayed.

B.4 Microdetrital tufa

B.4.1 Micritic tufa: the finest sediments consist of micrite, which comprises the majority of lake, pond and marsh deposits. It forms thin sheet deposits on slopes in association with bryophyte hummocks, and fills phytoherm frameworks. Though it may be structureless in thin-section, it is frequently clotted.

B.4.2 Peloidal tufa: this type is formed by the peloids having smooth elliptical outline to free form that are often grouped into poly-nucleate masses 10-70 μm in diameter. Deposits can be grain-supported but commonly "grow" or "compact" to form clotted textures.

CHAPTER V

TUFA DEPOSITS OF THE ANTALYA

V.1 Introduction

This chapter is based on the extensive and elaborate study of Glover and Robertson (2003) and observations made during field investigations in this study. This essential study examines the origin, environment and types of tufa deposits in the Antalya area. The proposed classification of the tufa facies of the Antalya area by Glover and Robertson (2003) forms the backbone for the attempted geotechnical characterization of Antalya tufa deposits in this study. After the general definition and environment for tufa systems have been given in the preceding chapter, geological origin and characteristics of the tufa deposits in the Antalya area will be introduced in this chapter.

V.2 Geomorphological setting of the Antalya tufa deposits

Antalya tufa has been deposited in the Antalya basin, which is located at the NW part of the Aksu basin (Glover and Robertson 1998a). The tufa rock mass is generally covered by karst forms, which are formed by successive dissolution and recementation of tufa. Antalya basin covers one of the largest (630 km^2) and the thickest (up to 250 m) tufa deposition in the world.

The morphology of the Antalya tufa basin is made up of two main plateaus, namely, lower and upper plateau (Figures 5 and 6). Numerous other terraces can be locally observed but cannot be traced across the entire basin. Three main spring groups debouch onto tufa terraces. The topographic levels of these spring groups have been determined as 300 m, 100 m and sea level, respectively (Burger, 1990).

The Köprü and Aksu river basins divide the Antalya tufa basin into two parts. Eğirdir and Beyşehir lakes, located in the north, are believed to be the main water sources for the

Köprü and Aksu basins (Glover and Robertson, 2003). The modern spring waters is observed to be discharging from karstic aquifers with very large groundwater reservoirs with the large Mesozoic carbonate platforms, notably the Bey Dağları to the west of the Aksu Basin (Figure 7).

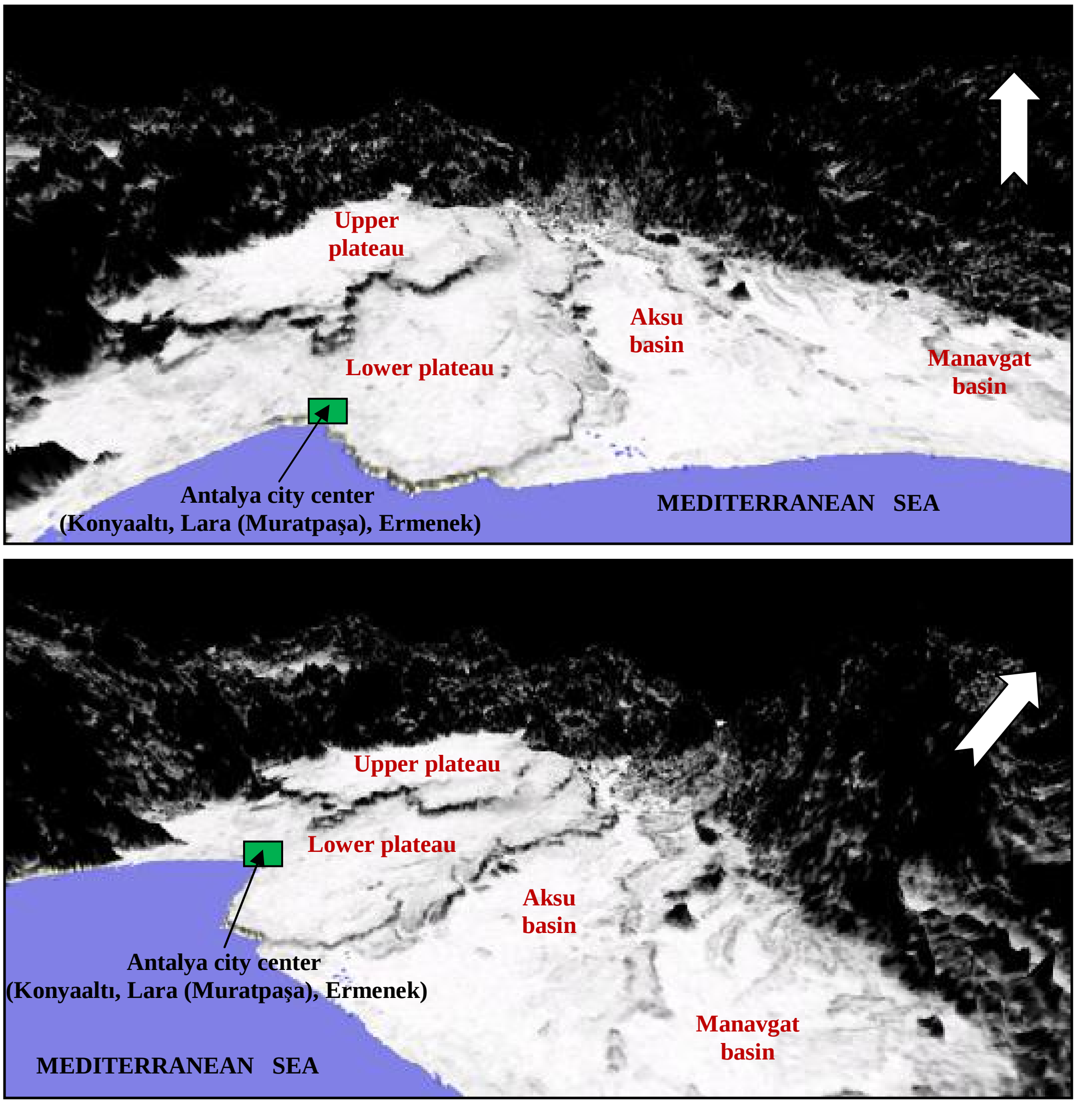

Figure 5. Digital elevation models illustrating the tufa plateaus of the Antalya basin (vertical exaggeration is x7).

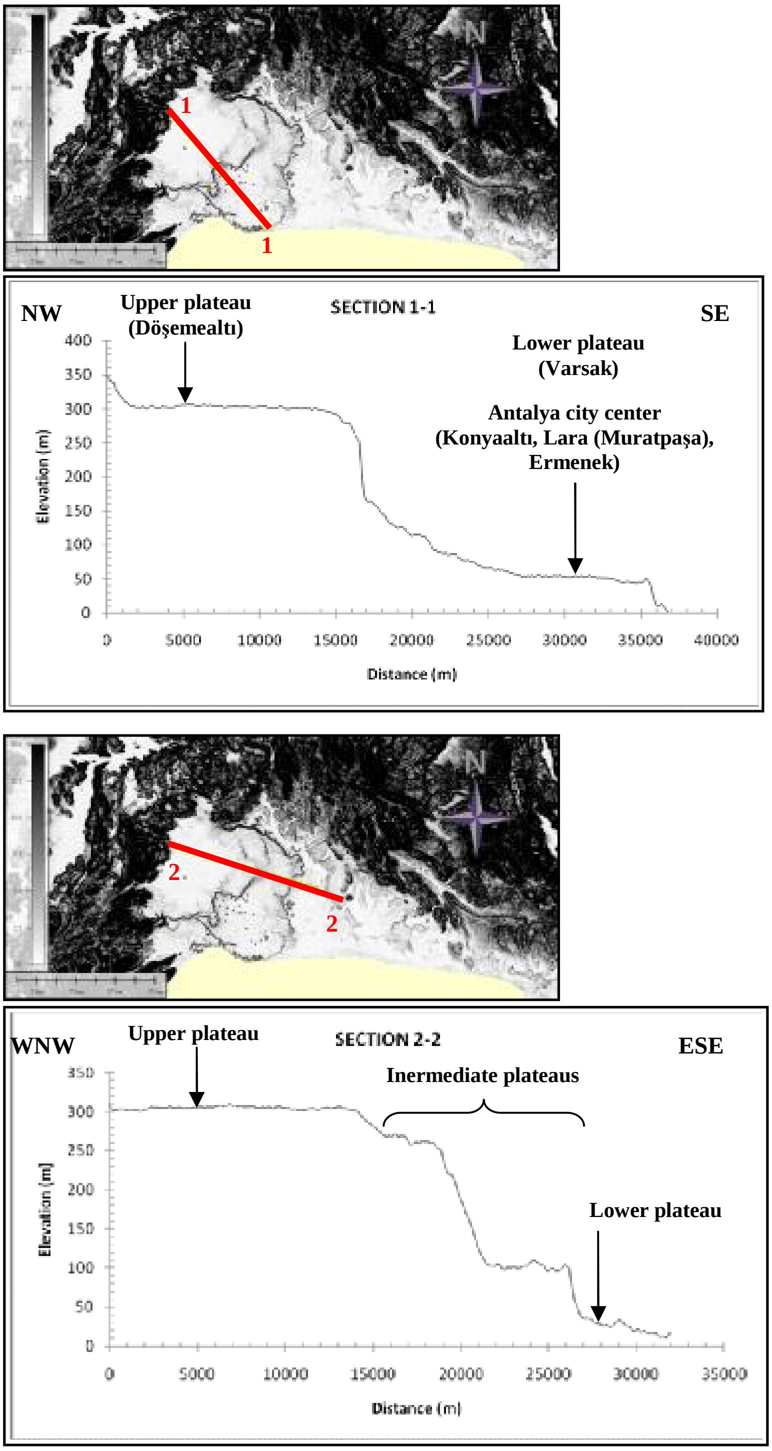

Figure 6. Cross sections revealing tufa terraces in the Antalya area.

Figure 7. Views from the modern spring discharging from the karstic carbonate platforms (July, 2009).

V.3 Origin of Antalya tufa deposits

Glover and Roberston (2003) mentioned that extensional tectonics has a significant effect in the localization of depocenters in the western Antalya basin. Due to the almost N-S trending normal fault, which produces a half-graben morphology in the basin, Pliocene and older rocks have been faulted and produced N-S trending, west dipping fault blocks. These fault blocks or grabens were sutiable for ponding small lakes where tufa first commenced to deposit, which later on produced barriers.

Burger (1990, 1992) has examined Antalya tufa samples, which yielded ages from c. 87 to 294 ka which revealed that Antalya tufa has been formed during mid-Late Quaternary. Glover and Robertson (2003) interpreted Burger's ages to reflect cascade-waterfall type tufa which buries older terrace deposits. They believed that the tufa deposition persisted from > 600 ka to recent. After a complete investigation period, they suggested that the Antalya tufa was mainly deposited from 2.0 to 1.5 Ma in lacustrine/paludal setting after Late Pliocene marine regression. The extensive tufa deposition was interrupted by tectonic uplift which created upper terrace at c. 300 m a.m.s.l. Rivers have been originated and evolved within the upper terrace. During mid-Quaternary marine transgression related with glacial cycles separated the lower terrace (100 – 200 m a.m.s.l.) forming coastal cliffs. Meanwhile, springs, rivers produced high-energy-type tufa. During tufa formation, tufa deposits possibly have experienced a number of glacial and interglacial periods. When the floral information is examined, it has been understood that cooler climatic conditions than today were prevailing.

According to borehole data published by Özüş (1992), the thickness of tufa within the upper plateau is up to 250 m thick in the west.

V.4 Antalya tufa settings and facies

Different depositional settings have been recognized by Robertson and Glover (2003) for the Antalya tufa. The modern and common tufa settings have been grouped into systems which have been listed below.

- Barrage/lake system
- Waterfall system
- Lacustrine/paludal system
- Fluvial system
- Slope system

Almost all tufa types identified by Pedley (1990) with further types discovered by Glover and Robertson (2003) are present in the Antalya tufa basin. The tufa types in the Antalya tufa basin are listed below (Glover and Robertson, 2003):

- microcrystalline tufa
- phytoherm framestone
- phytoherm boundstone
- phytoclast tufa
- intraclast tufa
- microdetrital tufa
- oncoidal tufa
- pisoliths
- tufa breccias

Among the tufa facies listed above, the first five listed tufa types are the subject of this study. The study area covers one of the largest (630 km^2) and the thickest (up to 250 m) tufa deposition in the world. Hence, it was not easy to study and examine the entire tufa deposition area. Accordingly, some representative parts, namely, Lara (Muratpaşa), Konyaaltı and Ermenek districts, which are located at the lower plateau of this large tufa deposition area, were studied. The aforementioned districts are densely populated and are situated very close to the sea shore. Hence, most of the time it was quite difficult to find tufa outcrops in these areas.

Starting from the mid of year 2007 up to 2011, numerous site visits were carried out to the study area in an attempt to identify the geological characteristics of the tufa deposits in the field through the observations of rock outcrops and man-made excavations. The types of tufa deposits were observed to be changing very frequently in short intervals in the field justifying the relation between facies and depositional environments of the Antalya tufa deposits that was mentioned in the previous studies.

The most common tufa types identified and studied during field excursions were the phytoherm framestone, the phytoherm boundstone, the microcrystalline, the phytoclast and the intraclast types. The representative outcrops of the each tufa type are given in the following pages (Figures 8, 9, 10, 11 and 12).

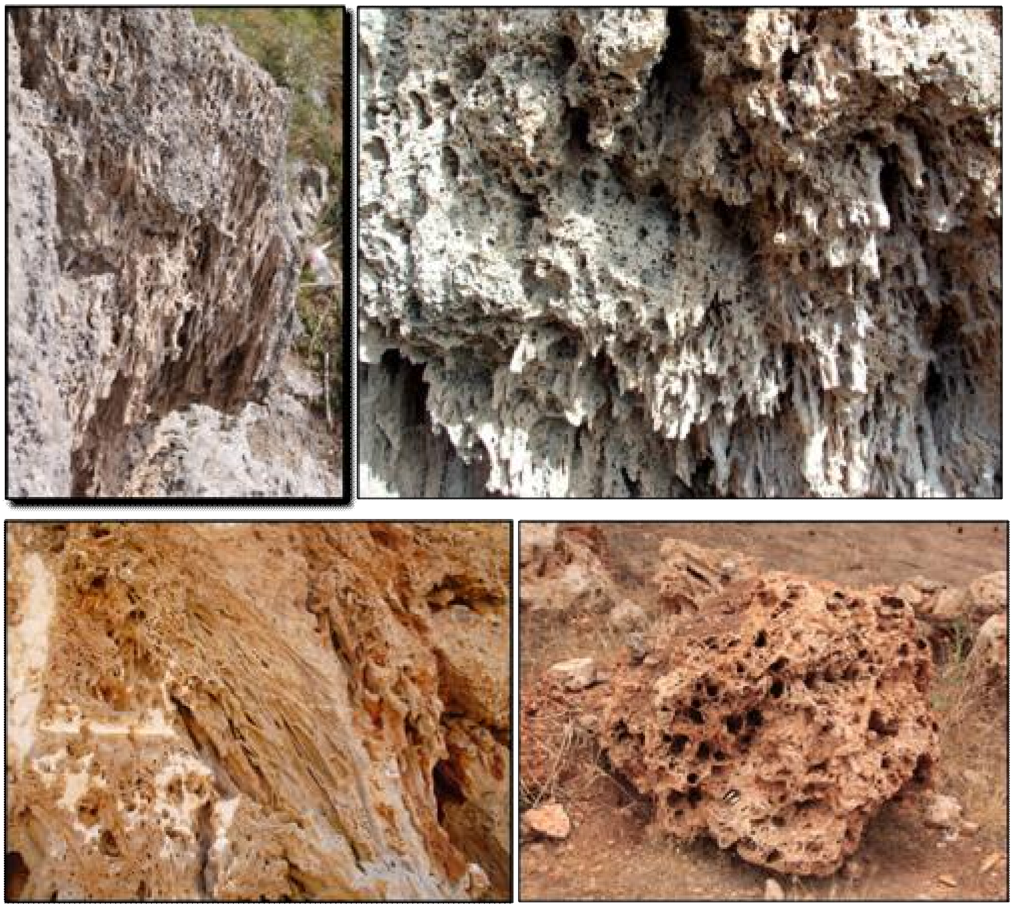

Figure 8. Images of the phytoherm framestone samples (July, 2009).

Figure 9. Images of the microcrystalline samples (October, 2009).

Figure 10. Images of the phytoclast samples (October, 2009).

Figure 11. Images of the phytoherm boundstone samples (April, 2010).

Figure 12. Images of the intraclast samples (October, 2009).

The Lara (Muratpaşa) district, which is located towards the east of the Antalya city center, was generally observed to posses the phytoherm framestone and the phytoclast types along the modern coast line (Figures 13 and 14). The inland areas, however, were observed to be represented mostly by the intraclast and the phytoclast types in the Lara district. It should be emphasized that these facies show lateral and vertical transitions into the other tufa types within the entire tufa deposition area.

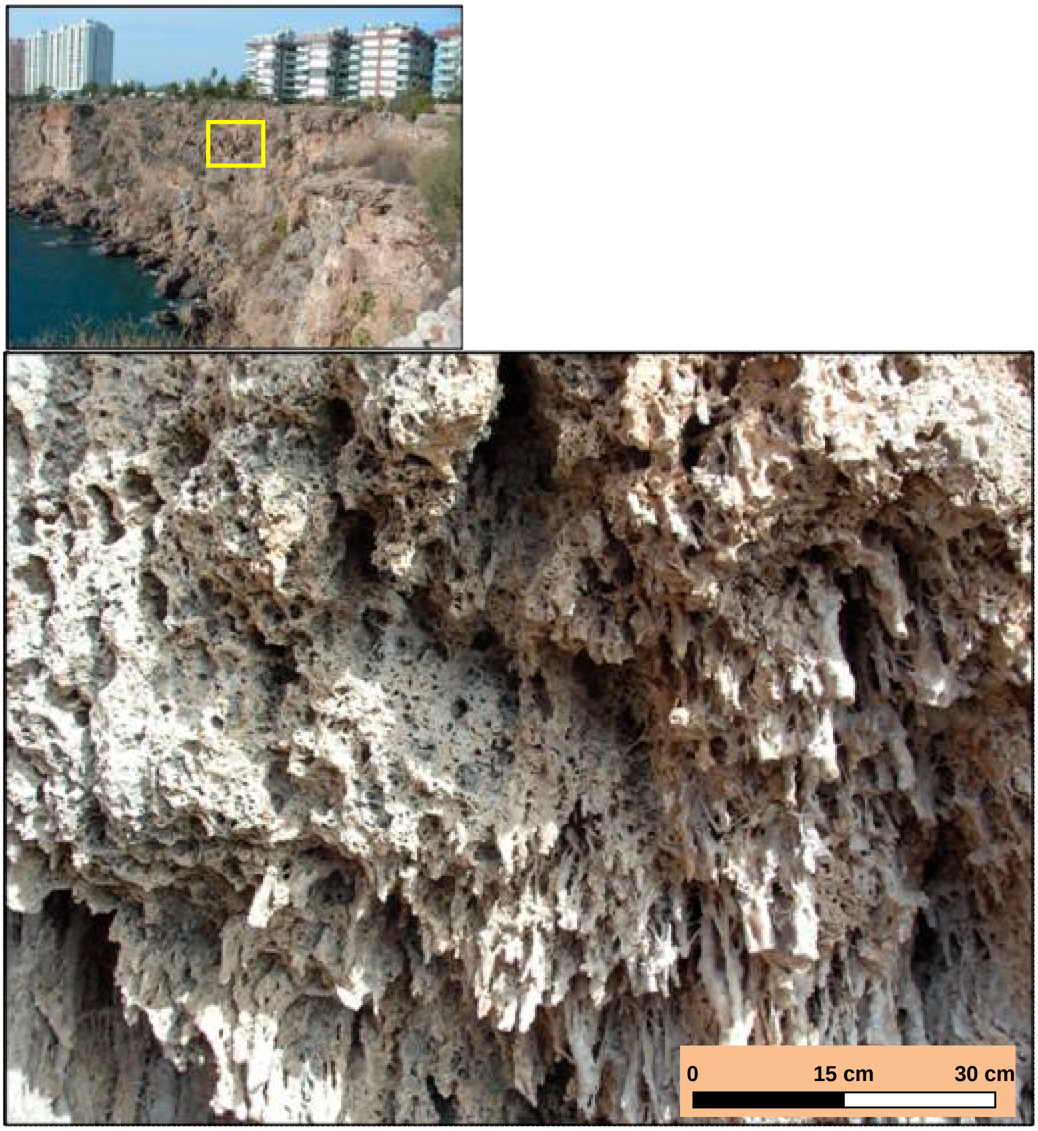

Figure 13. Tufa deposits of mainly phytoherm framestone close to the Lara Falls of the Düden river (October, 2007).

Figure 14. Lara Falls of the Düden River where new tufa deposition is observed adjacent to former deposits (August, 2009).

The lacustrine carbonate sediments were observed to be one of the major deposition types together with the microcrystalline tufa type and the fluvial clastic deposits were observed to be one of the major deposition types in the Konyaaltı district of western Antalya. In this region, mostly, the microcrystalline and intraclast types were observed in various excavations (Figures 15 and 16).

Figure 15. A view from a foundation excavation of a business center construction in the Konyaaltı district of western Antalya (August, 2008).

Figure 16. A view from excavations of the Antalya light railway construction (August, 2008).

The phytoherm framestone, the phytoherm boundstone and the microcrystalline tufa type deposits were mostly observed in the Ermenek district, towards to far east of the Antalya city center. In this region, two depression areas were also noticed. These sink hole-like depressions and the tufa outcrops around these depressions illustrate typical karst features (Figures 17 and 18).

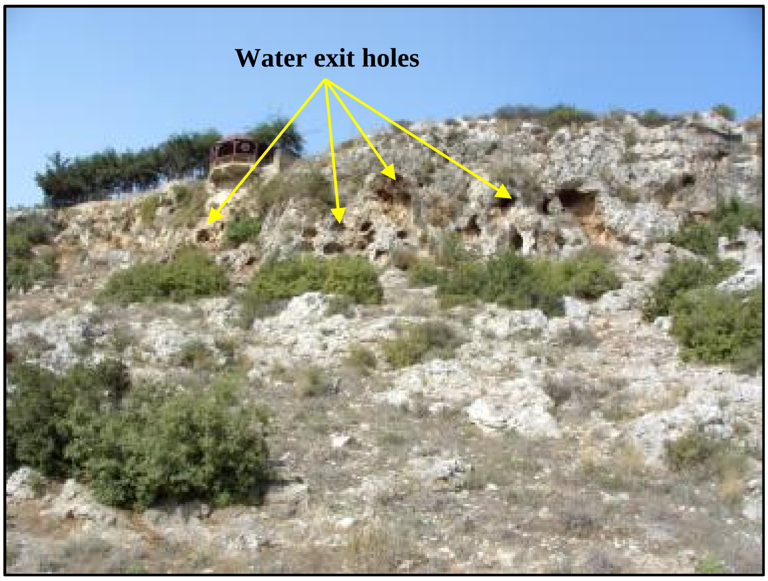

Figure 17. Water exit holes scattered around the main resurgence point of a spring in Ermenek (October, 2007).

Figure 18. Depressions around Ermenek (January, 2009).

CHAPTER VI

GEOTECHNICAL INVESTIGATIONS PERFORMED ON THE ANTALYA TUFA ROCK MASSES

VI.1 Introduction

This chapter introduces the geotechnical investigation performed for the geotechnical characterization of the Antalya tufa deposits. These geotechnical investigations could be grouped mainly into three categories, namely, *the field observations* based on surface geological considerations; *the field geotechnical studies* including drilling, trial pits, geophysical investigations and geotechnical field testing; and *the laboratory tests* covering soil and rock mechanics testing.

These geotechnical investigation methods, whose details and results will be discussed in the next chapter of this thesis, are introduced below.

Numerous block samples of the each tufa type were collected and transferred to the laboratories during site visits. 158 core samples with different L/D (length/diameter) ratios were recovered from more than 50 rock blocks in various dimensions by a portable drilling machine and then prepared for laboratory testing (Figures 19 and 20). Thin sections of each tufa type were prepared from these block samples for petrographic inspection. Furthermore, samples for Loss on Ignition (LOI), Differential Thermal Analyses (DTA), Thermogravimetric Analysis (TGA) and Scanning Electron Microscope (SEM) analysis including Energy-dispersive X-ray spectroscopy (EDS) were also prepared from these rock blocks.

Figure 19. Views during the collection of tufa rock block samples (April, 2010).

Figure 20. Views from the core sample preparation from the block samples of the Antalya tufa rock masses (July, 2010).

VI.2 Field geotechnical studies

During and after the field observations, a number of geological aspects of the tufa deposits, such as the porous texture and the formational contact relations, which could be important in controlling the mechanical behavior, were explored. In order to reveal the geological characteristics of the tufa deposits, various field geotechnical investigation techniques were carried out simultaneously, especially since the different tufa types mentioned in the preceding sections showed frequent lateral and vertical transitions. It needs to be mentioned that the non-homogeneous structure of the rock masses caused difficulties during sampling and testing.

The study area and its surroundings is a well-known karstic region, which has been thoroughly studied since many years by several researchers (Özgül, 1976; Koçyiğit, 1981;

Özgül, 1984; Yalçınkaya et al., 1986; Günay, 1981; Gürer et al., 1980; UNDP, 1983; Arıkan and Ekmekçi, 1985; Sipahi, 1985; Ekmekçi, 1987; Değirmenci, 1989; Denizman, 1989; Koyuncu, 2003). During the field observations, the porous structures, which could have originated from either karstification or mode of occurrence, were so distinctive. The size and geometry of these pores showed quite a wide variation from millimeters to meters (Figure 21). One of the aims of this study was to attempt to locate the cavities beneath the ground surface. For this purpose, geophysical methods, namely, Seismic Refraction Tomography (SRT) and Vertical Electrical Sounding (VES), which are referred to be appropriate geophysical techniques for cavity detection in the literature, were carried out (Table 3) (Figure 22). The details of these geophysical methods will be given in Chapter VII.2.1.

Table 3. ASTM Consensus Standard Methods for Assessing sinkholes and voids (ASTM D6429).

Method	**Consensus Standard**
Seismic Refraction	B
Electrical (DC)	B
Frequency Domain Electromagnetic	B
Ground Penetrating Radar	A
Gravity	A

A: Primary choice or preferred method, B: Secondary choice or alternate method

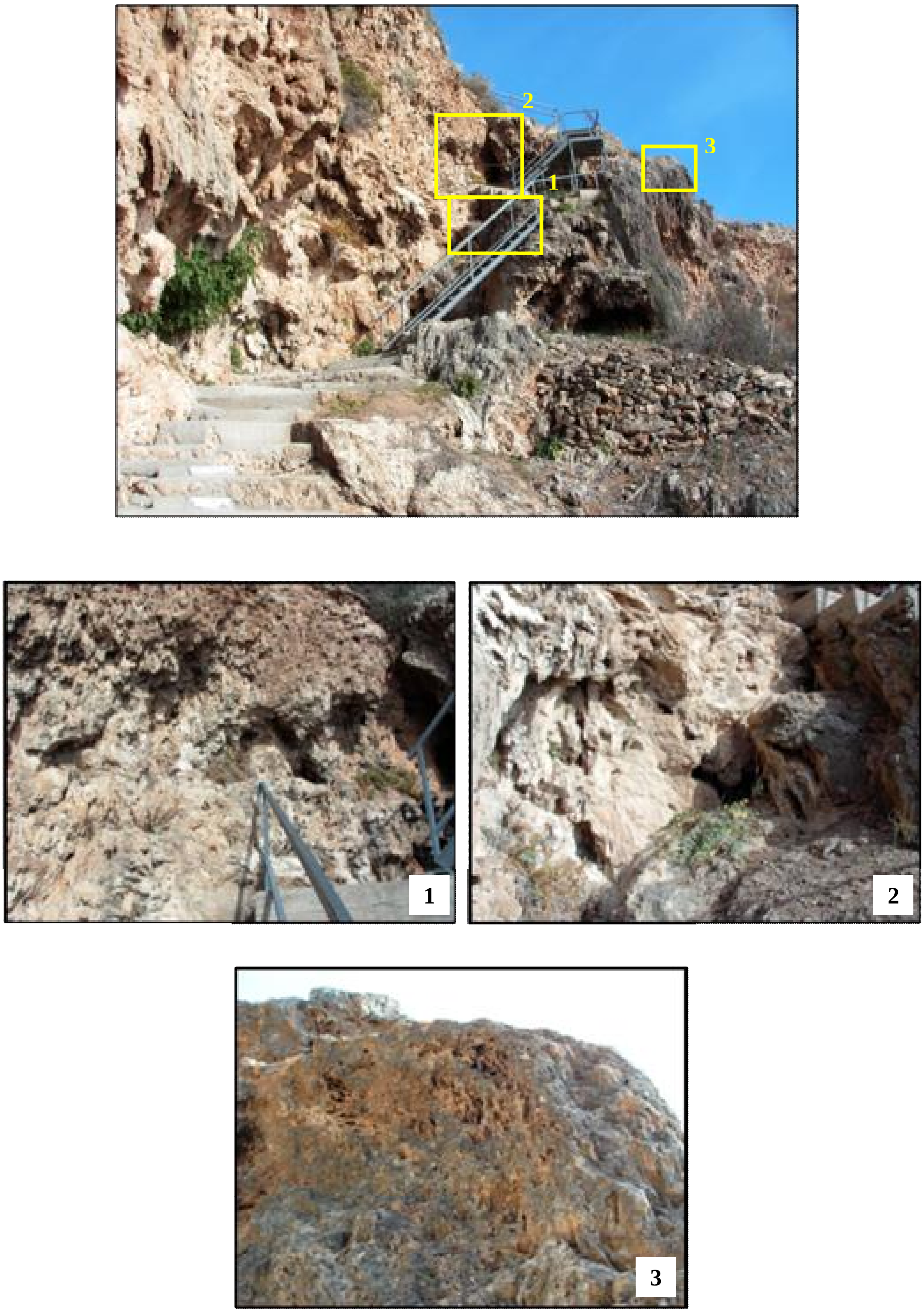

Figure 21. A typical view of tufa rock outcrop displaying quite a wide variation of pore size (October, 2007).

Seismic Refraction Tomography (SRT) Investigation

Vertical Electrical Sounding (VES) Investigation

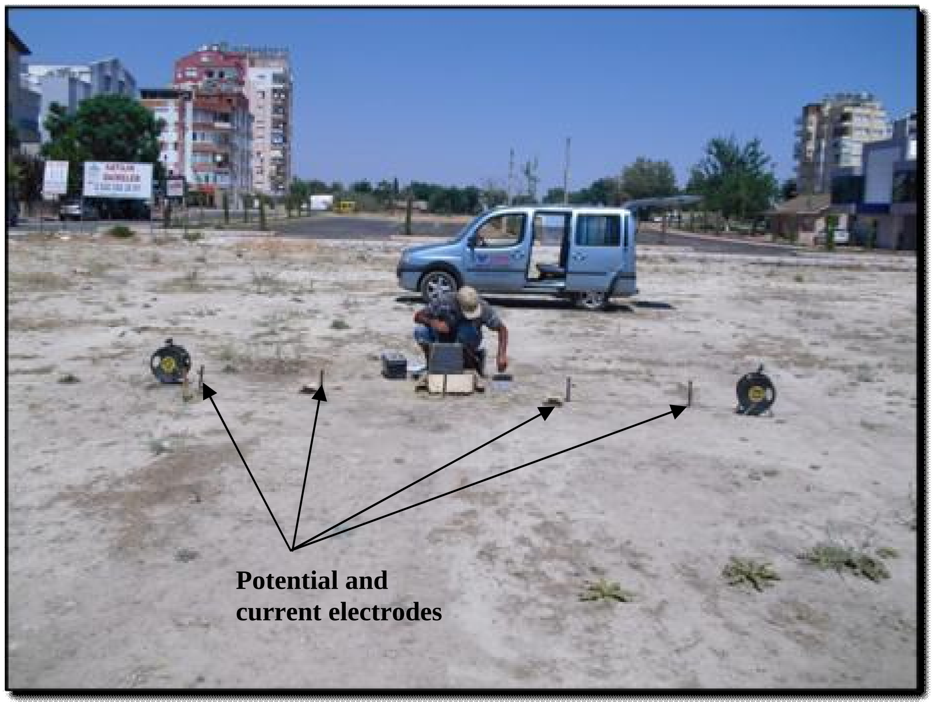

Figure 22. Views of the SRT and the VES investigations (October, 2009).

The results of the geophysical explorations also aided in selecting the borehole locations where within the scope of the field geotechnical studies, a total number of 9 boreholes were drilled by truck mounted rotary core drilling (Figure 23). The borehole locations were selected at particular locations showing an anomaly in the SRT investigations. One of the aims of drilling was to cross check the results of the SRT and VES investigations. In addition, NX (2-inch diameter) size core samples were obtained from these boreholes that enabled laboratory geomechanics, petrographic and index testing (Figure 24).

Figure 23. A view from Borehole SK-3 during drilling operations (October, 2009).

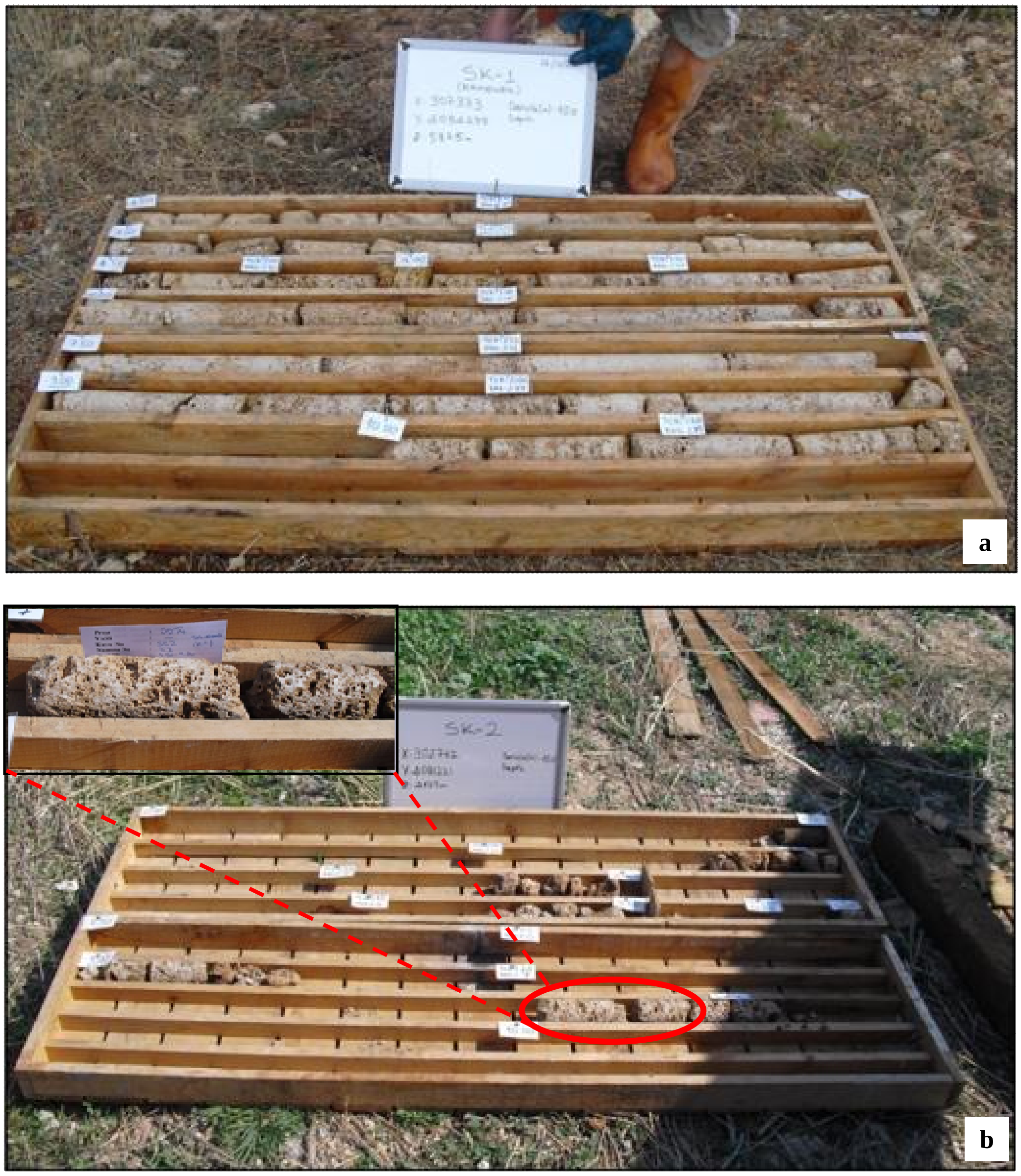

Figure 24. Core boxes. a) A view from core box of Borehole SK-1. b) A view from core box of Borehole SK-2 (October, 2010).

During drilling operations, 11 pressuremeter tests were carried out in boreholes where sampling through core barrels was not possible. A Menard type APAGEO brand pressuremeter instrument was employed for pressuremeter testing (Figure 25).

Figure 25. A view from a pressuremeter test carried out simultaneously during borehole drilling (October, 2010).

A total of 30 observation pits were excavated by a JCB (Joseph Cyril Bamford Excavators Limited) back hoe loader at different localities in the project area for the purpose of plate load testing and observations. A total of 38 plate load tests of which 30 of them were deemed reliable were carried out in order to investigate the bearing capacity of the tufa deposits (Figure 26). During plate loading testing, 30 mm thick plates with 300 mm and 762 mm diameters, respectively, were used.

Figure 26. Views from plate load tests (January, 2011).

VI.3 Laboratory testing

The geotechnical properties of the Antalya tufa deposits were also investigated through laboratory testing. In order to identify these parameters, a number of bulk and core samples were prepared from rock blocks obtained for each tufa type in the field.

Laboratory tests carried out on tufa samples could be grouped into three categories as follows:

a. *Petrographical and the mineralogical analyses*
b. *Geophysical tests*
c. *Geomechanics tests*

Brief information on laboratory tests for each testing category is presented below.

a. Petrographical and mineralogical analyses

The main aim of the petrographical and mineralogical analyses was to reveal the mineralogical composition and the microstructure that might give some clues about the controlling factors on the mechanical behavior of the tufa deposits. The sizes of the pore spaces and their interrelations (i.e., whether interconnected or not) together with the mineral types were also investigated.

The petrographical and mineralogical analyses carried out during this study covered optical microscopic examination, Loss on Ignition (LOI) testing, Differential Thermal Analysis (DTA), Thermogravimetric Analysis (TGA) and Scanning Electron Microscope (SEM) Analysis including Energy-dispersive X-ray spectroscopy (EDS).

The thin sections of the tufa types were prepared and analyzed in the Mineralogical Laboratory of the Department of Geological Engineering, Middle East Technical University (METU) for the purposes of mineral identification and alteration determination.

During SEM analyses, a ***JSM 6400 NORAN System 6 X-ray Microanalysis System and Semafore Digitizer*** device was used at the Metallurgical and Materials Engineering Department of METU (Figure 27.a). Examination of micro structure and mineral crystal surfaces with their composition were carried out.

The DTA/TGA analyses of the tufa deposits were carried out at the Central Laboratory at METU with a ***Setaram Labsys Simultaneous DTA/TGA*** device (Figure 27.b). The mineral and the organic species forming the tufa types were attempted to be identified in these analyses. DTA analyses were carried out with TGA analyses simultaneously in order to differentiate and identify the loss of mass due to dehydration during the heating, which was initiated from 25°C and elevated up to 600°C.

The LOI tests were carried out at the Technical Research Laboratory of DLH (Demiryollar, Limanlar ve Hava Meydanları İnşaatı Genel Müdürlüğü). The tufa samples were heated up to 1000°C and the differences in the mass of samples were measured before and after heating in order to detect the organic content within the mass (Figure 27.c). Since the loss in weight might be due to the release of free moisture, chemically combined or “hydroxy” water, CO_2 and SO_2 besides the release of any organic material, the results were correlated with the DTA/TGA results.

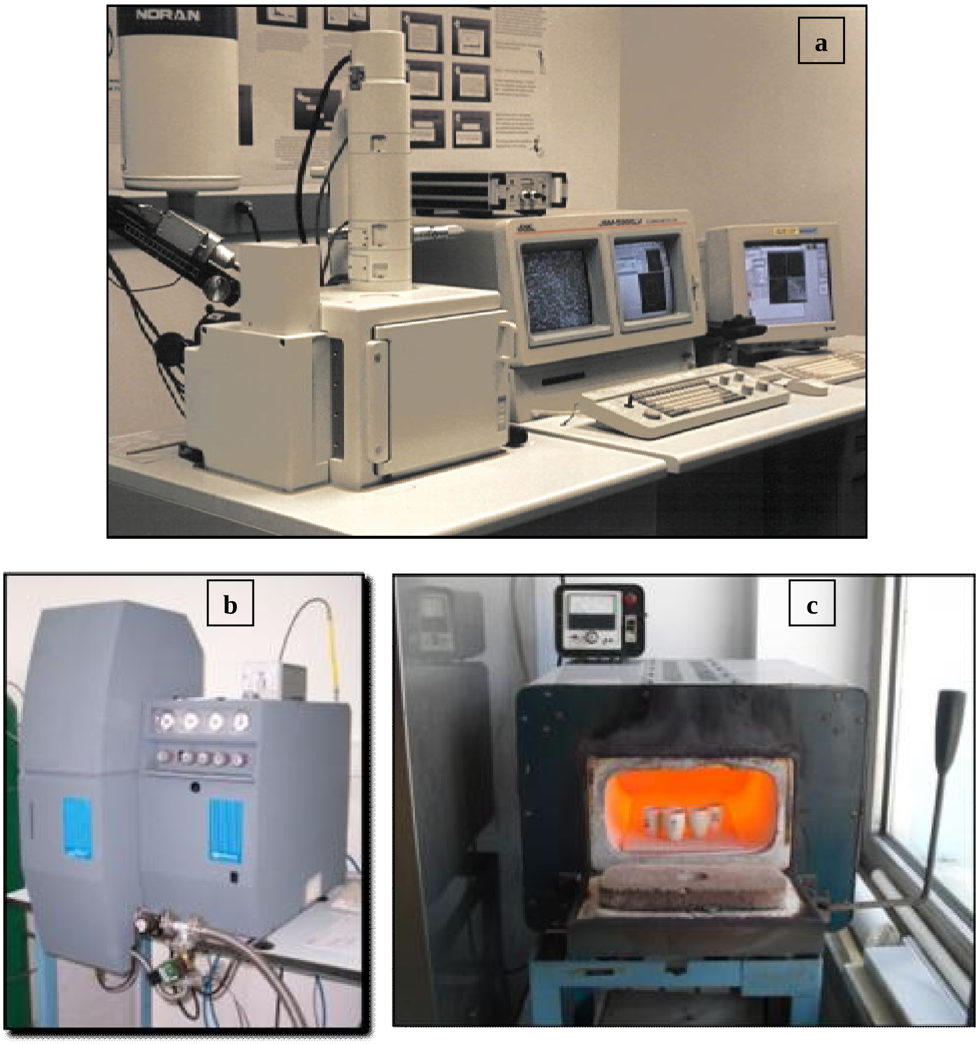

Figure 27. a) JSM 6400 NORAN System 6 X-ray Microanalysis System and Semafore Digitizer device used for SEM analyses. b) Setaram Labsys Simultaneous DTA/TGA device c) Ceramic inner liner oven for LOI analyses.

b.Geophysical tests

Geophysical parameters such as S-wave and the P-wave velocities may be very helpful when the geotechnical data is scarce and hard to obtain. Also, since these tests are non-destructive exploration methods, they allow the same samples to be used for other tests.

Regarding the above mentioned advantages, the ultrasonic velocity measurements were carried out on numerous tufa samples at the laboratory of DLH (Demiryollar, Limanlar ve Hava Meydanları İnşaatı Genel Müdürlüğü). A device manufactured by OYO Corporation with Model 5217A Sonic Viewer was used for the measurements (Figure 28) with the aim of determining the static and dynamic elastic constants. In addition, an attempt was made to establish the relationships between the geotechnical parameters, such as the uniaxial compressive strength, porosity and seismic wave velocities.

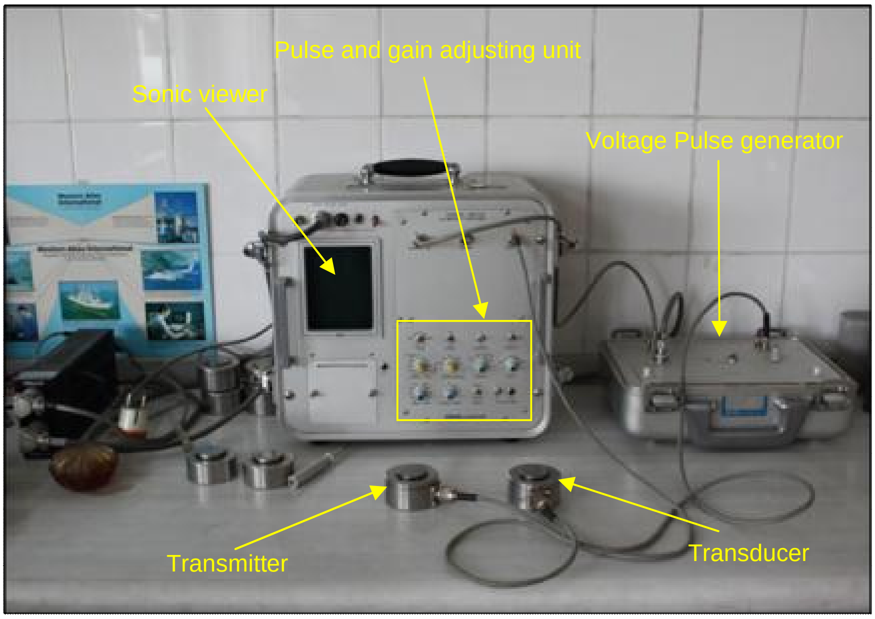

Figure 28. Views from the ultrasonic velocity measurement device and during testing.

c. Geomechanics tests

The geomechanics tests were carried out at the laboratories of; DSİ TAKK (Devlet Su İşleri Teknik Araştırma ve Kalite Kontrol Dairesi Başkanlığı), DLH, Geological

Engineering Department and Mining Engineering Department of METU. These tests included:

a. *Porosity and unit weight determination tests,*
b. *Uniaxial compressive strength (UCS) test (Figure 29),*
c. *Triaxial compressive strength test (Figure 30),*
d. *Brazilian indirect tensile strength test (Figure 31),*
e. *Point load strength test (Figure 32),*
f. *Slake durability test (Figure 33),*

The above mentioned geomechanics tests were performed to determine the shear strength, the uniaxial compressive strength, the elastic properties and their relationships with other parameters such as porosity and seismic velocity of the different tufa types (Figures 29-33).

Figure 29. A view of the uniaxial compressive strength test with measurement of Elastic properties.

Figure 30. A view of the triaxial compressive strength test.

Figure 31. A view of the Brazilian indirect tensile strength test.

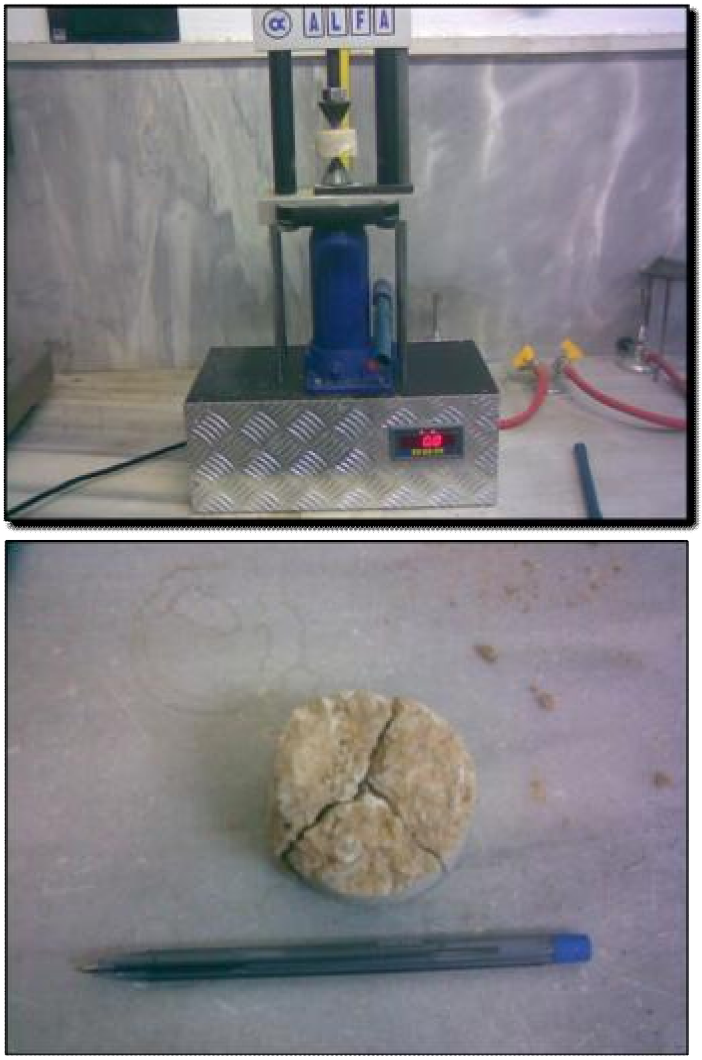

Figure 32. A view of the point load strength test.

Figure 33. A View of the slake durability test.

All of the geomechanics tests, except the UCS test, were carried out in accordance with the appropriate ASTM (American Society for Testing and Materials) or ISRM (International Society for Rock Mechanics) standards. Due to the porous nature of the tufa deposits, the rather rough side surfaces of the core samples prevented the strain gages for the measurement of elastic constants during UCS testing. Therefore, a special instrument, a circumferential extensometer, was used during UCS testing (Figure 34).

Figure 34. A circumferential extensometer used for the measurement of the elastic parameters of the tufa samples.

The MTS (Material Testing System) apparatus including microconsole and microprofiler was used during UCS testing. Tests were deformation controlled with the rate of 5/1000 mm/sec. While the lateral displacements were measured by the circumferential extensometer, the vertical displacements were measured by the LVDT (Linear Variable Differential Transformer). The uniaxial compressive strengths and the elastic constants (i.e., Elasticity modulus and Poisson’s ratio) of the tufa core samples were measured during UCS testing.

CHAPTER VII

GEOTECHNICAL CHARACTERIZATION OF THE ANTALYA TUFA ROCK MASSES

VII.1 Introduction

This chapter describes the methods utilized and the results of the rock mass characterization tests carried out on the Antalya tufa rock masses. These tests were conducted in two stages, namely, in-situ and the laboratory tests. The in-situ testing effort was divided into two tasks, namely, in-situ geophysical testing comprising of seismic refraction and electrical resistivity measurements, and in-situ geotechnical testing covering pressuremeter test and plate load test. The laboratory testing studies covered a fairly wide spectrum ranging from petrographical thin section examinations, SEM analyses, DTA and TGA analyses, unit weight and the porosity determination, uniaxial compressive strength testing, triaxial compression strength testing, indirect tensile strength (Brazilian) testing, point load strength index testing, slake durability testing, ultrasonic wave velocity measurement and loss on ignition (LOI) testing. Later in this chapter, the results of each test will be correlated with the results of the other tests in order to figure out the mutual relationships between the testing parameters for the purpose of geotechnical characterization of the tufa rock masses.

VII.2 In-situ tests

In-situ tests covering geophysical and geotechnical investigations, namely, pressuremeter tests, plate load tests, seismic refraction tomography and vertical electrical sounding methods were carried throughout the city of Antalya where areas of intense housing (settlement) prevented conducting an ideal investigation program. Figures 35 and 36 give the locations of the compiled (previous investigations) and conducted (present investigations) in-situ testing points.

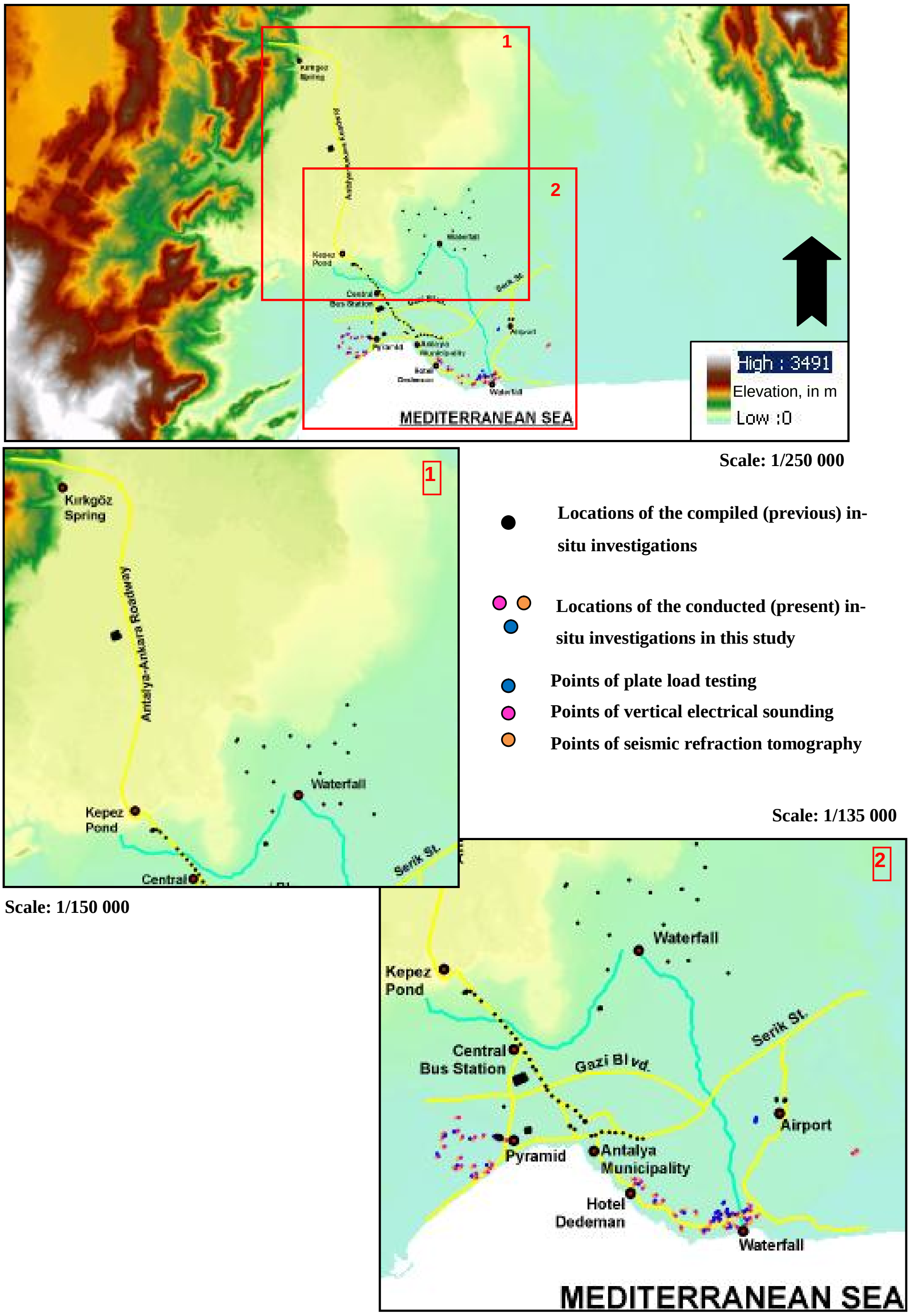

Figure 35. General layout of the locations of the compiled and conducted in-situ investigations performed in the Antalya area.

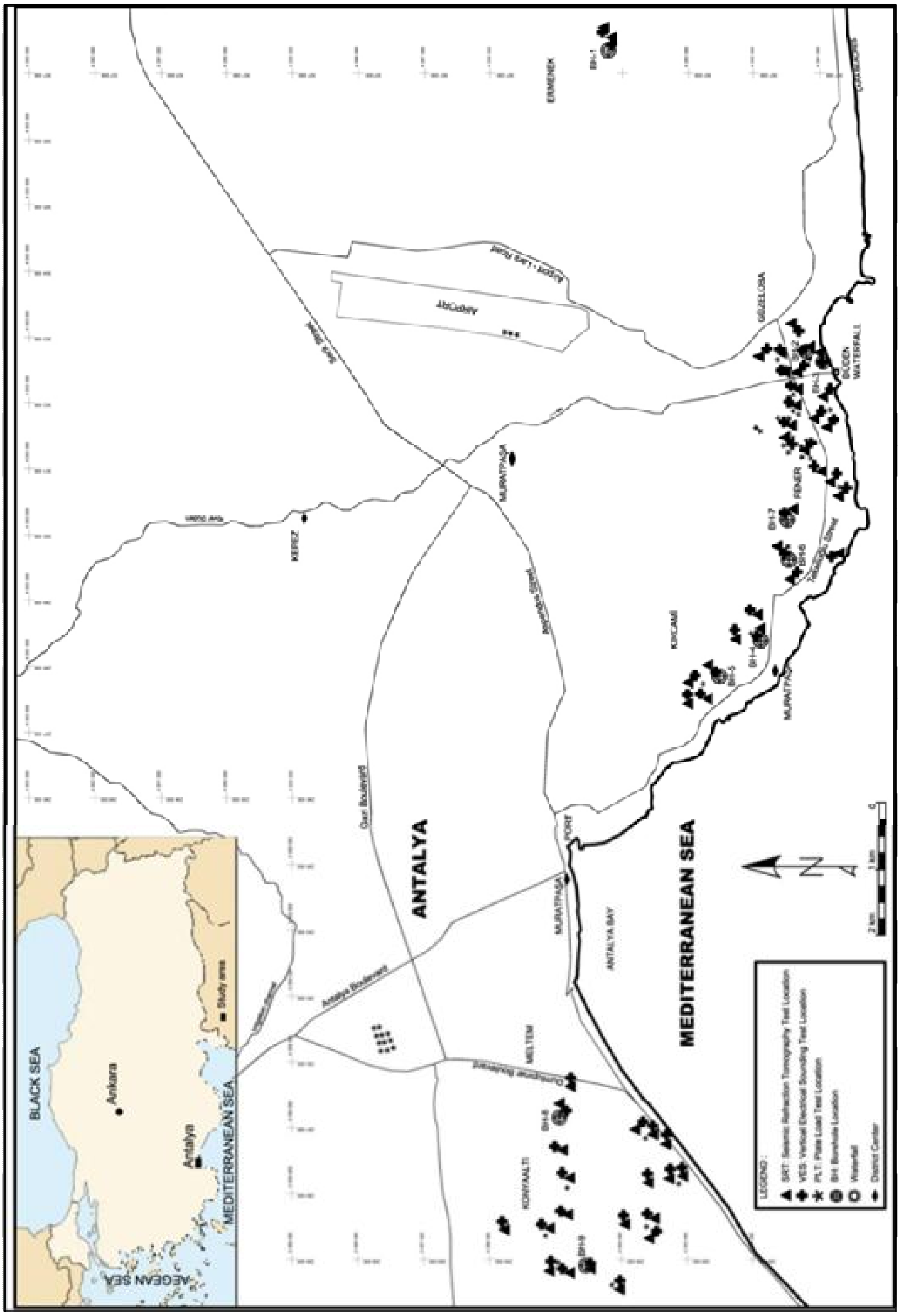

Figure 36. Detailed layout of the investigations performed in this study.In-situ geophysical tests

Field geophysical tests carried out were the seismic refraction tomography (SRT) and the vertical electrical sounding (VES). The main aim in applying geophysical investigations was to detect the voids or the cavities, whose diameter are more than100 cm, within the tufa rock mass near to the surface (< 15 m). It is well-known that the distribution and dimension of these cavities vary so much within the tufa rock mass. Since the foundation depth of the buildings in Antalya is mostly shallow (< 15 m), the investigations were focused down to 15 m to 20 m below the ground surface.

The other purpose of applying geophysical investigations was to measure the shear wave velocity and the primary wave velocity together with the earth resistivity of the rock masses. In order to correlate and compare the measurement results, both geophysical investigation methods have been utilized at each investigation area. A description of the methods and the test results are presented below.

VII.2.1.1 Seismic refraction tomography (SRT)

The conventional refraction inversion methods use a “layer cake” approach where the subsurface stratum is divided into a number of continuous constant velocity layers with velocities and thicknesses. These velocities and thicknesses are varied through interactive forward modeling to match the travel times, which are determined from the in-situ data. These methods require that the sections of the travel time curves be mapped to refractors (Sheehan et. al., 2005).

Being different than the conventional refraction methods, SRT does not require a model, which is broken into constant velocity continuous layers. Instead, the model is made up of numerous small constant velocity grid cells or nodes. Inversion is carried out by an automated procedure. This procedure involves ray tracing through an initial model and comparing the modeled travel times to the in-situ data, and adjusting the model grid-by grid in order to match the modeled travel times to the in-situ data. This process is iteratively repeated until a preset number of iterations are reached. Because there is no assumption of continuous constant velocity layers, SRT can model localized velocity anomalies (Sheehan et. al., 2005).

P-wave velocity profiles obtained by the SRT were planned to be used in cavity detection in this study since many literature studies suggest that is a successful method (ASTM, 1999; Thomas and Dobecki, 2006; Sheehan et. al., 2005). In order to detect the accuracy and the efficiency of the method, a particular SRT investigation was carried out at a location where a single relatively large cavity about 2.5 m below the surface was observed in the ground profile (Figure 37). The dimensions of the cavity were 1.25 m x 1.0 m x 0.6 m (width x length x height). A very narrow geophone spacing of 1.0 m, which supplies ahigh resolution measurement up to a depth of 8.0 m, with 12 geophones was adjusted for this purpose. Geophones were Oyo Geospace brand with a natural frequency of 14 Hz and standard coil resistance of 380 ohms. In addition, a rectangular led plate with 20 cm x 20 cm x 3 cm dimensions was fabricated to prevent noise interfering with the seismic record (Figure 37). In conventional commercial seismic applications, most of the time the P-wave velocity records are affected by the sound produced at the time the 6 kg-hammer hits the aluminum plate. However, the use of plate made up of lead, which is a soft metal, prevents the sound that could disturb the P-wave record.

Applying the above mentioned philosophy, SRT measurements were performed made in the particular study area mentioned above. A Geometrics ES-3000 device was utilized during SRT measurements. The system included ESOS data acquisition software and the ES-3000 seismodule was connected directly to a PC via the Ethernet port.

Figure 37. a) A view of a cavity which was attempted with the SRT method. b) The fabricated lead plate used during SRT measurements.

Along the seismic measurement line, P-wave velocities were measured with appropriate gain values that prevented the noise in the records. In order to measure P-wave velocities, a total of 13 shots, 2 of which had 3 m offset from the ends of the line and 11 were placed between geophones, were attempted in a single measurement line with P-wave recording geophones (Figure 38). Such a short 3 m-offset has been preferred during SRT measurements since primary waves could easily dissipate in short distances. All the seismic data were recorded by the PC and later processed by the software SeisImager. After processing seismic raw data by inversion techniques, P-wave contour profiles were obtained for the seismic measurement line as shown in Figures 38 and 39.

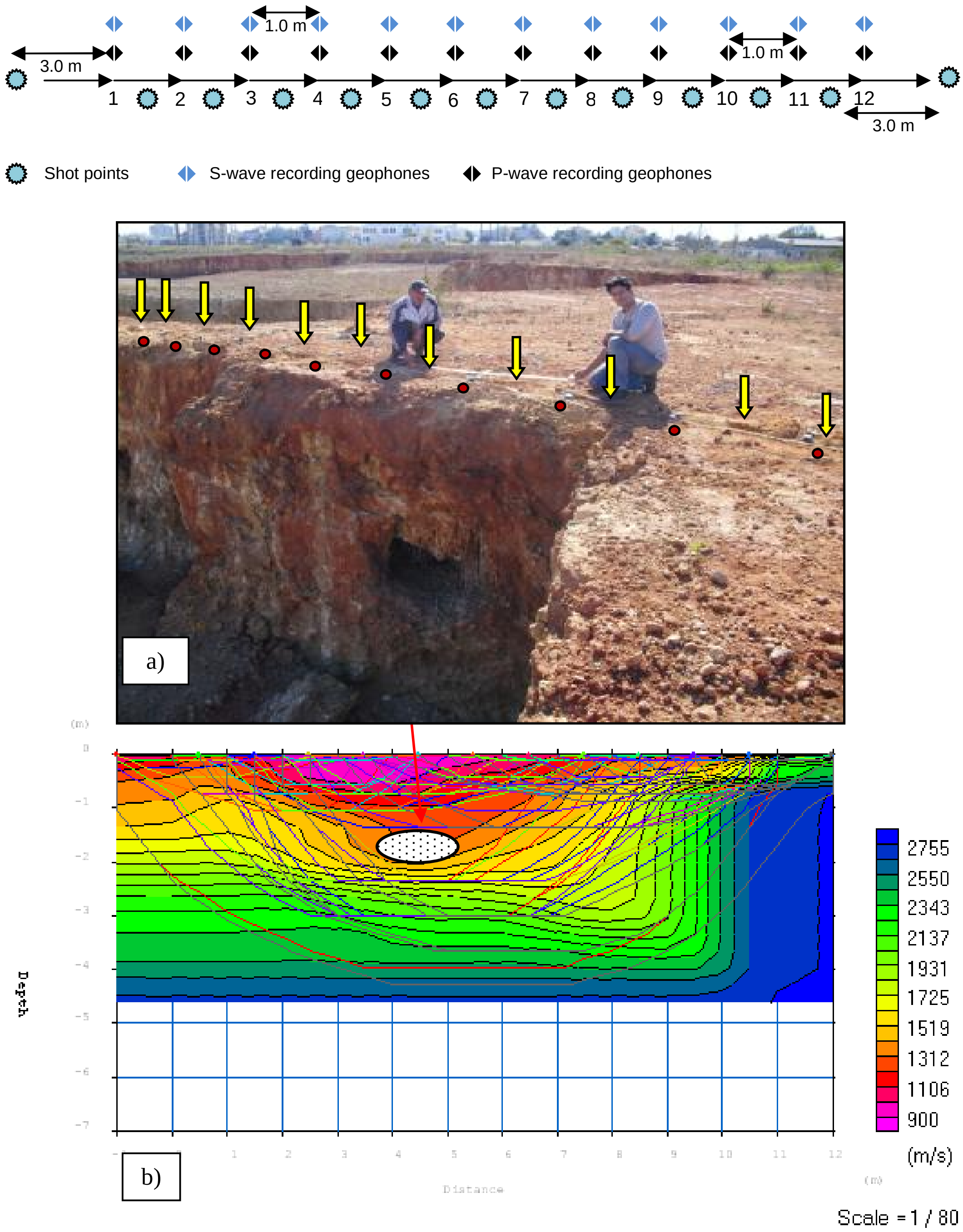

Figure 38. a) Seismic measurement line with S and P geophones and the location of the SRT measurement. b) P-wave profile of the measurement.

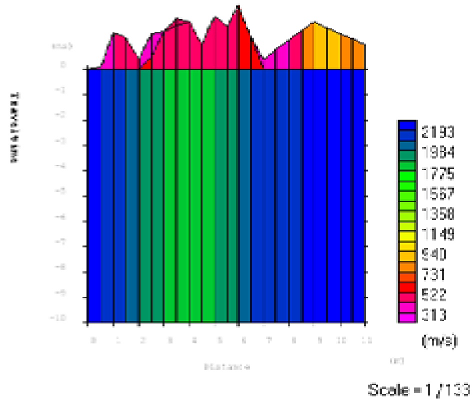

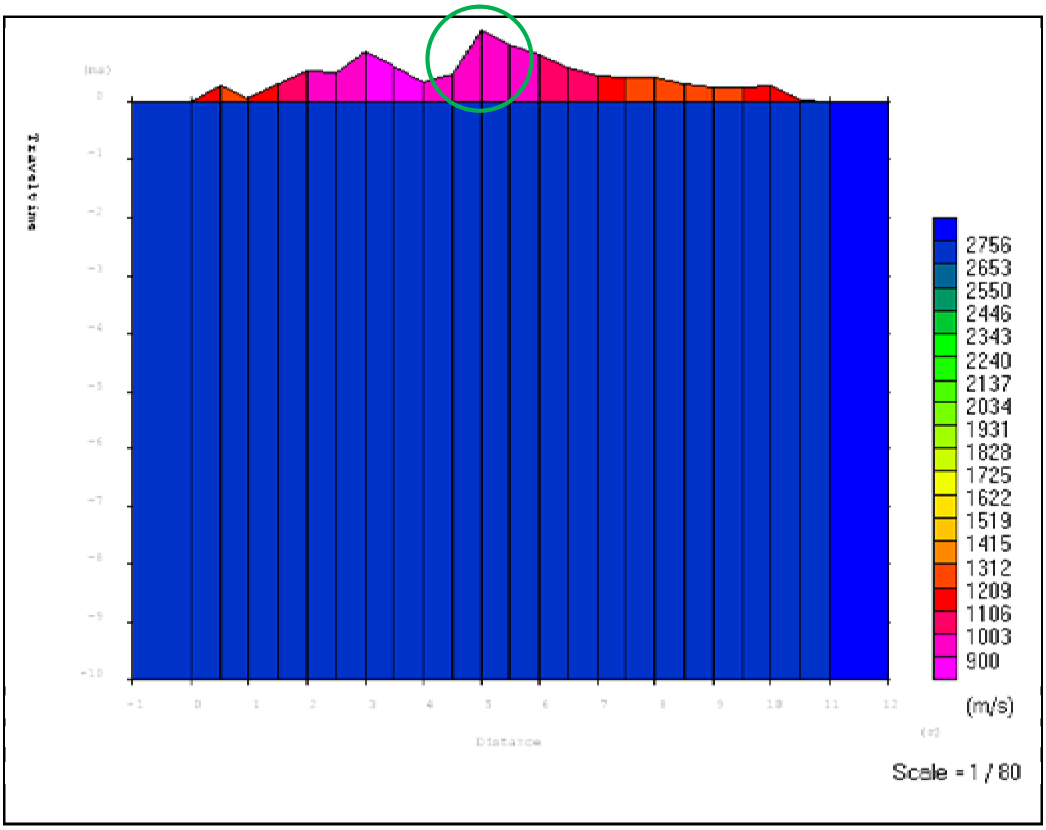

Figure 39. The graph of comparison between the observed and the calculated by inversion techniques travel times. Travel time curve of the measurement.

In the analysis of the seismic data, 1.3 ms and 1.0 ms delays due to cavity were observed at the 5th and 6th geophones, respectively. These were the geophones located just above the cavity. Though this method seems to be successful for detecting such a cavity, it has been realized that the interpretation of the SRT measurements needs very sensitive study especially for the case of smaller cavities which is the most common case in the Antalya region.

In order to support and the cross-check the SRT results, vertical electrical sounding (resistivity measurements) was applied with a Wenner configuration. The resistivity measurements with a Wenner configuration was carried out in three different electrode spacings of 1.0 m, 2.0 m and 3.0 m with a homebuilt device (Figure 40). According to the resistivity measurements, low resistivity values were determined between the 5th and 6th geophones. The cavity location was indicated by these low resistivity values (Figure 41).

Figure 40. The resistivity measuring device utilized during the investigations.

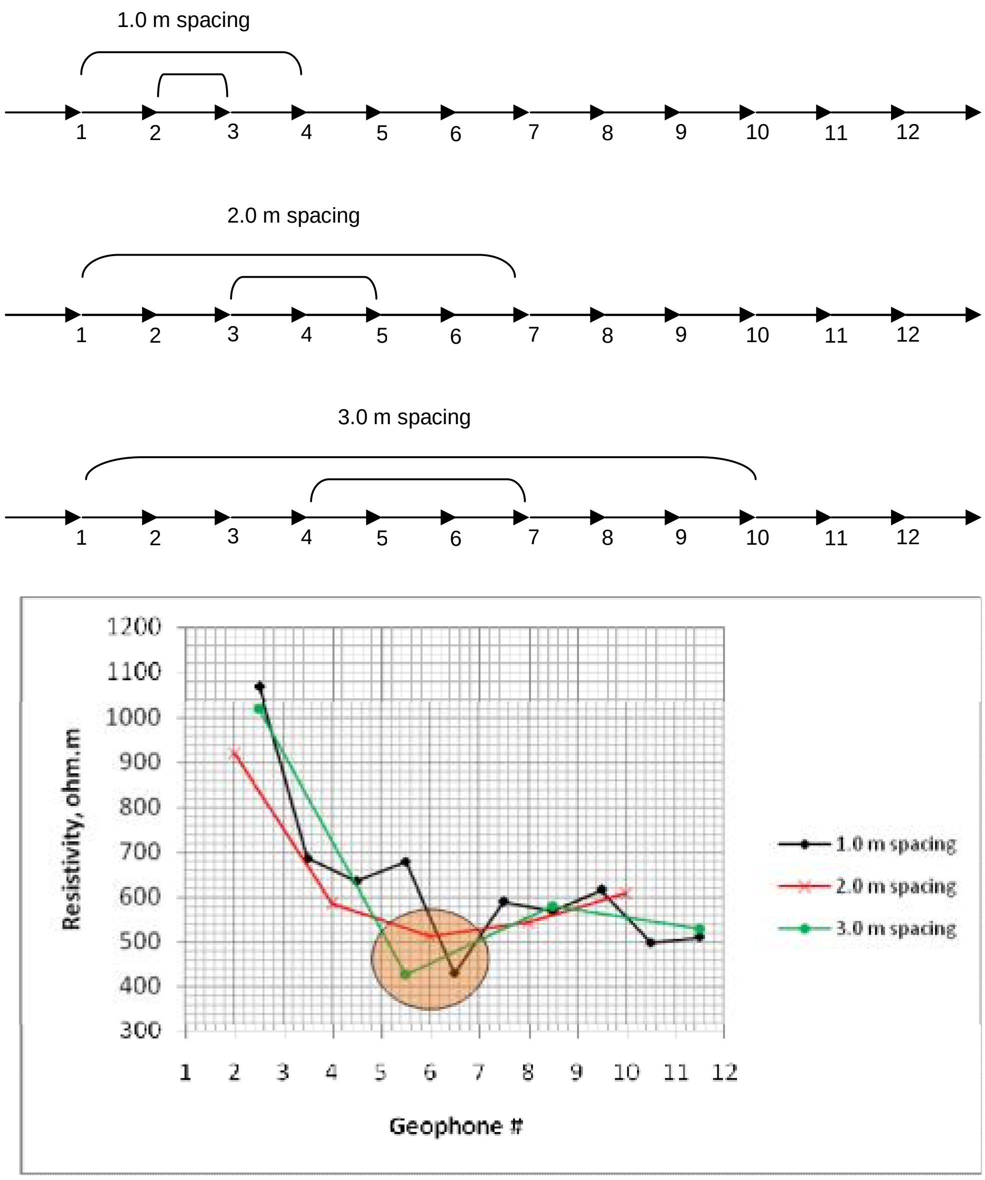

Figure 41. The three different electrode spacing scheme used during resistivity measurements along the same line that was measured by the SRT technique. The lower resistivity values measured between the 5th and 6th geophones coincided with SRT results.

As a conclusion, the results of the seismic and electrical surveys coincided and their results were consistent with the field observations.

Afterwards, approximately 50 SRT measurements were performed in different parts of the study area (Figure 42). In each seismic measurement line, P-wave and S-wave velocities were measured with the appropriate gain values that prevented noise in the records. In order to measure S-wave velocities, all the P-geophones were replaced with S-wave recording ones and 2 shots having 3 m offset from the ends of line were attempted for the same measurement line. In these investigations, in order to explore the deeper ground conditions (approximately 20 m), geophone spacing was adjusted as 3.0 m. The total length of the measurement lines was 36 m.

The seismic wave velocity profiles obtained from the SRT measurements were examined for possible anomalies that could be a sign for underground cavities (Figures 43, 44 and 45). It was observed during site visits that the dimensions of the cavities in the tufa or travertine rock masses showed a wide variation and only large cavities similar to the one in the pilot study could create anomalies which might be identifiable. Upon the identification of possible location of cavities, boreholes would be drilled in order to verify the SRT results.

Figure 42. Photographs taken during an SRT measurement.

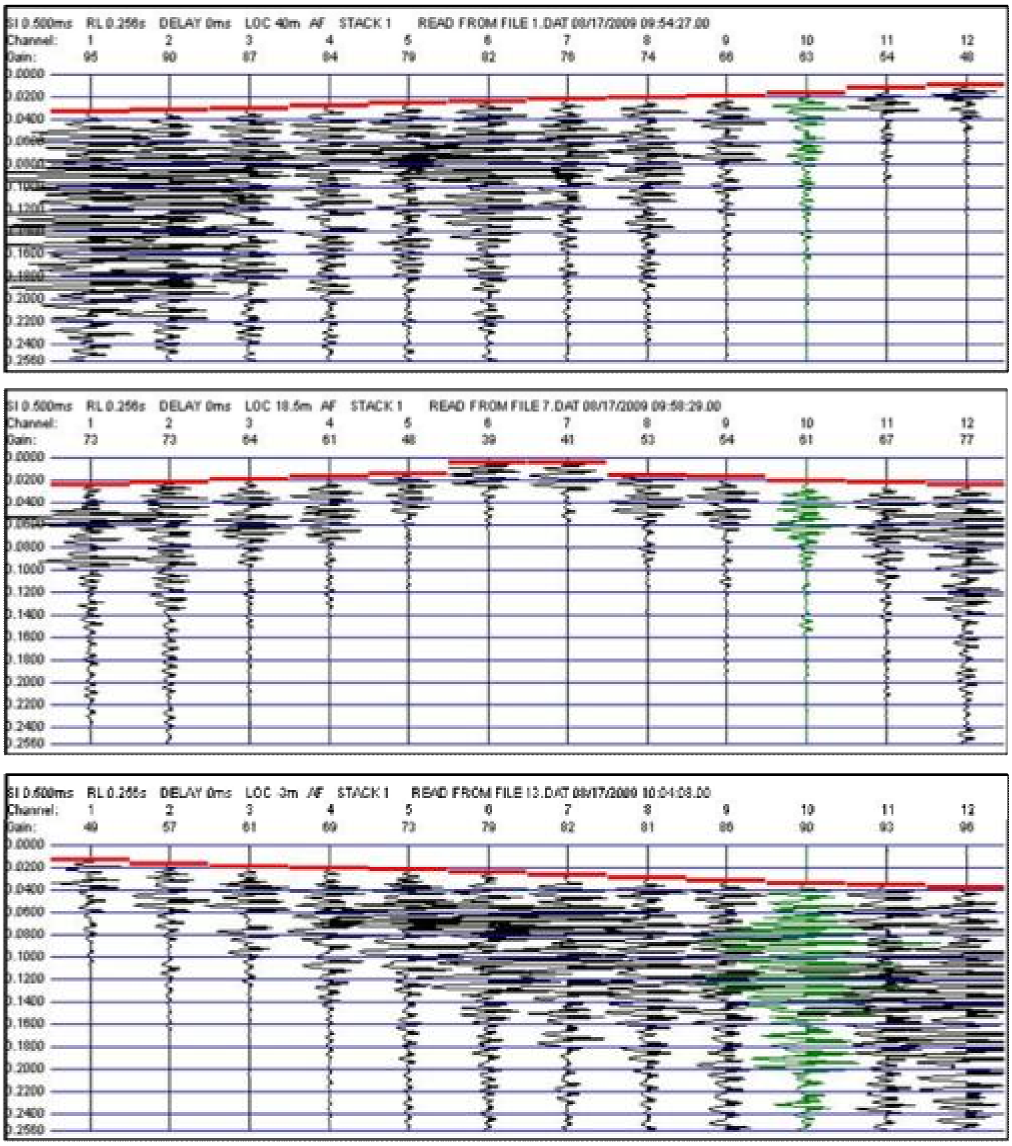

Figure 43. Sample records taken during hammer shots from the SRT studies. Shots at the first, middle and the last geophones are presented, respectively.

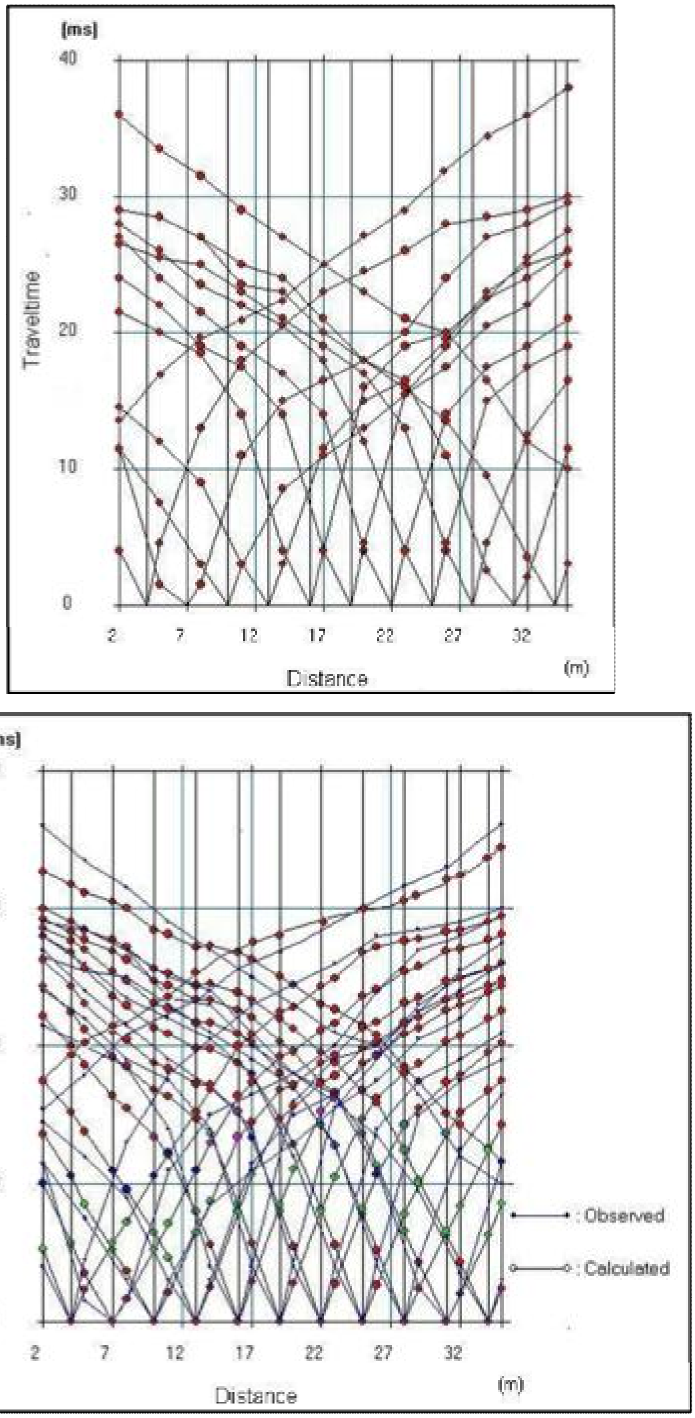

Figure 44. Sample records of travel time-distance graphs from SRT measurements.

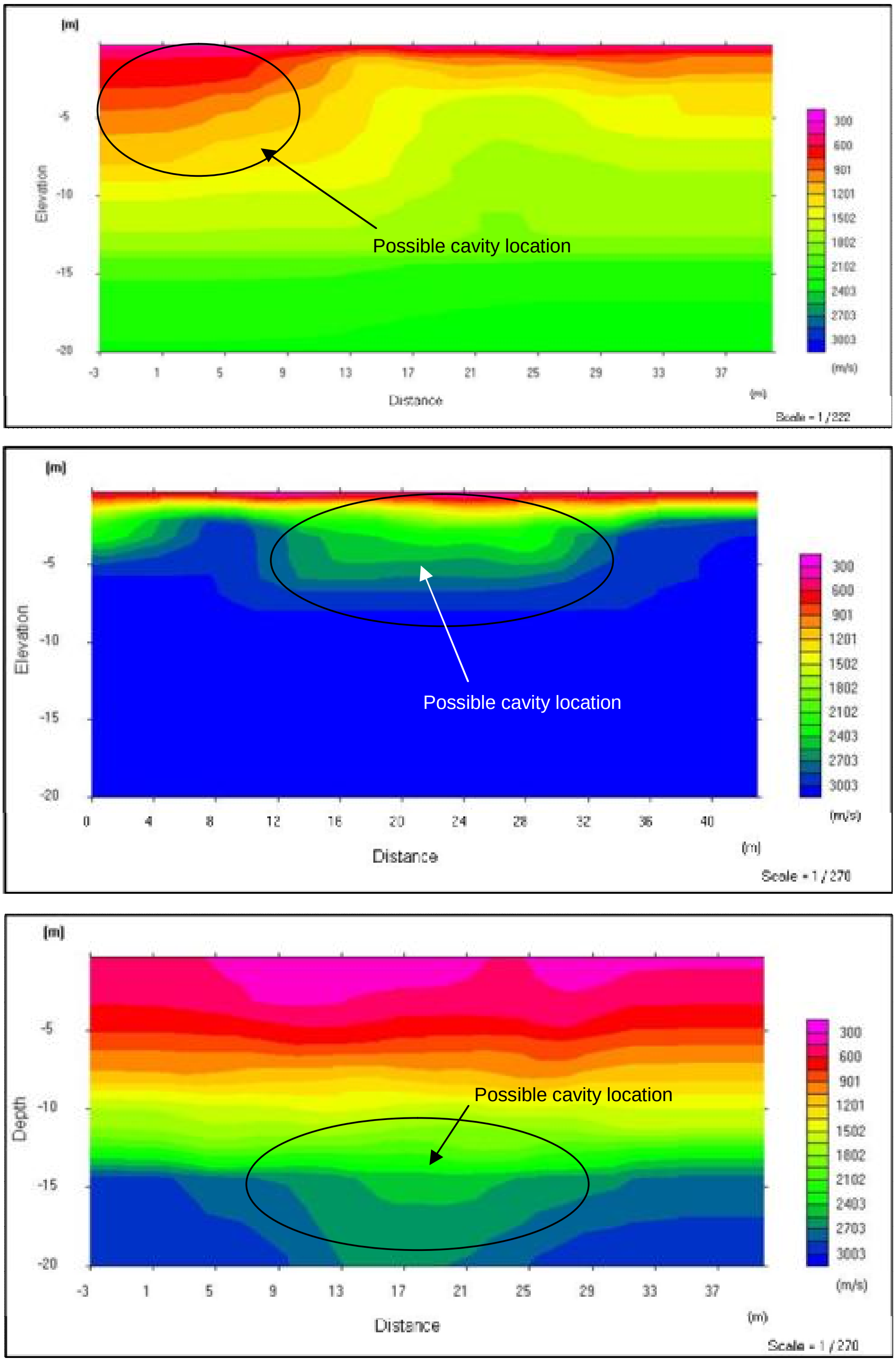

Figure 45. Ground tomographies based on the P-wave velocities measured during an SRT study.

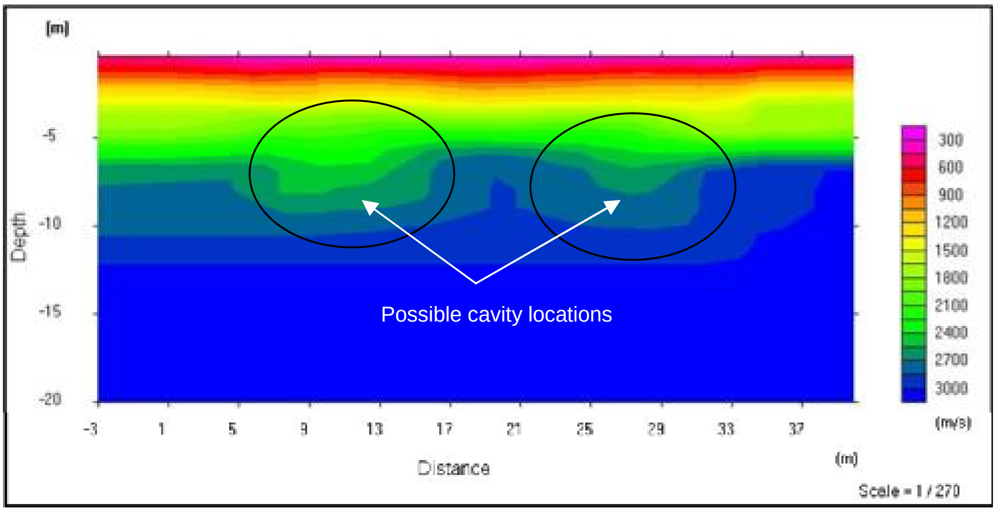

Figure 45 (cont'd.). Ground tomographies based on the P-wave velocities measured during an SRT study.

Five borehole locations with possible cavities were identified after 50 SRT measurements spread out in the study area. Moreover, P-wave and S-wave velocities with the natural period (To) of the tufa deposits together with terra rossa, which is the common weathering product of limestone in karstic landscapes, were recorded (Table 4, Eq. 1).

Table 4. Summary of the results of the SRT measurements.

Type / Parameters	P-wave velocity (m/s)	S-wave velocity (m/s)	To (s)
	Mean ± St.d.	Mean ± St.d.	Mean ± St.d.
Intraclast	1836 ± 496	693 ± 210	0.33 ± 0.09
Phytoclast	1713 ± 612	623 ± 203	0.38 ± 0.11
Porous M.crystalline	2116 ± 758	707 ± 173	0.31 ± 0.08
Phytoherm framestone	2350 ± 443	930 ± 71	0.23 ± 0.02
Terra rossa	878 ± 282	180 ± 56	-
Microcrystalline tufa	2299 ± 437	1234 ± 311	0.21 ± 0.04

$$T_o = 4 \times \left(\frac{h_1}{V_1} + \frac{50-h_1}{V_2}\right) \qquad \text{Eq. (1)}$$

Accordingly, the microcrystalline tufa has the highest S-wave velocity with the lowest ground natural period. On the contrary, the phytoclast tufa has the lowest S-wave velocity with the highest ground natural period.

VII.2.1.2 Vertical Electrical Sounding (VES)

The vertical electrical sounding method was used in locations of seismic refraction tomography in order to compare and verify the SRT results. In case of noisy SRT records, VES measurement could also be a substitute method. This method was used to investigate the vertical variation of earth resistivity, which might be the indication of cavity or groundwater. The Schlumberger method in which, the center of the four electrodes is fixed and the electrode spacing is increased so that the current penetrates progressively deeper, was applied (Figure 46). This method is faster than the Wenner method to apply since two potential electrodes need to be moved. Because the potential electrodes remain in a fixed location, the effects of near-surface lateral variations in resistivity are further reduced. However, both methods produce data of more or less similar quality.

Figure 46. A view of VES applicaion.

The VES measurements were carried out at two points along the same line of the SRT measurements performed at each study location. A homebuilt device was utilized during the VES studies. The measured values at two points along the line were interpolated to obtain a continuous resistivity profile (Figure 47). The Inverse-Distance Anisotropic modeling method, which is one of the "options" of the Inverse-Distance algorithm, was used in the analyses. This kind of directional search can improve the interpolation of voxel values that lie between data point clusters, and can be useful for modeling drill-hole based data in stratiform deposits. This configuration was planned to have the opportunity to compare the results of both geophysical methods.

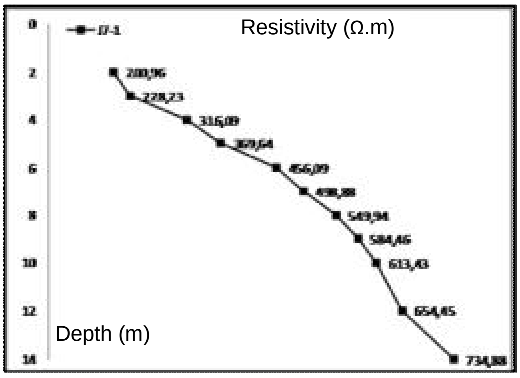

a)

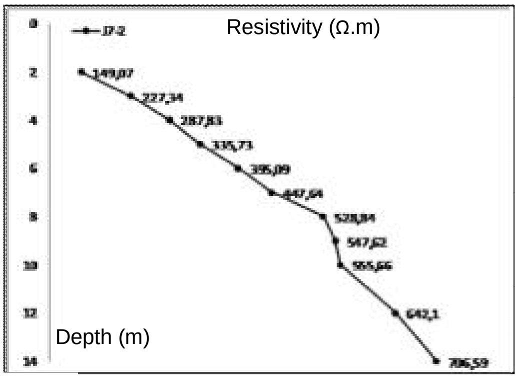

b)

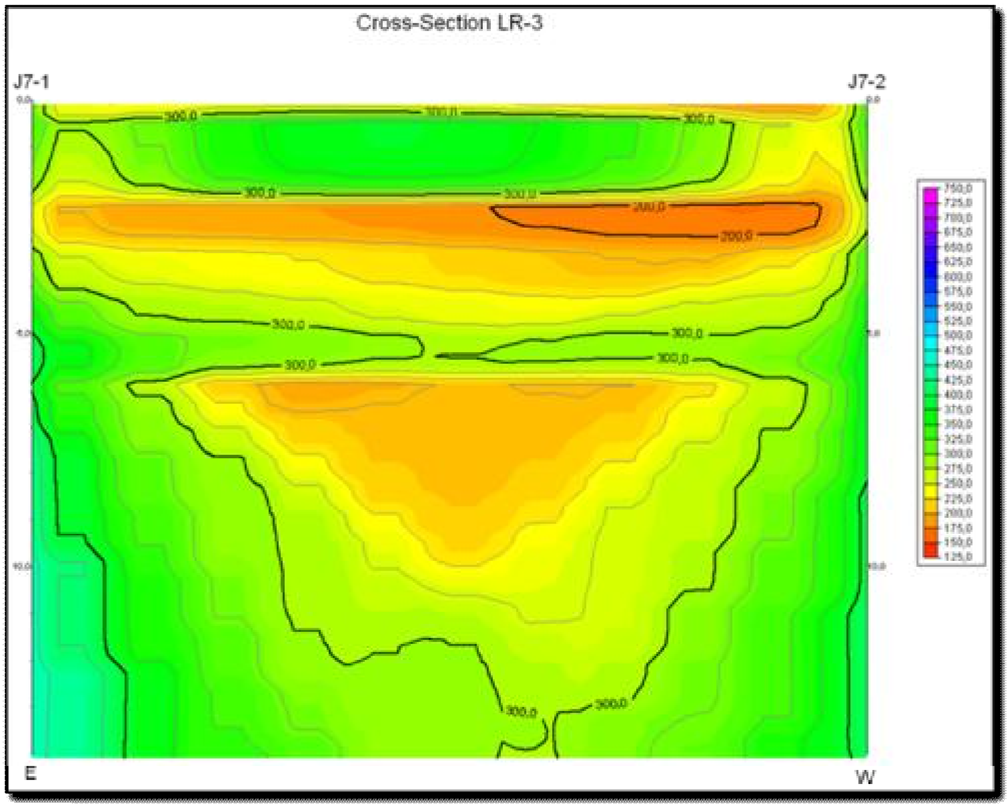

c)

Figure 47. a) Resistivity measurement at the 4th geophone along the line for 14 m depth. b) Resistivity measurement at the 9th geophone along the line for 14 m depth. c) Inverse distance anisotropic model between the 4th and 9th geophones along the line.

VII.2.2 In-situ geotechnical tests

In-situ geotechnical tests carried out in this investigation were borehole pressuremeter tests and plate load tests. A description of these methods and their results are given below.

VII.2.2.1 The pressuremeter tests

The pressuremeter tests were carried out in accordance with ASTM D 4719 – 07 standard during borehole drilling. The aim of conducting the pressuremeter tests was to get geotechnical data for those tufa rock masses that cores could not be obtained and hence, could not be tested in the laboratory due to their fragile texture (Figure 48).

Figure 48. The fragile tufa rock masses which are hard to core in order to obtain representative core samples for laboratory testing.

The pressuremeter tests were carried out with a Menard type APAGEO brand instrument possessing a load maximum load capacity of 80 bar (approximately 80 kgf/cm^2) and a maximum volume change measurement capacity of 800 cm^3. BX size (60 mm) probes were used during testing (Figure 49).

Figure 49. Menard type pressuremeter instrument utilized during testing

The pressuremeter tests were carried out in boreholes drilled in intraclast, phytoclast or phytoherm framestone types of tufa rock masses from which core samples were hardly recovered. Although the phytoherm framestone type mostly has a strong matrix, its porous structure formed irregular cores that prevented the extraction of the rock samples in the form of core samples from the boreholes. The irregular annular faces, resulting frm the irregular cores, tore apart pressuremeter probes in several instances during pressuremeter testing (Figure 50). On the other hand, the intraclast type tufa, which is weaker than most of the other tufa types, in several instances caused the expansion of the walls of the drilled boreholes in which it was not possible to perform pressuremeter testing due to the over enlargement of the boreholes.

a)

b)

c)

Figure 50. a. Pressuremeter probe torn apart by sharp edges of phytoherm framestone. b. Damaged slieve c. Repaired probe.

During the pressuremeter test, after the probe was lowered to the desired depth in the borehole where the test was going to be carried out, a total of two readings per minute (i.e., one reading at every 30 seconds) for each 5 bar increment (or 1 bar increment in case of weaker ground) were taken. These readings physically represent the volumetric change of the probe inside the borehole. Accordingly, two measurements for each pressure increment were taken. In case the two readouts for the same pressure increment were so close within a precision of 0.01, it was assumed that the probe provided full contact with the sidewalls of the borehole and that the next measurements after that point gave information directly related to the stress-strain relationship of the tufa rock mass.

The measured and corrected volume changes were plotted against the corrected applied pressures during pressuremeter tests. Figure 51 illustrates an example of volume versus pressure graphs for one of these tests performed in the rather weak types of the tufa rock mass (i.e., the intraclast and phytoherm framestone tufa types).

Table 5 gives the results of the entire pressuremeter tests performed in the rather weak types of the tufa rock mass (i.e., the intraclast and phytoherm framestone tufa types). The mean and the standard deviation of the Elasticity modulus for intraclast and phytoherm framestone types were calculated as 42.7 MPa ± 39.6 and 43.6 MPa ± 43.3, respectively.

In order to determine the limit pressure and the related net limit pressure along with the deformation modulus, double hyberbolic curve plots have also been drawn particularly for the pressuremeter tests at which the pressure in the probe was not sufficient to break the rock in the borehole (ISO, 2008). The results of the pressuremeter tests through double hyperbolic curve ploting are given in Table 6. The mean and the standard deviation of the Elasticity modulus for phytoherm framestone and intraclast tufa types were calculated as 105 MPa ± 121 and 181 MPa ± 148, respectively. This conflicting relationship is attributed to the variable nature of the Antalya karstic rock mass.

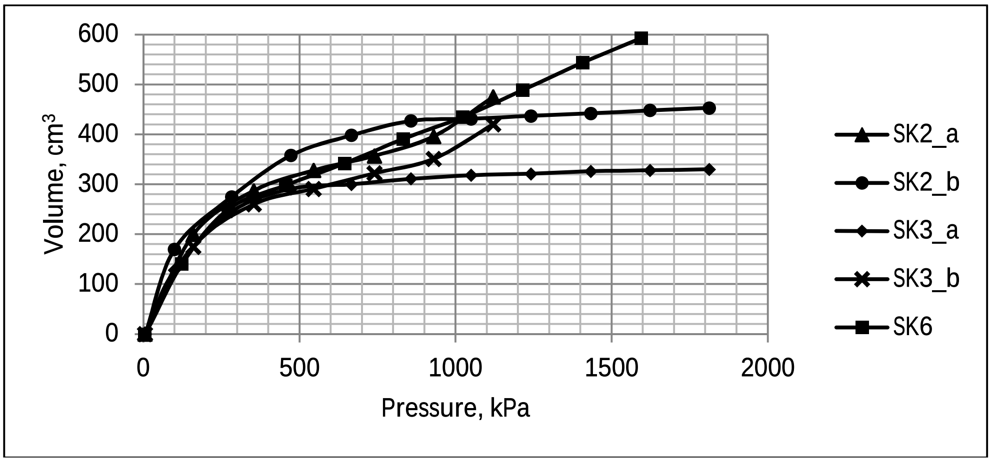

a)

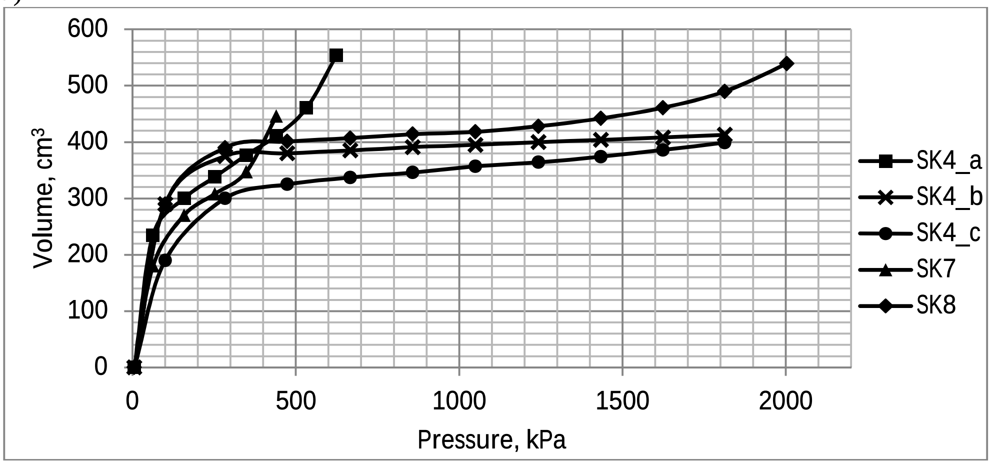

b)

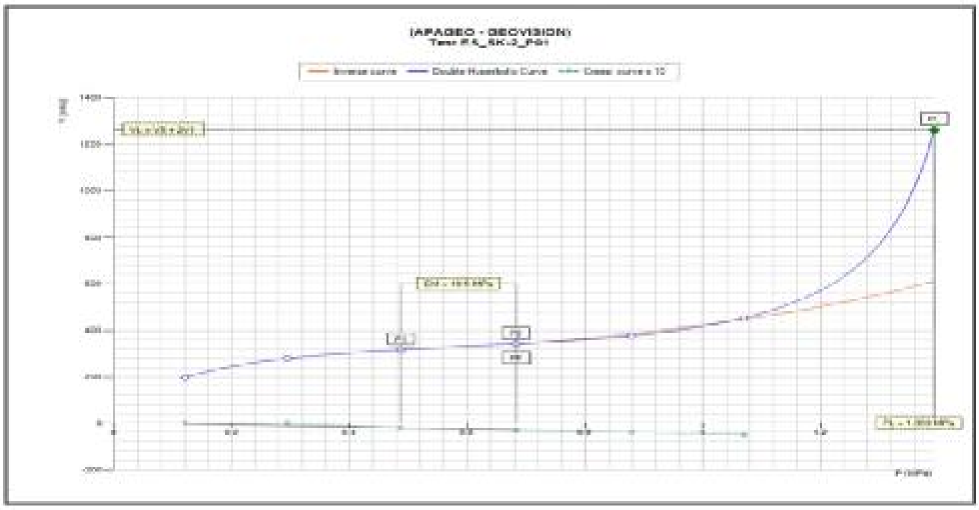

c)

Figure 51. Graphs of pressuremeter test results. a) phytoherm framestone tufa type b) intraclast tufa type c) sample result for double hyperbolic curve plotting.

Table 5. Results of pressuremeter tests on intraclast and phytoherm framestone tufa types.

Borehole	Depth (m)	Lithology	PL (kPa)	PLn (kPa)	E (MPa)
SK-4	2.50	Intraclast tufa	785	627	5.70
SK-4	10.0	Intraclast tufa	≥ 2000	≥ 2000	99.5
SK-4	13.0	Intraclast tufa	≥ 2000	≥ 2000	43.2
SK-7	8.00	Intraclast tufa	588	431	5.54
SK-8	1.50	Intraclast tufa	2452	1978	59.6
SK-2	3.50	Phytoherm framestone	1569	1215	12.3
SK-2	9.50	Phytoherm framestone	≥ 2000	≥ 2000	95.3
SK-3	2.50	Phytoherm framestone	≥ 2000	≥ 2000	86.4
SK-3	6.00	Phytoherm framestone	1765	1411	14.2
SK-6	1.50	Phytoherm framestone	2059	1603	98.4
SK-5	4.50	Soil	687	529	7.94
Mean ± Standard deviation:					
Intraclast type			1565 ± 826	1407 ± 805	42.7 ± 39.6
Phytoherm framestone type			1878 ± 207	1646 ± 351	43.6 ± 43.3

Table 6. Results of pressuremeter tests on intraclast and phytoherm framestone tufa types via double hyperbolic curve plotting method.

Borehole	Depth (m)	Lithology	PL (kPa)	PLn (kPa)	E (MPa)
SK-4	2.50	Intraclast tufa	620	6000	7.00
SK-4	10.0	Intraclast tufa	1940	1850	329
SK-4	13.0	Intraclast tufa	1970	1860	329
SK-7	8.00	Intraclast tufa	630	560	6,30
SK-8	1.50	Intraclast tufa	2570	2560	231,8
SK-2	3.50	Phytoherm framestone	1390	1360	19,5
SK-2	9.50	Phytoherm framestone	1890	1800	240
SK-3	2.50	Phytoherm framestone	1880	1860	234
SK-3	6.00	Phytoherm framestone	1100	1050	17,7
SK-6	1.50	Phytoherm framestone	1640	1630	11.4
SK-5	4.50	Soil	510	470	11,7
Mean ± Standard deviation:					
Intraclast type			1546 ± 889	1486 ± 898	181 ± 148
Phytoherm framestone type			1580 ± 338	1540 ± 336	105 ± 121

According to the pressuremeter test results, it could be concluded that phytoherm framestone and intraclast tufa types have similar bearing capacity. However, intraclast tufa has been observed to have higher deformation modulus values according to the results of the double hyperbolic curve plotting method.

VII.2.2.2 The plate load test

Plate load tests were carried out in accordance with the ASTM D 1196 – 93 standard. The purpose of applying plate load test was to get additional geotechnical data such as deformation modulus, particularly for the intraclast type tufa, which was hard to sample.

Plate load tests were carried out using a truck (possessing a weight of 16 tonnes) or a JCB back-hoe loader (possessing a weight of 8 tonnes) as a loading device, hydraulic jack assembly, bearing plates with diameters of 300 mm and 762 mm, respectively, three dial gages and a deflection beam (Figure 52). During testing, the plate was unloaded between the two cycles of loading. The settlement values of the ground just below the plate were measured by three dial gages for each incremental load. Three dial gages were placed on the deflection beam in an equilateral triangle arrangement where each gage was located at the corners of the equilateral triangle. Then, the load on the plates was increased with 5 bar increments up to 30 bars. Following the loading cycle, the unloading cycle was carried out in a similar manner and the settlement readings were taken at 20 bars, 10 bars and 5 bars, respectively. The last settlement record at the time of zero load illustrated whether the ground swelled or not. The unloading cycle was followed by the second loading cycle with the same pressure increments. During all of the loading cycles, the settlement records were taken at the instant where all three gages showed constant (i.e., minimum fluctuating) values.

Figure 52. Views of plate load tests performed with 300 mm and 762 mm diameter plates.

The modulus of deformation has been calculated from both the first and the second loading cycles. It has been determined from the loading cycle, as the inclination of the secant line between two points given by the value of the 0.3- and 0.7-multiple of the maximum load, using the Eq. (2).

$$E_v = 1.5 \cdot r \cdot \frac{\Delta\sigma}{\Delta s} \qquad \text{Eq. (2)}$$

where,

E_v is static modulus of deformation (MPa),

r is load plate radius, i.e., 0.15 (m),

$\Delta\sigma$ is difference in the value of the 0.3- and 0.7-multiple of the maximum load (MPa),

Δs *is* difference in the load plate insertion between the value of the 0.3- and 0.7-multiple of the maximum load (m)

Plate load tests were carried out on four tufa types, namely, intraclast, phytoclast, microcrystalline and phytoherm framestone. Furthermore, some measurements were also taken for terra-rossa, which is a type of red-clay-soil produced by the weathering of the karstic rock masses.

Table 7 gives the results of the plate load tests. The mean and the standard deviation of the deformation modulus for the first and second loading cycles for each type are also given in Table 7. Figures 53 and 54 give plots of the plate load tests.

Plate load tests marked with an asterix in Table 7 have been excluded during the calculations of average and standard deviation values since they have been evaluated as outlier values as compared to rest of the data.

The modulus of deformation values obtained from plate load tests by using 300 mm plate have been observed to be 1.5 to 3.0 times higher than the values obtained from plate load tests by using 762 mm plate. Hence the scale effect led to a factor of 1.5 to 3.0 for the different diameter tests.This result has shown that appropriate plate sizes should be utilized during plate load tests for the purpose of an engineering design.

Table 7. Results of the plate load tests

PLT No.	Lithology	E_{S1} (MPa)	E_{S2} (MPa)	E_{s2}/E_{s1}	Subgrade modulus $1000*t/m^3$
PLT-1	Intraclast tufa	78.8	116	1.47	24.6
PLT-2	Intraclast tufa	31.5	170	5.38	10.6
PLT-6	Intraclast tufa	71.1	110	1.55	14.1
PLT-8	Intraclast tufa	32.0	78.8	2.46	11.8
PLT-10*	Intraclast tufa	290	630	2.17	103
PLT-11*	Intraclast tufa	71.1	441	6.20	27.3
PLT-23	Intraclast tufa	50.1	91.9	1.83	14.6
PLT-27	Intraclast tufa	49.0	78.8	1.61	20.6
PLT 28	Intraclast tufa	81.2	122	1.50	18.9
PLT 29	Intraclast tufa	82.4	130	1.58	11.0
PLT 30	Intraclast tufa	37.3	43.1	1.16	5.23
PLT 31	Intraclast tufa	20.0	23.3	1.17	4.53
PLT 32	Intraclast tufa	20.0	25.5	1.28	3.70
PLT 33	Intraclast tufa	29.5	35.0	1.19	5.52
PLT 34	Intraclast tufa	25.5	29.5	1.16	5.07
Mean ± Standard deviation		**46.8 ± 23.8**	**81.0 ± 47**		**11.6 ± 6.8**
PLT-12	Microcrystalline tufa	98.4	459	4.67	53.4
PLT-13	Microcrystalline tufa	162	339	2.09	53.8
PLT-14	Microcrystalline tufa	408	286	0.70	199
PLT-16	Microcrystalline tufa	71.1	276	3.88	29.3
PLT-17	Microcrystalline tufa	137	882	6.44	58.6
PLT-20*	Microcrystalline tufa	1131	1460	1.29	503
Mean ± Standard deviation		**175 ± 135**	**449 ± 253**		**78.8 ± 68.2**
PLT 35	Phytoclast tufa	102	140	1.38	14.7
PLT 36	Phytoclast tufa	90.3	98.3	1.09	17.1
PLT 37	Phytoclast tufa	77.8	80.0	1.03	14.9
Mean ± Standard deviation		**90 ± 12**	**106 ± 30.8**		**15.6 ± 1.31**
PLT-3	Phytoherm framestone	27.6	170	6.15	11.1
PLT-9	Phytoherm framestone	63.0	116	1.84	24.7
PLT-19	Phytoherm framestone	91.5	479	5.24	31.6
Mean ± Standard deviation		**60.7 ± 32.0**	**255 ± 196**		**22.5 ± 10.4**
PLT-18	Terra-rossa	22.1	73.5	3.33	6.78
PLT-22	Terra-rossa	88.9	88.6	1.00	34.2
PLT-24	Terra-rossa	121	134	1.11	37.7
PLT-26	Terra-rossa	43.2	63.9	1.48	18.8
Mean ± Standard deviation		**68.8 ± 44.7**	**90.1 ± 31.3**		**24.4 ± 14.3**

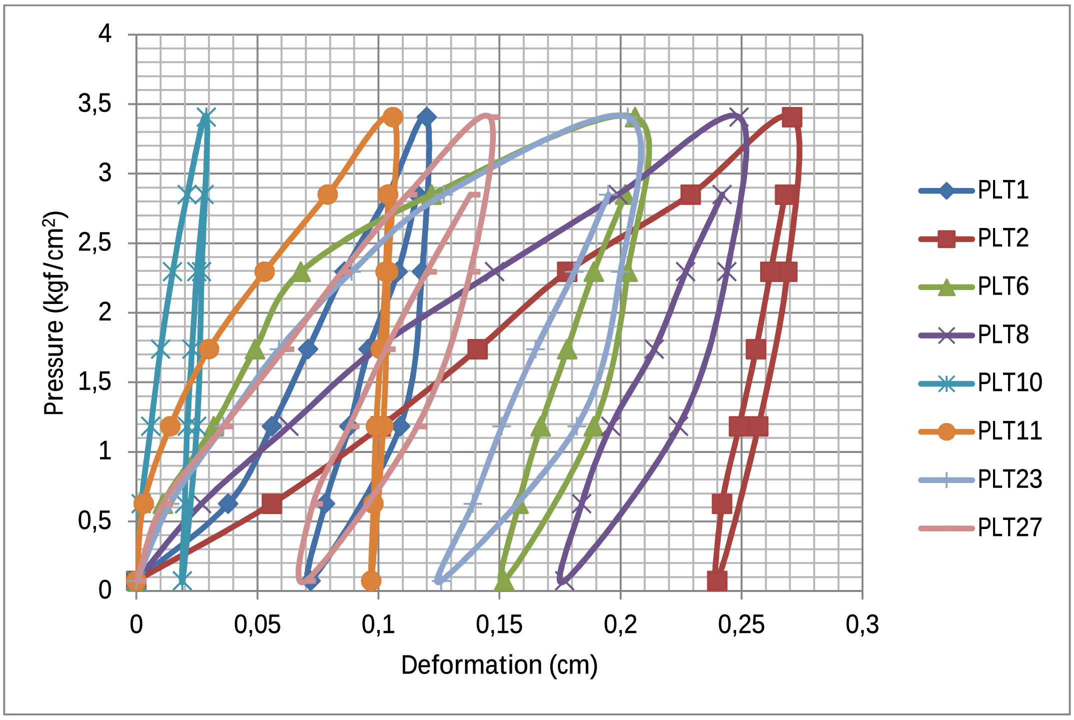

a)

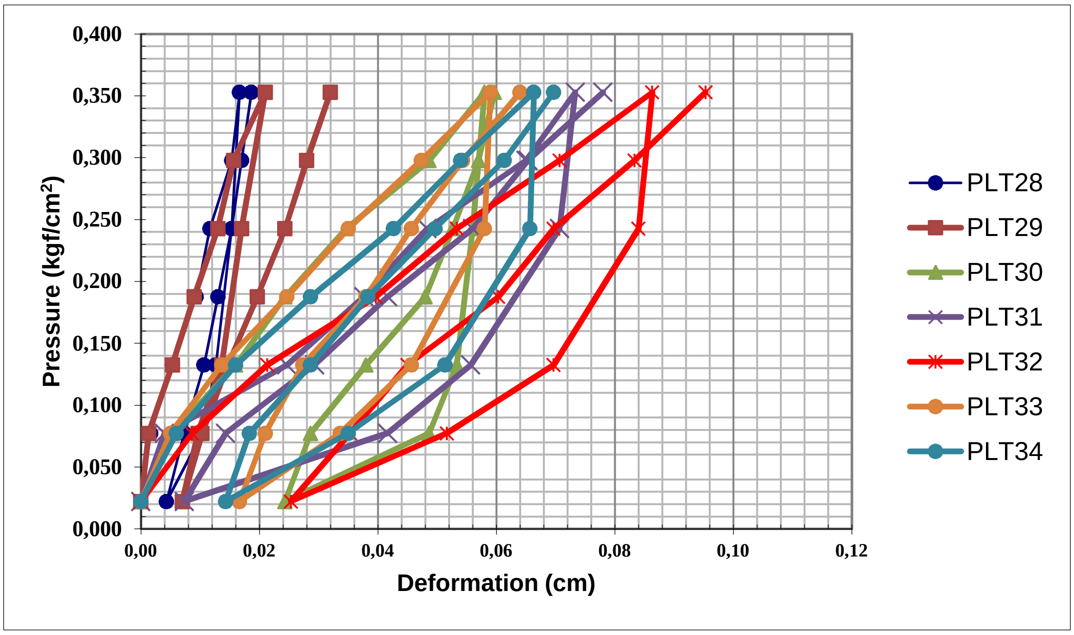

b)

Figure 53. Graphs of plate load test for Intraclast type tufa. a) 300 mm diameter plate b) 762 mm diameter plate.

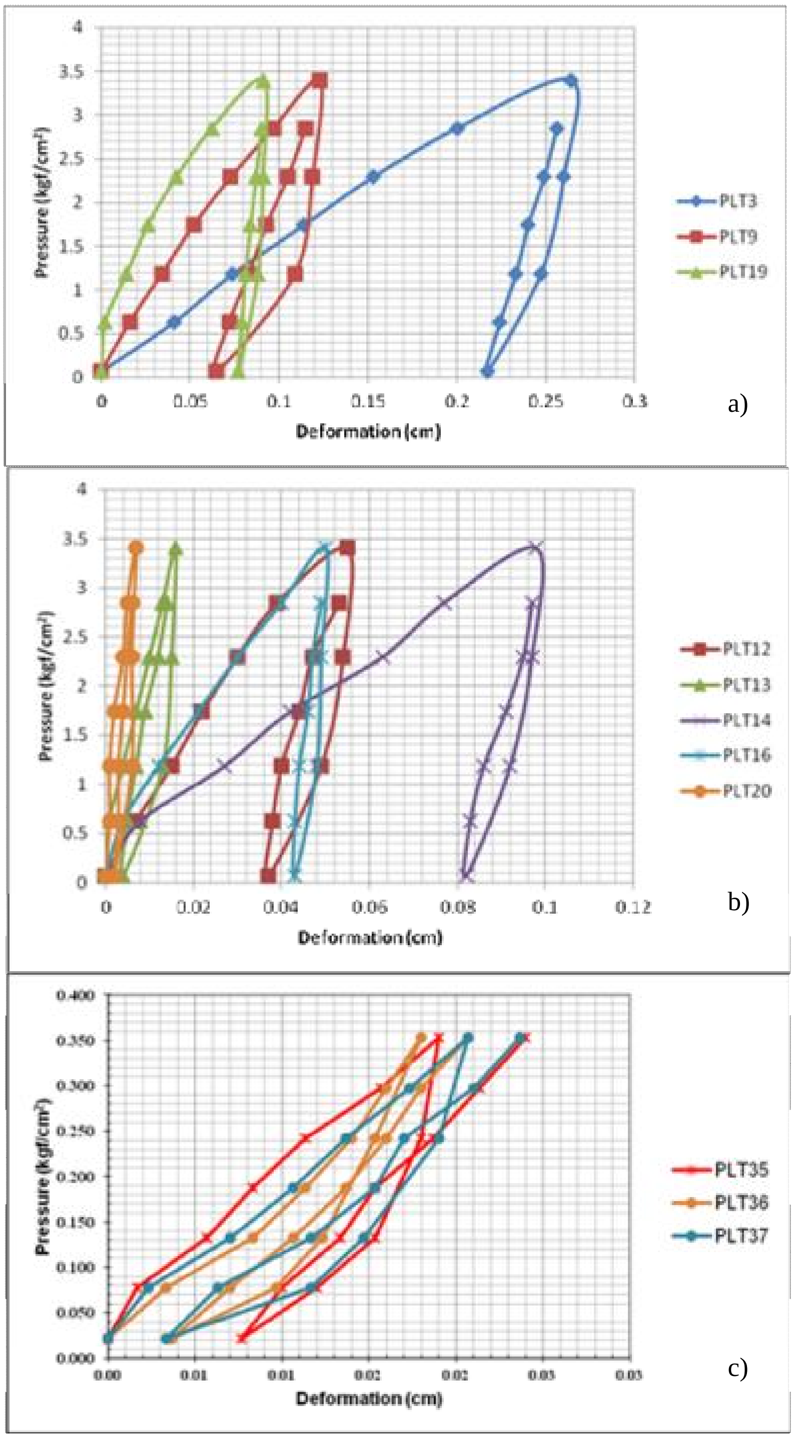

Figure 54. Graphs of plate load tests. a) Phytoherm framestone type. b) Microcrystalline type c) Phytoclast type (plate diameter is 762 mm for all tests)

The deformation modulus values calculated from pressuremeter tests and plate load tests have common intervals due to large standard deviations. Deformation modulus values calculated for intraclast tufa have been determined as 181 MPa ± 148 and 81.0 MPa ± 47 from pressuremeter and plate load tests, respectively. Similarly, deformation modulus values calculated for phytoherm framestone have been determined as 105 MPa ± 121 and 255 MPa ± 196 from pressuremeter and plate load tests, respectively.

VII.2.3 Laboratory tests

Laboratory tests carried out during this dissertation study can be grouped broadly into three categories as:

- *petrographical* or the *mineralogical* analyses; which included thin section examination via microscope, LOI, SEM, EDS, DTA and TGA studies,
- *geophysical* tests, namely, ultrasonic velocity measurement, and
- *geomechanics* tests covering uniaxial compressive strength (UCS) test, triaxial test, point load strength index test, Brazilian indirect tensile strength test, slake durability test, porosity and unit weight determination test.

Numerous samples were collected from the field for subjecting the samples to the above mentioned laboratory tests. Table 8 summarizes the number of samples from each tufa rock type that were subjected to laboratory testing.

Table 8. The number and type of laboratory tests carried out in this study.

Test type / Tufa type	Quantity					**Total**
	Microcrsytalline tufa	Phytoherm framestone	Phytoherm boundstone	Phytoclast tufa	Intraclast tufa	
Porosity and unit weight determination	37	36	32	47	4	**156**
Loss on ignition	5	5	5	5	5	**25**
Uniaxial compressive strength test	10	7	13	7	3	**40**
Triaxial test	6	5	5	3	0	**19**
Brazilian indirect tensile strength test	11	9	13	14	0	**47**
Slake durability test	5	8	8	10	3	**34**
Point load strength index test	13	14	13	12	0	**52**
Ultrasonic velocity measurement	37	36	32	47	4	**156**
Total	**124**	**120**	**121**	**145**	**19**	**529**

VII.2.3.1 Petrographical and mineralogical analyses

VII.2.3.1.1 Thin section examination

Thin section examinations of the Antalya tufa rock mass have been carried out at mineralogy laboratory of the Department of Geological Engineering at METU by a Nikon Eclipse E200 microscope. In the following paragraphs, photographs of the thin section and their explanations are presented.

In the microcrystalline sample (Figure 55), the coarse and micritic crystals have been observed to be uniformly distributed. Some porous structures have also been noticed. It has been interpreted that the smoky appearance might be due to existence of clay mineral. The presence of the black colored opaque mineral has been interpreted as organic matter content.

In phytoherm framestone sample (Figure 56), hollow circles which are common for staglagmite-stalactites have been observed where the hollow circles were observed to be filled with sparry and micritic calcite crystals. Brown iron oxide together with clay filtered through soil horizons may also fill these pores. Lesivage or clay migration may be observed.

In the phytoherm framestone sample (Figure 57), concentric calcite and clay depositions around pore spaces have been observed to be quite common. Organic matter or lesivage structures were almost non-existent. Calcite deposition has been observed in the alternation form of coarse and micritic crystals. Coarse calcite crystals have been mostly observed within the inner sides of the pore spaces while micritic crystals were close to the outer rims.

In the phytoherm boundstone sample (Figure 58), homogeneously distributed micritic calcite crystals with some irregular small pore spaces have been observed. Numerous black opage minerals or organic matter have been observed as impurities.
In the other microcrystalline sample (Figure 59), some structures related to dissolution and re-deposition have been observed. Brown colored iron oxide has been observed to be intruding the calcite crystals and abundant finer calcite crystals as compared to the other samples have been observed. Due to abundance of the fine crystals, more a compact structure has been noticed.

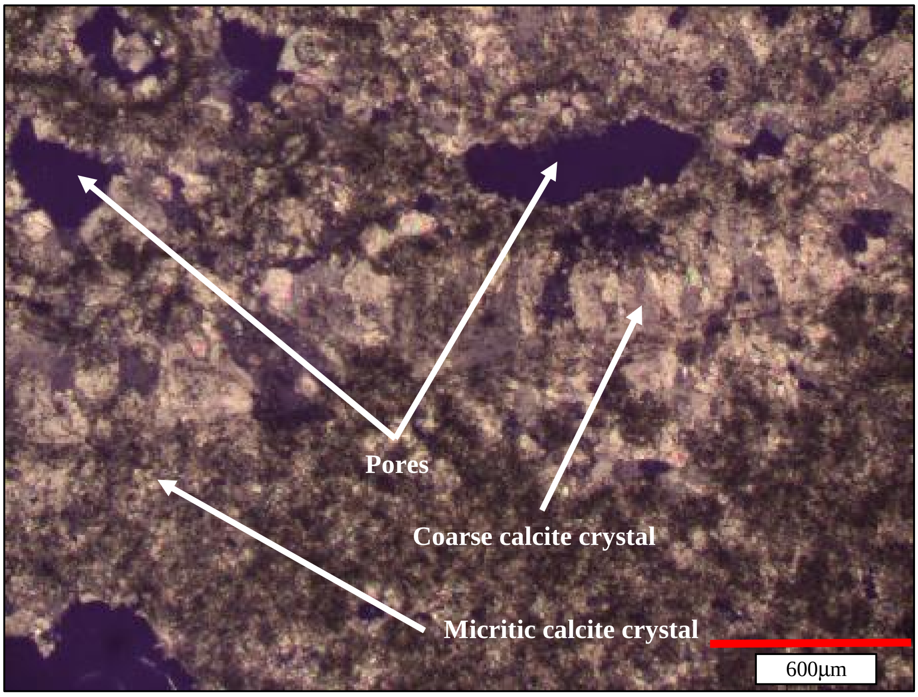

Analyzer in 4X view

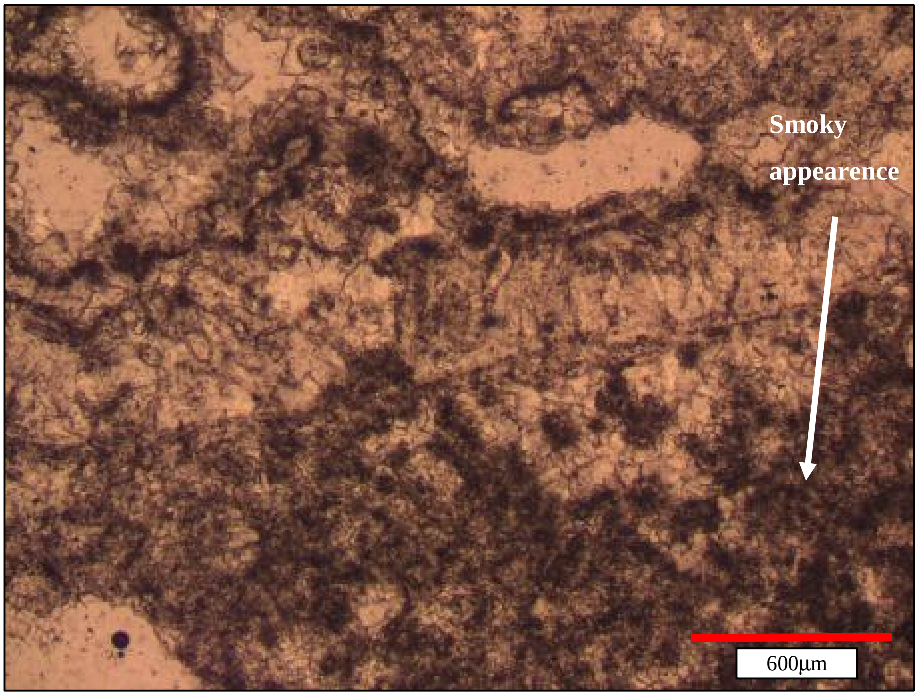

Analyzer out 4X view

Figure 55. Thin section photographs of the microcrystalline sample.

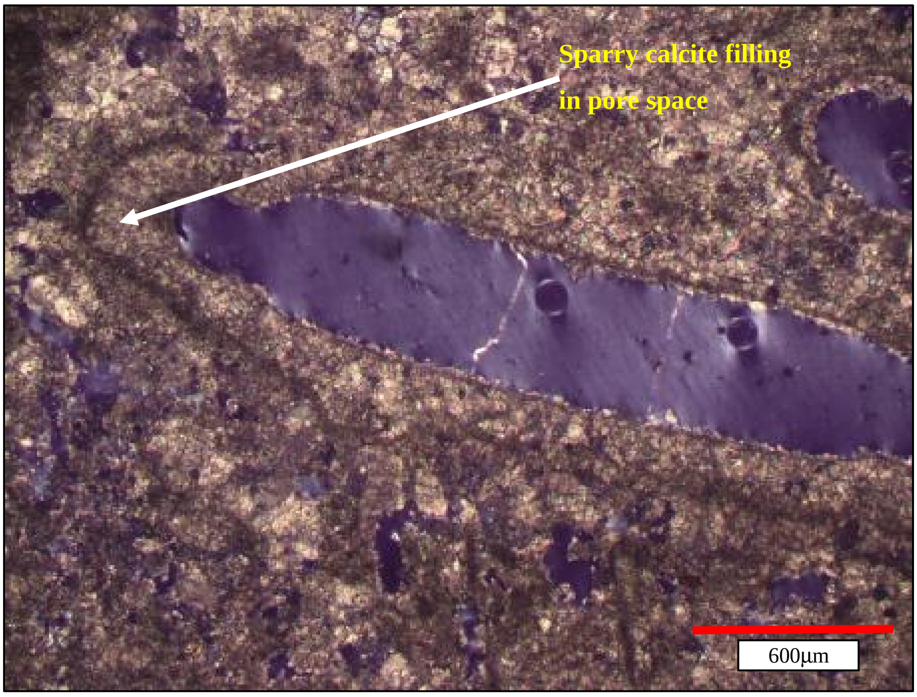

Analyzer in view

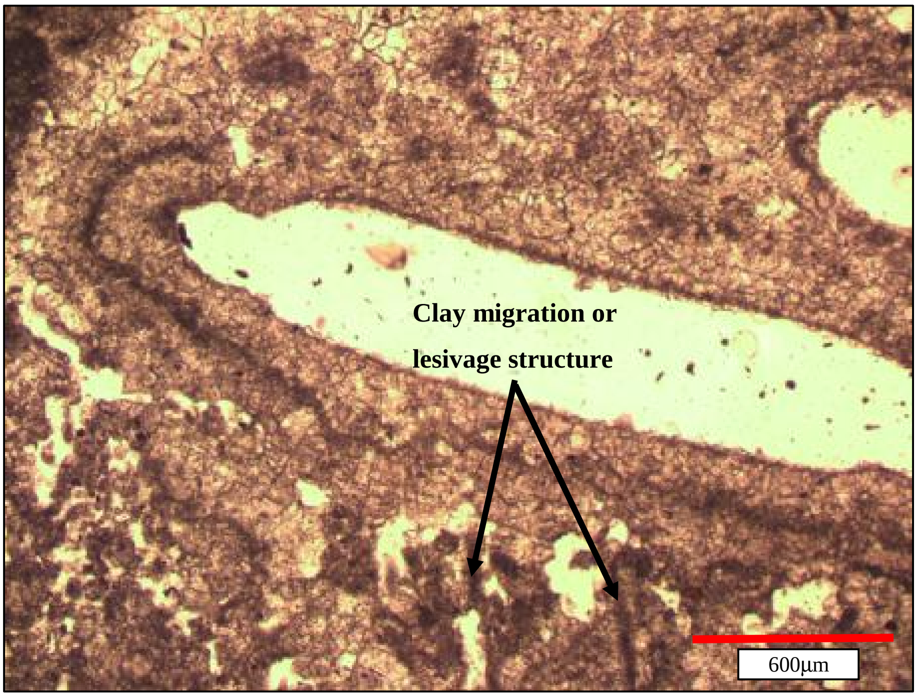

Analyzer out view

Figure 56. Thin section photographs of phytoherm framestone sample.

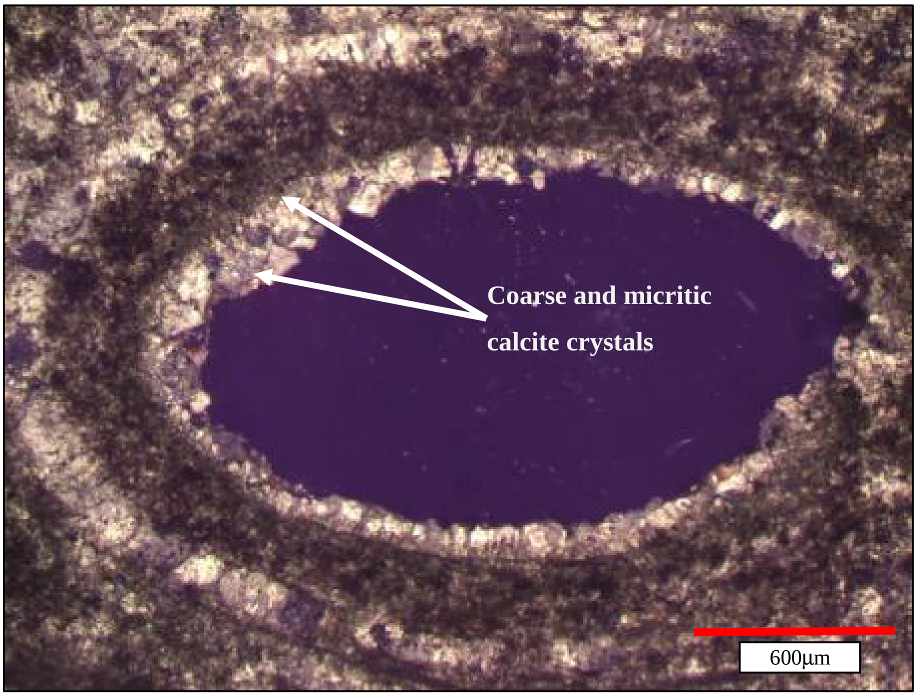

Analyzer in view

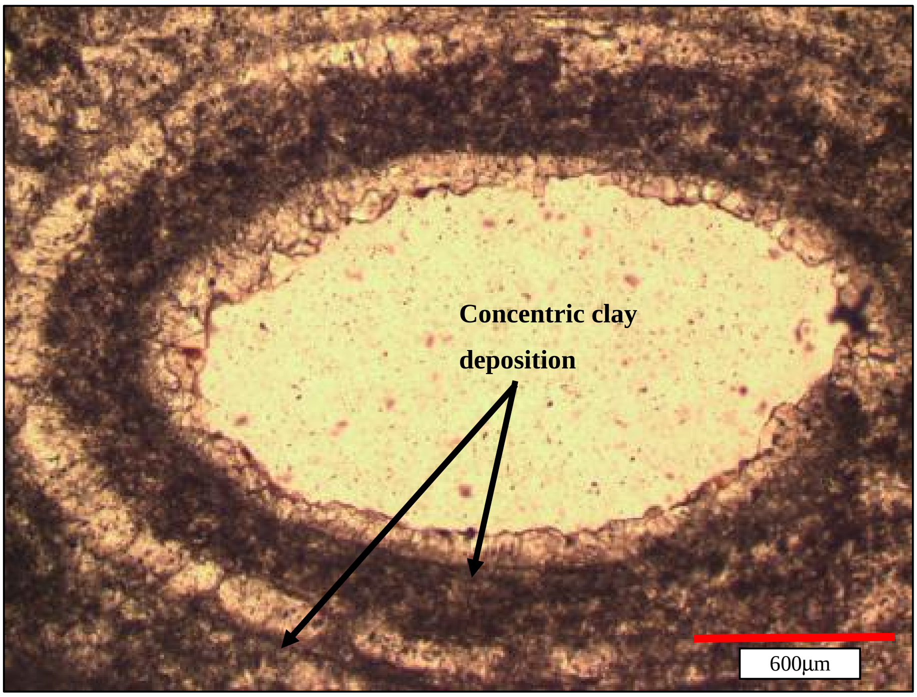

Analyzer out view

Figure 57. Thin section photographs of other phytoherm framestone sample.

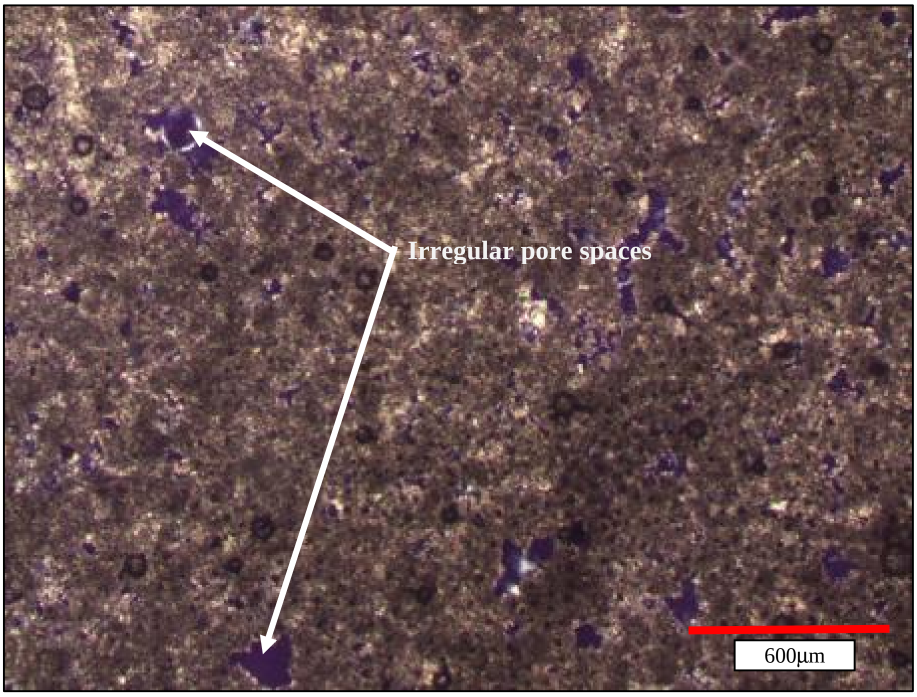

Analyzer in view

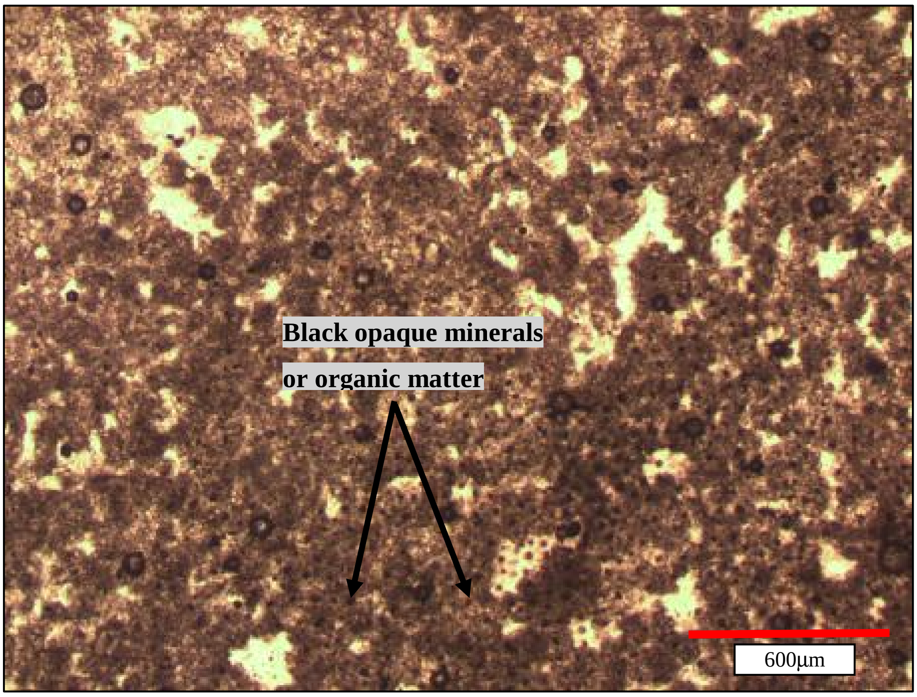

Analyzer out view

Figure 58. Thin section photographs of phytoherm boundstone sample.

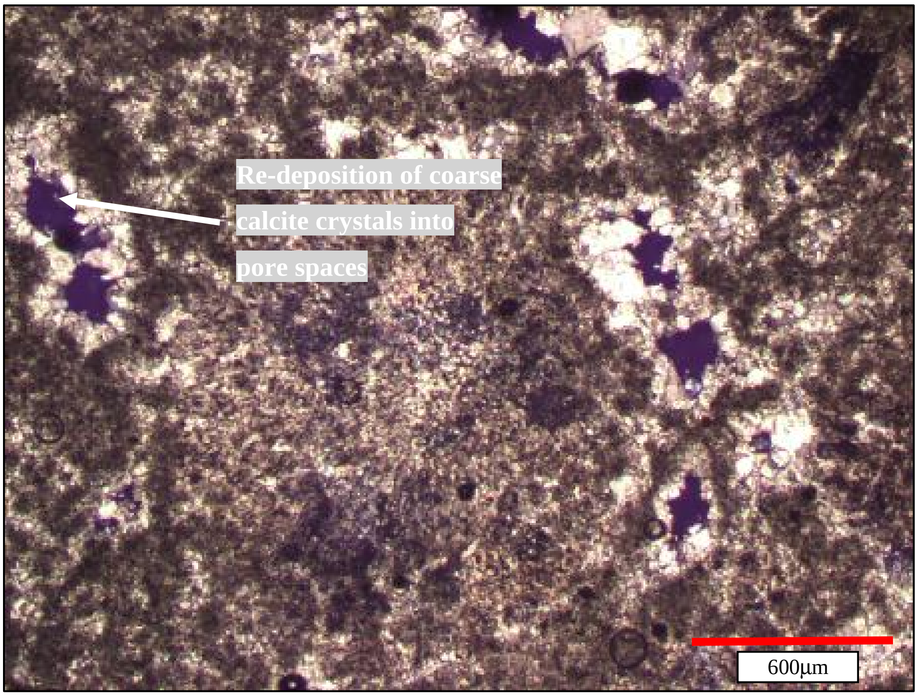

Analyzer in view

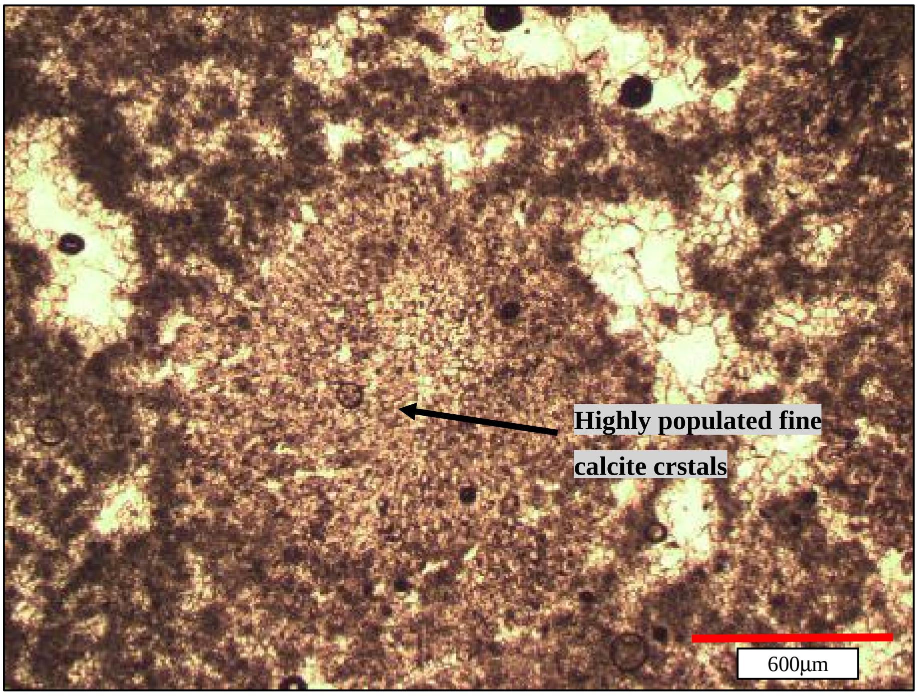

Analyzer out view

Figure 59. Thin section photographs of other microcrystalline sample.

VII.2.3.1.2 Loss on ignition tests

Loss on ignition tests were carried out in accordance with the ASTM C25 standard. A total of twenty five samples, five from each tufa rock type, were tested in the laboratory. The main purpose was to determine the organic content, whose effects might govern the mechanical behavior of the tufa rock masses.

According to the LOI test results, except for the microcrystalline tufa type, the other types possessed almost similar LOI (%) values around 42 (Table 9). The microcrystalline tufa rock type, on the other hand, had lower LOI (%) values which ranged from 9 to 20. This outcome can be interpreted as that most of the tufa rock masses lose significant amount of organic matter composing of carbon when heated. The total loss in the mass cannot be solely due to only the organic matter in the mass. Some dehydration takes place during heating. In order to find this proportion these results will be compared with the results of DTA and TGA analyses. Apart from the dehydration phenomenon, the results of the LOI tests might independently offer one of the explanations to “why the microcrystalline type is stronger than other tufa types”.

Table 9. Results of the loss on ignition (LOI) tests.

Lithology	Sample no.	Mass of container (g)	Mass of container + sample (g)	Mass of sample (g)	Mass of container + sample after burning (g)	LOI (%)	Mean ± St.D.
Microcrystalline tufa	M3	14.2	15.8	1.63	15.6	9.16	15.7 ± 5.08
Microcrystalline tufa	M2	14.2	15.5	1.25	15.2	17.6	
Microcrystalline tufa	M4	12.9	14.2	1.28	13.9	19.5	
Microcrystalline tufa	M1	14.6	15.8	1.18	15.7	11.5	
Microcrystalline tufa	M3	14.6	15.6	1.07	15.4	20.7	
Phytoclast tufa	PF1	14.2	15.3	1.11	14.8	43.1	43.2 ± 0.08
Phytoclast tufa	PF2	14.2	15.2	1.02	14.8	43.3	
Phytoclast tufa	PF3	12.9	14.2	1.33	13.6	43.2	
Phytoclast tufa	PF4	14.6	15.9	1.32	15.4	43.2	
Phytoclast tufa	PF5	14.6	16.1	1.56	15.4	43.3	
Phytoherm boundstone	B1	14.2	16.2	2.08	15.4	41.1	42.6 ± 0.86
Phytoherm boundstone	B2	14.2	15.7	1.50	15.1	42.9	
Phytoherm boundstone	B4	12.9	14.5	1.62	13.8	43.1	
Phytoherm boundstone	B4	14.6	16.1	1.46	15.5	42.9	
Phytoherm boundstone	B3	14.6	16.3	1.78	15.6	42.9	
Intraclast tufa	I1	14.2	16.2	2.01	15.3	42.3	42.1 ± 0.21
Intraclast tufa	I1	14.2	16.2	2.00	15.4	41.9	
Intraclast tufa	I1	12.9	15.1	2.21	14.2	42.3	
Intraclast tufa	I1	14.6	16.2	1.59	15.6	41.9	
Intraclast tufa	I1	14.6	16.4	1.88	15.6	42.2	
Phytoherm framestone	P1	14.2	15.5	1.37	14.9	42.9	42.5 ± 0.78
Phytoherm framestone	P2	14.2	16.2	1.95	15.3	42.9	
Phytoherm framestone	P3	12.9	14.3	1.43	13.7	42.9	
Phytoherm framestone	P3	14.6	16.4	1.80	15.7	42.5	
Phytoherm framestone	P6	14.6	15.9	1.37	15.4	41.2	

VII.2.3.1.3 Scanning electron microscope (SEM) analyses

A total of five samples, one sample of each tufa type identified in the field, were prepared for SEM analyses. Together with SEM, Energy-dispersive X-ray spectroscopy (EDS) analysis was also carried out for element analyses of the tufa types (Figures 60, 61, 62, 63 and 64). All the tufa types have been observed to possess a high calcium percentage of calcium by weight. While all autochthonous types have higher calcium percentage other than silica and aluminum, the allochthonous types have relatively higher percentages of silica and aluminum. This observation could point out that allochthonous types possess a higher proportion of elements other than calcium due to the erosion, transportation and deposition phenomena of the autochthonous deposits (Table 10).

Table 10. Results of the EDS analyses.

Sample Type	Element	Weight Conc %	Atom Conc %
1.Phytoherm framestone			
	Al	2.00	2.90
	Si	5.54	7.72
	K	0.83	0.83
	Ca	88.21	86.15
	Fe	3.42	2.40
2. Phytoherm boundstone			
	Ca	100.0	100.0
3. Microcrystalline			
	Ca	100.0	100.0
4. Phytoclast			
	Al	11.38	14.25
	Si	30.54	36.75
	Ca	58.09	48.99
5. Intraclast			
	Mg	0.90	1.38
	Al	5.47	7.57
	Si	9.44	12.56
	Ca	84.20	78.49

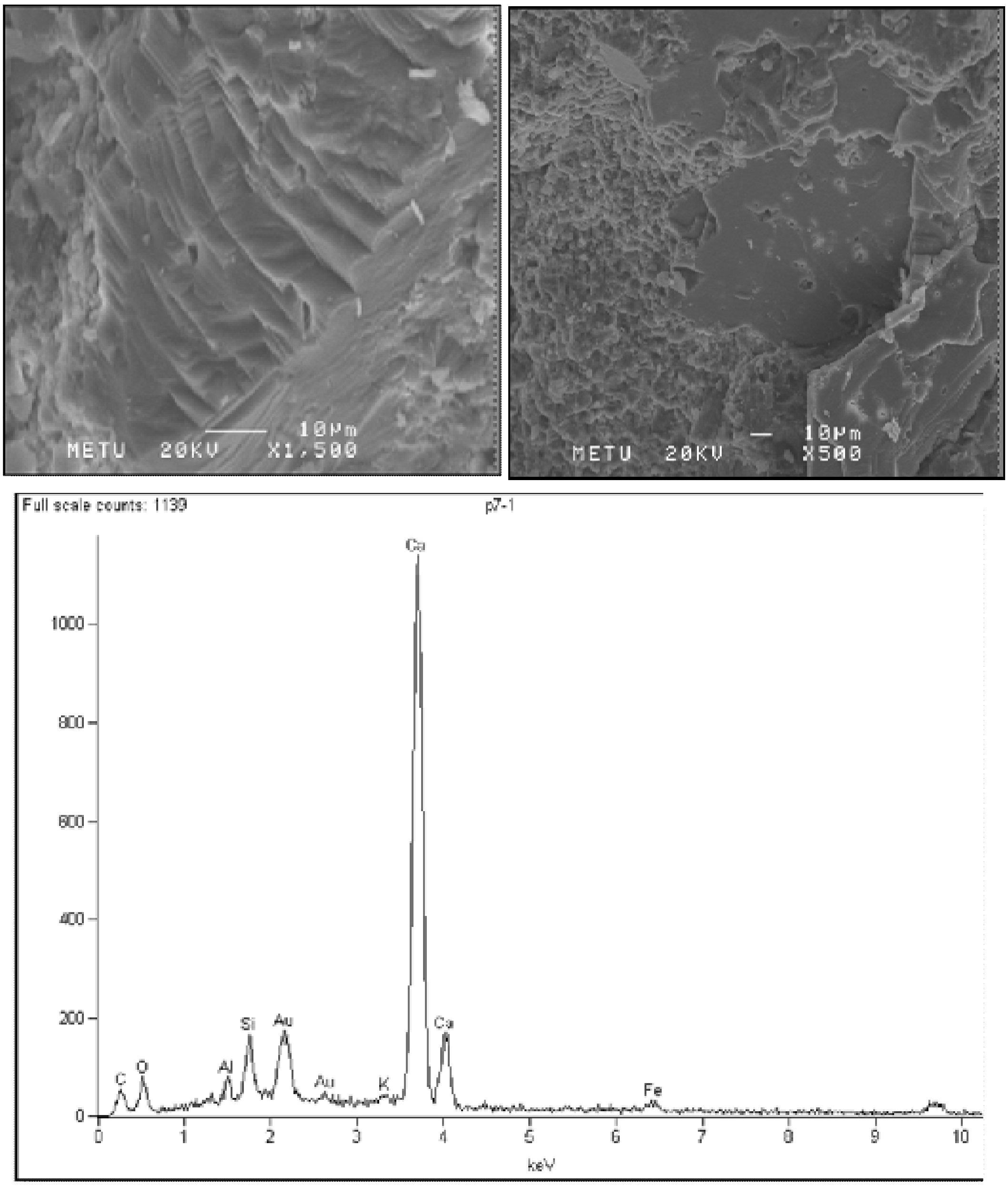

Figure 60. Results of the SEM and EDS analyses for phytoherm framestone tufa.

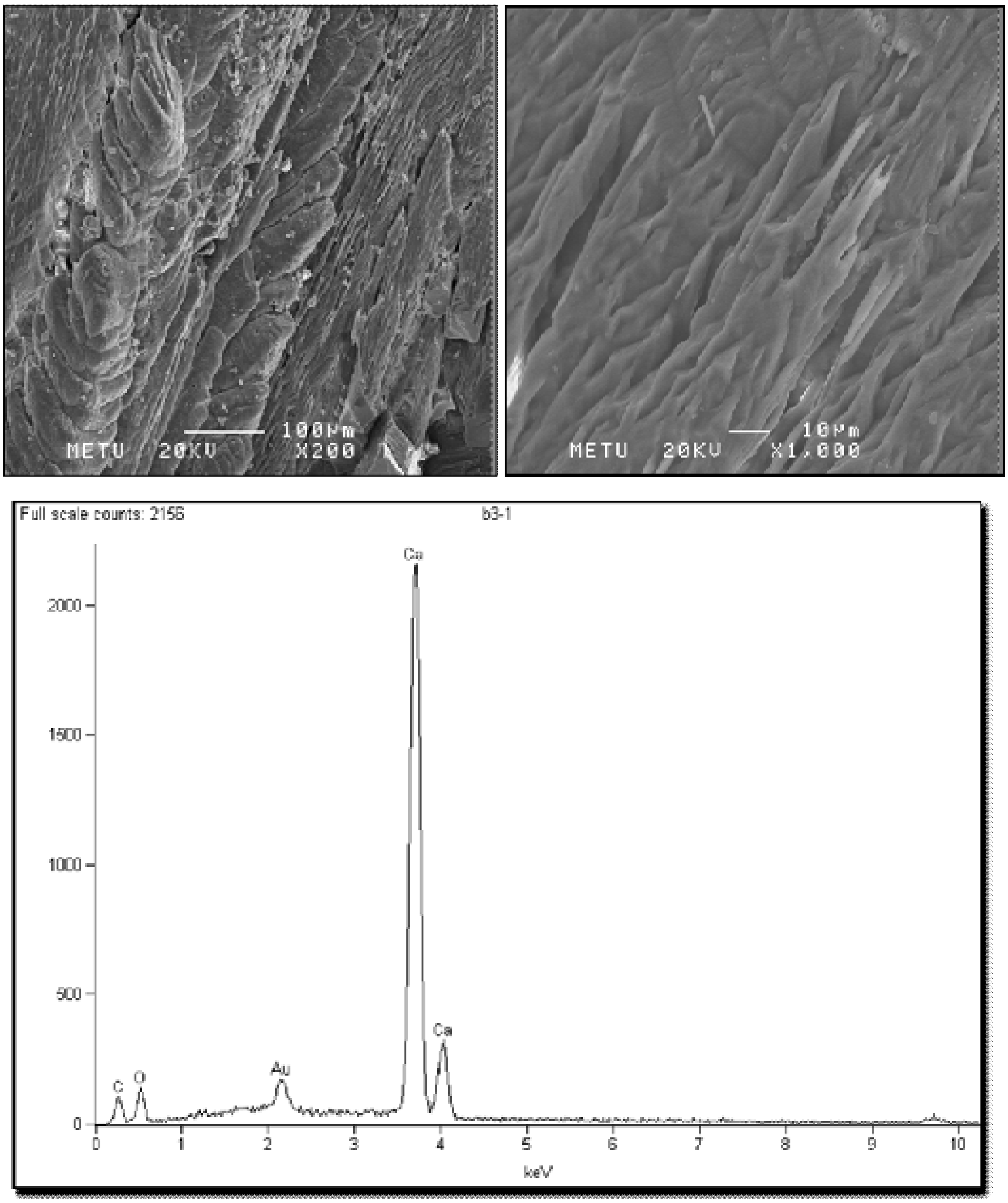

Figure 61. Results of the SEM and EDS analyses for phytoherm boundstone tufa.

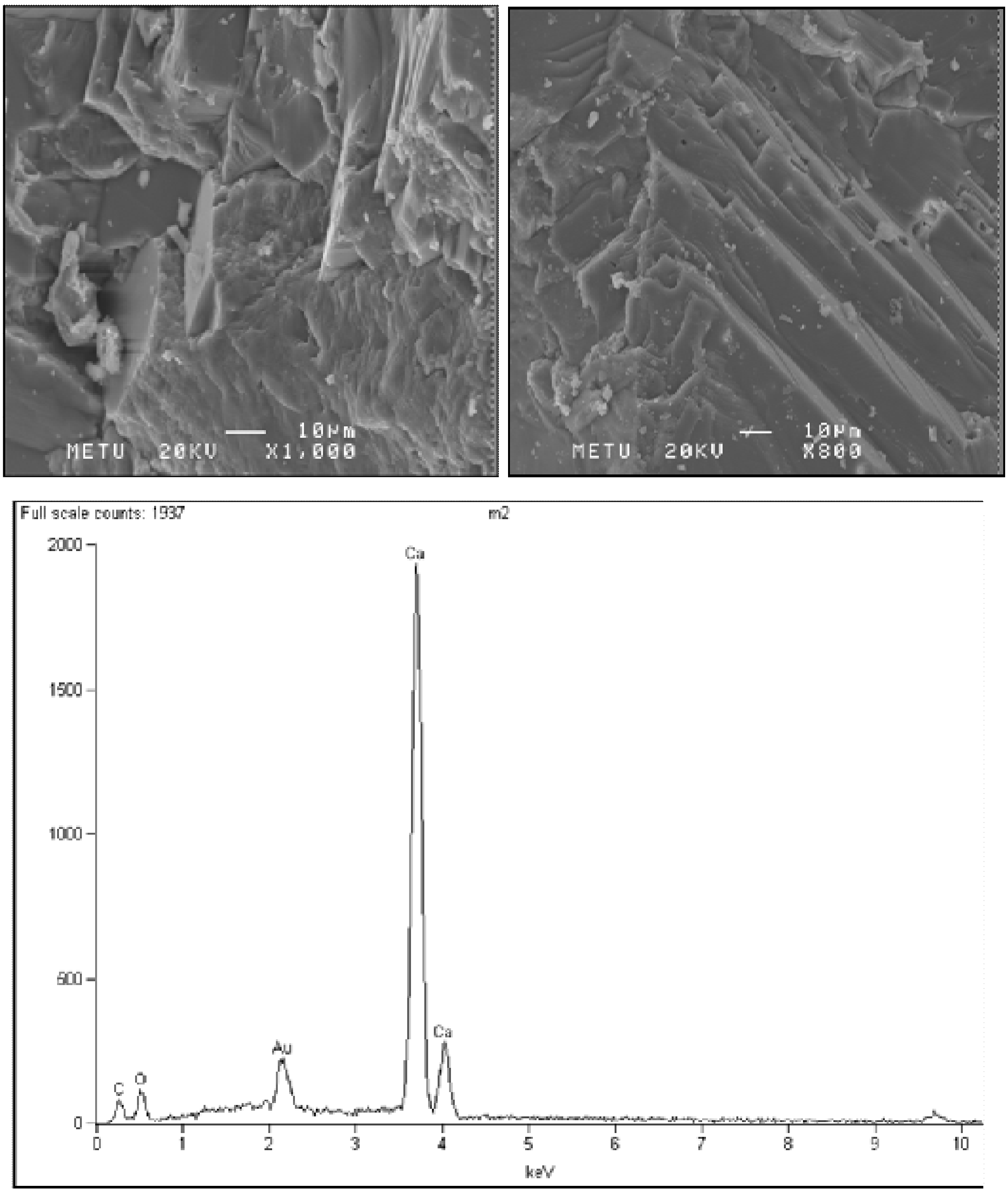

Figure 62. Results of the SEM and EDS analyses for microcrystalline tufa.

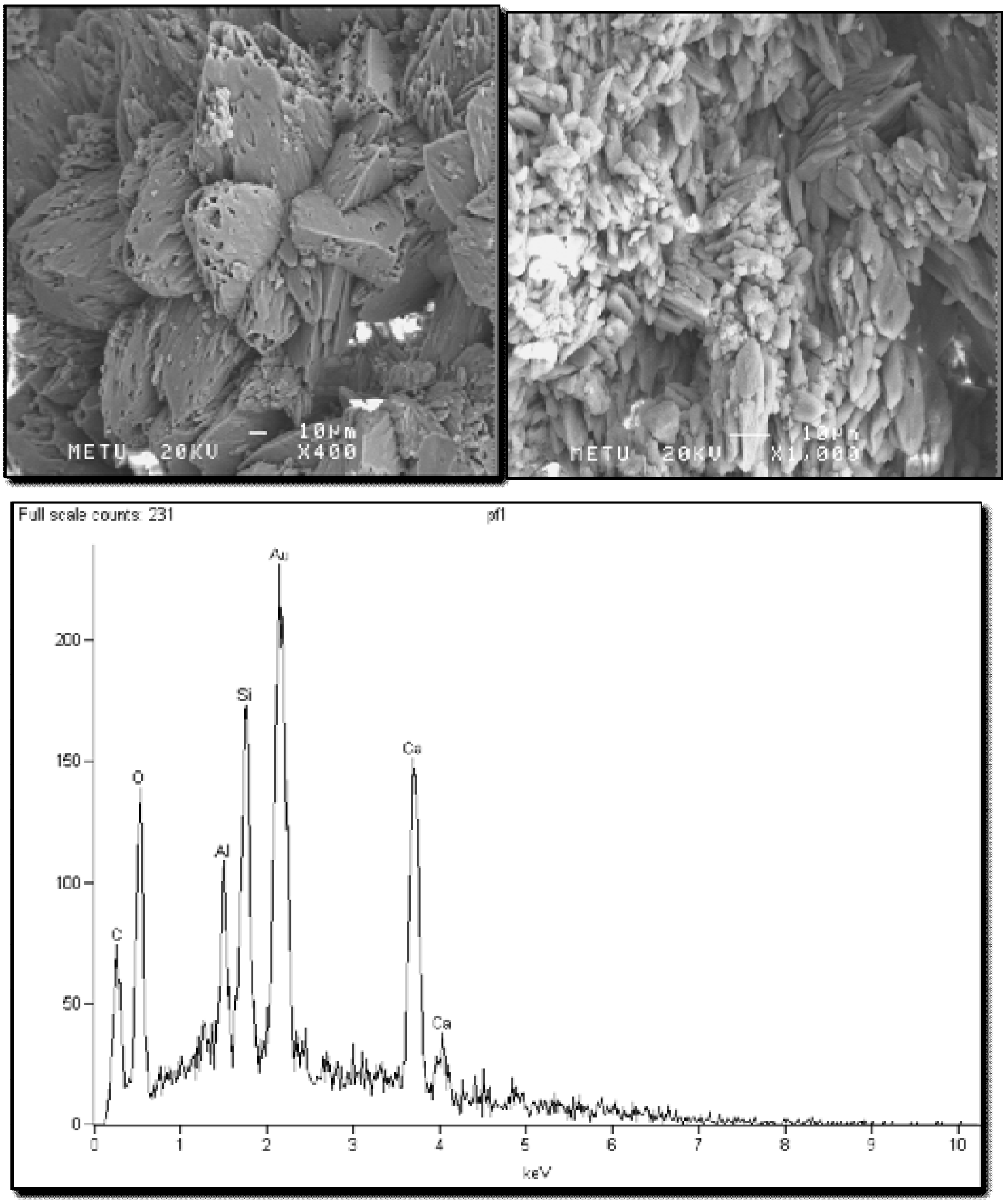

Figure 63. Results of the SEM and EDS analyses for phytoclast tufa.

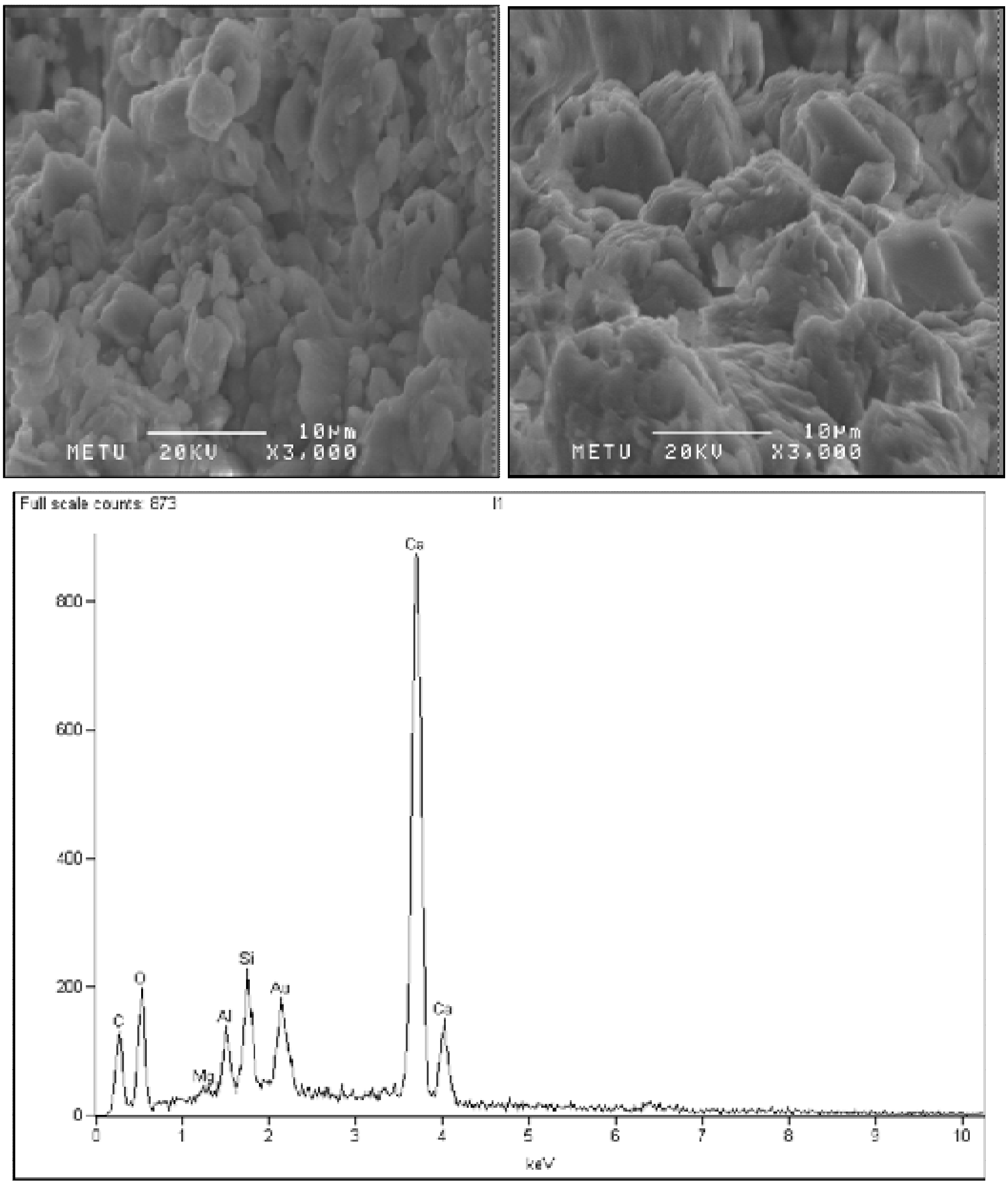

Figure 64. Results of the SEM and EDS analyses for intraclast tufa.

VII.2.3.1.4 Differential Thermal Analyses (DTA)

A total of five samples, one for each tufa type identified in the field, were prepared for DTA. Together with DTA, Thermogravimetry analysis (TGA) was also carried out for element analyses of the tufa types (Figure 65). In order to determine the organic component of the tufa types, samples have been heated up to 600 °C with a heating rate of 15 °C/min.

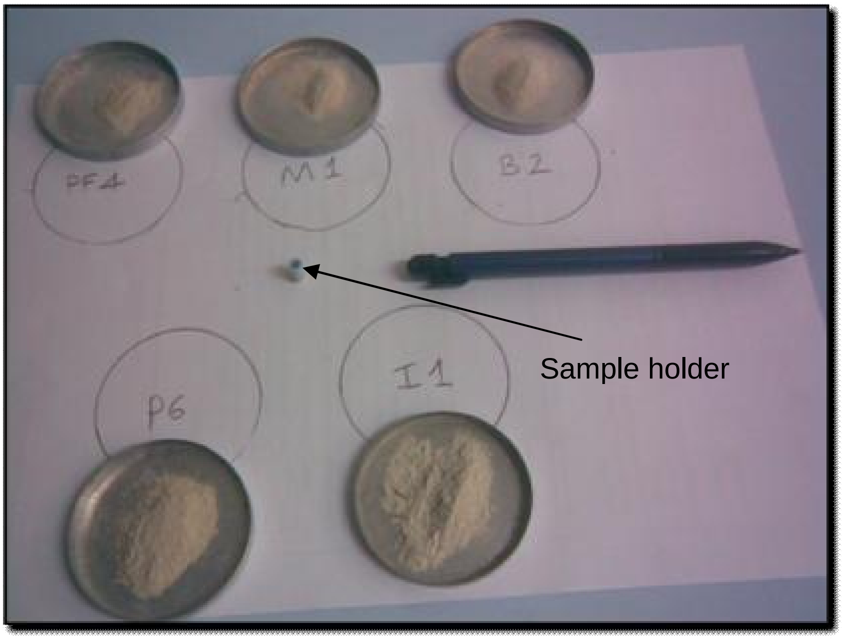

Figure 65. Tufa samples prepared for DTA and TGA.

“Different organic matter constituents have different thermal stabilities, so the formation of a peak in a certain temperature range can be related to the decomposition of specific organic matter structures. These include a labile, a recalcitrant and a refractory pool. The labile organic matter fraction decomposes during thermal analysis at 300–350 °C while the more recalcitrant organic matter decomposes at 400–500 °C. The refractory fraction has been reported to decompose at 450–600 °C” (Gretel, F. et. al., 2009).

“Differential thermal analysis (DTA) thermograms show that when a dried, powdered sample containing organic material and calcium carbonate is heated in a muffle furnace, the organic material begins to ignite at about 200 °C and is completely ignited by the time the furnace temperature has reached approximately 550 °C. Evolution of CO_2 from the calcium carbonate will begin at about 800 °C and proceed rapidly so that most of the CO_2 has been evolved by the time the furnace has reached 850 °C. If any dolomite is present in the sample, it will evolve CO_2 at a lower temperature than calcite (ca. 700-750 °C)” (Walter, E.D., Jr., 1974).

Examination of the DTA curves of the tufa samples revealed that apart from the microcrystalline type, all the other tufa types possessed almost identical DTA curves (Figures 66, 67, 68 and 69). The peaks (Peak 1 and Peak 2) before 200 C° observed on DTA curves represent the exothermic reactions (Peaks 1, 2 and 3) related to the burning of organic matter. The microcrystalline type has a lower number of peaks that is most probably representative of lesser amount of organic matter. This outcome was in agreement with the LOI test results.

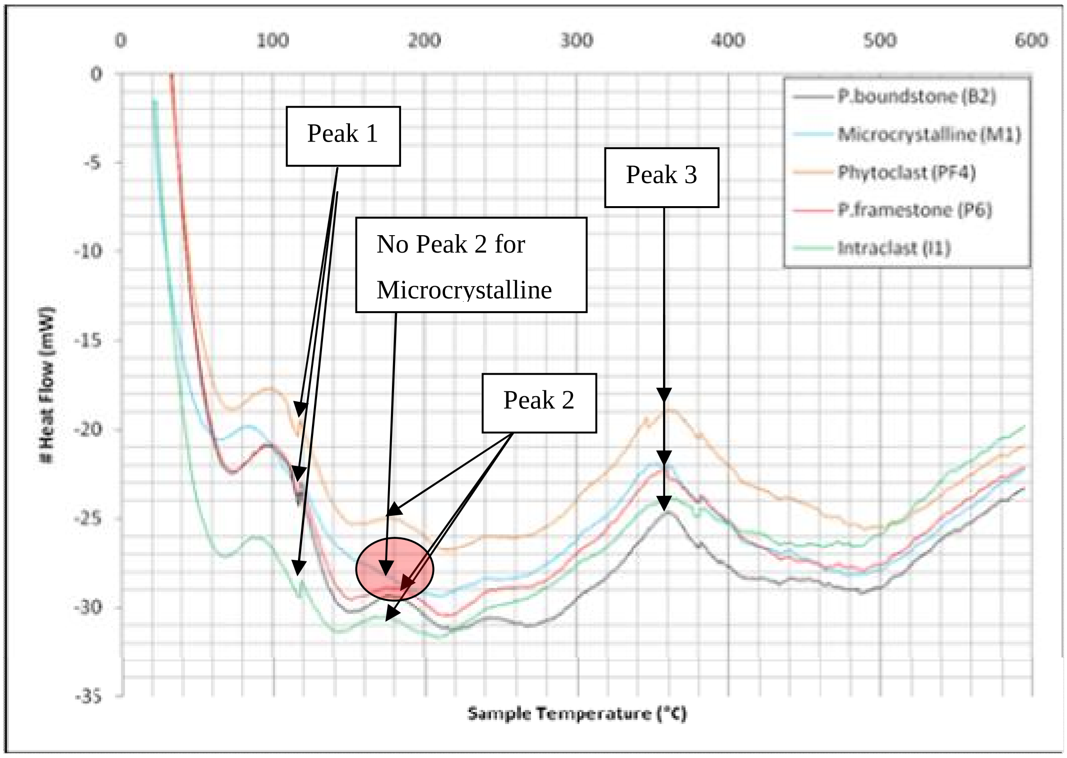

Figure 66. DTA curves for the Antalya tufa rock mass types.

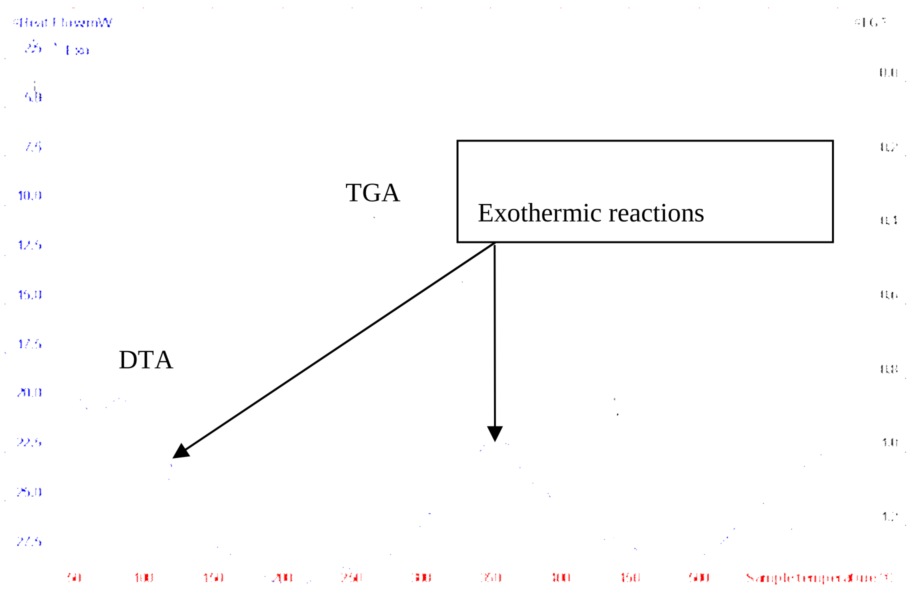

Figure 67. DTA and TGA curves for microcrystalline tufa.

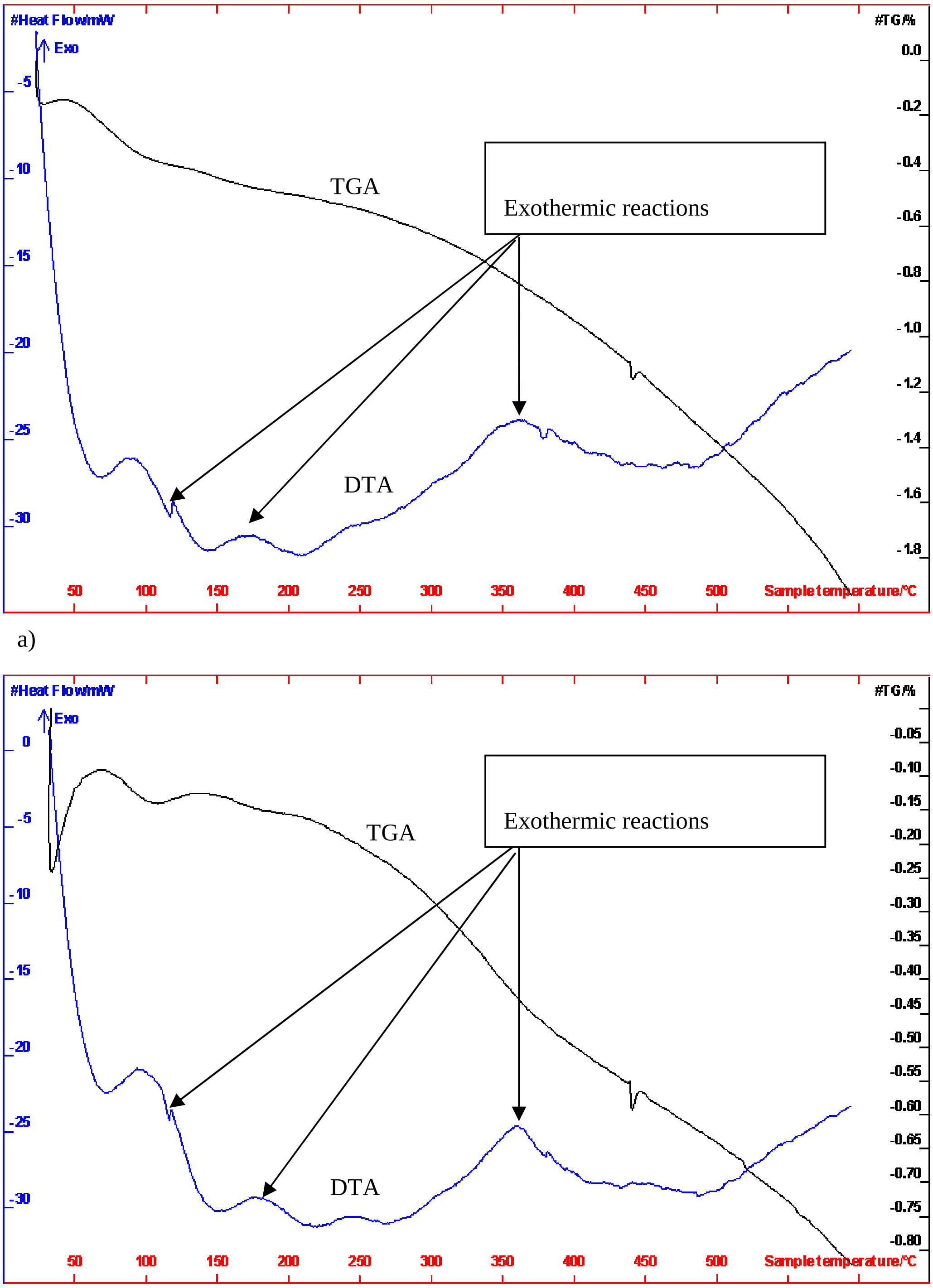

a)

b)

Figure 68. DTA and TGA curves. a) intraclast tufa b) phytoherm boundstone tufa.

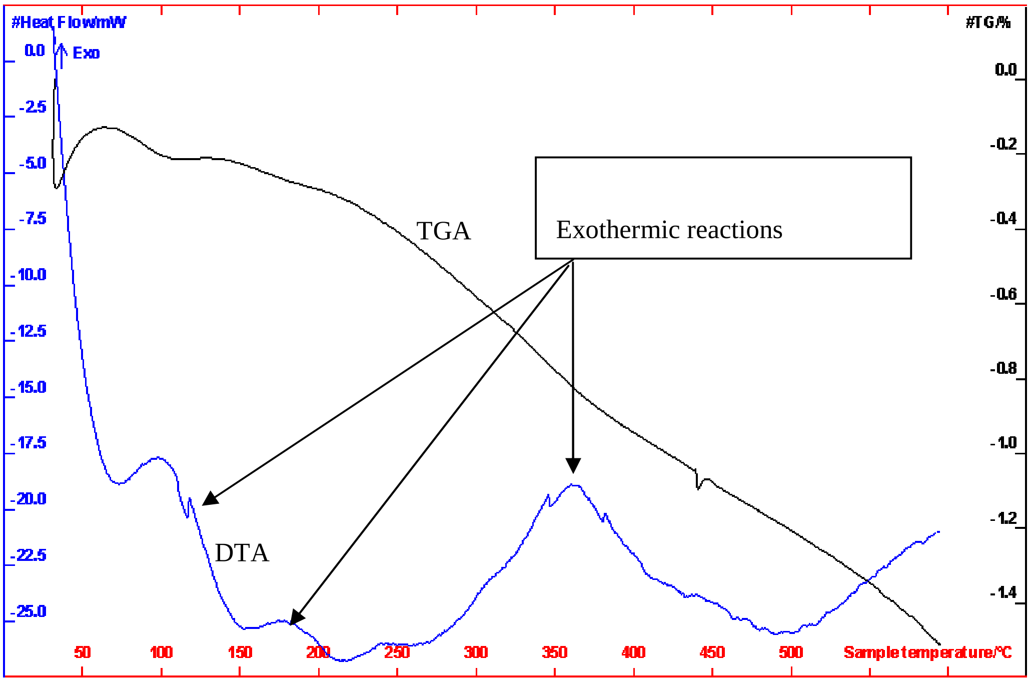

a)

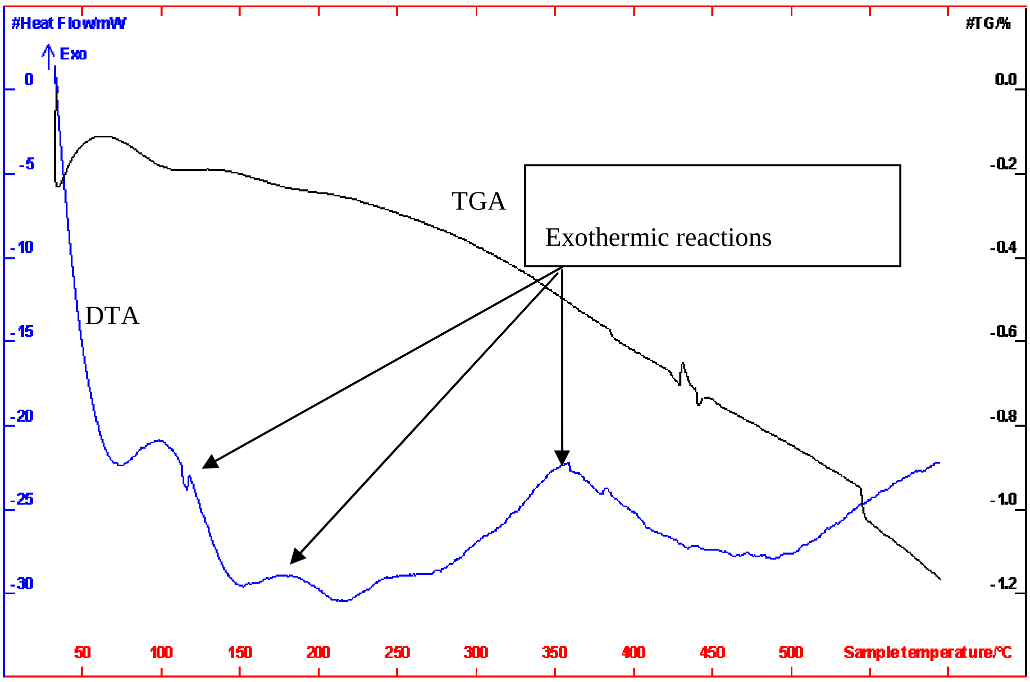

b)

Figure 69. DTA and TGA curves. a) phytoherm framestone b) phytoclast tufa.

VII.2.3.2 Geophysical tests (ultrasonic velocity measurements)

The ultrasonic velocity measurements were carried out in accordance with ASTM E 494; ASTM D 2845 and ISRM, 1981 standards. As a non destructive testing method, this test provided a chance for the correlation of P-wave and S-wave velocity of the tufa rock mass with its strength parameters, such as point load strength index and uniaxial compressive strength along with the elastic constants. The correlations of the seismic wave velocities with the other geotechnical parameters will be discussed later in this chapter. A total of 156 samples were tested for the ultrasonic wave velocity measurements. The mean values of the measurements for the different type of tufa rock masses are presented by Table 11 and Figures 70 and 71.

Table 11. Results of ultrasonic velocity measurements.

Tufa type	Vp (m/s)		Vs (m/s)	
	Mean	Std. Dev.	Mean	Std. Dev.
Microcrystalline tufa	4262	931	1969	322
Phytoherm framestone	3686	1344	1725	581
Phytoherm boundstone	3515	665	1599	354
Phytoclast tufa	3417	525	1543	303
Intraclast tufa	2722	276	1444	42
Antalya tufa rock mass	3684	960	1696	428

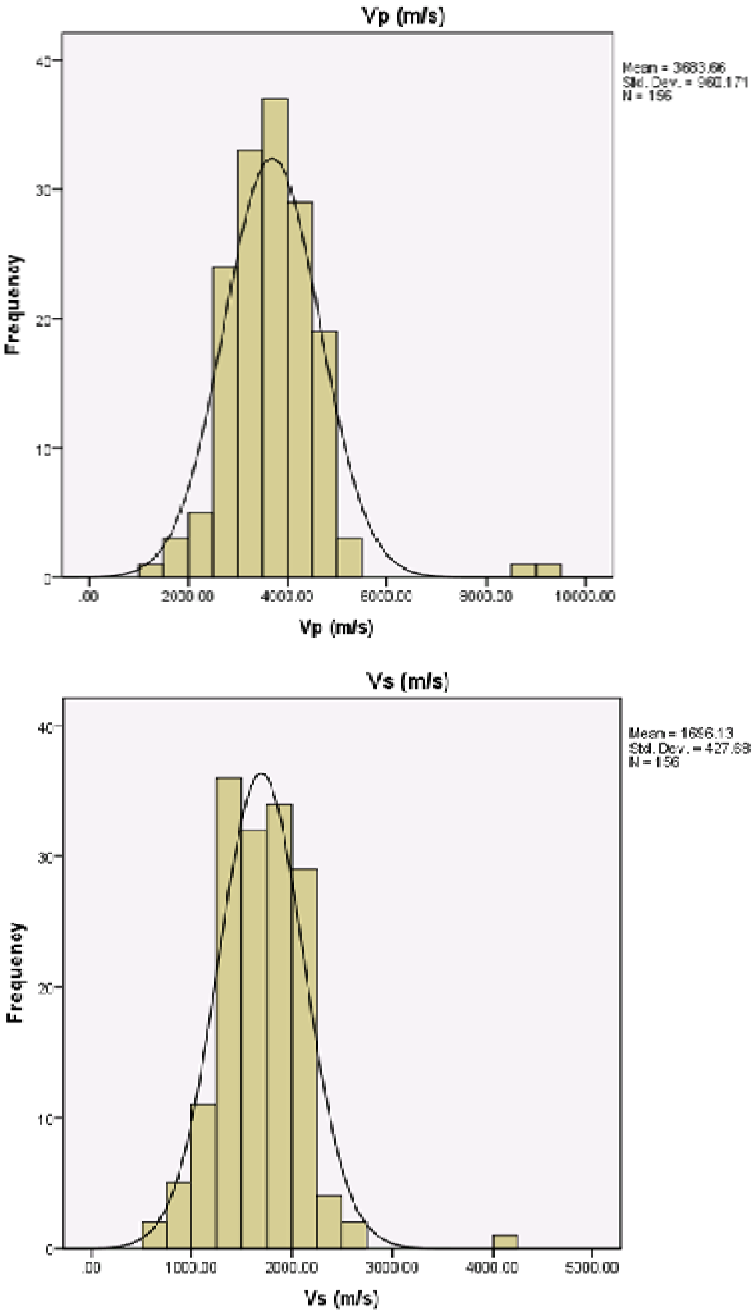

Figure 70. Histograms that illustrate the mean values and standard deviations of Vs and Vp of the samples of the Antalya tufa rock mass.

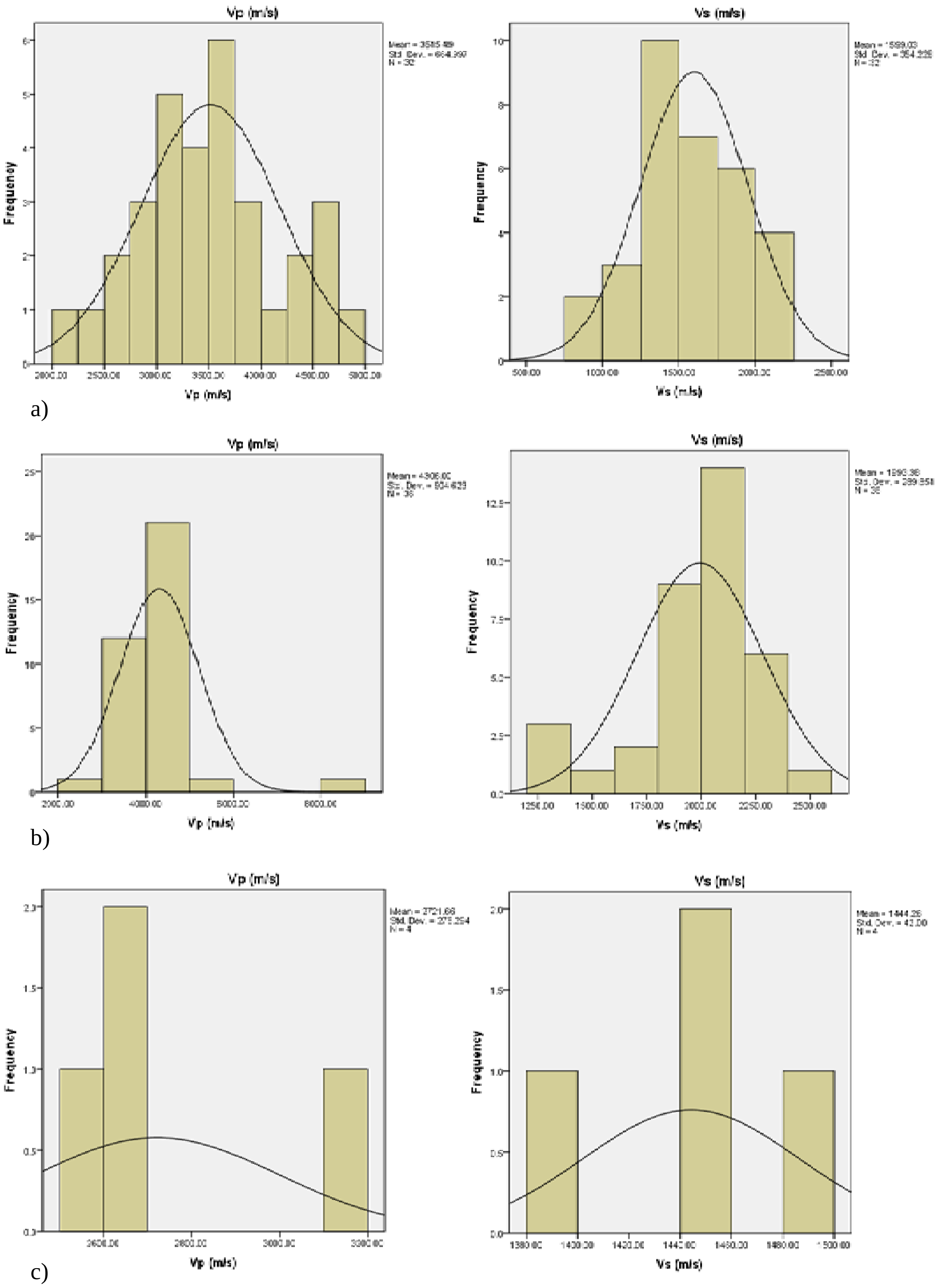

Figure 71. Histograms that illustrate the mean values and standard deviations of Vs and Vp of the samples. a) phytoherm boundstone tufa. b) microcrystalline tufa. c) intraclast tufa.

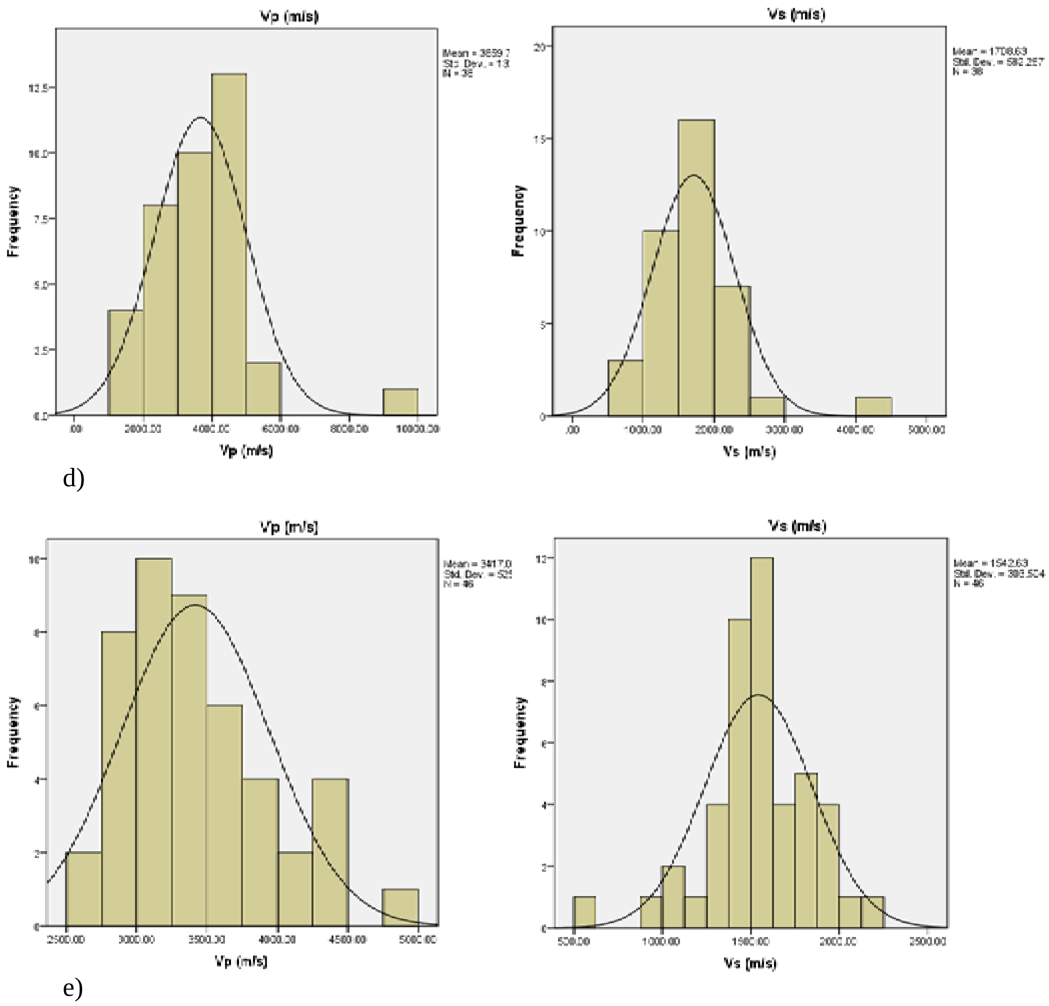

Figure 71 (cont'd.). Histograms that illustrate the mean values and standard deviations of Vs and Vp of the samples. d) phytoherm framestone tufa. e) phytoclast tufa.

As it can be seen from Table 10 and Figures 70 and 71, the microcrystalline tufa, which is stronger and massive, has the highest P-wave and S-wave velocities, while the intraclast tufa has the lowest values.

A fairly strong mathematical relationship between the measured P-wave and S-wave velocities of the tufa rock masses has been obtained as demonstrated by Eq. (3) and as illustrated by Figure 72. Figure 73 gives similar relationships for the individual tufa rock mass types.

$V_s = 0.423V_p + 163.9, \; R^2 = 0.812$ Eq. (3)

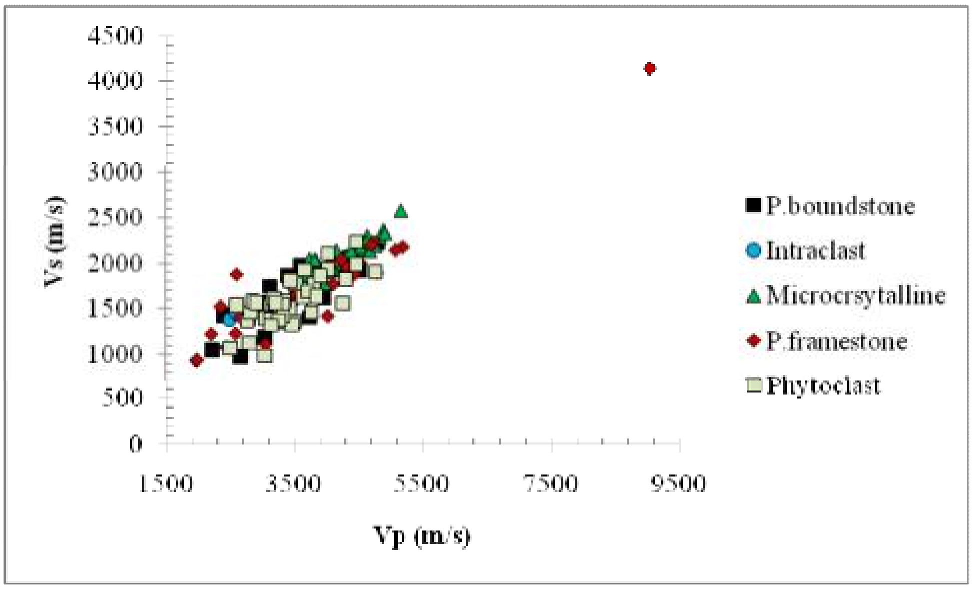

a)

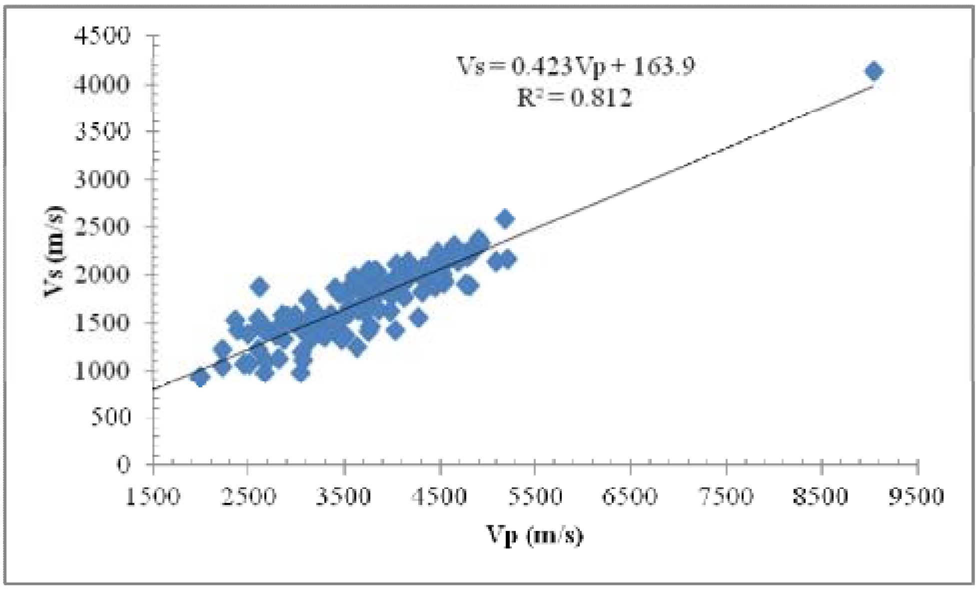

b) N= 148

Figure 72. The ultrasonic wave velocity measurements for the entire tufa rock samples tested. a) an illustration of the sample set of individual tufa types. b) regression equation and regression line of the same sample set.

Strong relationships between these parameters have also been obtained for the individual tufa rock masses except the intraclast type from which very limited core samples have been obtained since it is the lowest strength tufa rock type. It is believed that if an adequate number of samples were able to be taken, a stronger correlation would most probably be obtained for this type also. Figure 73 gives Vs and Vp relationships for the individual tufa rock types.

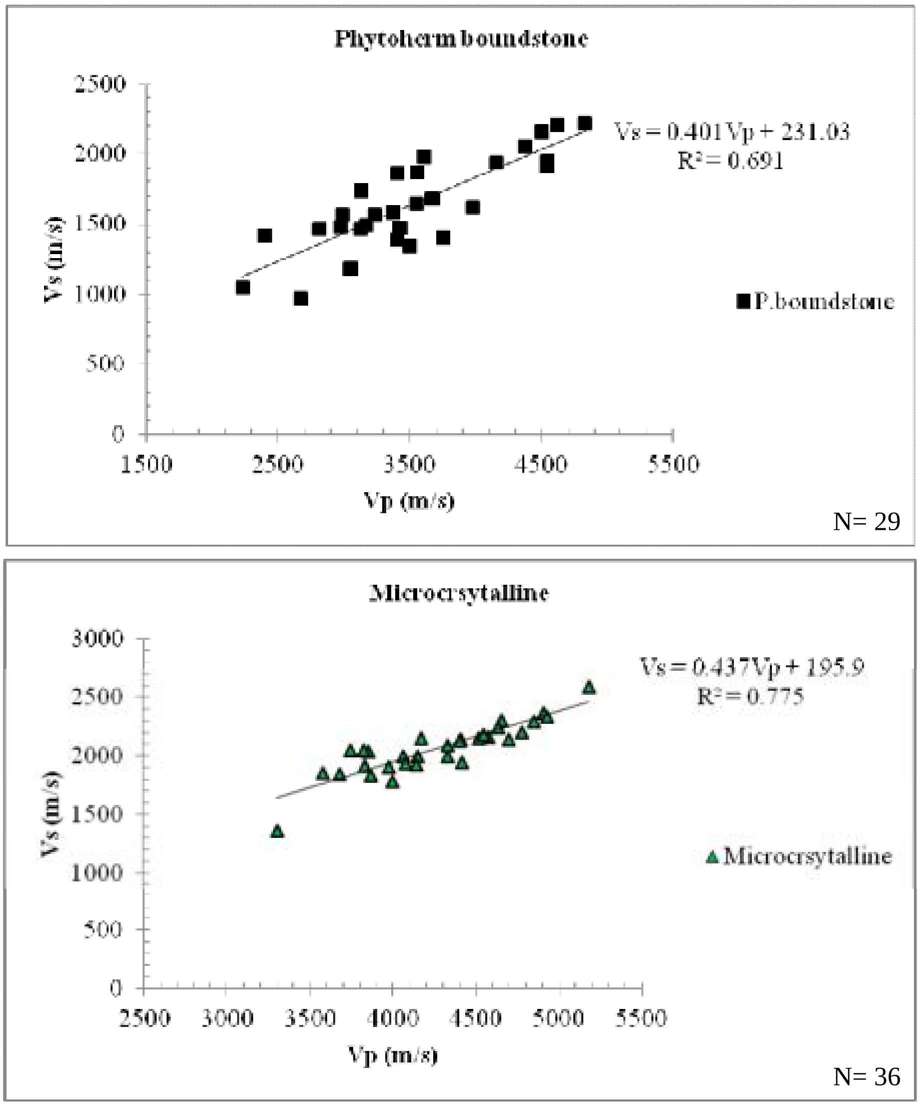

Figure 73. Vs and Vp relationships for the individual tufa rock types.

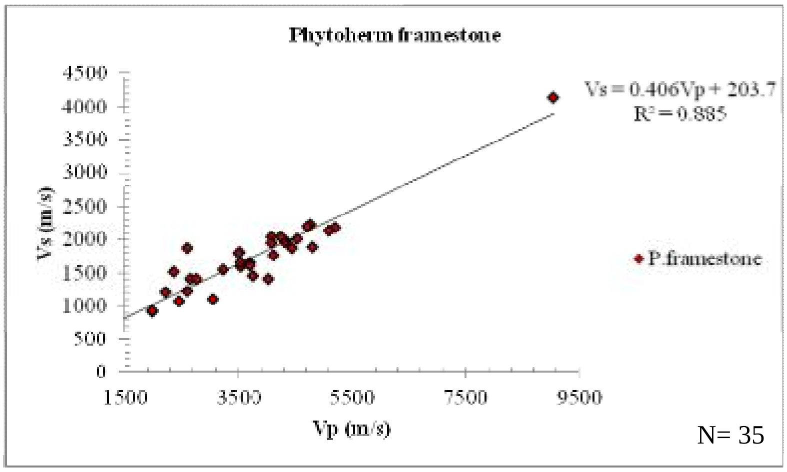

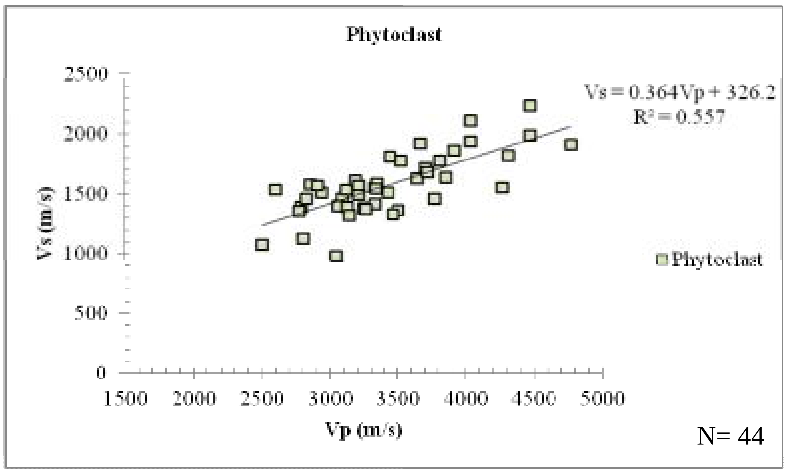

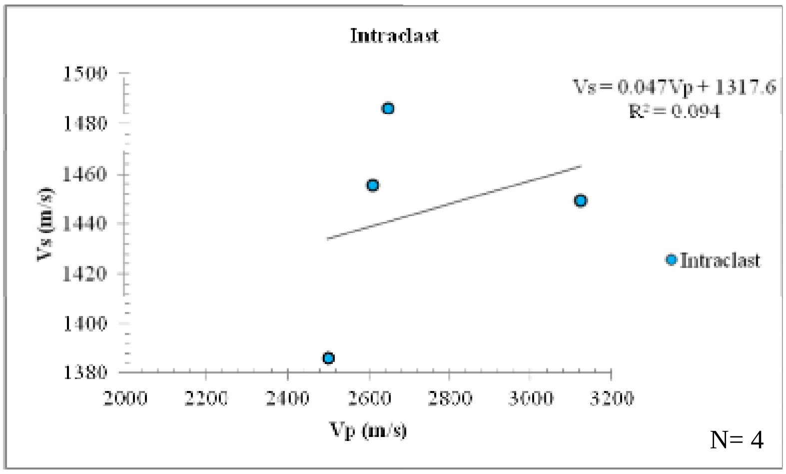

Figure 73 (cont'd.). Vs and Vp relationships for the individual tufa rock types.

Table 12 summarizes the Vp and Vs relationships for the tufa rock types with the relevant coefficient of determinations.

Table 12. Vp and Vs relationships and relevant coefficient of determinations for the tufa rock types.

Tufa type	Vp and Vs relation	Coefficient of determination (R^2)
Antalya tufa rock mass	$V_s = 0.423V_p + 164$	0.812
Phytoherm framestone	$V_s = 0.406V_p + 203.7$	0.885
Phytoherm boundstone	$V_s = 0.401V_p + 231.03$	0.691
Microcrystalline	$V_s = 0.437V_p + 195.9$	0.775
Phytoclast	$V_s = 0.364V_p + 326.2$	0.557
Intraclast	$V_s = 0.047V_p + 1317.6$	0.094

Dynamic deformation modulus and shear modulus of Antalya tufa rock masses have also been determined in Table 13.

Table 13. Dynamic deformation modulus and shear modulus for the tufa rock types.

Tufa type	Dynamic deformation modulus (GPa)	Shear modulus (GPa)
Phytoherm framestone	15 ± 9	5.5 ± 3.5
Phytoherm boundstone	14 ± 7	5.2 ± 2.5
Microcrystalline	22 ± 7	8.1 ± 2.9
Phytoclast	12 ± 4	4.3 ± 1.7
Intraclast	11 ± 1	4.3 ± 0.3

VII.2.3.3 Geomechanics tests

VII.2.3.3.1 Unit weight and porosity determination

The unit weight and porosity of a total of 156 tufa rock samples obtained from rock blocks have been measured. According to the measured values, the tufa rock mass in general has at mean unit weight of 19.5 kN/m^3 and a mean porosity of 14.7 %. Table 14 summarizes the measured unit weight and porosity values of the tufa rock types.

Table 14. Results of the unit weight and porosity measurements of the tufa rock types.

Tufa types	Porosity (%)		Unit weight (kN/m^3)	
	Mean	Std. D.	Mean	Std. D.
Microcrystalline	10.6	3.9	20.9	1.3
Intraclast tufa	14.0	5.6	20.8	0.9
Phytoherm boundstone	14.3	9.6	20.3	2.9
Phytoherm framestone	14.0	5.9	18.6	2.4
Phytoclast	18.2	5.0	18.1	1.5
Antalya tufa rock mass	14.7	7.1	19.5	2.3

According to the results of the porosity measurements, the Antalya tufa rock mass is generally included in the medium to high porosity class (Table 15).

Table 15. Classification of porosity (FAO, 2006)

No.	Description	n %
1	Very low	< 2
2	Low	2 – 5
3	Medium	5 – 15
4	High	15 – 40
5	Very high	> 40

The relationship between the measured unit weight and the measured porosity values of the tufa rock types is given by Eq. (4) and by Figure 74.

$$n = -2.7\gamma + 68, \; R^2 = 0.769 \qquad \text{Eq. (4)}$$

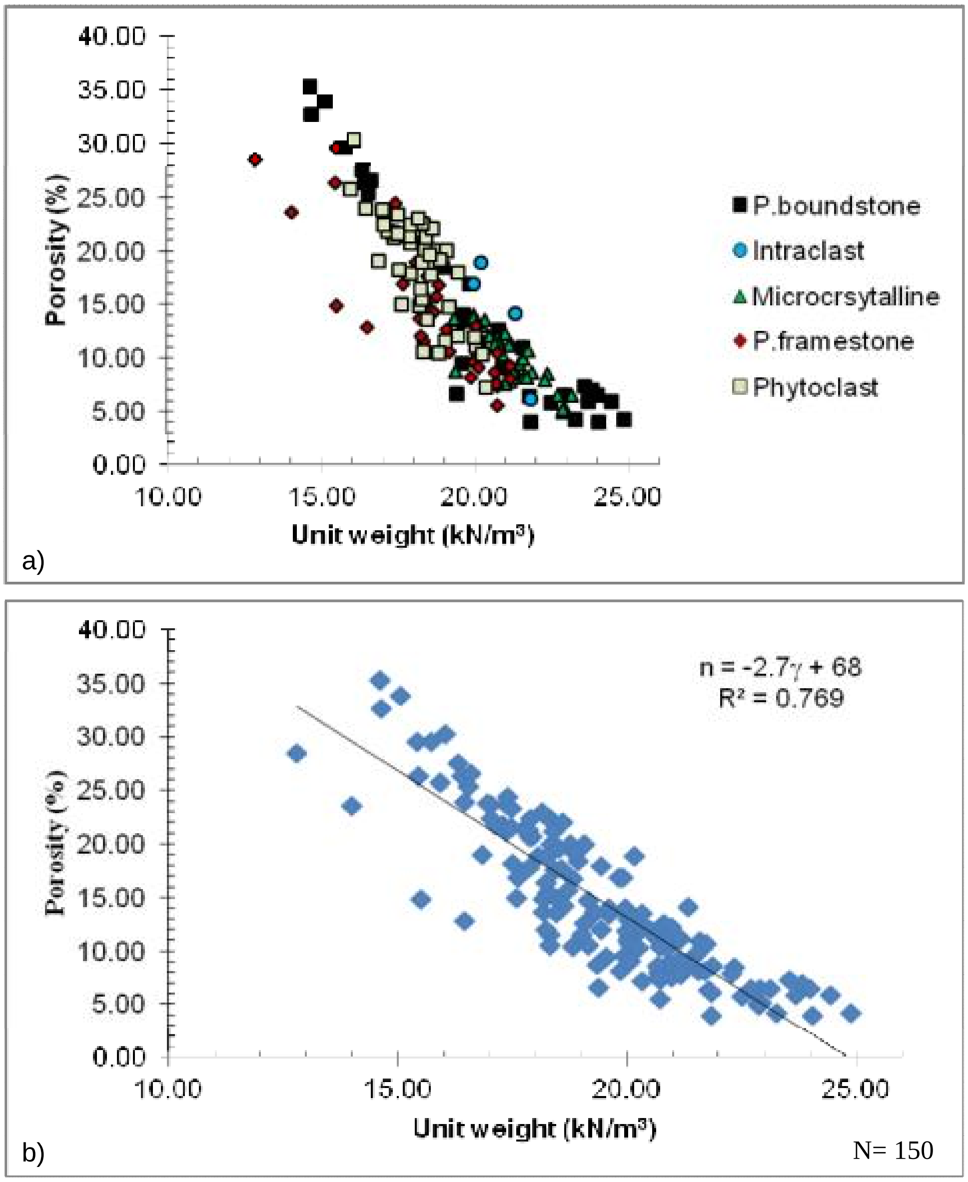

Figure 74. The unit weight and porosity measurements for the entire tufa rock samples tested. a) an illustration of the sample set of individual tufa types. b) regression equation and regression line of the same sample set.

The relationship between these two parameters for the individual tufa rock types have also been calculated with relatively high coefficient of determination values (Figure 75 and Table 16).

Table 16. The correlations between unit weight and porosity of the Antalya tufa rock types.

Tufa type	Unit weight and porosity relation	Coefficient of determination (R^2)
Phytohern framestone	$n = -2.6\gamma + 63$	0.718
Phytoherm boundstone	$n = -3.0\gamma + 75$	0.887
Microcrystalline	$n = -2.6\gamma + 65$	0.803
Phytoclast	$n = -3.7\gamma + 86$	0.609
Intraclast	$n = -5.5\gamma + 128$	0.789

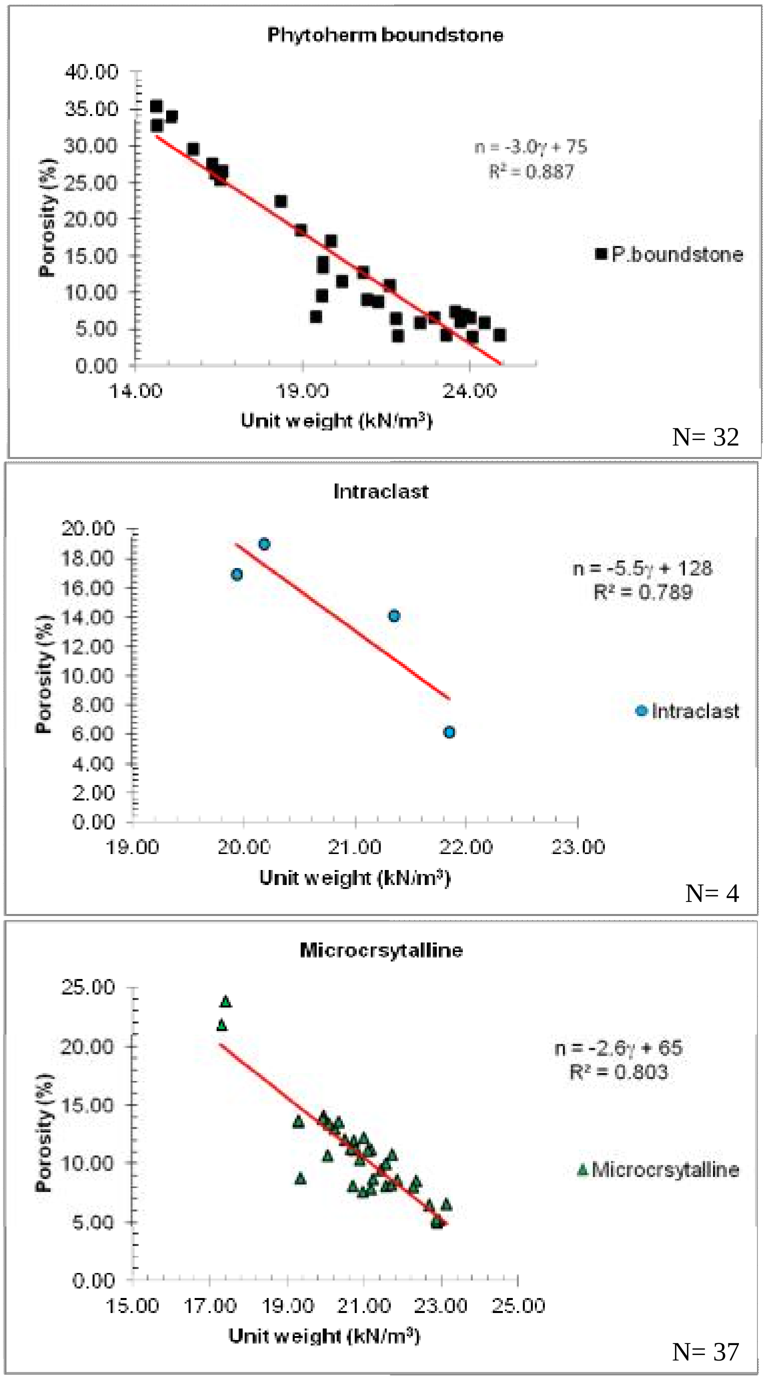

Figure 75. Unit weight and porosity relationships for the individual tufa rock types.

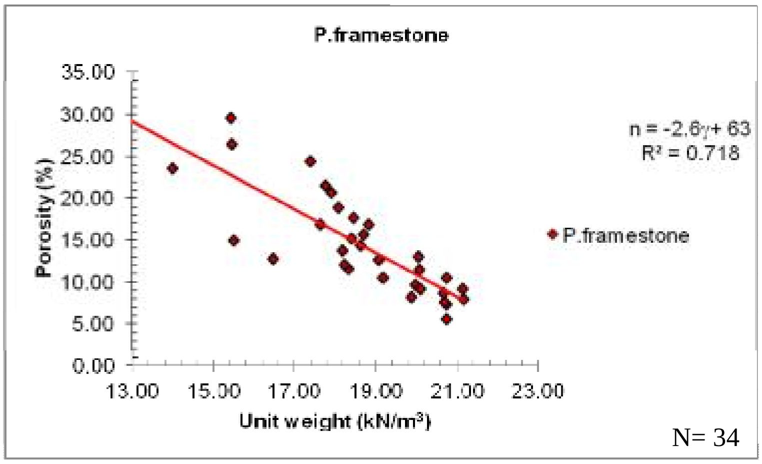

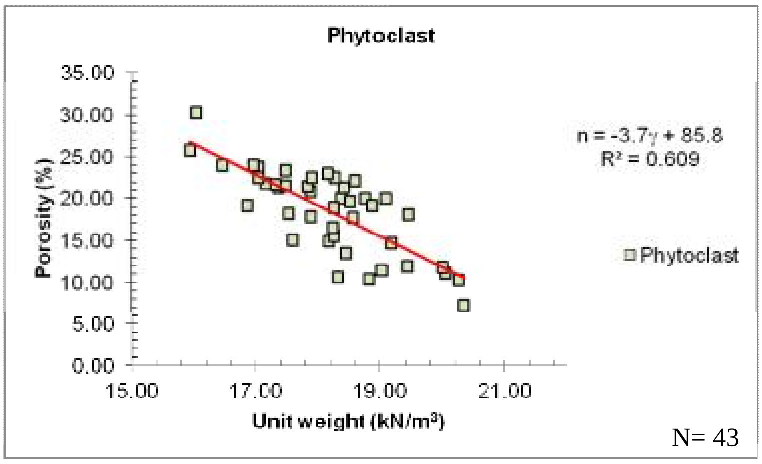

Figure 75 (cont'd.). Unit weight and porosity relationships for the individual tufa rock types.

VII.2.3.3.2 Uniaxial compressive strength (UCS) test

The UCS tests were carried out in accordance with *ASTM D 2938; ASTM D 7012* standards in order to determine the uniaxial compressive strength and elastic constants such as Elasticity modulus (E) and Poisson's ratio (ν) of the entire tufa rock mass and for the individual tufa rock types. The UCS measurements were not possible with conventional method including strain gauge measurements for lateral deformations since the irregular side surfaces of the core samples inhibited strain gauges to be glued on the rock core surface. Therefore, a special instrument, namely, circumferential extensometer, has been used to measure the lateral deformations accurately to calculate the Poisson's ratio of the tufa rock types. The tufa core samples had a diameter (D) of 54 mm and a minimum length (L) of about 108 mm to satisfy a minimum L/D ratio of 2.0. A total of 23 UCS tests have been performed. In addition to these 23 UCS tests including elastic constant measurements, additional 17 UCS tests have been carried out during the triaxial compressive strength tests with zero confining pressure leading to a total 40 uniaxial compressive strength and 23 elastic constant measurements (Table 17).

Table 17. UCS and elastic constant values of the tufa rock types tested.

Sample no	Tufa type	UCS (MPa)	E (GPa)	ν
B1a	P. boundstone	7.36	3.54	0.03
B2a	P. boundstone	12.1	5.17	0.12
B3a	P. boundstone	8.61	5.31	2.04
B6b	P. boundstone	17.2	4.19	0.021
B78a*	P. boundstone	1.41	-	-
B6d	P. boundstone	7.12	-	-
B78e	P. boundstone	0.57	0.764	0.026
I1a	Intraclast	4.72	2.23	0.45
I1b	Intraclast	3.29	1.05	0.12
I1c	Intraclast	5.96	1.34	1.19
M1a	Microcrystalline	26.2	7.52	0.05
M1b*	Microcrystalline	8.76	-	-
M3a	Microcrystalline	44.9	18.5	0.13
M3b	Microcrystalline	77.0	22.5	0.13
M3d*	Microcrystalline	13.4	-	-
M3f	Microcrystalline	29.5	13.4	0.09
M4a	Microcrystalline	8.91	4.40	0.04
M4c*	Microcrystalline	20.1	-	-
M5a*	Microcrystalline	25.0	-	-
M5e*	Microcrystalline	16.6	-	-
P1a	P. framestone	4.15	3.21	0.12
P1b*	P. framestone	4.68	-	-
P1c	P. framestone	2.45	1.23	0.18
P1d	P. framestone	2.92	2.46	0.05
P9a	P. framestone	19.0	8.03	0.07
P3a*	P. framestone	0.28	-	-
P6a*	P. framestone	4.98	-	-
P6b	P. framestone	6.36	7.10	0.14
P8a*	P. framestone	5.33	-	-
P8b*	P. framestone	8.65	-	-
P8c*	P. framestone	5.52	-	-
P9b*	P. framestone	15.3	-	-
P9g*	P. framestone	13.8	-	-
PF3a*	Phytoclast	9.36	-	-

Table 17 (cont'd.). UCS and elastic constant values of the tufa rock types tested

Sample no	Tufa type	UCS (MPa)	E (GPa)	ν
PF4a	Phytoclast	5.76	2.95	0.02
PF4c	Phytoclast	6.70	2.38	0.09
PF5b	Phytoclast	3.23	1.56	0.01
PF6h	Phytoclast	3.67	2.61	0.03
PF6j	Phytoclast	5.41	1.80	0.01
PF7a*	Phytoclast	4.35	-	-

*Triaxial compressive strength test results with zero confining pressure.

According to the UCS test results, the microcrystalline tufa has the highest UCS value while the intraclast tufa has the lowest value. This was an expected result due to the massive and strong appearance of the microcrystalline tufa (Table 18 and Figure 76). Elasticity modulus of the samples has been calculated from the slopes of linear best fit curves between data points at the 30 % and 80 % of the failure load from the axial stress vs. axial strain plots (Figure 77). Similarly, higher Elasticity modulus values were determined for the microcrystalline tufa type. It was observed that the values of Poisson's ratio obtained have large variance and some irrelevant values were also encountered. This was thought to be most probably due to the irregular rock core surfaces that prevented a tight fit of the circumferential extensometer that led to erratic results in the lateral displacement measurements.

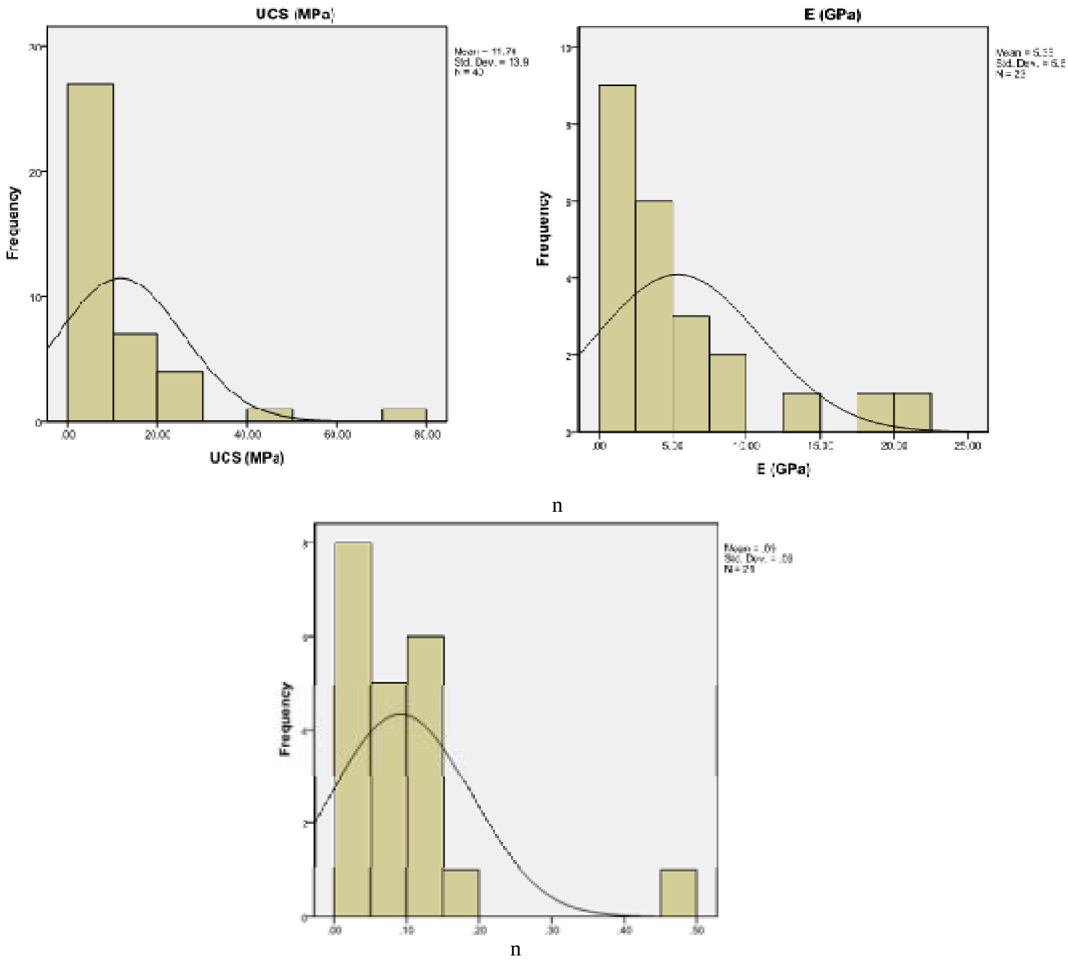

Figure 76. Statistical analysis of UCS, Elasticity modulus and Poisson’s ratio of the Antalya tufa rock masses.

Table 18. Results of the UCS, Elasticity modulus and Poisson’s ratio of the tufa rock types.

Tufa type	UCS (MPa)		E (GPa)		ν	
	mean	Std. D.	mean	Std. D.	mean	Std. D.
Antalya tufa	11.8	13.9	5.35	5.62	0.09	0.09
Microcrystalline	27.0	20.7	13.3	7.47	0.09	0.04
P. boundstone	7.76	5.79	3.79	1.84	0.05	0.05
P. framestone	7.18	5.52	4.41	2.99	0.11	0.05
Phytoclast	5.49	2.09	2.26	0.571	0.03	0.03
Intraclast	4.66	1.34	1.54	0.614	0.29	0.23

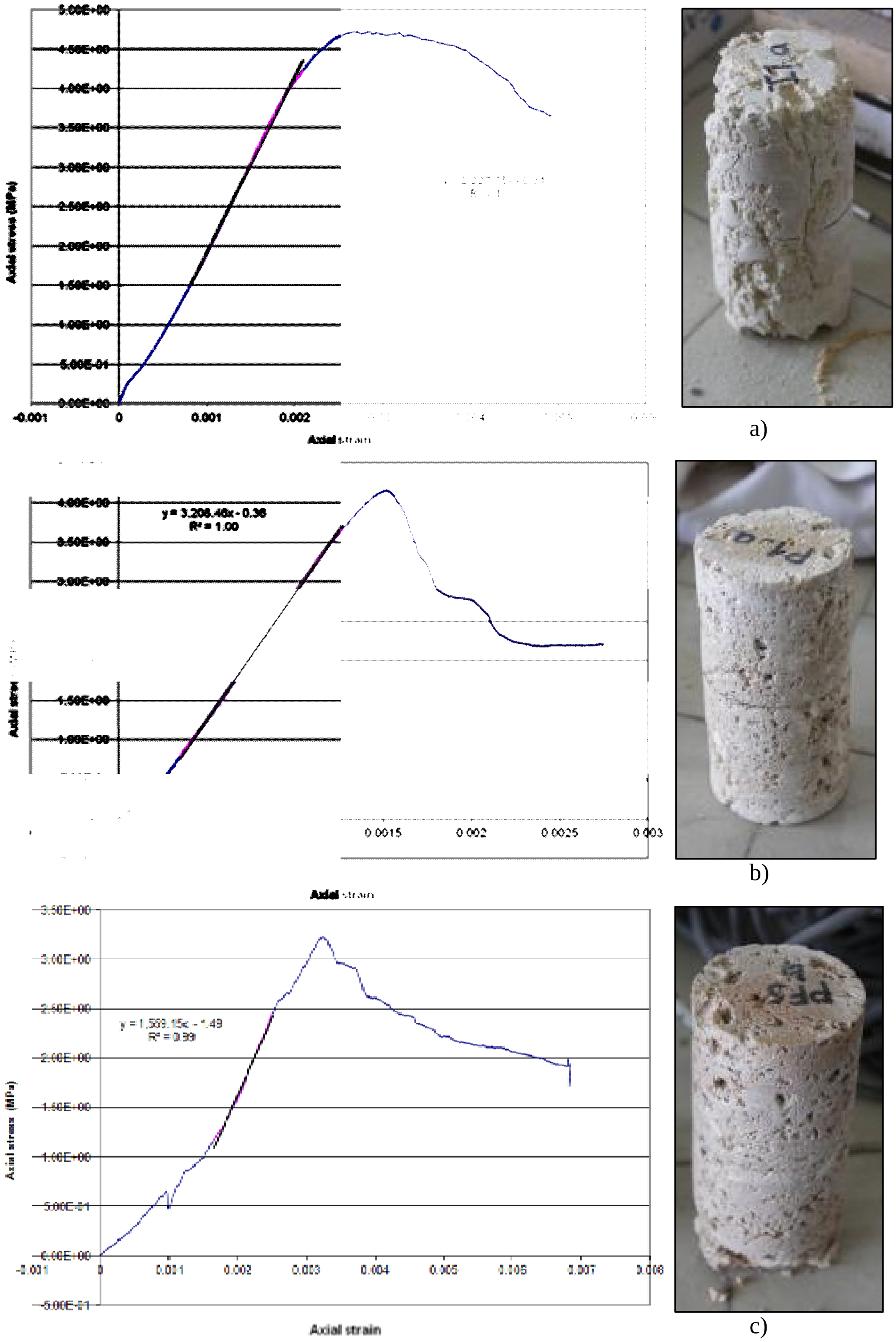

Figure 77. Views from axial stres vs. axial strain plots from which Elasticity modulus of the samples has been calculated. a.Intraclast tufa b. Phytoherm framestone c. Phytoclast tufa d. Microcrystalline tufa e.Phytoherm boundstone.

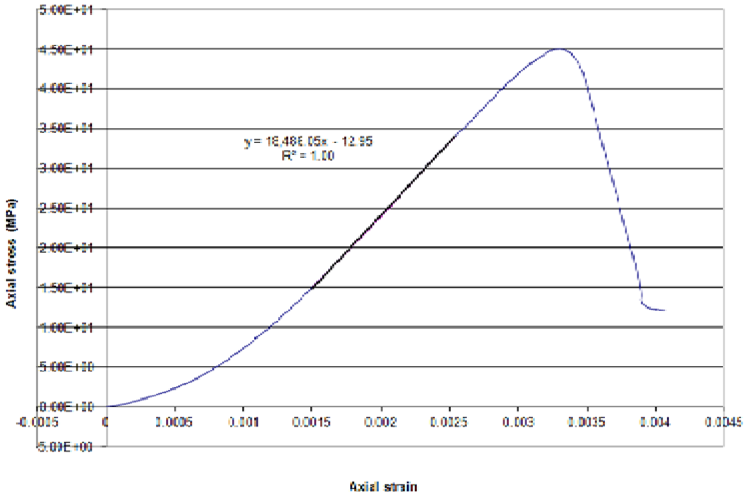

d)

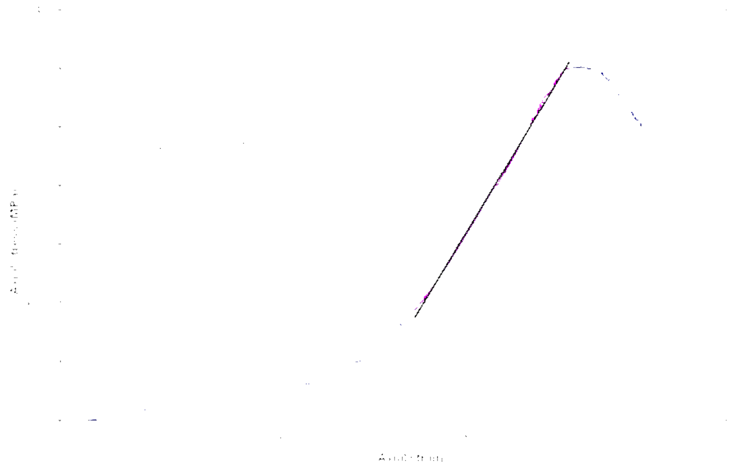

e)

Figure 77 (cont'd.). Views from axial stres vs. axial strain plots from which Elasticity modulus of the samples has been calculated. a.Intraclast tufa b. Phytoherm framestone c. Phytoclast tufa d. Microcrystalline tufa e.Phytoherm boundstone.

During testing, it was observed that the porous tufa types (e.g., the phytoherm framestone type) showed intermediate failures during loading before the final failure point. This observation was interpreted as the closure of individual pores before the final failure of the rock material took place (Figure 78).

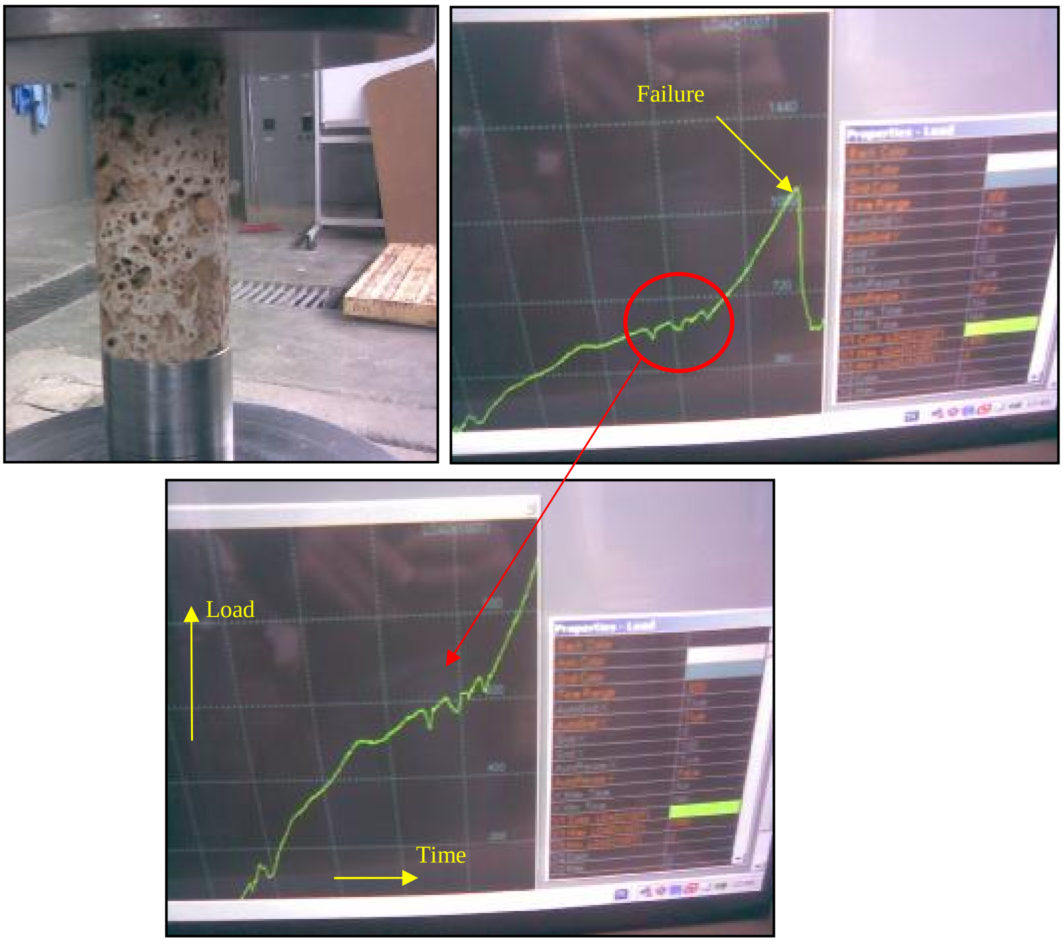

Figure 78. Snapshot views taken during uniaxial loading of the phytoherm framestone sample showing intermediate failures prior to the ultimate load.

VII.2.3.3.3 Triaxial compressive strength tests

Triaxial tests have been carried out according to ISRM (International Society of Rock Mechanics) standard (ISRM, 1981). The main aim in applying the triaxial compressive strength tests was to observe the changes in the strength of the tufa rock masses with changing confining pressure and to obtain the rock mass parameter m_i of the Hoek and Brown (1997) criterion. A total of 19 sample sets, each of which possessed 3 samples, were tested (Table 19). As a result of triaxial testing, the mean value of the m_i parameter for the entire tufa rock mass was determined to be 14 (Table 20 and Figure 79).

Table 19. The results of the triaxial compressive strength tests for the entire tufa rock types.

Sample no	d (mm)	A (mm^2)	F (N)	σ_1 (MPa)	σ_3 (MPa)	m_i	c (MPa)	ϕ °
B1	54.00	2916.00	21461.76	7.36	0	50	2.337	56.4
B1	54.15	2302.96	42394.15	18.4	1			
B4	54.14	2302.11	89220.9	38.8	0.5			
B2	54.00	2916.00	35137,8	12.1	0	2.305	4.714	19.5
B5	54.12	2300.41	40511.27	17.6	0.5			
B5	54.31	2316.59	34117.34	14.7	1			
B3	54.00	2916.00	25106.76	8.6	0	25.454	1.107	54.9
B3	54.43	2326.8	25232.51	10.8	0.5			
B6	54.37	2321.71	42354.92	18.2	1			
B5	54.06	2295.31	22339.55	9.78	1	50	0.513	54.8
B5	53.61	2257.26	67665.89	29.9	2			
B6	54.17	2304.66	68224.86	29.6	3			
B78	54.23	2309.77	3265.614	1.41	0	1	0.575	9.4
B78	54.05	2294.46	6060.51	2.64	1			
B78	53.82	2274.97	9522.257	4.19	2			
M1	54.00	2916.00	76486.68	26.2	0	1.833	8.25	19.5
M1	54.43	2326.84	44639.87	19.2	0.5			
M1	53.84	2276.66	63821.68	28.0	1			
M1	53.83	2275.82	19946.73	8.76	0	31.301	1.4	53.8
M1	54.1	2298.71	40373.98	17.6	1			
M1	54.13	2301.26	63282.31	27.5	2			
M3	54.00	2916.00	131161.68	44.9	0	1	14.431	0
M3	54.25	2311.47	69342.82	29.9	0.5			
M3	54.21	2308.06	30282.94	13.1	1			
M3	54.12	2300.41	30783.07	13.4	0	1.316	5.791	12.1
M3	54.24	2310.62	38991.24	16.9	1			
M3	54.06	2295.31	74756.09	32.6	2			
M4	54.00	2916.00	25981.56	8.91	0	12.502	1.448	47.2
M4	54.34	2319.15	17661.78	7.62	0.5			
M4	54.15	2302.96	35529.49	15.4	1			
M5	54.25	2311.47	57663.1	24.9	0	50	2.823	63.1
M5	54.32	2317.44	88916.9	38.4	1			
M5	54.26	2312.32	138509.1	59.9	2			
P1	54.00	2916.00	12101,4	4.15	0	1	2.217	0
P1	53.97	2287.67	18034.43	7.89	2			
P1	54.17	2304.66	14327.52	6.22	3			
P3	53.91	2282.59	637.4323	0.28	0	1	0.113	0
P3	54.21	2308.06	2451.663	1.06	1			
P3	53.81	2274.13	4981.778	2.19	2			
P6	54.00	2916.00	18545.76	6.36	0	1.367	4.524	9.2
P6	54.14	2302.11	50563.09	21.9	2			
P6	53.88	2280.05	27115.39	11.9	4			
P8	54.24	2310.62	12748.65	5.52	0	6.016	2.823	63.1
P8	54.08	2297.01	23781.13	10.4	1			
P8	54.45	2328.55	27115.39	11.6	2			

Table 19 (cont'd.) The results of the triaxial compressive strength tests for the entire tufa rock types.

Sample no	d (mm)	A (mm^2)	F (N)	σ_1 (MPa)	σ_3 (MPa)	m_i	c (MPa)	ϕ °
P9	54.00	2916.00	55258.2	18.9	0	11.335	4.721	43.6
P9	54.49	2331.97	72029.84	30.9	0.5			
P9	54.42	2325.98	56721.66	24.4	1			
PF4	54.00	2916.00	16796.16	5.76	0	18.637	0.653	51.7
PF3	53.97	2287.67	8982.891	3.93	0.5			
PF3	54.06	2295.31	32293.3	14.1	1			
PF5	54.00	2916.00	9418.68	3.23	0	3.614	1.524	21.5
PF5	53.94	2285.13	18407.08	8.06	0.5			
PF5	54.13	2301.26	12415.22	5.39	1			
PF6	54.00	2916.00	15775.56	5.41	0	4.099	1.578	28.3
PF6	54.18	2305.51	29910.28	12.9	1			
PF6	54.33	2318.29	21662.89	9.34	2			

Table 20. Mean values of cohesion, internal friction angle and mi obtained through triaxial compressive strength tests for each of the tufa rock types along with the tufa rock mass.

Tufa type	c (MPa)	ϕ (°)	m_i
Microcrystalline	5.7 ± 5.1	33 ± 25	16 ± 20
Phytoherm framestone	2.9 ± 2.0	23 ± 29	4 ± 5
Phytoherm boundstone	1.8 ± 1.8	39 ± 23	26 ± 24
Phytoclast	1.3 ± 0.5	34 ± 18	9 ± 9
Tufa rock mass	3.2 ± 3.4	32 ± 23	14 ± 18

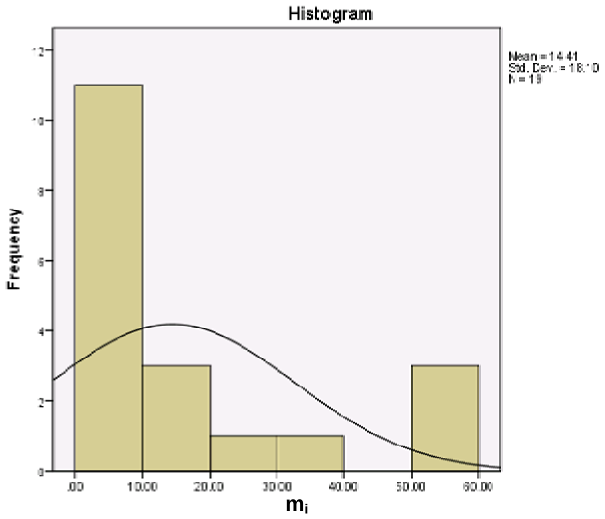

Figure 79. A histogram illustrating the m_i values of the Antalya tufa rock mass.

The Mohr circles constructed from the triaxial tests of the Antalya tufa rock types are presented in Figure 80.

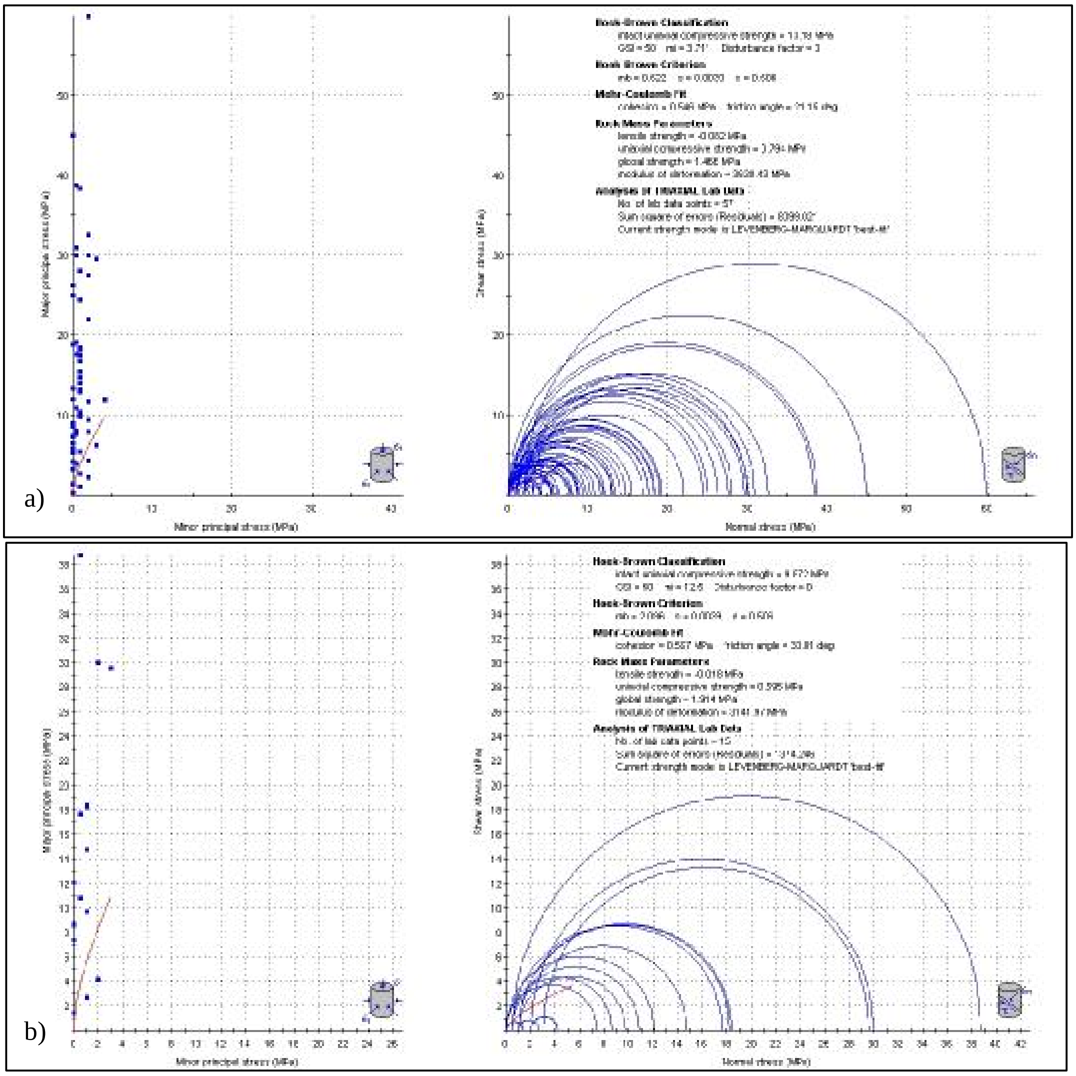

Figure 80. Mohr circles of the Antalya tufa rock types. a.Antalya tufa rock mass. b. Phytoherm boundstone c. Microcrystalline d. Phytoherm framestone e. Phytoclast

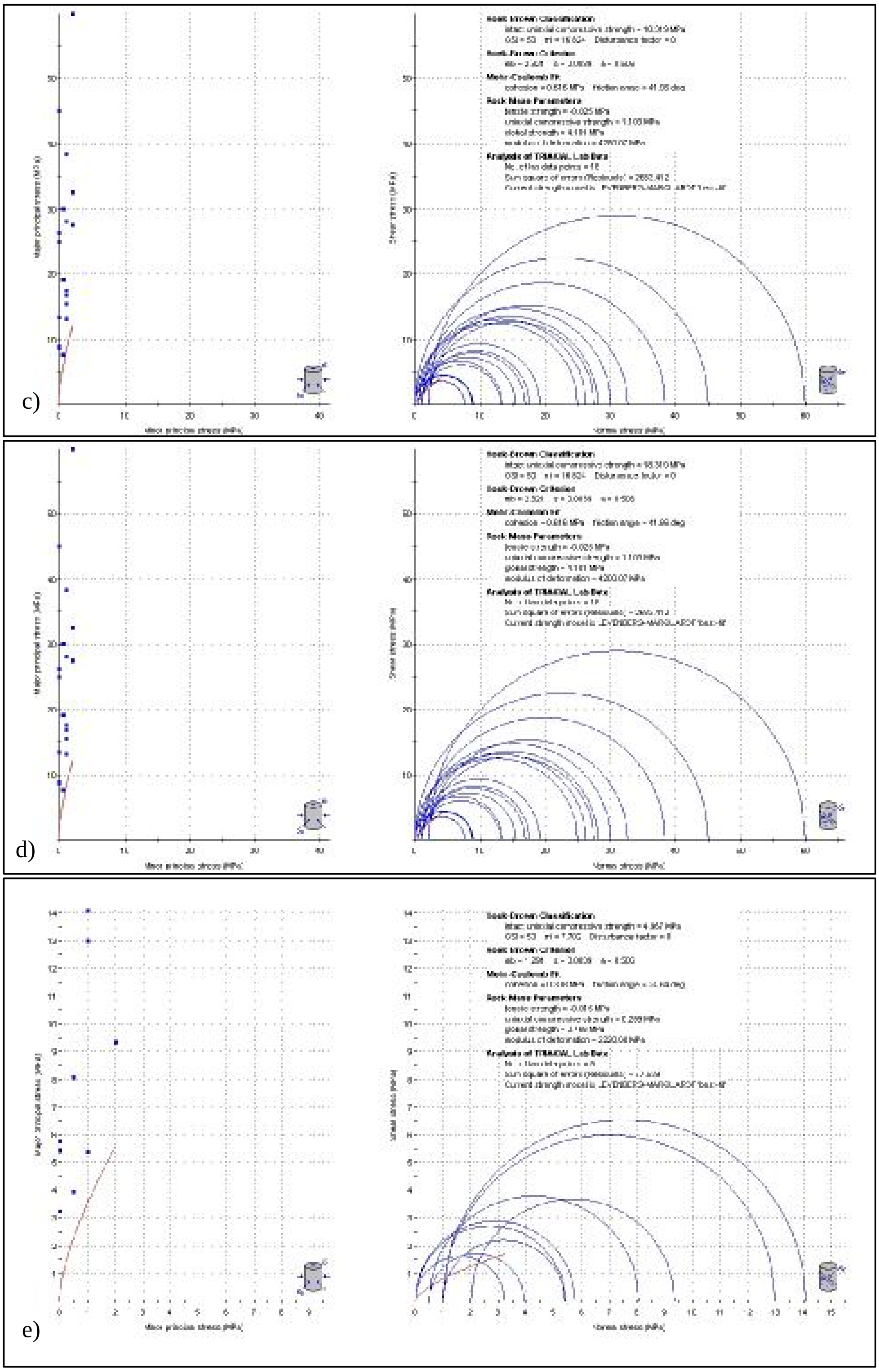

Figure 80 (cont'd.). Mohr circles of the Antalya tufa rock types. a.Antalya tufa rock mass. b. Phytoherm boundstone c. Microcrystalline d. Phytoherm framestone e. Phytoclast

According to the results of the triaxial compressive strength tests, the Antalya tufa rock mass could be said to be mostly brittle in regards to the brittle-ductile transition criterion proposed by Mogi (1966, Figure 81). The brittle-ductile transition has been proposed by Mogi as follows (Eq. 5):

$$\sigma_1 \geq 4.4\sigma_3 \qquad \text{Eq. (5)}$$

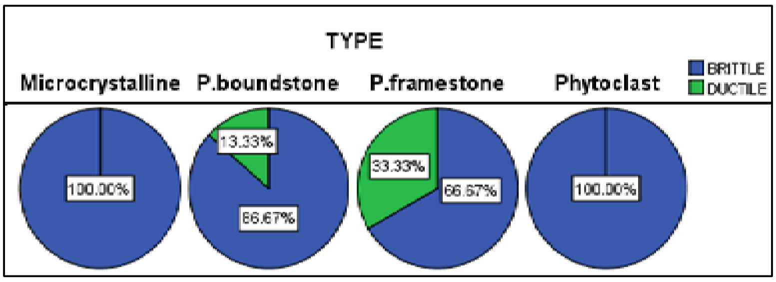

Figure 81. Proportion of the brittle and ductile samples of the Antalya tufa rock types.

VII.2.3.3.4 Brazilian indirect tensile strength test

In order to determine the indirect tensile strength of the tufa rock types, Brazilian indirect tensile strength tests have been carried out in accordance with the relevant ISRM standard. Table 21 and Figure 82 present the results of the 47 samples tested. The mean Brazilian tensile strength value of the tufa rock mass ± one standard deviation has been determined to be 1.84 MPa ± 1.36 (Table 22). Brazilian indirect tensile strength of the tufa rock samples have been calculated by Eq. (6):

$$T = \frac{2P}{\pi t D} \qquad \text{Eq. (6)}$$

where,

T is the tensile strength, P is the maximum load at failure, D is the diameter and t is the thickness of the sample.

Table 21. The results of the Brazilian indirect tensile strength tests.

Sample No.	Thickness (mm)	Diameter (mm)	Failure load (kgf)	Indirect tensile strength (MPa)
B3c	79.0	54.00	582	0.85
B3d	63.0	54.34	450	0.82
B3e	45.0	54.00	524	1.35
B4b	60.0	54.25	624	1.20
B4c	31.0	53.80	189	0.71
B5e	73.0	53.90	980	1.55
B5f	54.0	54.37	1214	2.58
B5g	44.0	54.13	978	2.56
B5h	27.0	54.00	160	0.69
B6e	48.4	54.00	631	1.51
B6g	24.9	53.80	480	2.24
B6f	15.4	54.40	950	7.08
B78f	43.7	54.00	127	0.34
M1g	56.5	54.00	2401	4.91
M1h	52.0	54.13	1482	3.29
M3i	46.5	54.20	1190	2.95
M3j	53.0	54.58	1702	3.67
M3k	55.5	54.33	621	1.29
M4e	43.0	54.38	1400	3.74
M4f	51.0	54.34	1331	3.00
M5j	36.8	53.90	1166	3.67
M5i	41.4	54.00	298	0.83
M5k	32.0	54.00	1132	4.09
M5l	23.6	54.00	446	2.18
P1h	54.0	54.34	232	0.49
P3c	55.0	54.26	240	0.50
P3d	58.5	54.13	55	0.11
P8e	59.7	54.00	895	1.73
P8f	45.9	54.20	748	1.88
P8g	33.3	54.30	600	2.07
P8g	36.2	54.00	360	1.15
P9e	30.7	53.90	463	1.75
P9f	32.7	54.00	686	2.43
PF2a	49.0	54.13	215	0.51
PF2b	59.0	54.13	556	1.09
PF2c	36.0	54.00	132	0.42
PF3d	35.5	54.28	154	0.50
PF4e	51.0	54.16	1057	2.39
PF4f	53.5	54.50	841	1.80
PF5d	75.0	54.08	476	0.73
PF5e	53.0	54.13	834	1.81
PF5f	60.5	54.10	492	0.94
PF6l	50.0	54.30	357	0.82
PF6m	34.0	54.00	391	1.33
PF6n	21.9	54.20	230	1.21
PF6o	24.4	54.00	467	2.21
PF7e	60.2	54.00	727	1.40

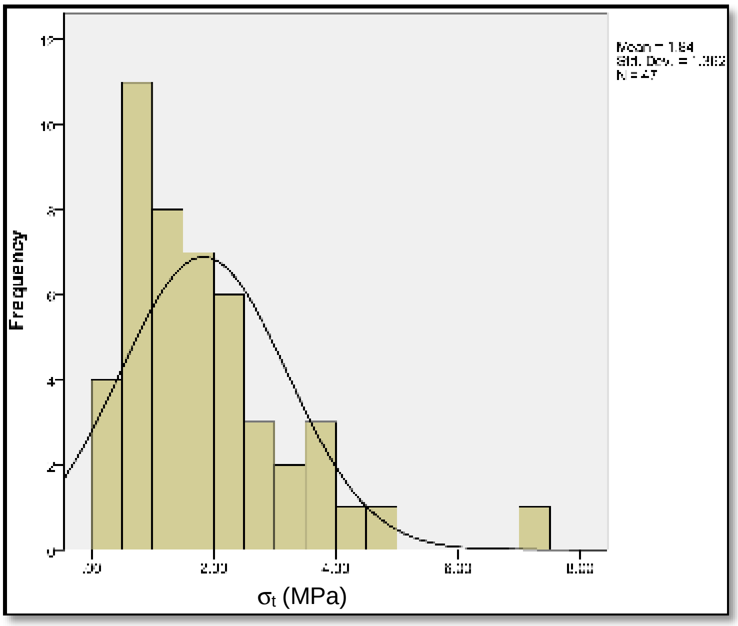

Figure 82. A histogram illustrating the Brazilian tensile strength values of the Antalya tufa rock mass.

Table 22. The mean Brazilian tensile strength value of the tufa rock types and the tufa rock mass ± one standard deviation.

Tufa type	σ_t (MPa)
Microcrystalline	3.1 ± 1.2
Phytoherm boundstone	1.8 ± 1.7
Phytoherm framestone	1.4 ± 0.8
Phytoclast	1.2 ± 0.6
Tufa rock mass	1.8 ± 1.4

Figure 83 represents the Brazilian tensile strength test results of the tufa rock types tested where the microcrystalline tufa and the phytoclast tufa yield the highest and lowest tensile strength capacity values, respectively. Since it was not possible to recover samples from the intraclast type, no information on its tensile strength capacity has been obtained. However, it is believed that it would have been more or less the same of the phytoclast type.

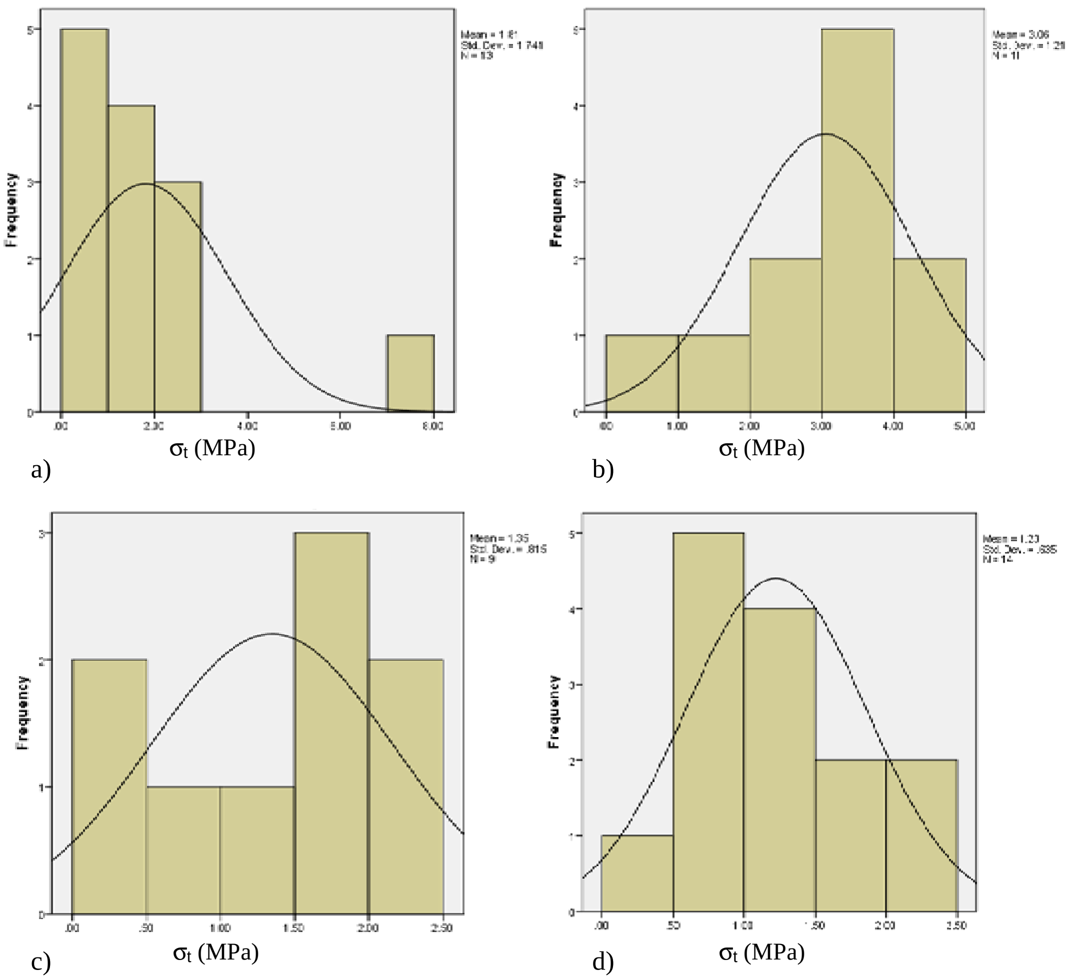

Figure 83. Histograms of tensile strength values of Antalya tufa rock types. a. Phytoherm boundstone. b. Microcrystalline. c. Phytoherm framestone. d. Phytoclast.

VII.2.3.3.5 Point load strength index tests

The point load strength index tests of the tufa rock masses have been carried out in accordance with the relevant ISRM standard (ISRM, 1981) in order to measure the point load strength index of the tufa rock types and the tufa rock mass. Another purpose of estimating the point load strength index was to determine the uniaxial compressive strength (UCS) of the tufa rock mass through various correlations available between the point load strength index and the uniaxial compressive strength of rock materials in the literature, where the results of these tests are thought to be valuable in case of the absence of UCS data. A total of 52 point load strength index tests have been carried out as tabulated in Table 23. The mean index value including both the diametral and the axial cases of the tufa rock mass ± one standard deviation has been determined to be 1.34 ± 1.24 MPa (Table 24). Point load strength index of the tufa rock samples have been calculated by the Eq. (7).

$$I_{s(50)} = F \times I_s \qquad \text{Eq. (7)}$$

where,

$I_s = P/{D_e}^2$

$F = size\ correction\ factor = \left(D_e/50\right)^{0.45}$

P= failure load,

D_e= equivalent core diameter: D^2 for diametral core tests, $4A/\pi$ for axial, block and lump tests (Figure 84),

A= WD = minimum cross sectional area of a plane through the platen contact points (Figure 84).

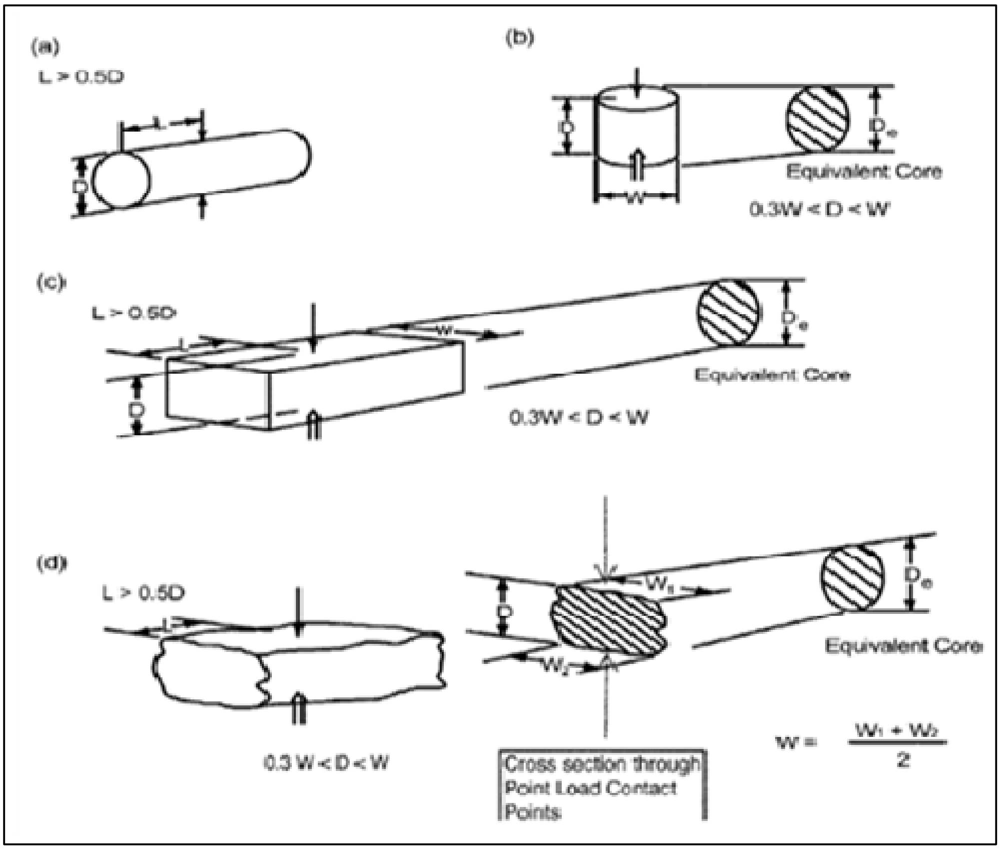

Figure 84. Load configurations and specimen shape requirement for (a) the diametral test, (b) the axial test, (c) the block test, and (d) the irregular lump test.

Table 23. The results of the point load strength index tests.

Sample No.	D	L	w_1	w_2	W	P	Diametral $I_{s(50)}$	Axial $I_{s(50)}$	Diametral	Axial
	(mm)	(mm)	(mm)	(mm)	(mm)	(kgf)	(MPa)	(MPa)	k	k
B4-1	25.0	26.5	53.5	42.3	47.9	545	-	3.14	-	21.0
B4-2	39.0	44.0	68.2	48.9	58.6	1099	-	3.84	-	23.6
B4-2A	29.0	32.0	-	-	56.0	159	-	0.72	-	22.1
B4-2B	38.0	42.0	-	-	41.4	415	-	1.93	-	22.0
B4-2C	24.0	31.0	-	-	41.5	2000	-	13.28	-	20. 5
B4-3	36.0	30.0	82.0	71.0	76.5	969	-	2.92	-	24.5
B4-4	57.2	41.0	-	-	76.7	356	-	0.75	-	27.1
B4-5	73.0	34.0	-	-	46.0	792	-	2.05	-	25.5
B3-1	31.0	51.0	-	-	51.0	182	-	0.84	-	22.0

Table 23 (cont'd.). The results of the point load strength index tests.

Sample No.	D	L	w_1	w_2	W	P	Diametral $I_{s(50)}$	Axial $I_{s(50)}$	Diametral	Axial
	(mm)	(mm)	(mm)	(mm)	(mm)	(kgf)	(MPa)	(MPa)	k	k
B3-2	53.0	63.0	-	-	80.6	172	-	0.37	-	26.9
B3-2A	84.0	33.0	-	-	48.0	90	-	0.20	-	26.6
B2-1	60.6	31.0	-	-	62.0	304	-	0.72	-	26.2
B2-2	59.0	41.0	55.0	50.0	52.5	379	-	1.04	-	25.1
M1-1	28.0	45.0	50.0	60.0	55.0	394	-	1.87	-	21.9
M1-2	36.0	26.0	38.0	34.0	36.0	339	-	1.83	-	21.3
M1-3	42.0	42.0	-	-	77.0	234	-	0.62	-	25.3
M1-4	51.0	36.0	-	-	68.0	308	-	0.78	-	25.7
M1-4A	38.0	33.0	74.8	44.0	59.4	327	-	1.15	-	23.5
M4-1	23.54	-	-	-	54.2	294	-	1.61	-	21.3
M4-2	35.7	-	-	-	53.9	284	-	1.13	-	22.8
M4-3	16.0	-	-	-	54.0	251	-	1.86	-	20.0
M4-4	54.3	39.0	-	-	-	652	2.25	-	23.6	-
M3-1	30.0	30.0	-	-	72.0	650	5.63	-	19.5	-
M3-2	32.0	26.0	62.0	40.6	51.3	521	4.08	-	19.8	-
M3-3	48.0	43.0	80.0	47.0	63.5	893	3.73	-	22.6	-
M3-4	45.0	45.0	53.7	78.0	65.9	848	3.92	-	22.1	-
P1-1	73.5	42.0	-	-	65.5	278	0.60	-	26.9	27.7
P1-2	33.0	48.0	46.0	61.0	53.5	405	3.03	-	20.0	22.5
P1-3	59.0	38.0	72.0	60.0	66.0	188	0.57	-	24.4	26.4
P2-1	30.45	-	-	-	50.1	68	-	0.32	-	21.9
P2-2	65.5	-	-	-	53.1	154	-	0.39	-	25.7
P3-1	49.3	-	-	-	52.3	44	-	0.14	-	24.1
P3-2	32.4	-	-	-	61.8	92	-	0.36	-	22.9
P3-3	43.0	-	-	-	49.2	49	-	0.18	-	23.2
P3-4	53.0	-	-	-	62.3	209	-	0.55	-	25.4
P3-4A	58.0	-	-	-	58.0	175	-	0.45	-	25.5
P3-5	46.0	53.0	77.0	57.5	67.3	125	-	0.34	-	25.1
P3-5A	46.0	53.0	74.0	54.0	64.0	250	-	0.72	-	24.8
P3-6	40.0	34.0	59.6	50.0	54.8	86	-	0.31	-	23.4
P3-7	30.5	55.0	58.5	58.1	58.3	222	-	0.94	-	22.5
PF2-1	47.7	44.0	75.3	57.9	66.6	175	-	0.47	-	25.2
PF2-1A	51.9	-	-	-	51.8	95	-	0.29	-	24.4
PF2-2	50.4	51.8	55.3	59.3	57.3	57	-	0.17	-	24.7

Table 23 (cont'd.). The results of the point load strength index tests.

Sample No.	D	L	w_1	w_2	W	P	Diametral $I_{s(50)}$	Axial $I_{s(50)}$	Diametral	Axial
	(mm)	(mm)	(mm)	(mm)	(mm)	(kgf)	(MPa)	(MPa)	k	k
PF3-1	50.5	25.2	-	-	-	187	0.72	-	22.9	14.4
PF3-1A	30.0	-	-	-	50.5	34	-	0.16	-	21.9
PF3-1B	40.5	-	-	-	50.5	228	-	0.87	-	23.1
PF3-2	54.1	48.0	-	-	-	541	1.88	-	23.597	14.4
PF3-2A	52.5	-	-	-	54.1	218	-	0.64	-	24.6
PF4-1	30.0	46.0	50.0	74.5	62.3	403	-	1.64	-	22.7
PF4-2	58.0	38.0	-	-	54.0	404	-	1.10	-	25.1
PF4-3	47.0	39.0	-	-	60.0	405	-	1.20	-	24.6
PF4-3A	47.0	35.0	-	-	44.0	406	-	1.53	-	23.1

In Figure 85, the mean point strength index value including both the diametral and axial cases of the tufa rock mass types ± one standard deviation has been illustrated by means of histograms.

Table 24. The mean point load strength index value of the tufa rock types and the tufa rock mass ± one standard deviation.

Tufa type	I_{s50} (MPa)
Microcrystalline	2.34 ± 1.52
Phytoherm boundstone	1.59 ± 1.26
Phytoherm framestone	0.64 ± 0.72
Phytoclast	0.89 ± 0.59
Tufa rock mass	1.34 ± 1.24

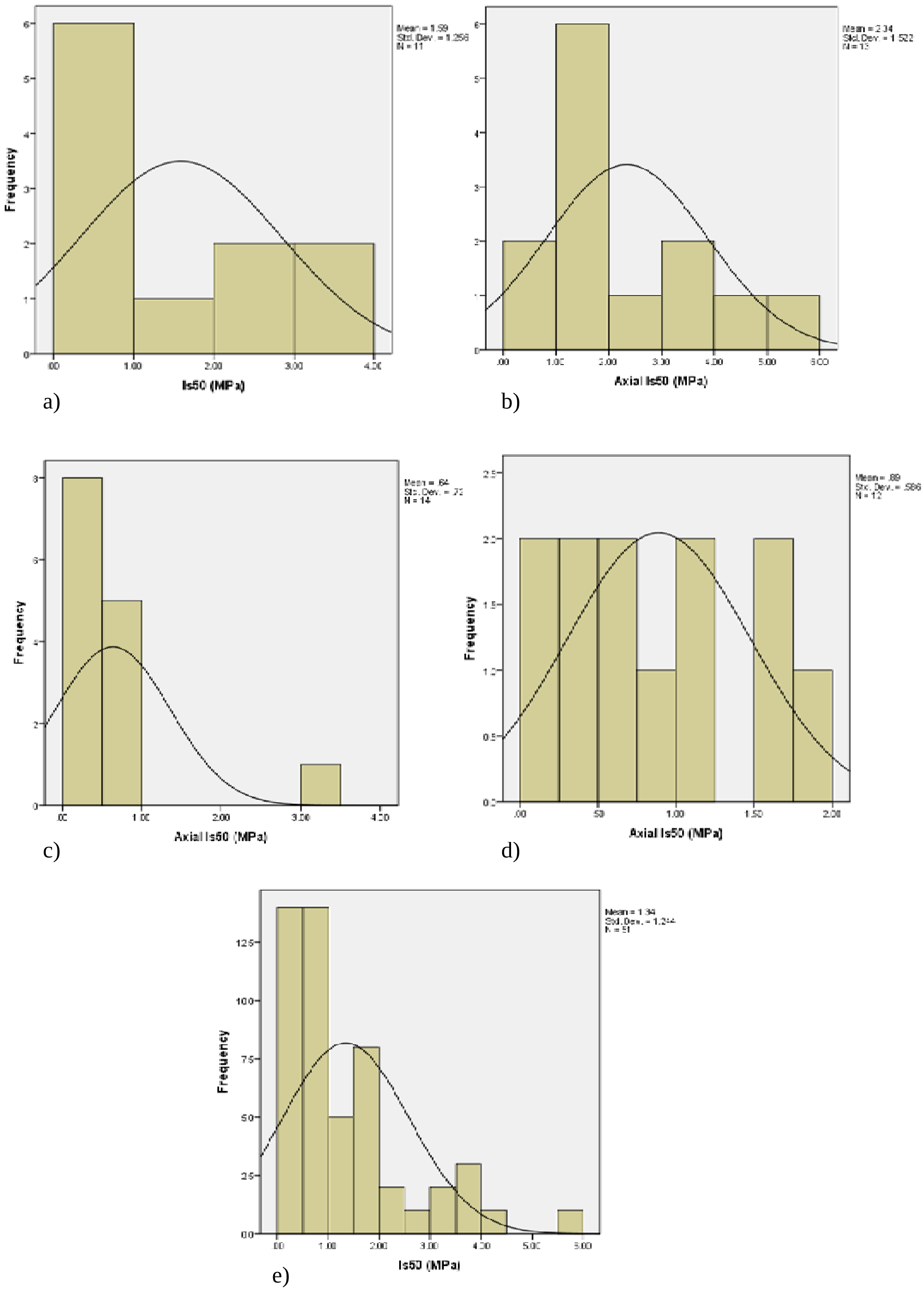

Figure 85. Histograms of point load strength index values of the Antalya tufa. a) Phytoherm boundstone. b) Microcrystalline. c) Phytoherm framestone. d) Phytoclast e) Antalya tufa rock mass

VII.2.3.3.6 The slake durability test

The slake durability test is one of the methods utilized to determine the durability of the weak rock masses. The main purpose is to accelerate the weathering of the rock samples with slaking, rotation and sieving processes. A total number of 34 slake durability tests have been carried out in accordance with the relevant ISRM standard (ISRM, 1981) and with the ASTM D4644 standard. Although two cycles are mentioned to be sufficient in these standards, more than two cycles have been employed in the slake durability testing of a number of tufa rock samples in this study. The aim was to observe the effects of further weathering and water reaction.

Table 25 illustrates the results of the slake durability tests. According to the weathering classes proposed based on the slake durability index by Franklin and Chandra (1972), the majority of the tufa samples tested were in the extremely high (Id_2= 95%-100 %) and very high (Id_2= 90%-95 %) class (Figure 86 and Table 26).

Table 25. Classification of durability (Franklin and Chandra, 1972)

Ground	Classification of durability	Slake durability index Id_2 (%)
SOIL	Very low	0 – 25
	Low	25 – 50
	Medium	50 – 75
	High	75 – 90
ROCK	Very high	90 – 95
	Extremely high	95 – 100

Table 26. The results of the slake durability tests.

Sample No.	Id-1* (%)	Id-2 (%)	Id-3 (%)	Id-4 (%)	Id-5 (%)	Id-6 (%)	Id-7 (%)	Id-8 (%)	Id-9 (%)	Id-10 (%)
B1	97.66	96.66	95.99	94.98	-	-	-	-	-	-
B2	99.40	99.00	98.59	98.19	-	-	-	-	-	-
B2	99.40	99.00	98.59	98.19	97.59	96.59	96.18	95.98	95.78	95.38
B3	93.33	89.05	-	-	-	-	-	-	-	-
B3	94.10	91.20	-	-	-	-	-	-	-	-
B3	94.30	91.60	-	-	-	-	-	-	-	-
B4	98.98	98.73	-	-	-	-	-	-	-	-
B5	98.86	98.86	-	-	-	-	-	-	-	-
I1	91.70	87.30	-	-	-	-	-	-	-	-
I1	93.20	90.20	-	-	-	-	-	-	-	-
I1	79.38	75.26	72.68	70.62	-	-	-	-	-	-
M1	99.62	98.87	-	-	-	-	-	-	-	-
M2	98.70	98.10	-	-	-	-	-	-	-	-
M2	98.40	97.60	-	-	-	-	-	-	-	-
M3	99.42	99.23	-	-	-	-	-	-	-	-
M5	99.18	98.77	-	-	-	-	-	-	-	-
P1	99.57	97.39	-	-	-	-	-	-	-	-
P3	100.00	99.27	-	-	-	-	-	-	-	-
P3	98.44	89.56	-	-	-	-	-	-	-	-
P6	98.56	98.15	-	-	-	-	-	-	-	-
P7	97.40	96.90	-	-	-	-	-	-	-	-
P7	97.10	96.40	-	-	-	-	-	-	-	-
P7	98.98	98.47	97.97	97.46	-	-	-	-	-	-
P8	97.08	97.08	95.38	94.89	-	-	-	-	-	-
PF1	99.80	99.39	-	-	-	-	-	-	-	-
PF1	95.20	92.10	-	-	-	-	-	-	-	-
PF1	95.50	94.50	-	-	-	-	-	-	-	-
PF2	96.80	95.20	94.00	93.20	-	-	-	-	-	-
PF3	99.39	99.39	-	-	-	-	-	-	-	-
PF4	98.99	98.79	-	-	-	-	-	-	-	-
PF4	99.02	98.85	97.54	97.05	-	-	-	-	-	-
PF4	98.99	98.79	97.79	96.78	95.98	94.57	93.36	92.35	91.55	90.74
PF5	96.36	92.91	-	-	-	-	-	-	-	-
PF6	97.67	96.40	95.34	94.07	-	-	-	-	-	-

* Id-1, Id-2, through Id-n represent the number of cycles employed during testing.

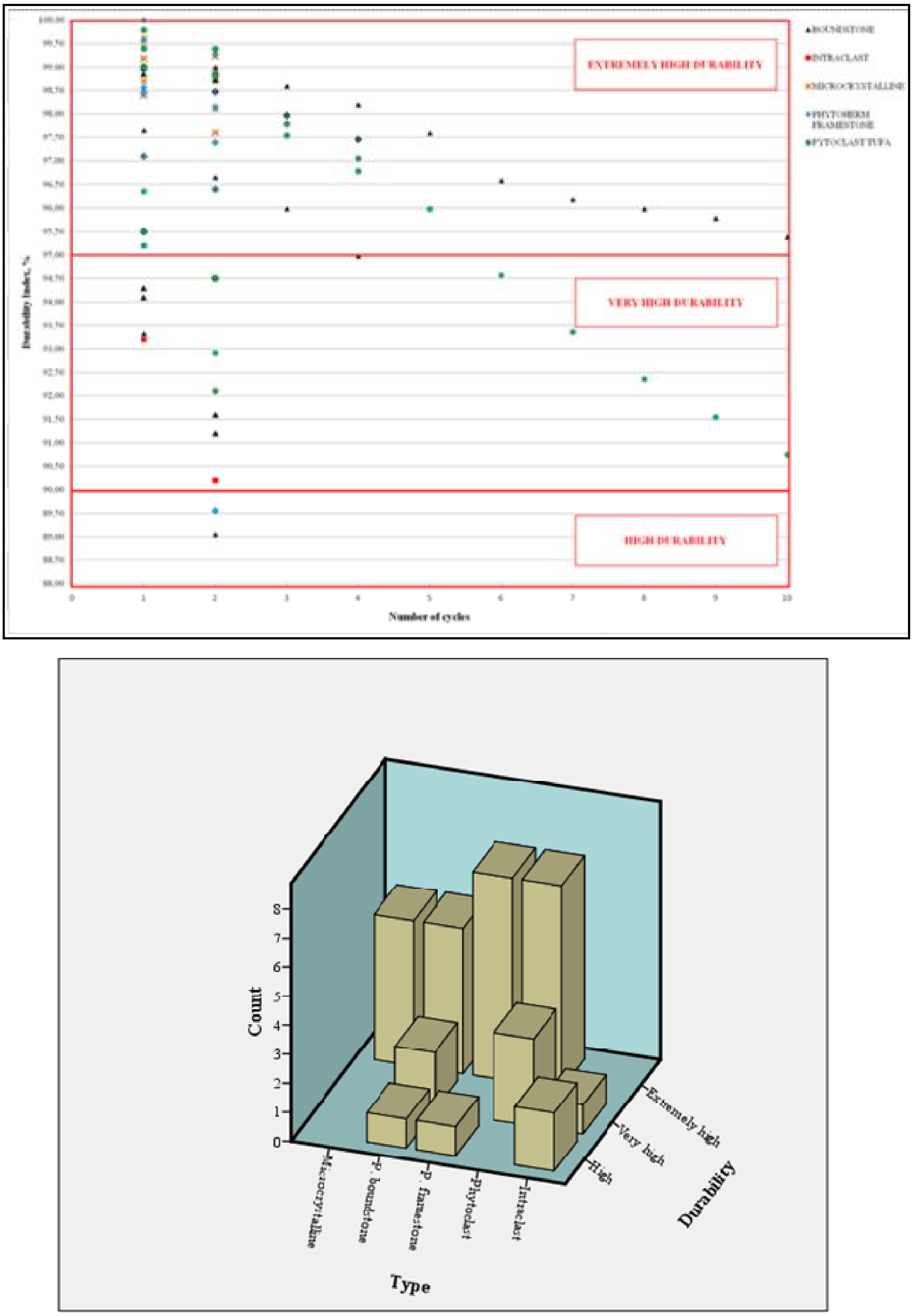

Figure 86. Results of slake durability tests of the Antalya tufa rock types.

VII.3 Correlations between the strength parameters of the Antalya tufa rock mass

Upon completion of the above mentioned in-situ and the laboratory geotechnical investigations, some relationships between the strength parameters of the tufa rock types have been observed. Correlations between these parameters have been made for both the entire tufa rock mass and for the individual tufa rock types as described in the following sections.

VII.3.1 Correlations between the uniaxial compressive strength and other parameters of the Antalya tufa rock mass

1. UCS and unit weight correlations of the Antalya tufa rock mass

In addition to the results of the 40 UCS laboratory tests carried out in this study, 333 UCS laboratory test results have been compiled from previous site investigation studies that were mentioned in Chapter II. The distribution of the 373 UCS test results according to the tufa rock types is presented by Table 27.

Table 27. The number of UCS tests performed on each tufa rock type.

Tufa type	Number of UCS tests
Microcrsytalline	275
P. framestone	75
P. boundstone	10
Intraclast	4
Phytoclast	9
Total	**373**

All of the results of the UCS tests possessed the unit weight data, as well. A correlation between the UCS and the unit weight (γ) of the tufa rock types is presented by Figure 87. Figures 88 through 93 illustrate the regression plots for the Antalya tufa rock types.

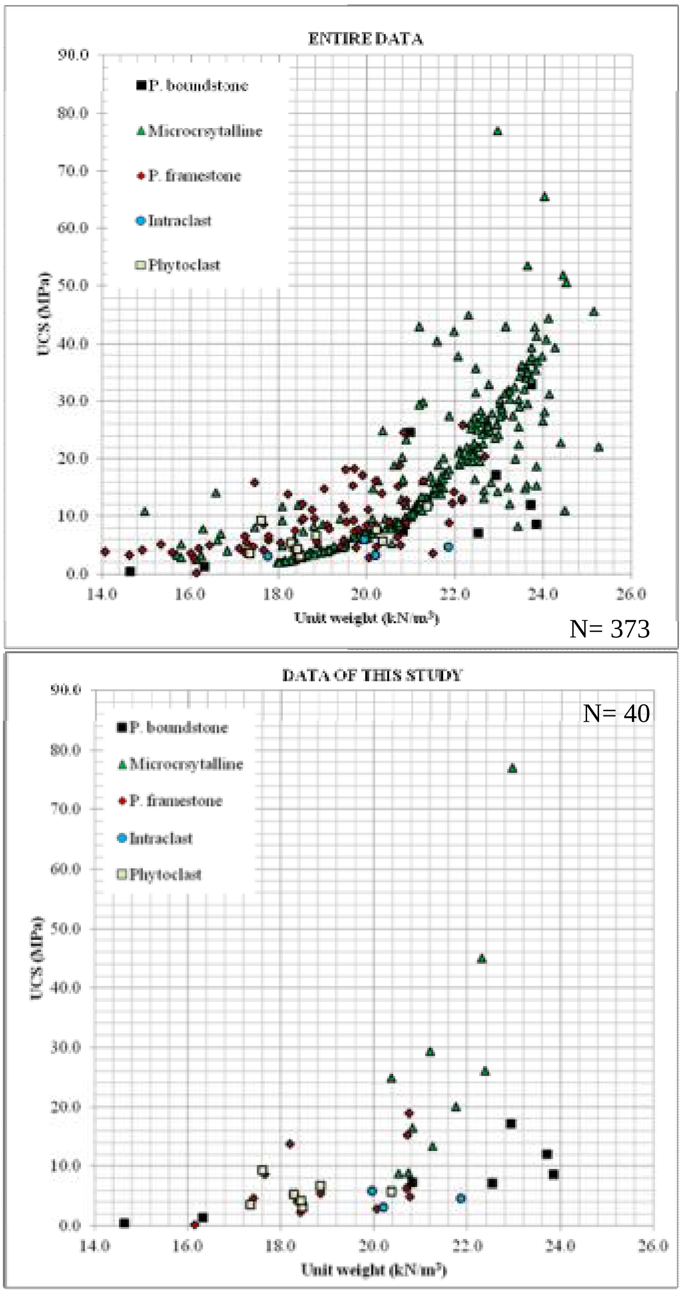

Figure 87. Plots of UCS versus unit weight of the Antalya tufa rock types.

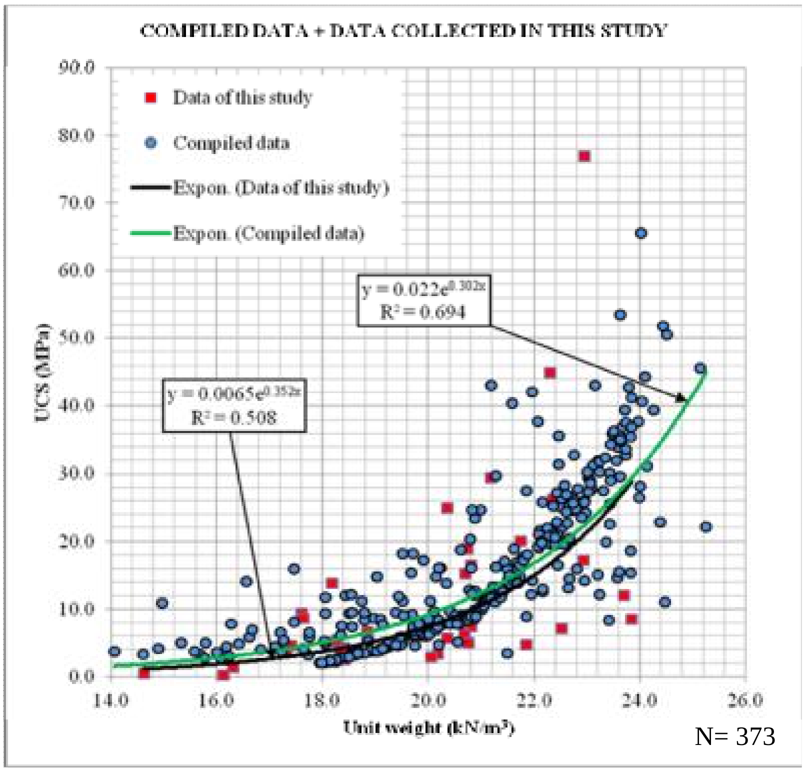

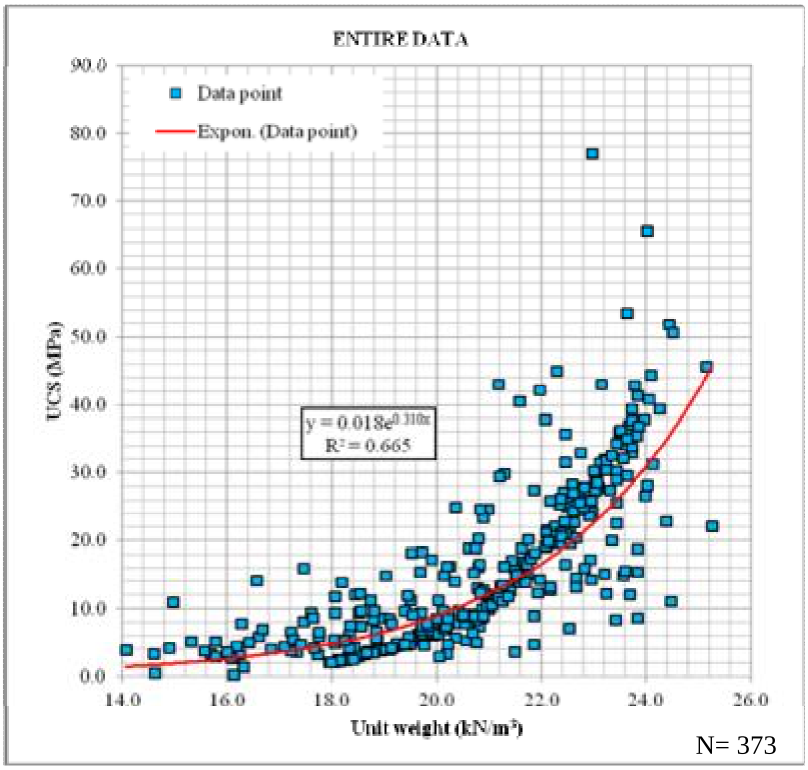

Figure 88. Regression plots of UCS vs. unit weight of the Antalya tufa rock mass.

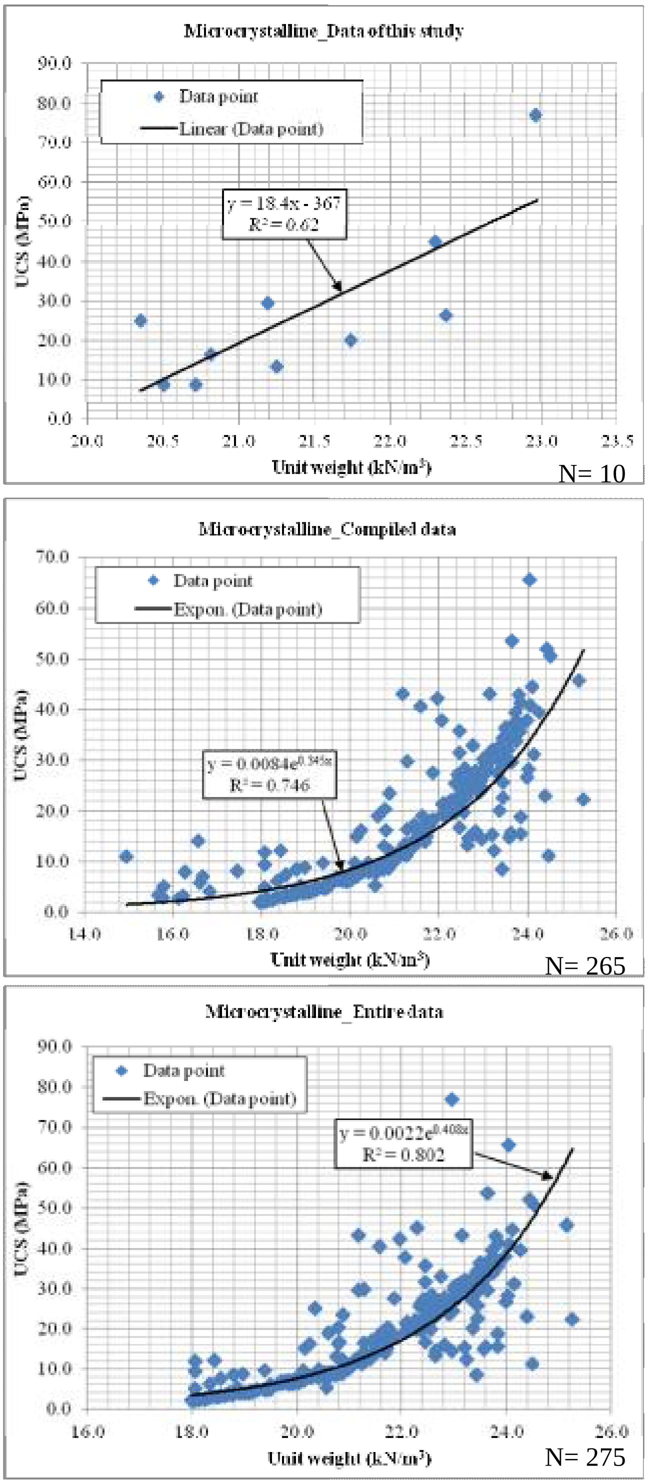

Figure 89. Regression plots of UCS vs. unit weight for the microcrsytalline tufa type.

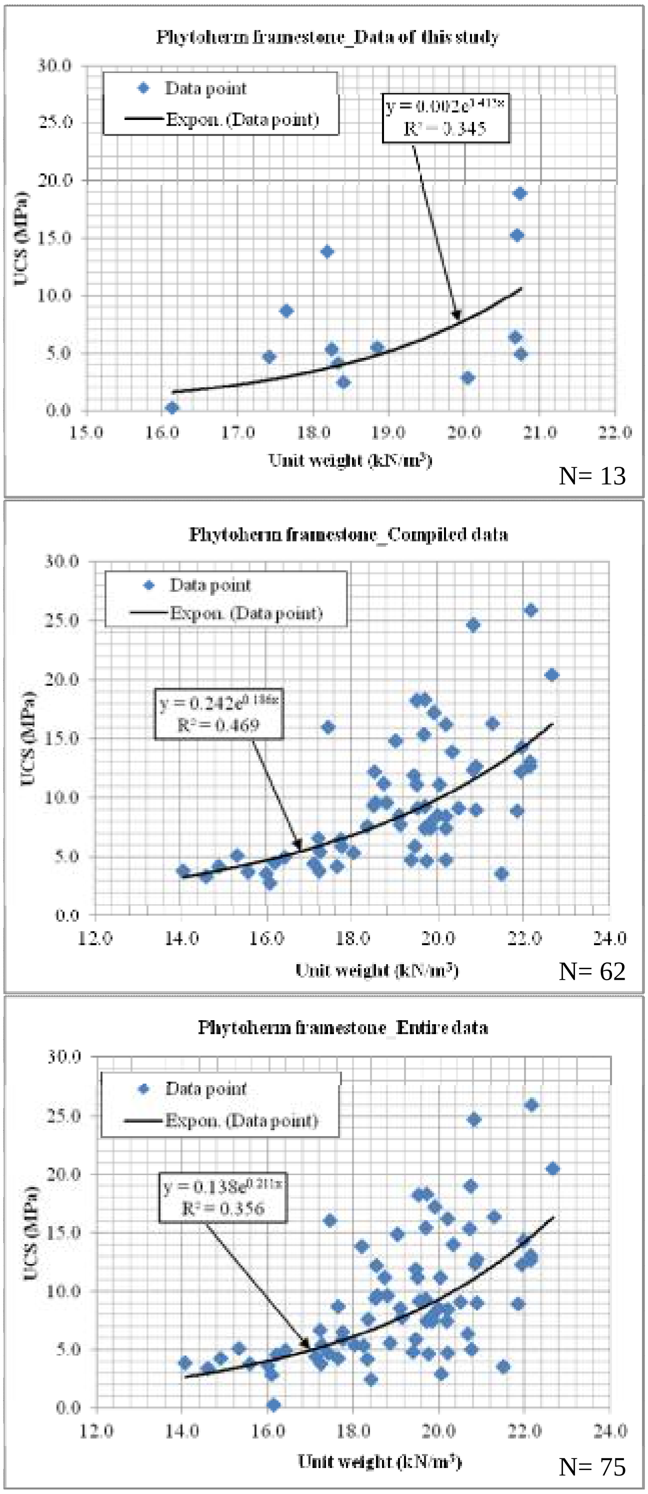

Figure 90. Regression plots of UCS vs. unit weight for the phytoherm framestone tufa type.

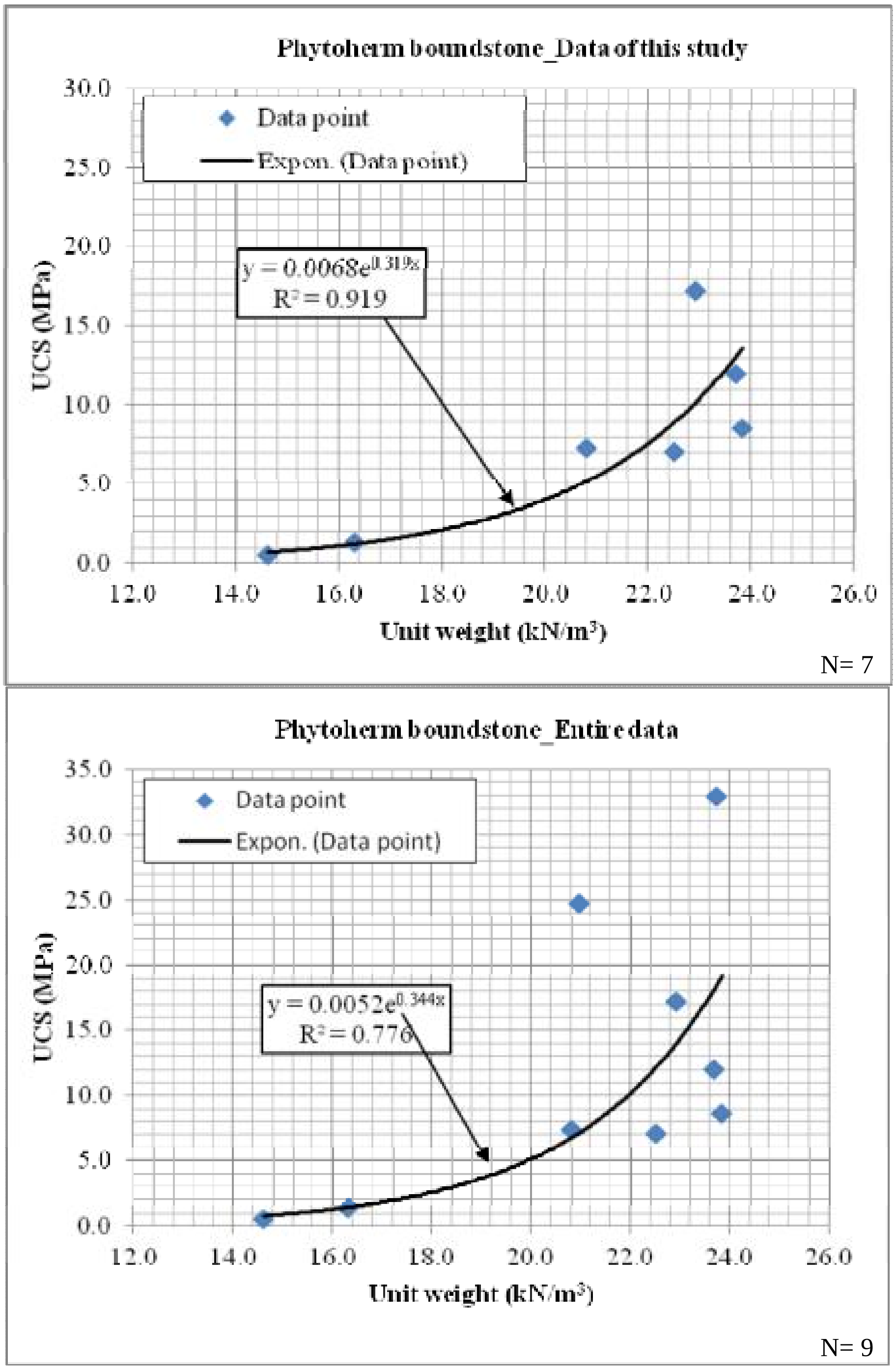

Figure 91. Regression plots of UCS vs. unit weight for the phytoherm boundstone tufa type.

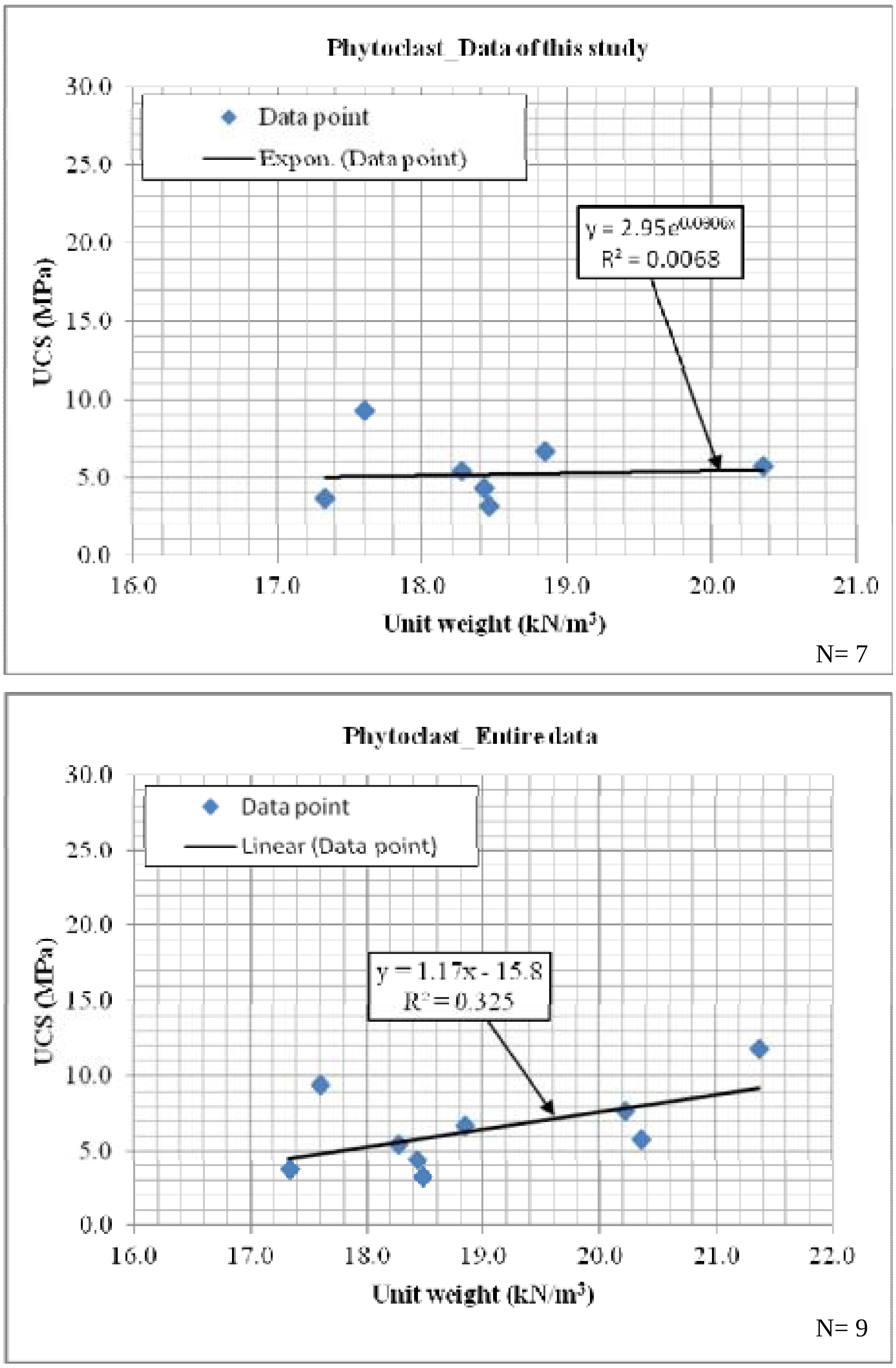

Figure 92. Regression plots of UCS vs. unit weight for the phytoclast tufa type.

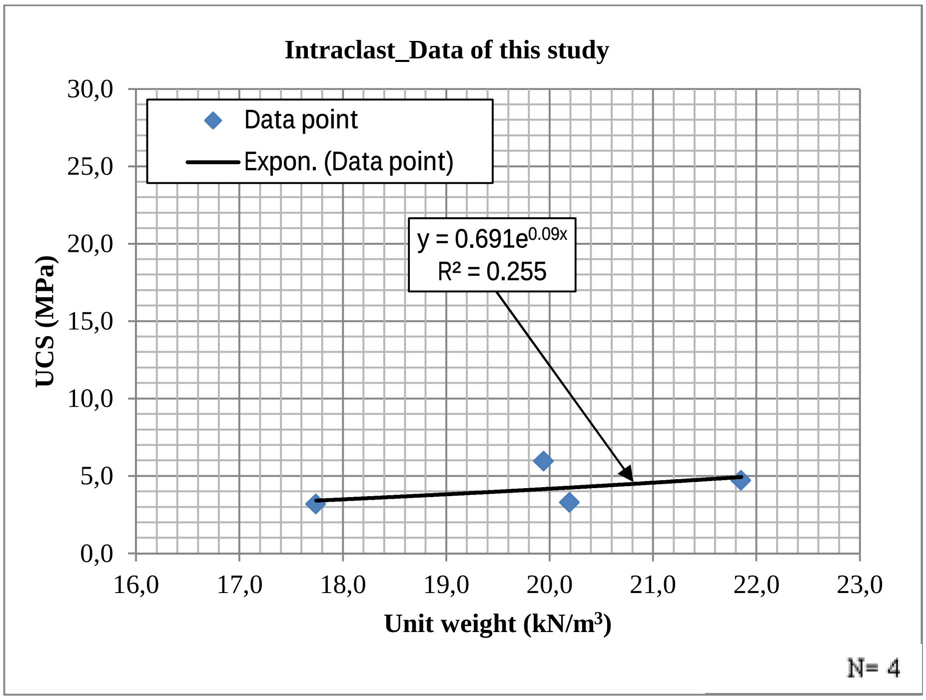

Figure 93. Regression plots of UCS vs. unit weight for the intraclast tufa type.

2. UCS and porosity correlations of the Antalya tufa rock mass

In order to correlate the UCS of the Antalya tufa rock masses with its porosity (n) values, only the data obtained from this study have been used. It is believed that there were many unreliable data in the previous studies. Accordingly, 40 measurements from this study have been utilized to determine the relation between UCS and the porosity (n) of the Antalya tufa rock mass and of the rock types (Figure 94).

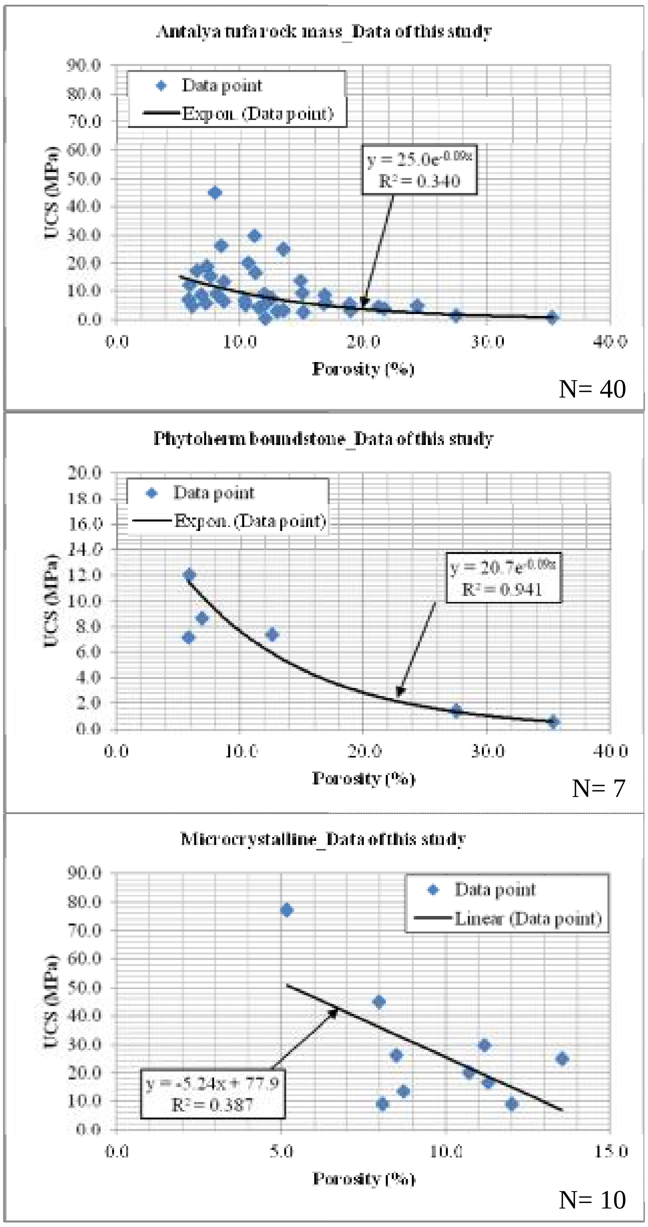

Figure 94. Regression plots of UCS vs. porosity for the Antalya tufa rock mass and tufa rock types.

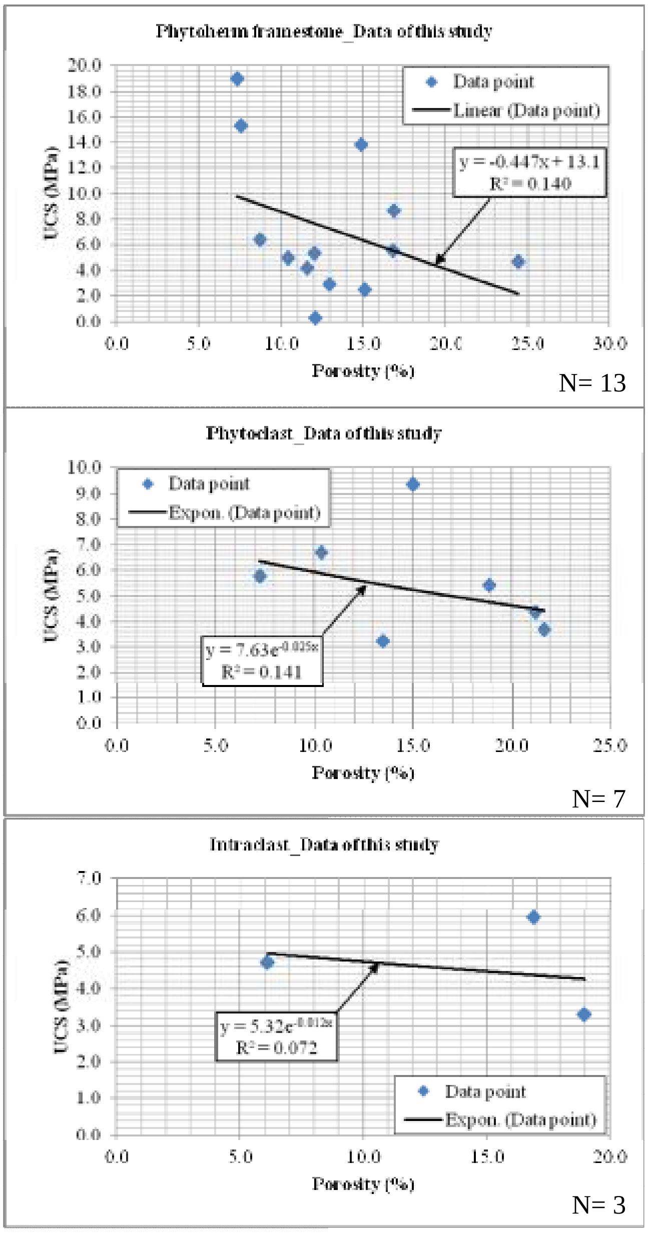

Figure 94 (cont'd.). Regression plots of UCS vs. porosity for the Antalya tufa rock mass and tufa rock types.

3. UCS and Elasticity modulus correlations of the Antalya tufa rock mass

The only reliable and available data set for the correlation between UCS and the Elasticity modulus (E) of the Antalya tufa rock mass has been obtained through UCS tests performed for this study. Accordingly, the following relations between the UCS and the Elasticity modulus of the Antalya tufa rock mass have been determined (Figures 95 and 96).

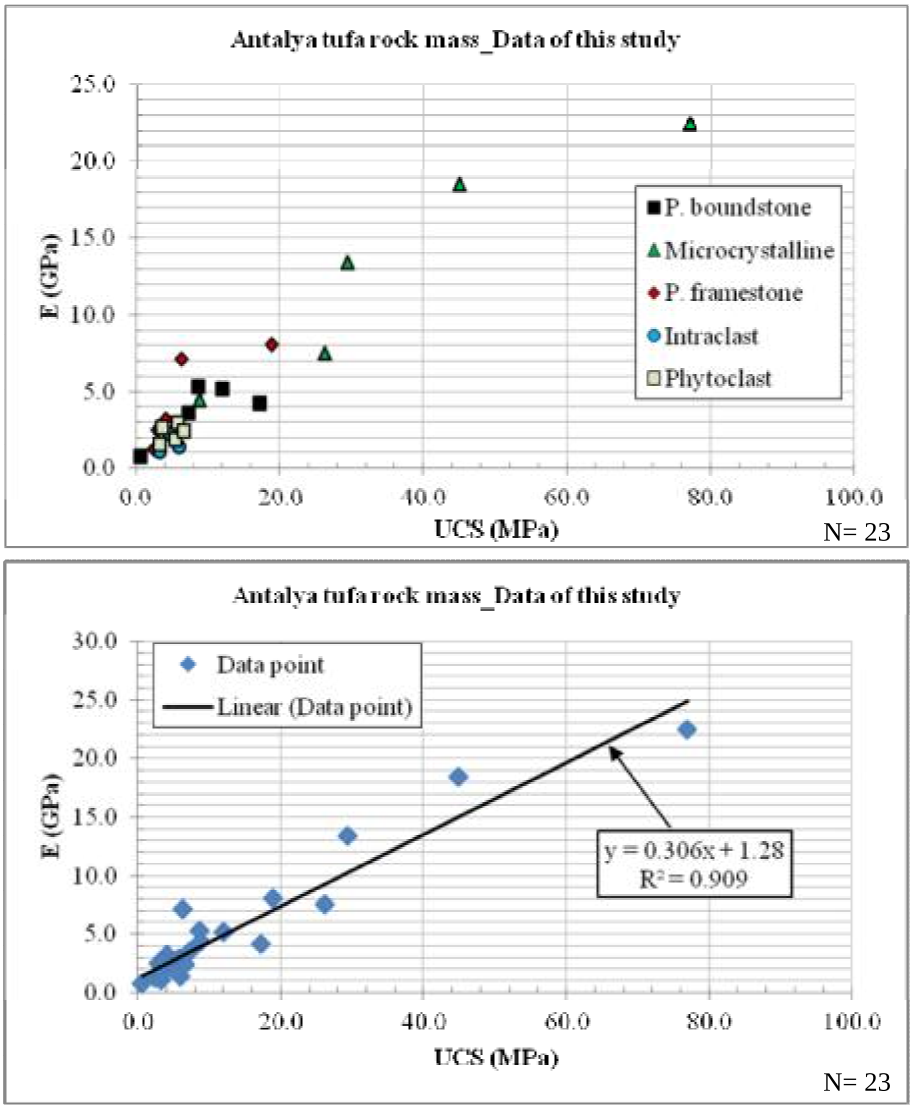

Figure 95. Regression plots of UCS vs. Elasticity modulus for the Antalya tufa rock mass.

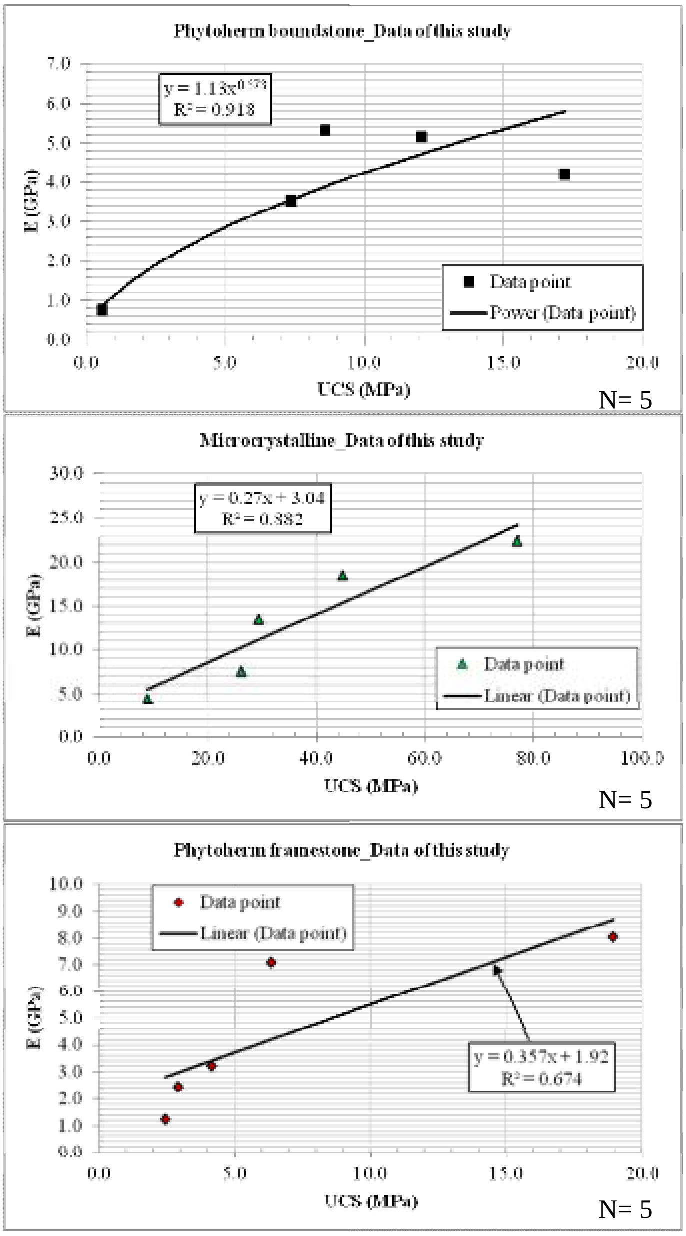

Figure 96. Regression plots of UCS vs. Elasticity modulus for the Antalya tufa rock types.

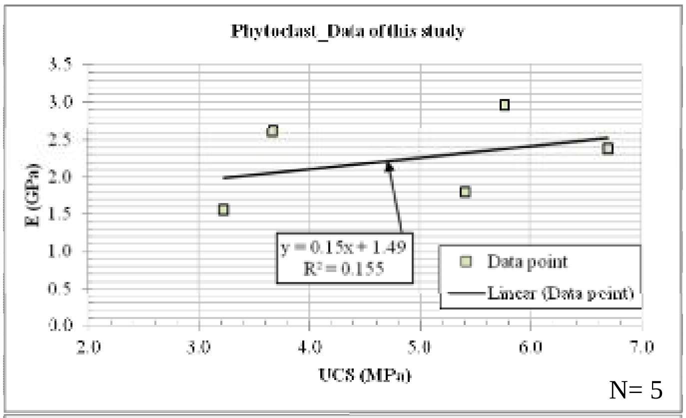

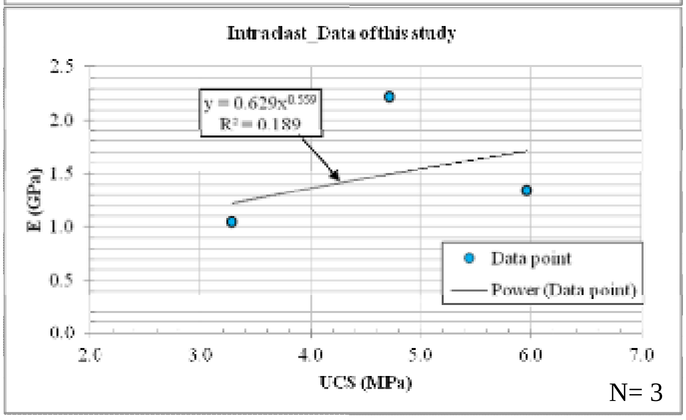

Figure 96 (cont'd.) Regression plots of UCS vs. Elasticity modulus for the Antalya tufa rock types.

<u>*4. UCS and tensile strength correlations of the Antalya tufa rock mass*</u>

The only reliable data set for the correlation between UCS and the tensile strength (σ_t) of the Antalya tufa rock types except the intraclast type has been obtained through the tests carried out during this study. Accordingly, the following relations between UCS and the tensile strength of the Antalya tufa rock mass and tufa rock types have been determined (Figure 97).

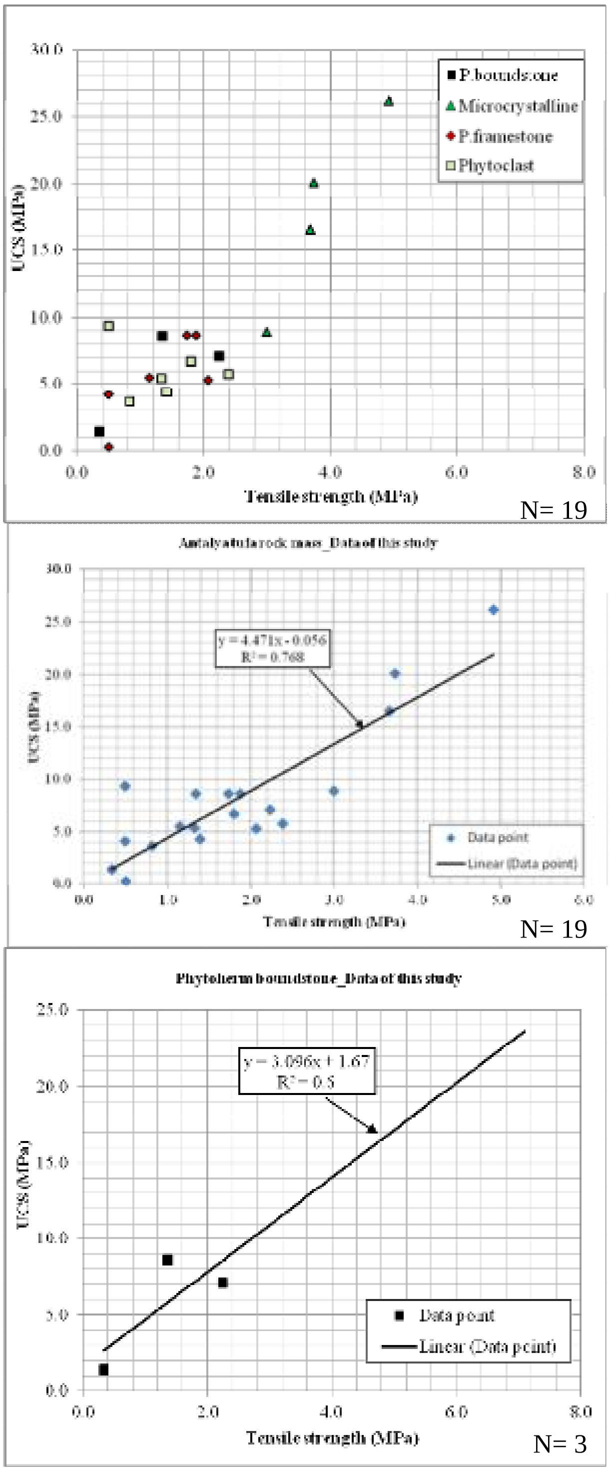

Figure 97. Regression plots of UCS vs. tensile strength for the Antalya tufa rock mass and rock types.

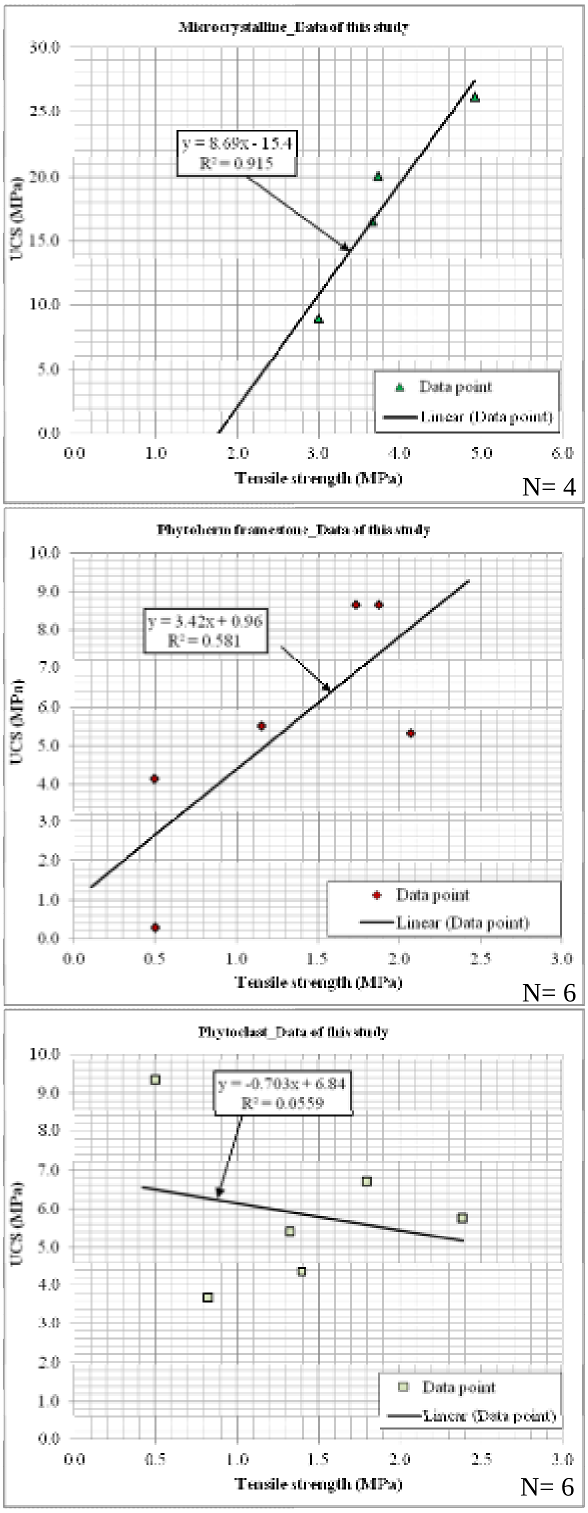

Figure 97 (cont'd.) Regression plots of UCS vs. tensile strength for the Antalya tufa rock mass and rock types.

5. UCS and point load strength index correlations of the Antalya tufa rock mass

The correlation between UCS and point load strength index (Is_{50}) of the Antalya tufa rock mass has been made based on the data set developed in this study as follows (Figure 98).

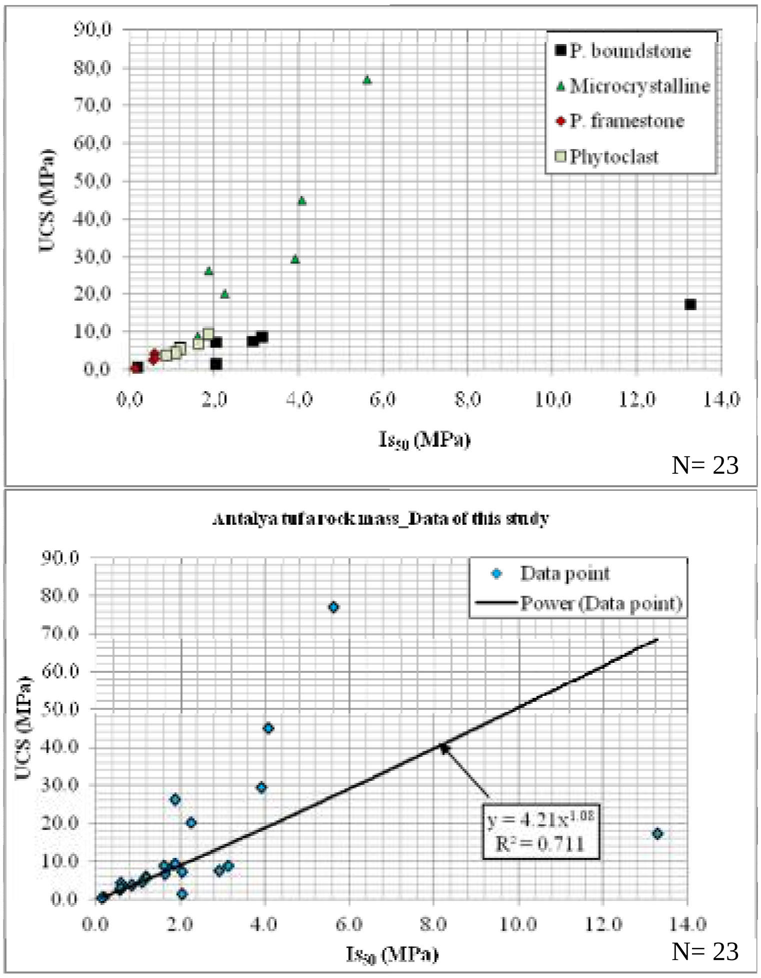

Figure 98. Regression plot of UCS vs. point load strength index for the Antalya tufa rock mass and tufa rock types.

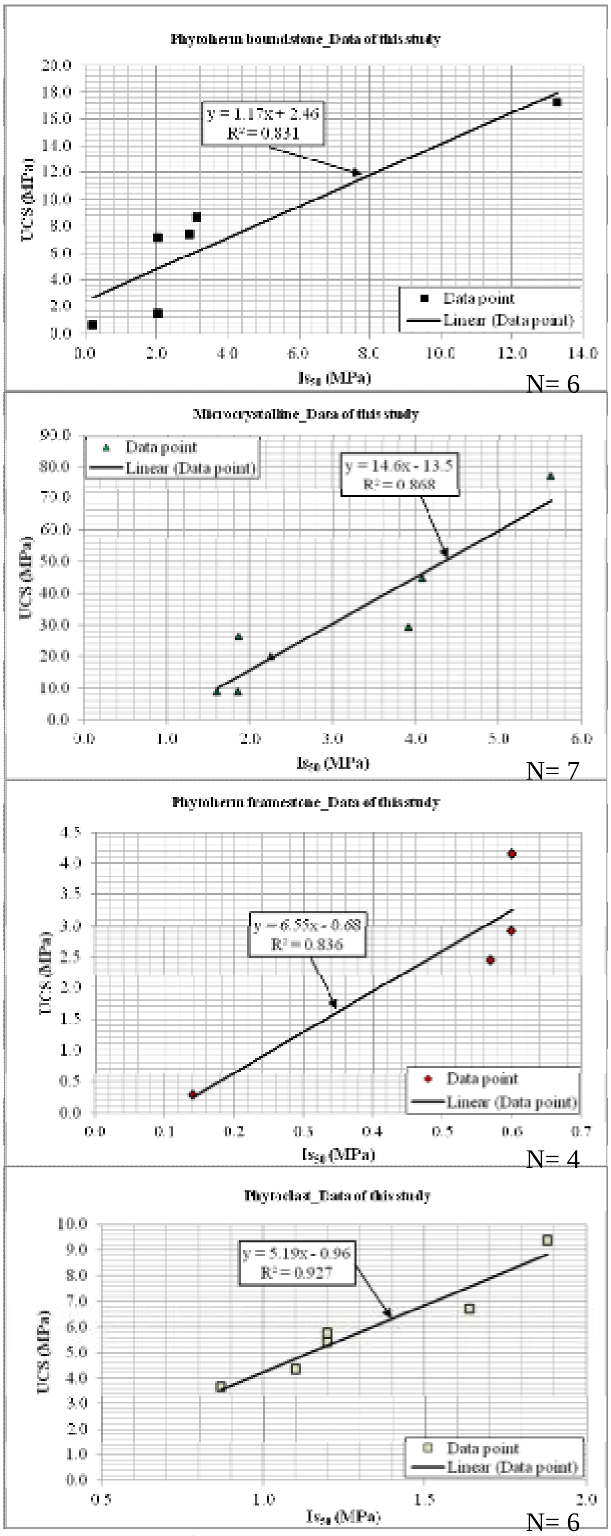

Figure 98 (cont'd.). Regression plot of UCS vs. point load strength index for the Antalya tufa rock mass and tufa rock types

6. UCS and slake durability correlations of the Antalya tufa rock mass

The correlation between UCS and slake durability index (Id_2) of the Antalya tufa rock mass has been made based on the data set developed in this study as follows (Figure 99).

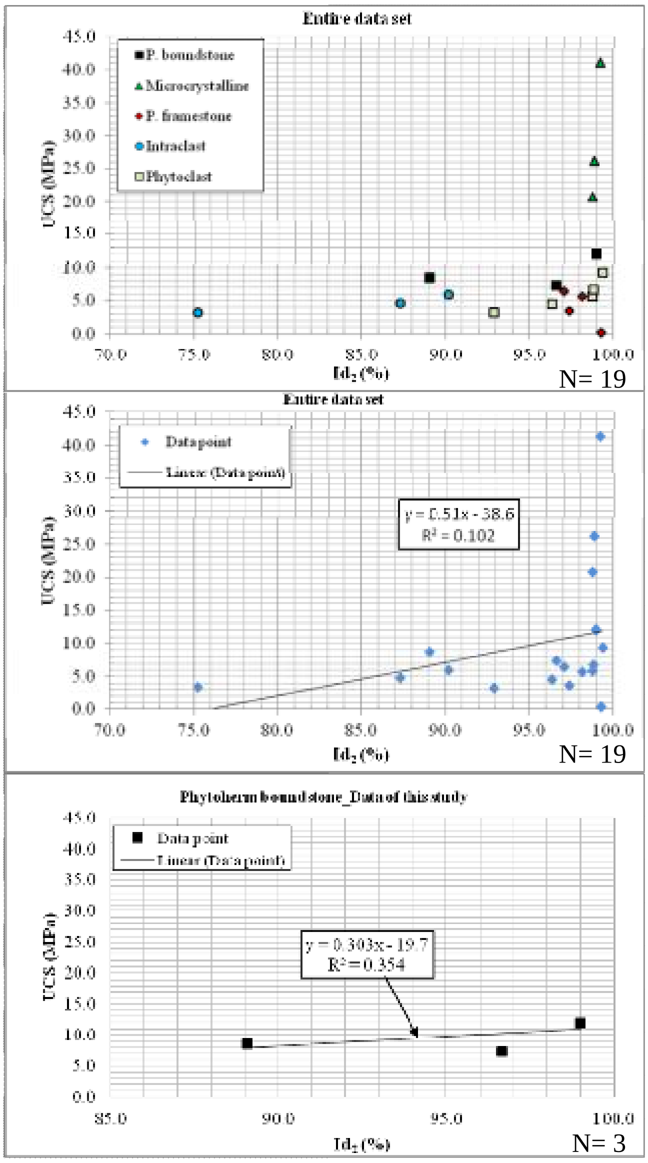

Figure 99. Regression plots of UCS vs. slake durability index of the Antalya tufa rock mass and tufa rock types.

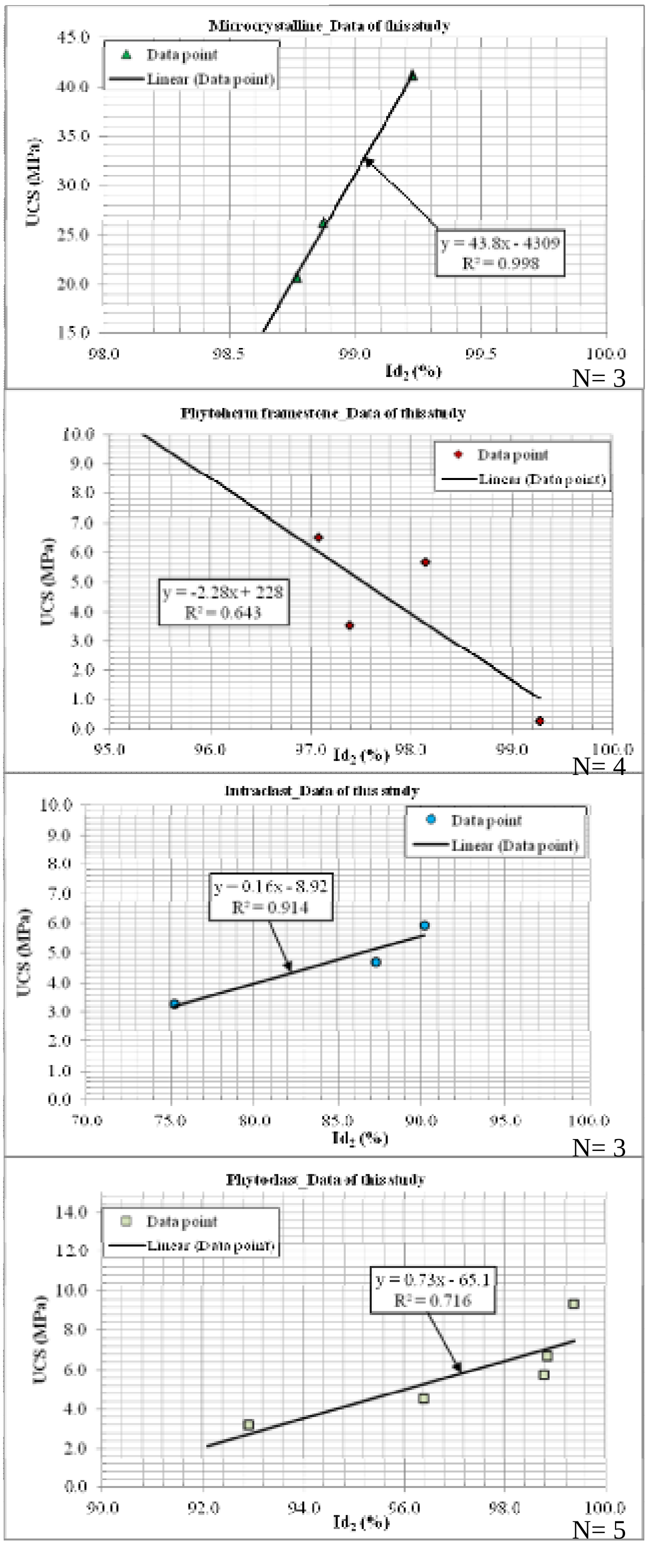

Figure 99 (cont'd.). Regression plots of UCS vs. slake durability index of the Antalya tufa rock mass and tufa rock types.

7. UCS and seismic wave velocity correlations of the Antalya tufa rock mass

Correlations between the UCS and the seismic wave velocities Vp and Vs of the Antalya tufa rock mass have been developed as illustrated in Figures 100 and 101, respectively.

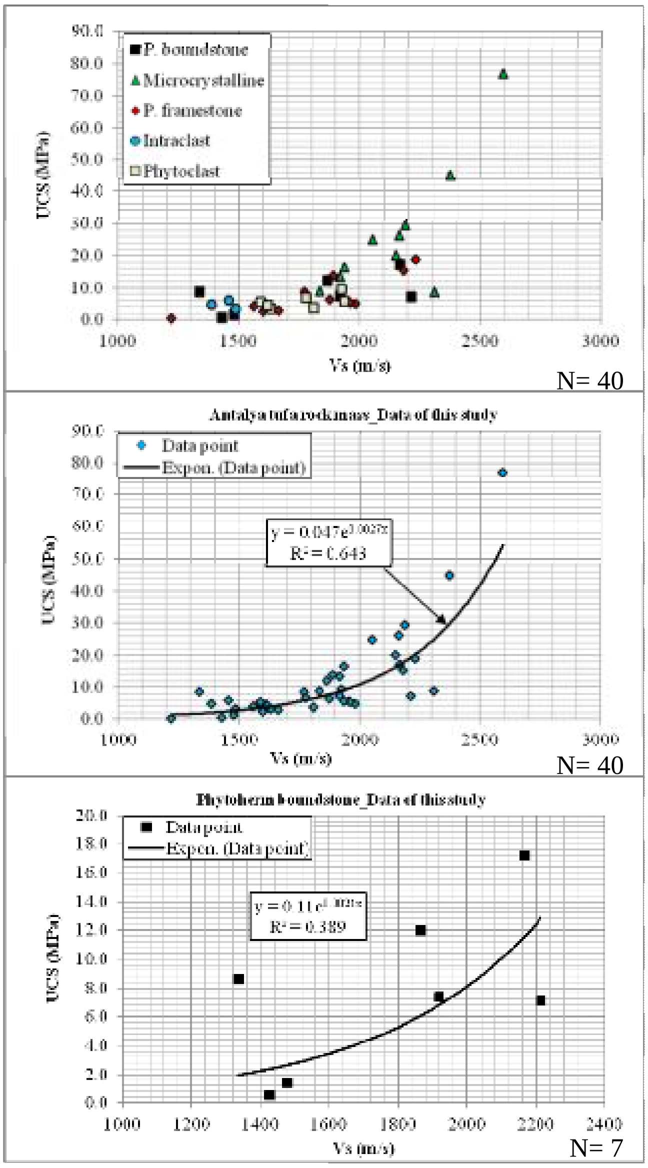

Figure 100. Regression plot of UCS vs. Vs for the Antalya tufa rock mass and tufa rock types.

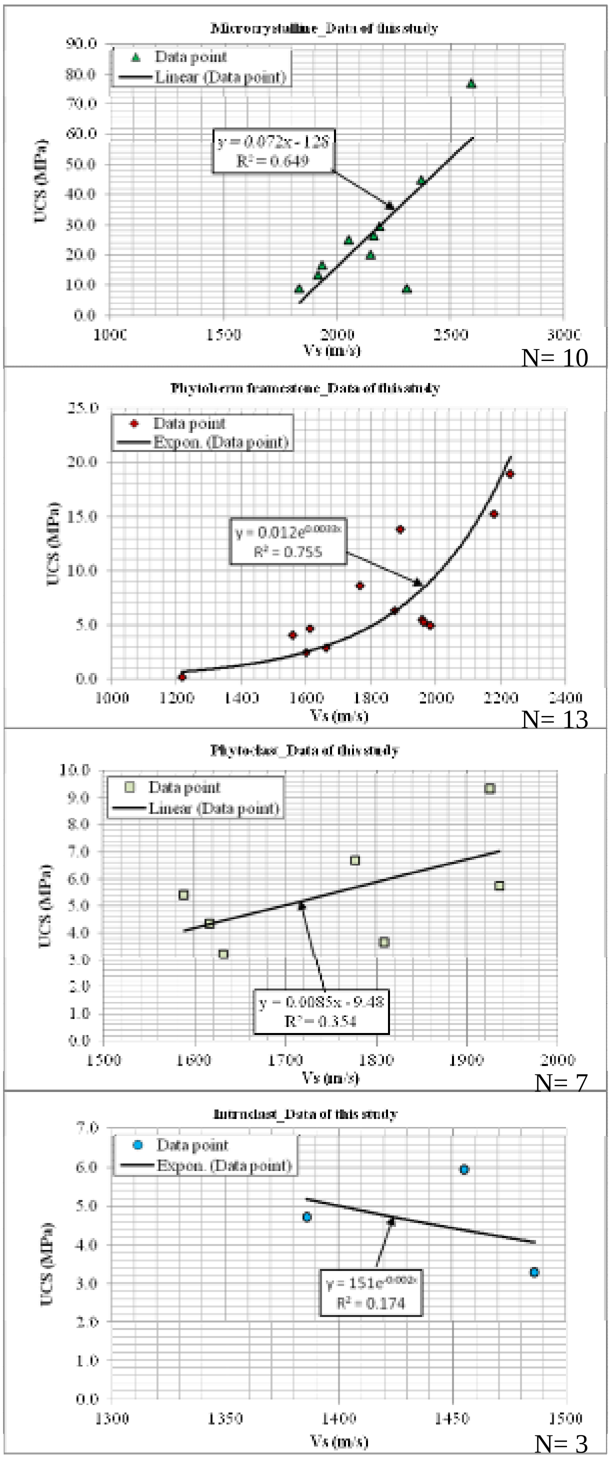

Figure 100 (cont'd.). Regression plot of UCS vs. Vs for the Antalya tufa rock mass and tufa rock types.

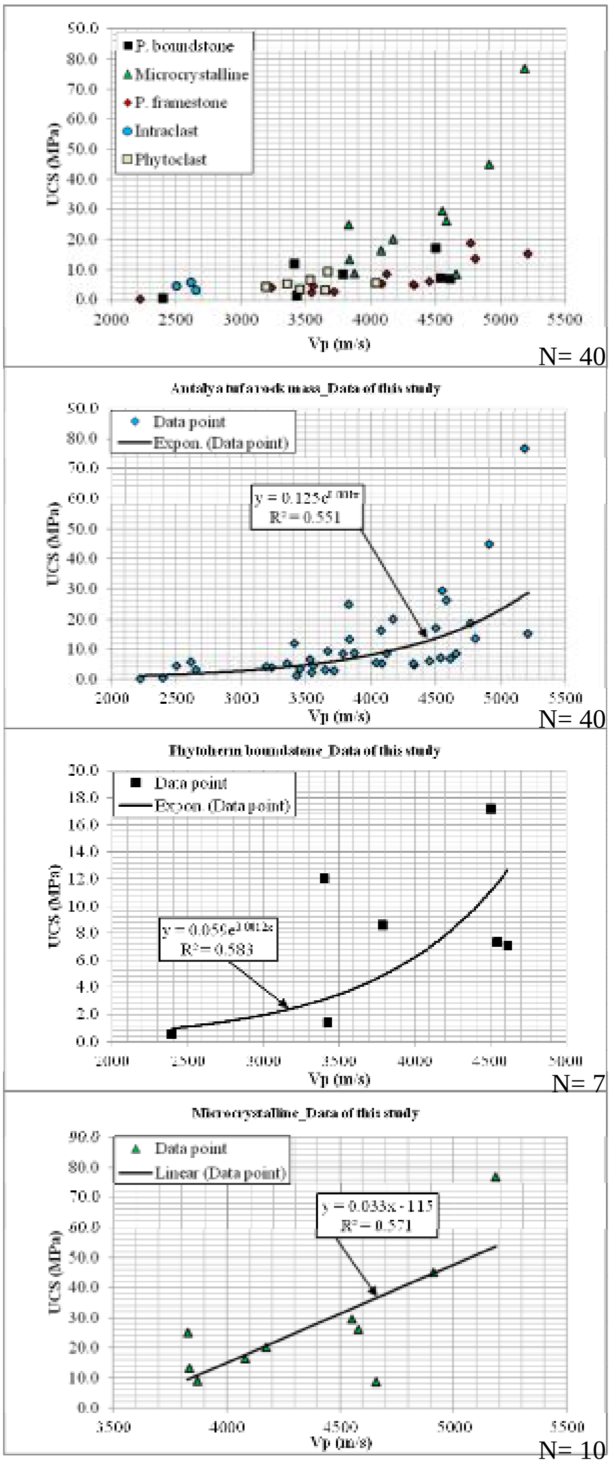

Figure 101. Regression plot of UCS vs. Vp for the Antalya tufa rock mass and tufa rock types.

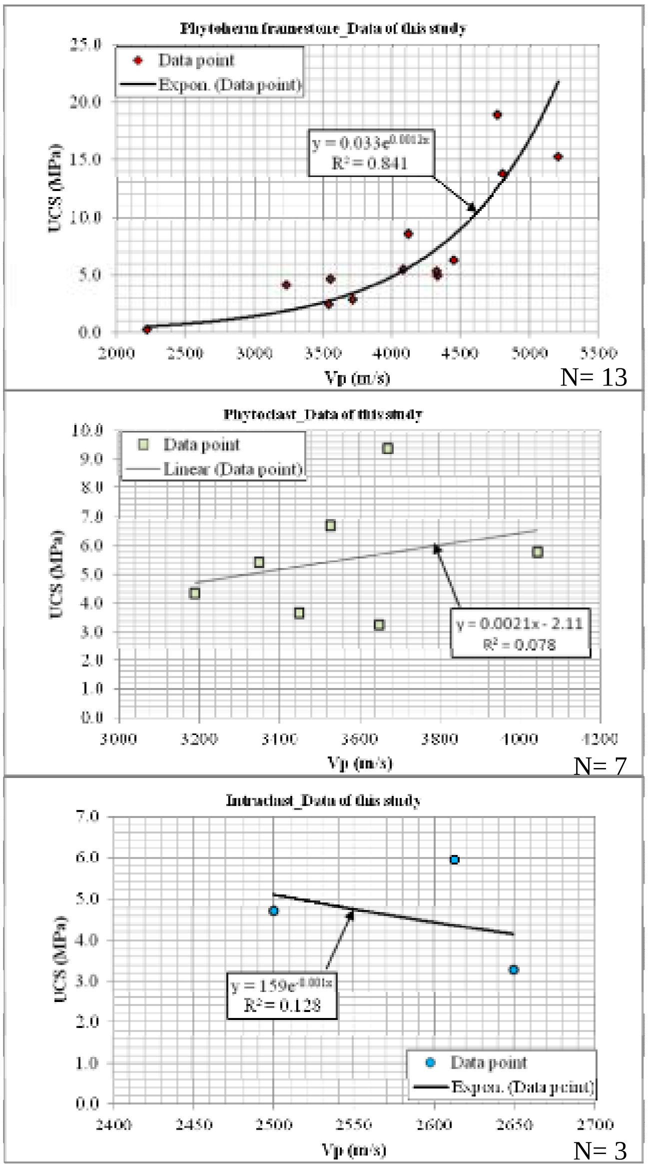

Figure 101 (cont'd.). Regression plot of UCS vs. Vp for the Antalya tufa rock mass and tufa rock types.

VII.3.2 Correlations between the Elasticity modulus and the other parameters of the Antalya tufa rock mass

Since the correlation between the Elasticity modulus and the UCS of the Antalya tufa rock mass has been presented in the previous section, this section will entail correlations between the Elasticity modulus and other strength parameters.

1.Elasticity modulus and unit weight correlations of the Antalya tufa rock mass

Correlation between the Elasticity modulus and unit weight (γ) of the tufa rock mass has been developed as presented by Figure 102.

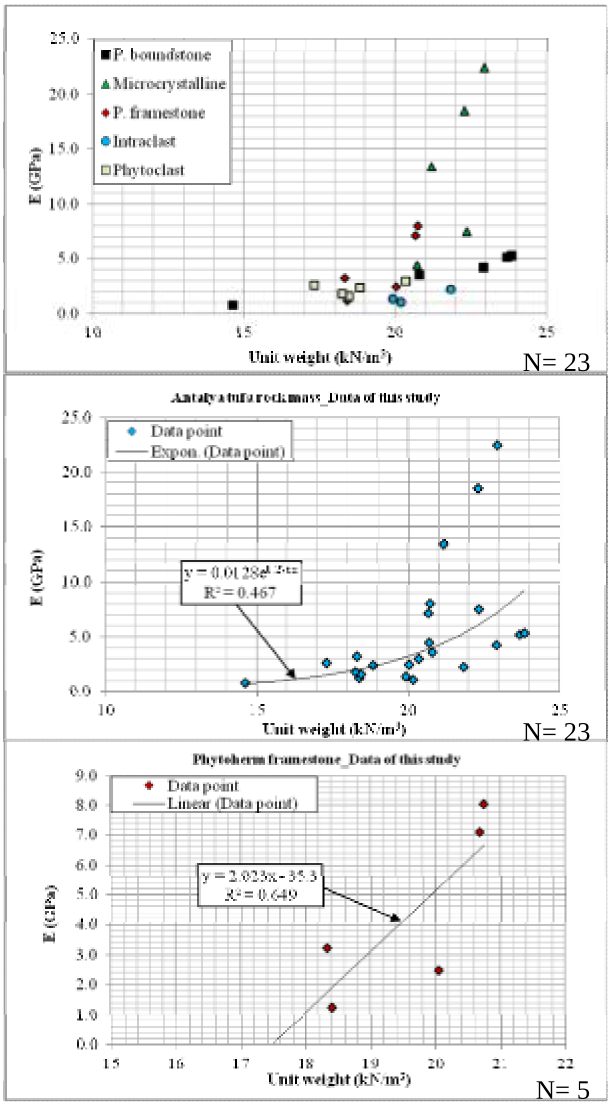

Figure 102. Regression plots of Elasticity modulus vs. unit weight for the Antalya tufa rock mass and tufa rock types.

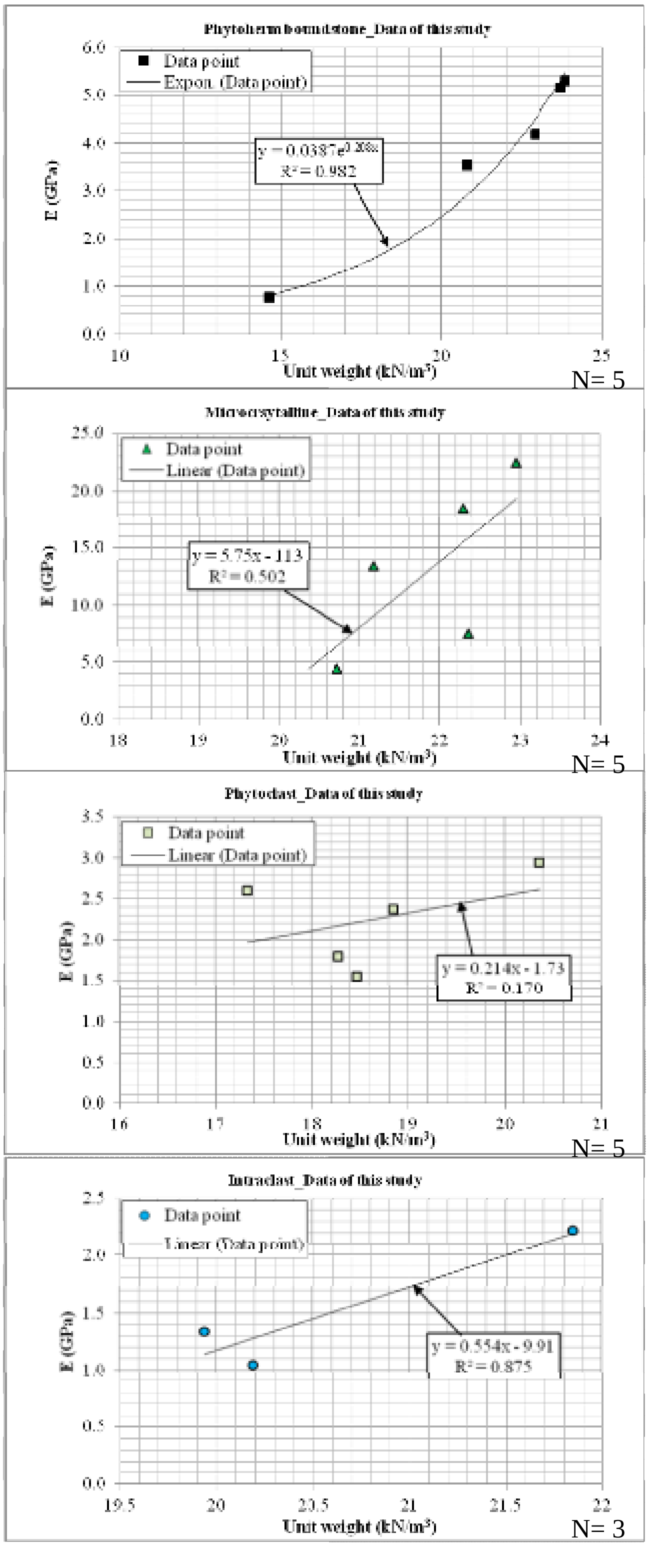

Figure 102 (cont'd.). Regression plots of Elasticity modulus vs. unit weight for the Antalya tufa rock mass and tufa rock types.

2. Elasticity modulus and porosity correlations of the Antalya tufa rock mass

In order to correlate the Elasticity modulus (E) of the Antalya tufa rock mass with its porosity (n) values, only the data obtained from this study have been used. Accordingly, 23 measurements from this study have been utilized to determine the relation between the E and the porosity (n) of the Antalya tufa rock masses (Figure 103).

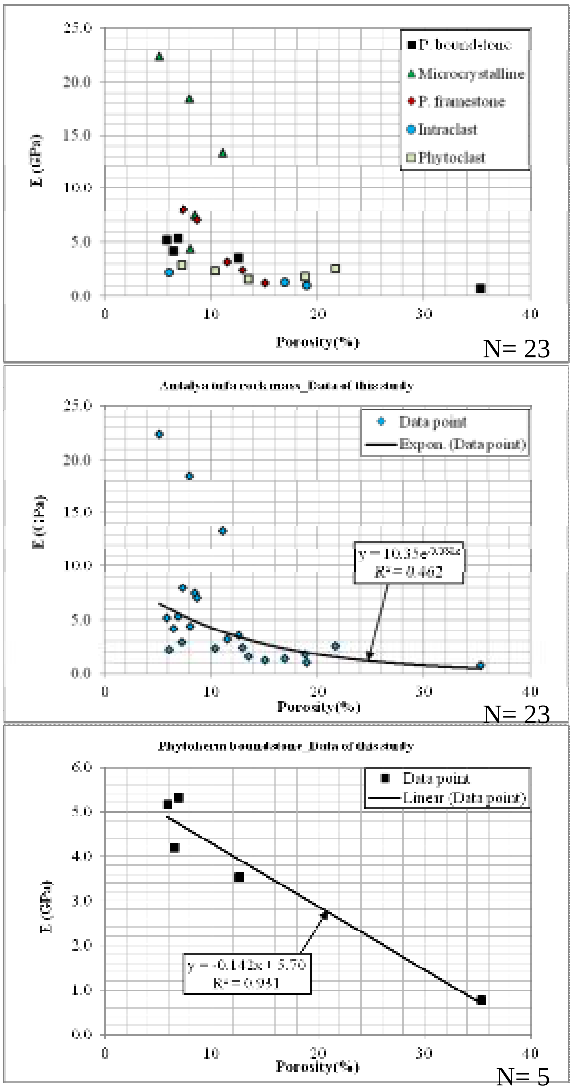

Figure 103. Regression plots of Elasticity modulus vs. porosity for the Antalya tufa rock mass and tufa rock types.

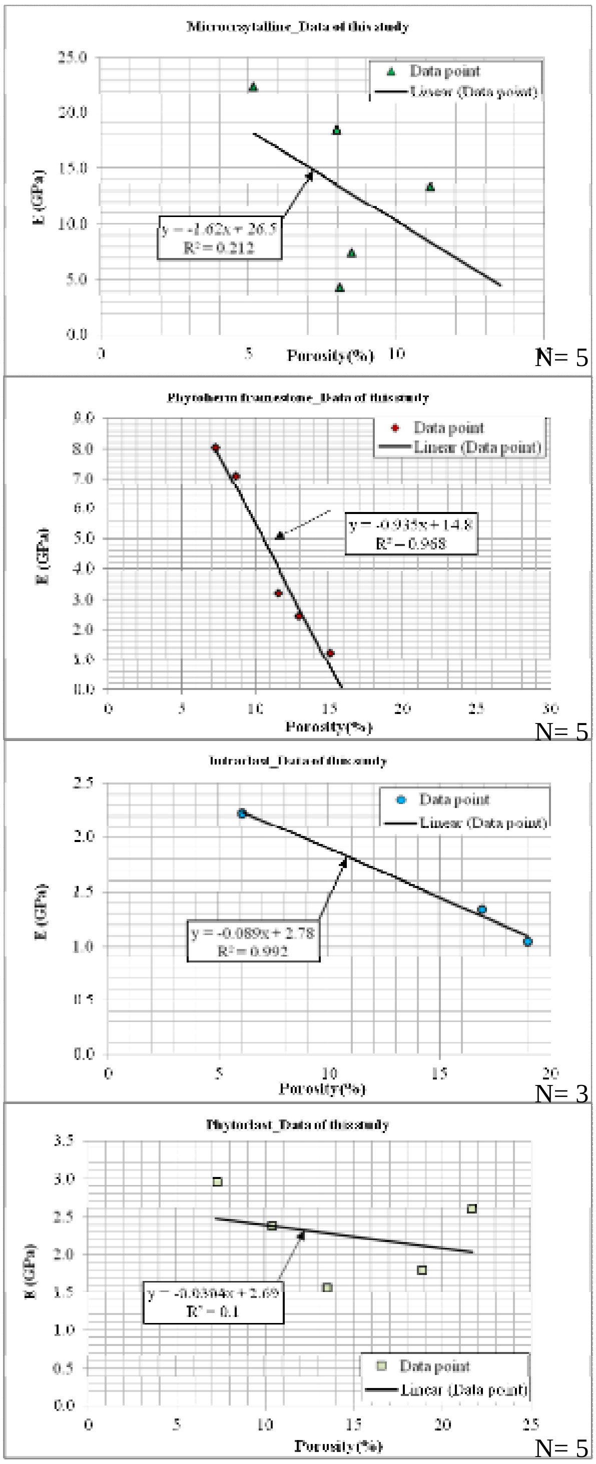

Figure 103 (cont'd.). Regression plots of Elasticity modulus vs. porosity for the Antalya tufa rock mass and tufa rock types.

3. Elasticity modulus and seismic wave velocity of the Antalya tufa rock mass

Correlations between the Elasticity modulus (E) and seismic wave velocities (Vp and Vs) of the Antalya tufa rock mass have been developed as illustrated in Figures 104 and 105.

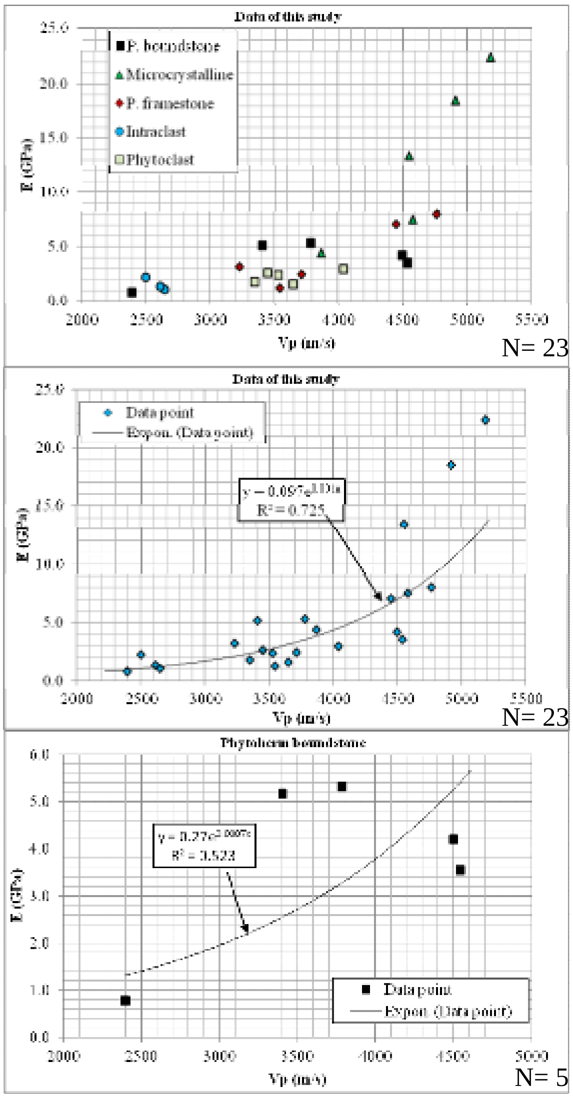

Figure 104. Regression plots of Elasticity modulus vs. seismic velocity (Vp) for the Antalya tufa rock mass and tufa rock types.

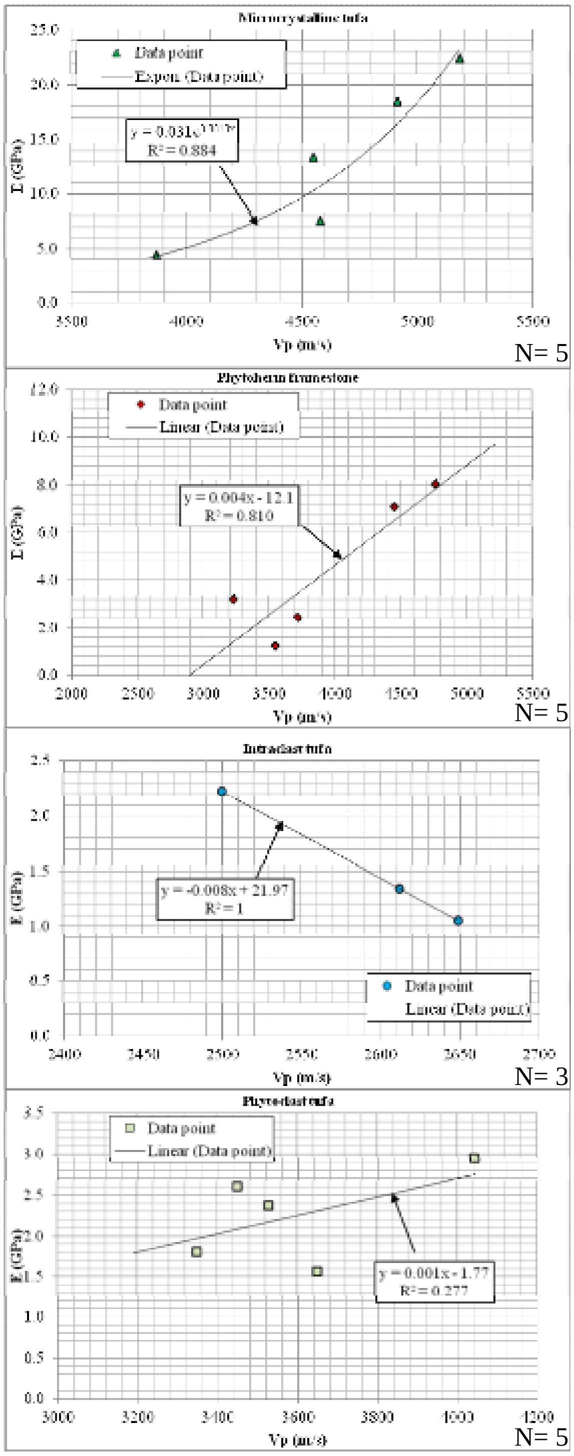

Figure 104 (cont'd.). Regression plots of Elasticity modulus vs. seismic velocity (Vp) for the Antalya tufa rock mass and tufa rock types.

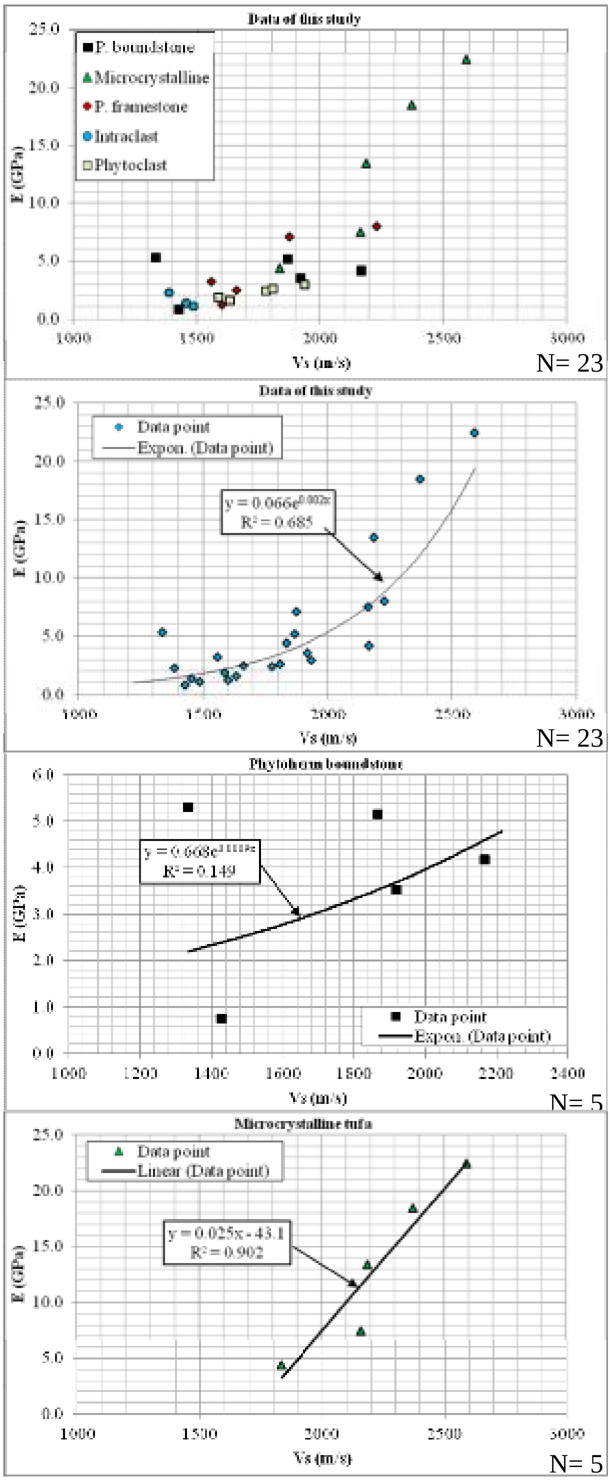

Figure 105. Regression plots of Elasticity modulus vs. seismic velocity (Vs) for the Antalya tufa rock mass and tufa rock types.

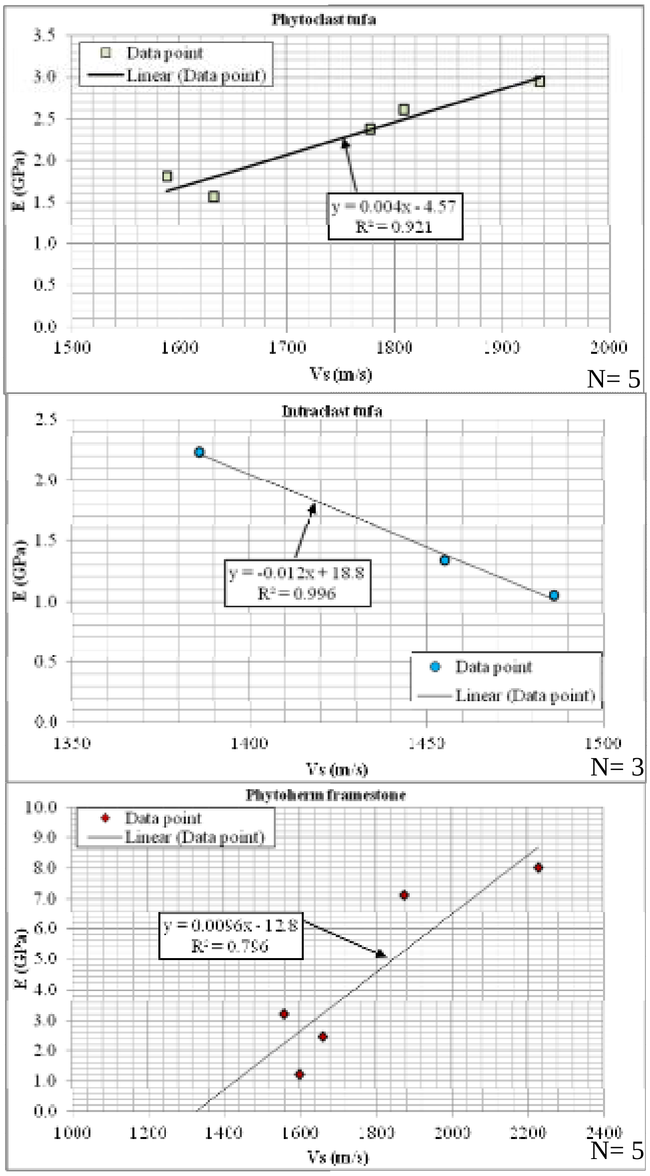

Figure 105 (cont'd.). Regression plots of Elasticity modulus vs. seismic velocity (Vs) for the Antalya tufa rock mass and tufa rock types.

<u>*4. Elasticity modulus and point load strength index of the Antalya tufa rock mass*</u>

The correlation between the Elasticity modulus (E) and the point load strength index (Is_{50}) of the Antalya tufa rock mass has been made based on the data set developed in this study as follows (Figure 106).

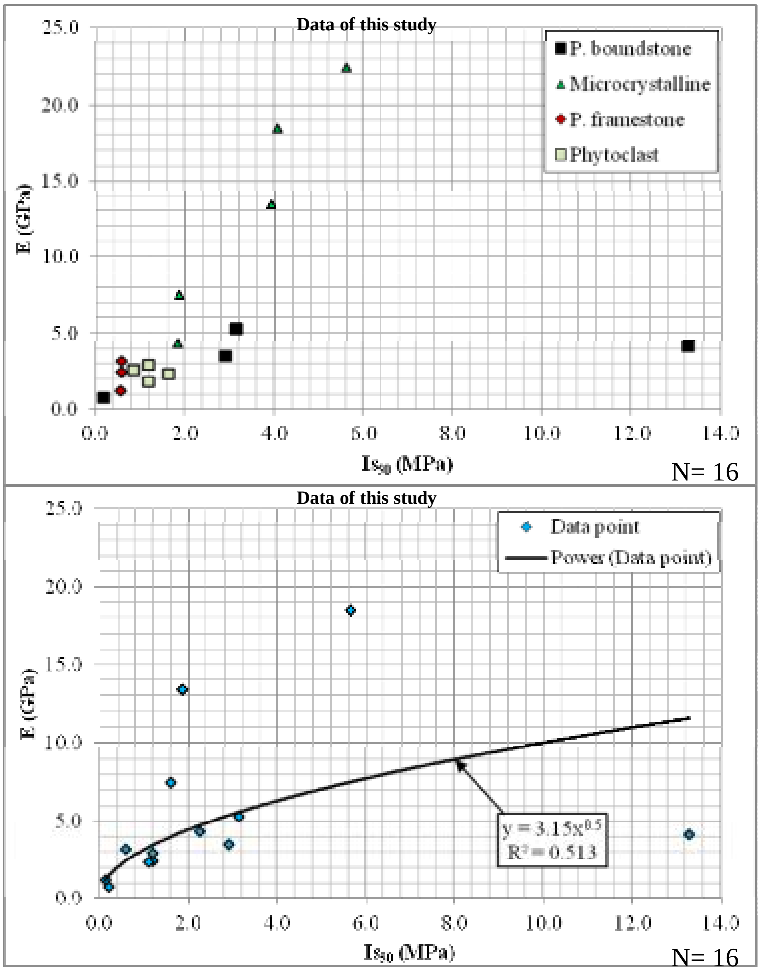

Figure 106. Regression plots of Elasticity modulus vs. the point load strength index (Is_{50}) for the Antalya tufa rock mass and tufa rock types.

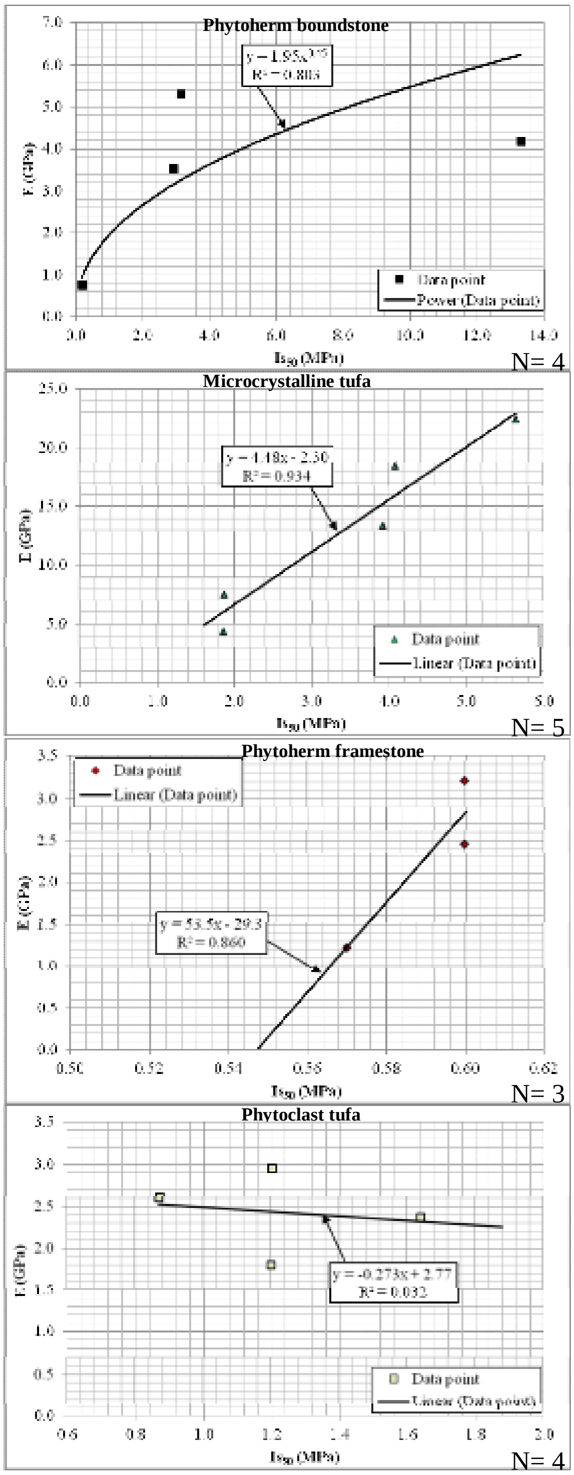

Figure 106 (cont'd.). Regression plots of Elasticity modulus vs. the point load strength index (Is_{50}) for the Antalya tufa rock mass and tufa rock types.

5. Elasticity modulus and slake durability index of the Antalya tufa rock mass

Correlation between Elasticity modulus (E) and slake durability index (Id_2) of the Antalya tufa rock mass has been made based on the data set developed in this study as follows (Figure 107).

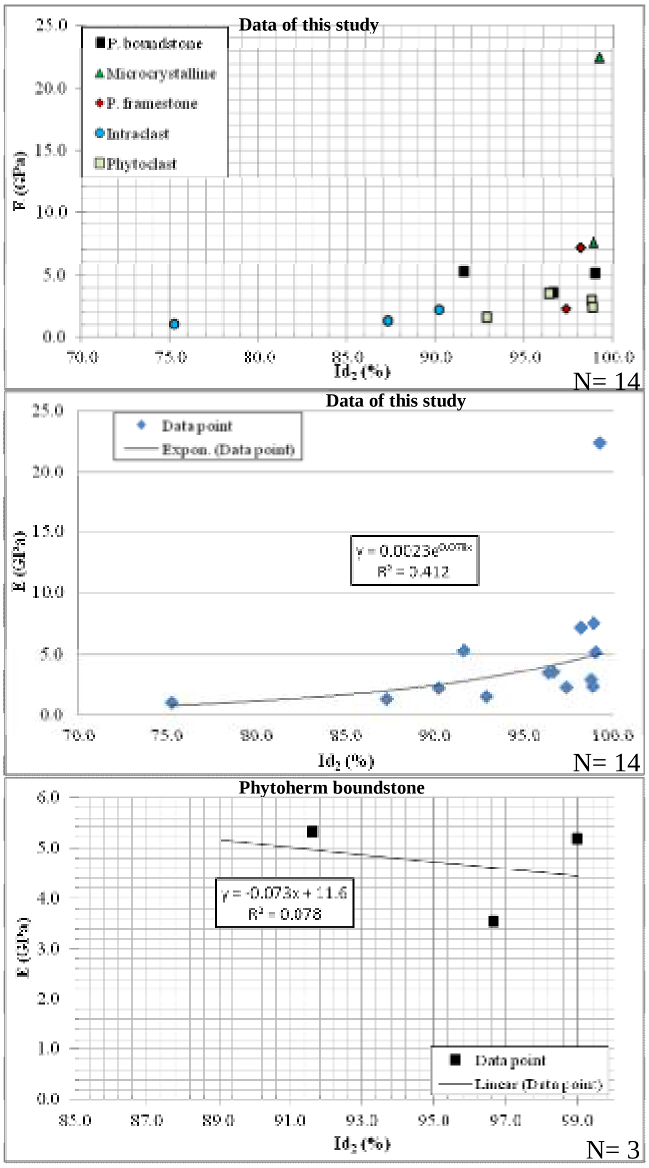

Figure 107. Regression plots of Elasticity modulus vs. slake durability index (Id_2) for the Antalya tufa rock mass and tufa rock types.

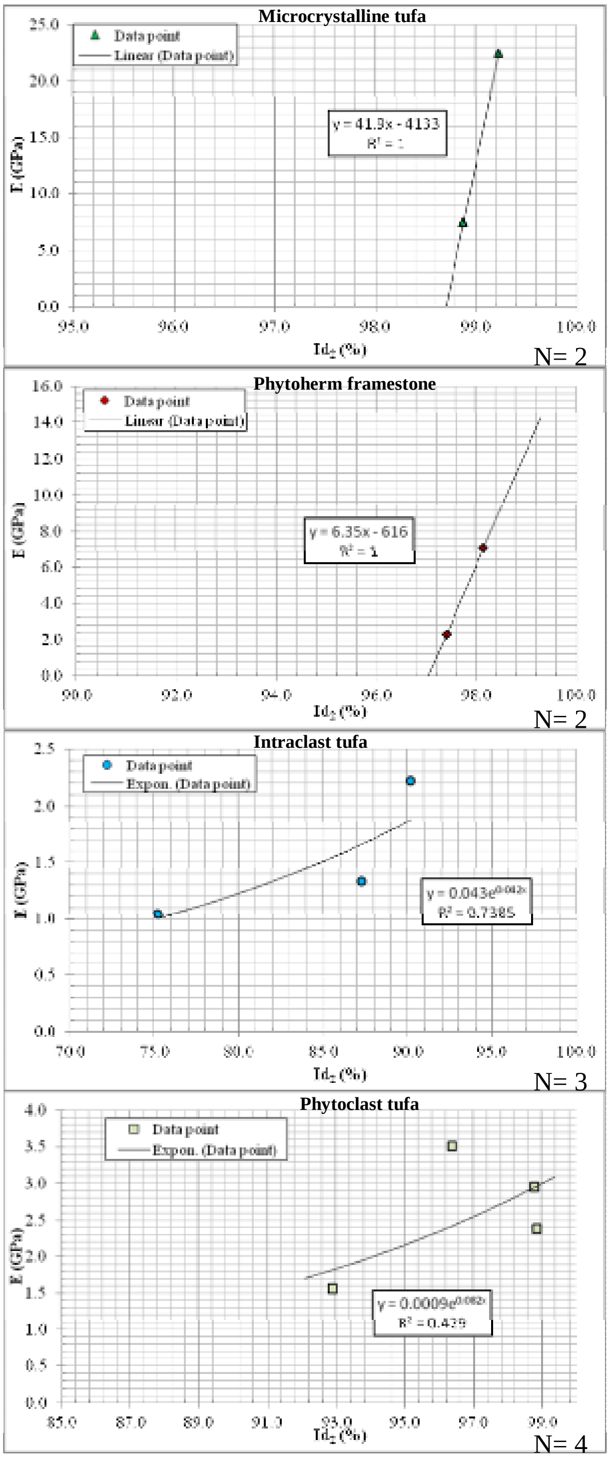

Figure 107 (cont'd.). Regression plots of Elasticity modulus vs. slake durability index (Id_2) for the Antalya tufa rock mass and tufa rock types.

6.Elasticity modulus and tensile strength of the Antalya tufa rock mass

According to the data set obtained through the tests carried out during this study, the following relations between the Elasticity modulus (E) and tensile strength (σ_t) of the Antalya tufa rock mass have been determined (Figure 108).

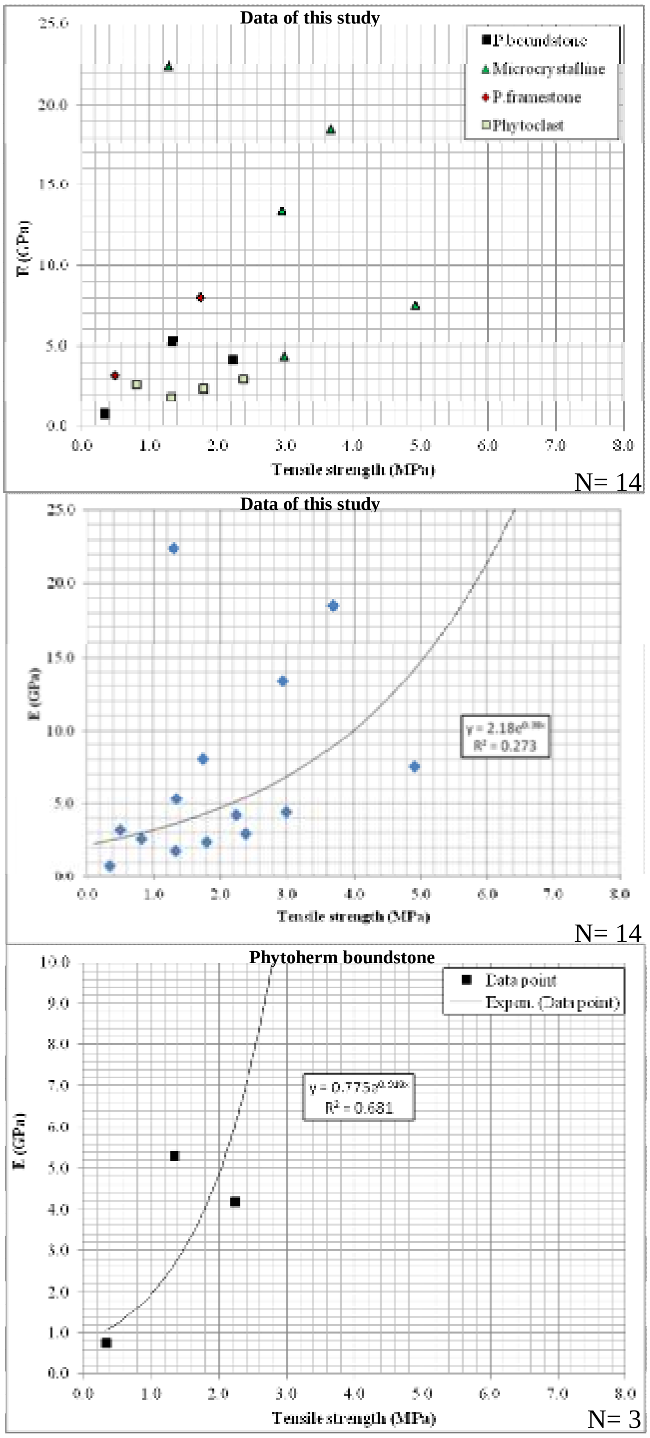

Figure 108. Regression plots of Elasticity modulus vs. tensile strength (σ_t) for the Antalya tufa rock mass and tufa rock types.

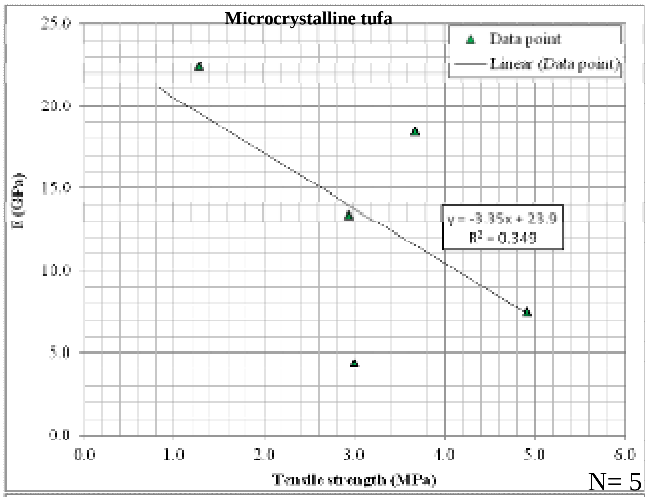

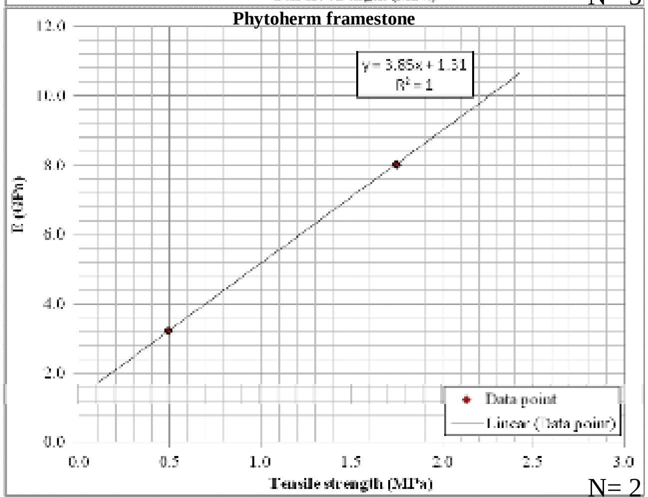

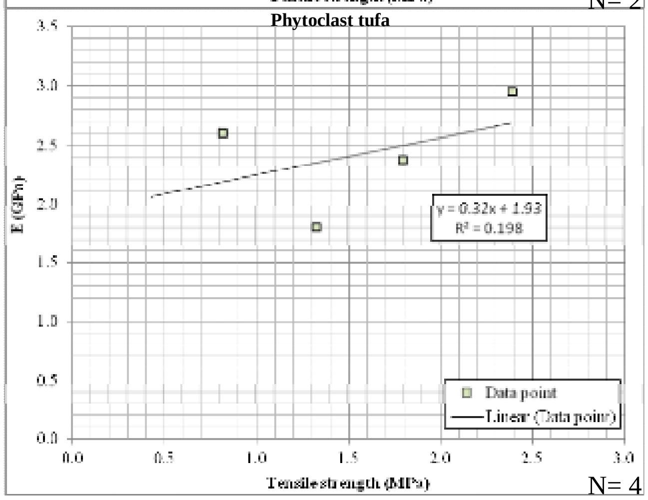

Figure 108 (cont'd.) Regression plots of Elasticity modulus vs. tensile strength (σ_t) for the Antalya tufa rock mass and tufa rock types.

VII.3.3 Correlations between the tensile strength and other parameters of the Antalya tufa rock mass

Since correlations between the tensile strength (σ_t) vs. uniaxial compressive strength (UCS), and between the tensile strength vs. Elasticity modulus (E) of the Antalya tufa rock mass have already been presented in the previous sections, this section will present correlations between the tensile strength and the other strength parameters.

1.Tensile strength and unit weight of the Antalya tufa rock mass

Correlation between the tensile strength (σ_t) and unit weight (γ) of the tufa rock mass is presented by Figure 109.

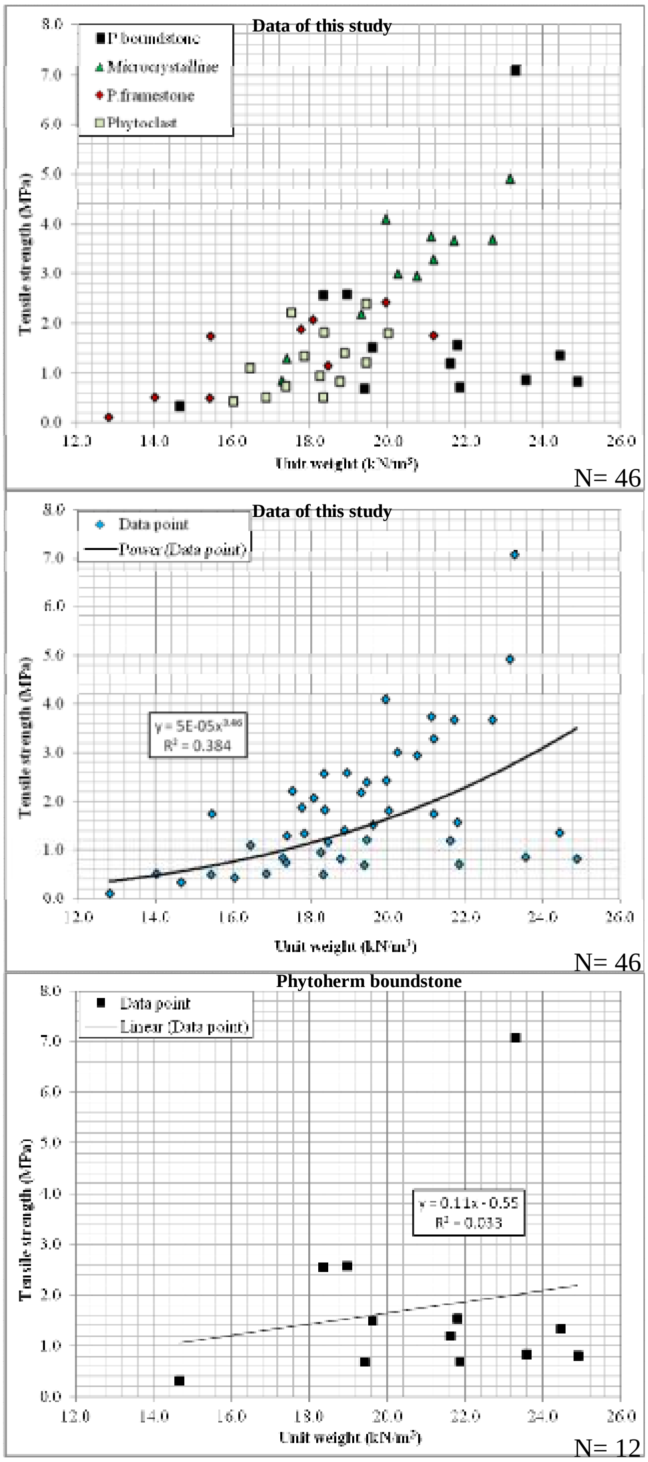

Figure 109. Regression plots of tensile strength (σ_t) vs. unit weight (γ) for the Antalya tufa rock mass and tufa rock types.

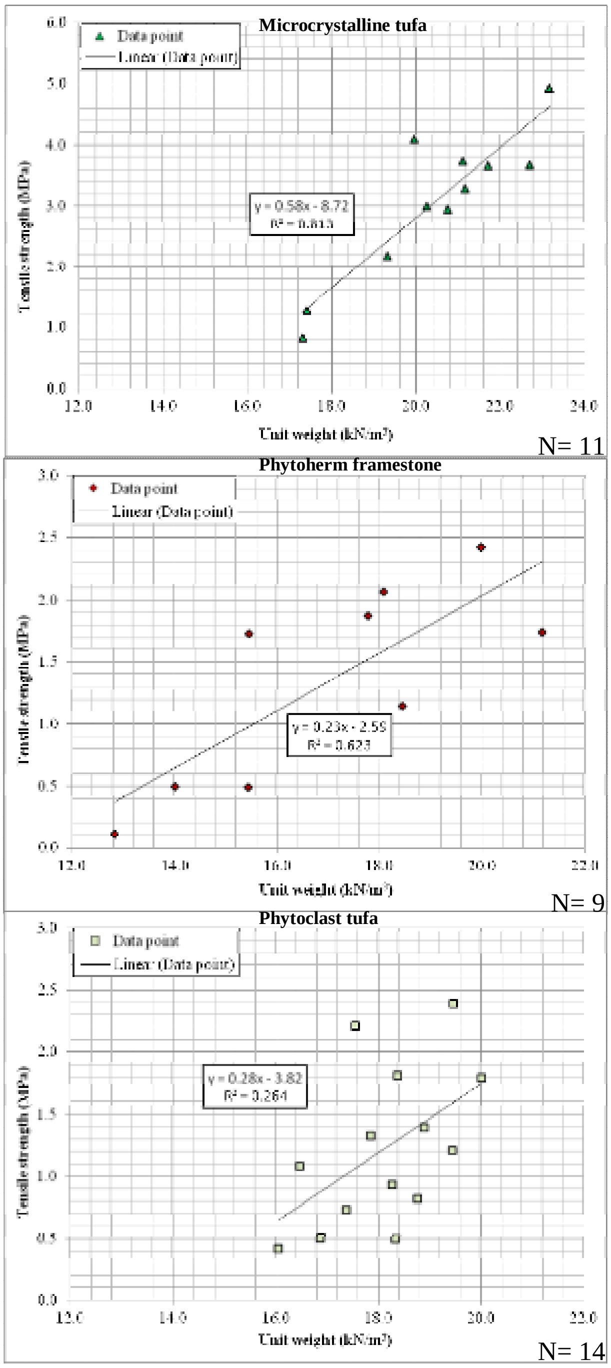

Figure 109 (cont'd.). Regression plots of tensile strength (σ_t) vs. unit weight (γ) for the Antalya tufa rock mass and tufa rock types.

2. Tensile strength and porosity of the Antalya tufa rock mass

Correlation between the tensile strength (σ_t) and porosity (n) of the Antalya tufa rock mass is given by Figure 110.

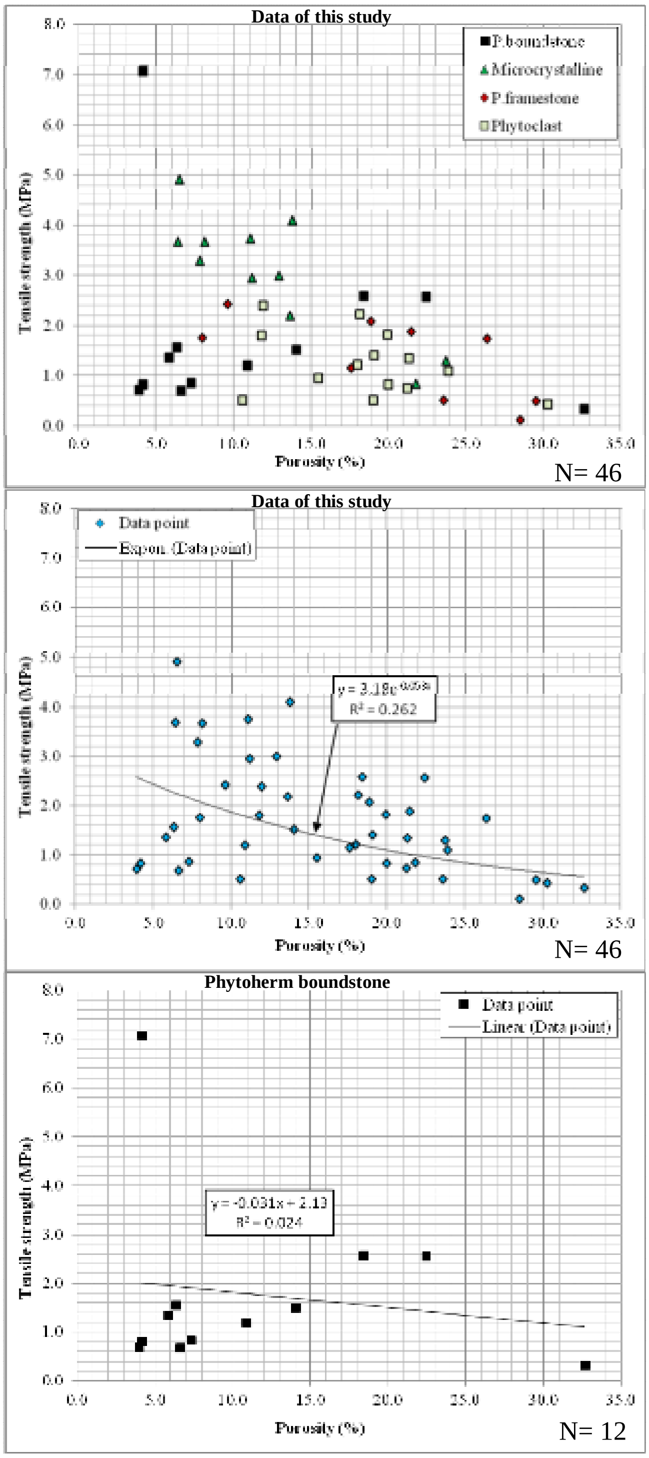

Figure 110. Regression plots of tensile strength (σ_t) vs. porosity (n) for the Antalya tufa rock mass and tufa rock types.

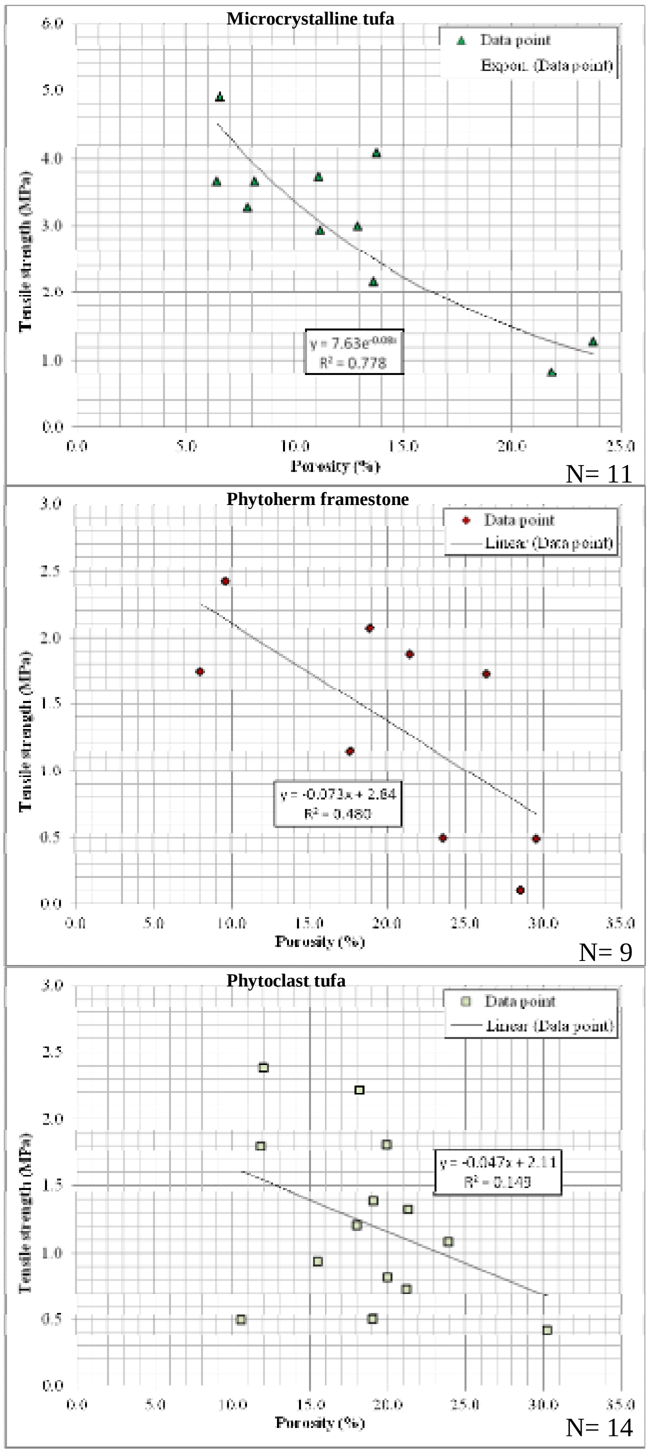

Figure 110 (cont'd.). Regression plots of tensile strength (σ_t) vs. porosity (n) for the Antalya tufa rock mass and tufa rock types.

3. Tensile strength and point load strength index of the Antalya tufa rock masses

Correlation between the tensile strength (σ_t) and point load strength index (Is_{50}) of the Antalya tufa rock mass is given by Figure 111.

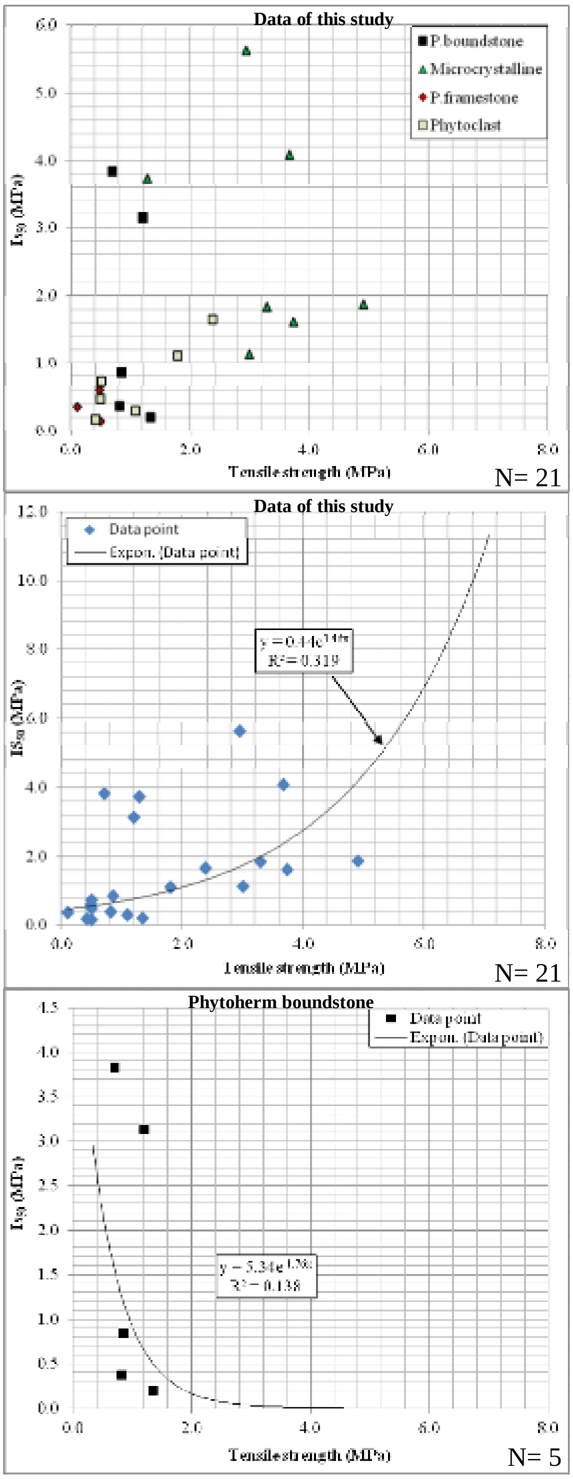

Figure 111. Regression plots of tensile strength (σ_t) vs. point load strength index (Is_{50}) for the Antalya tufa rock mass and tufa rock types.

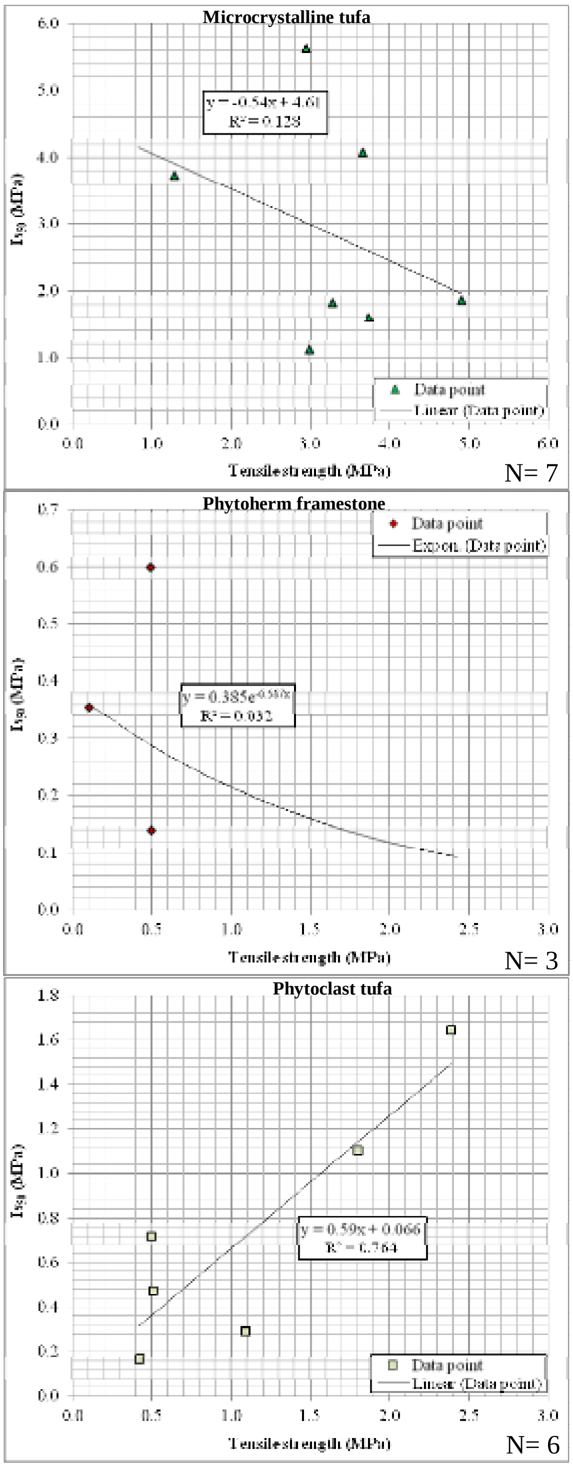

Figure 111 (cont'd.). Regression plots of tensile strength (σ_t) vs. point load strength index (Is_{50}) for the Antalya tufa rock mass and tufa rock types.

4. Tensile strength and seismic wave velocity correlations of the Antalya tufa rock mass

Correlations between the tensile strength (σ_t) and seismic wave velocities (Vp and Vs) of the Antalya tufa rock mass have been developed as illustrated by Figures 112 and 113, respectively.

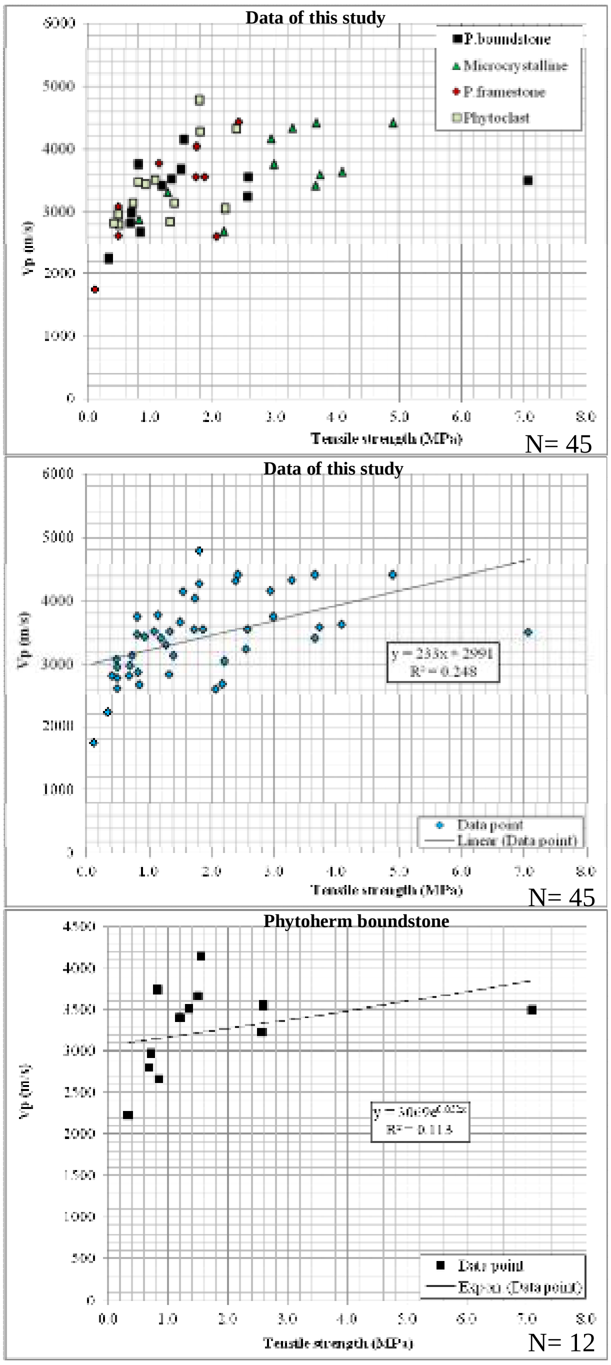

Figure 112. Regression plots of tensile strength (σ_t) vs. seismic wave velocity (Vp) for the Antalya tufa rock mass and tufa rock types.

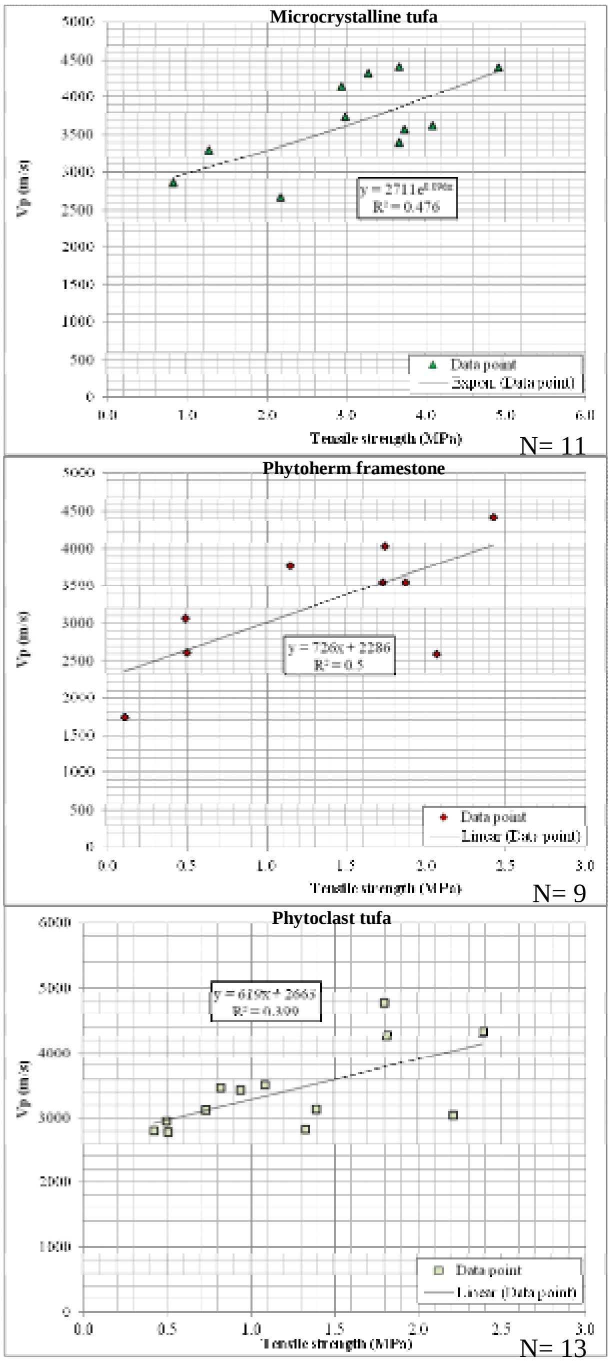

Figure 112 (cont'd.). Regression plots of tensile strength (σ_t) vs. seismic wave velocity (Vp) for the Antalya tufa rock mass and tufa rock types.

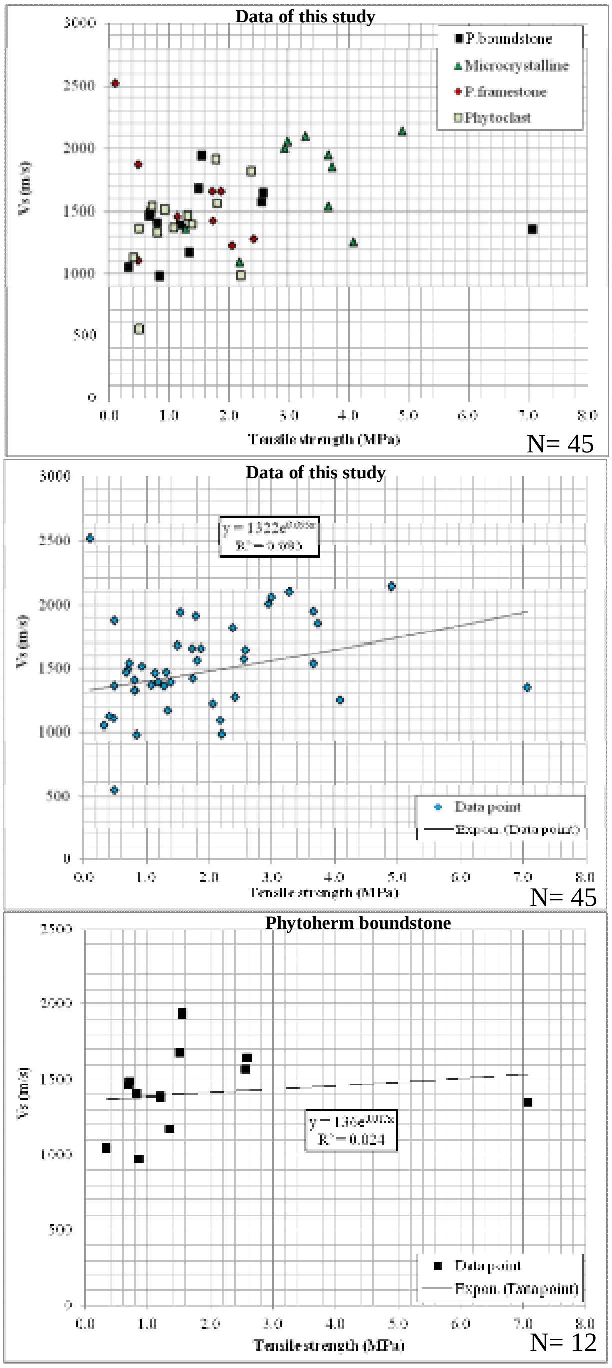

Figure 113. Regression plots of tensile strength (σ_t) vs. seismic wave velocity (Vs) for the Antalya tufa rock mass and tufa rock types.

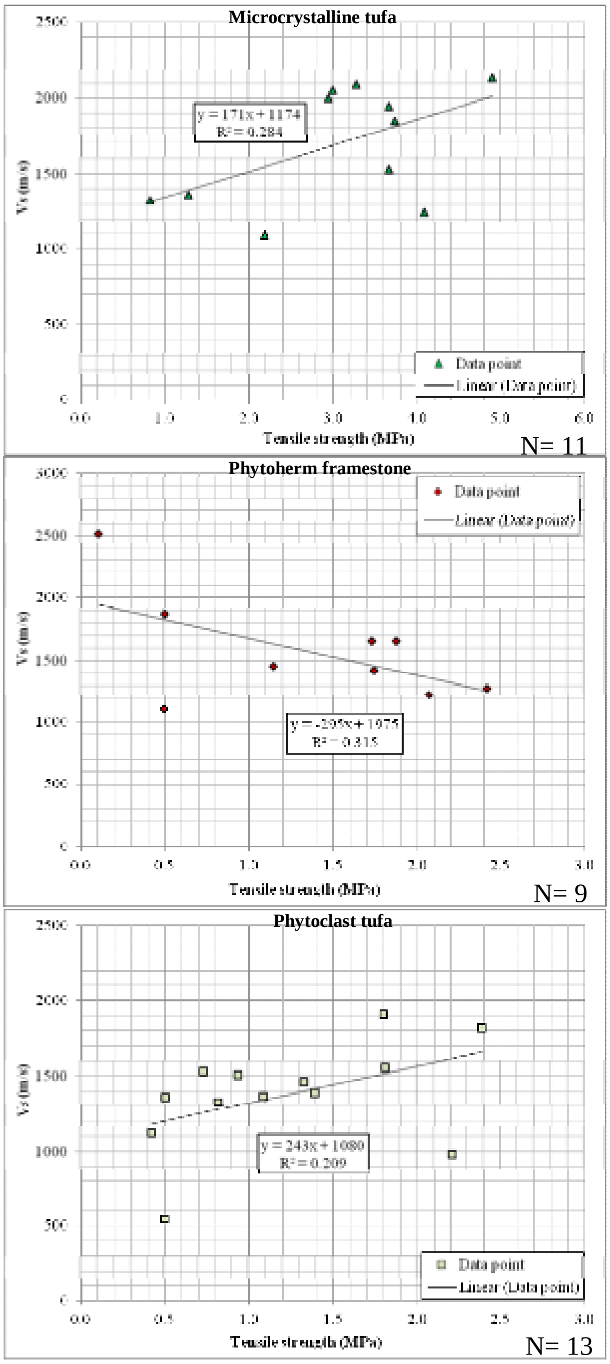

Figure 113 (cont'd.). Regression plots of tensile strength (σ_t) vs. seismic wave velocity (Vs) for the Antalya tufa rock mass and tufa rock types.

5. Tensile strength and slake durability correlations of the Antalya tufa rock mass

Correlation between the tensile strength (σ_t) and slake durability index (Id_2) of the Antalya tufa rock mass is presented by Figure 114.

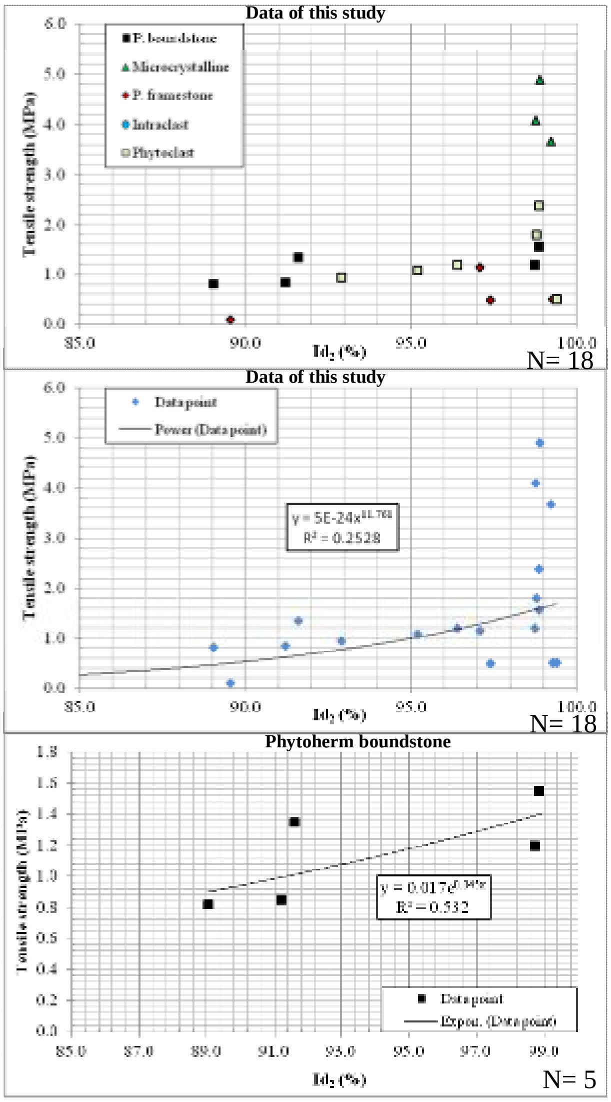

Figure 114. Regression plots of tensile strength (σ_t) vs. slake durability index (Id_2) for the Antalya tufa rock mass and tufa rock types.

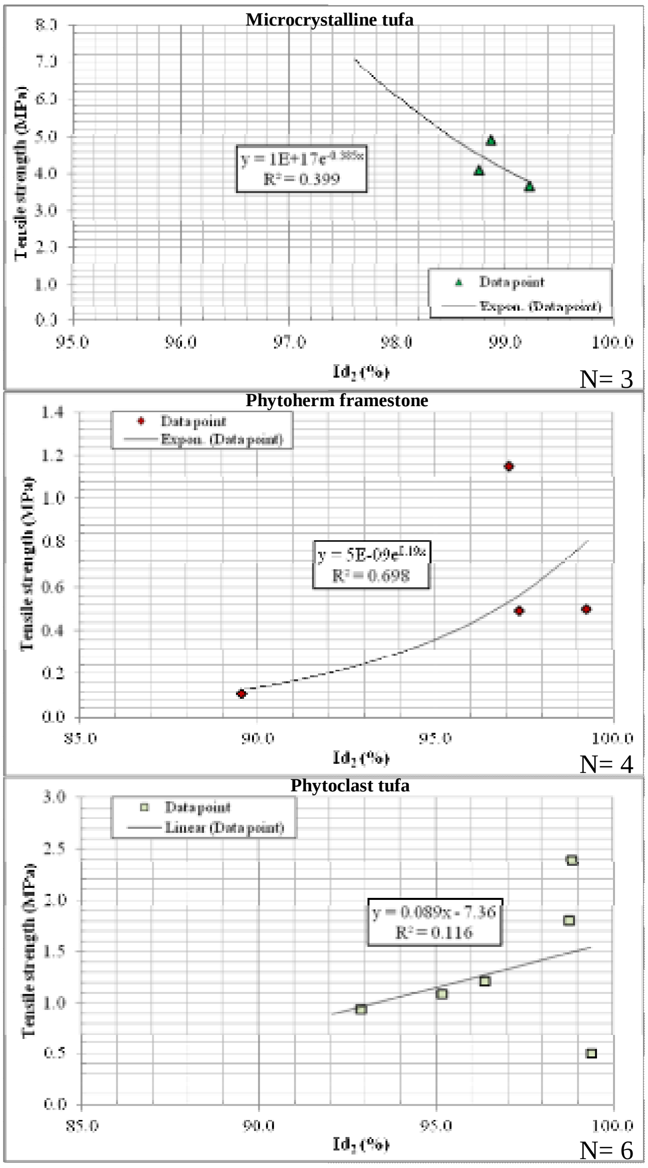

Figure 114 (cont'd.). Regression plots of tensile strength (σ_t) vs. slake durability index (Id_2) for the Antalya tufa rock mass and tufa rock types.

VII.3.4 Correlations between point load strength index and other parameters of the Antalya tufa rock mass

Since correlations between the point load strength index (Is_{50}) and uniaxial compressive strength (UCS), between point load strength index and Elasticity modulus (E), and between point load strength index and tensile strength (σ_t) of the Antalya tufa rock mass have been presented in the previous sections, the correlation between point load strength index and other strength parameters will be given in this section.

1. Point load strength index and unit weight of the Antalya tufa rock mass

Correlation between point load strength index (Is_{50}) and unit weight (γ) of the Antalya tufa rock mass is presented by Figure 115.

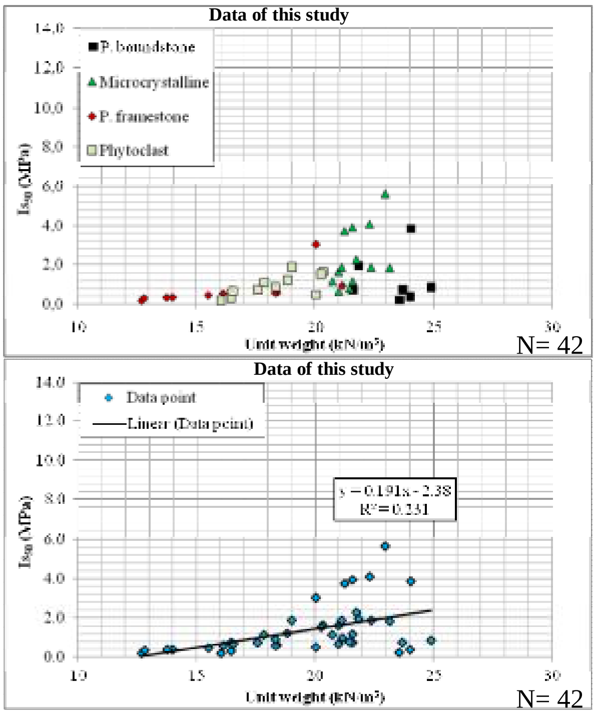

Figure 115. Regression plots of point load strength index (Is_{50}) vs. unit weight (γ) for the Antalya tufa rock mass and tufa rock types.

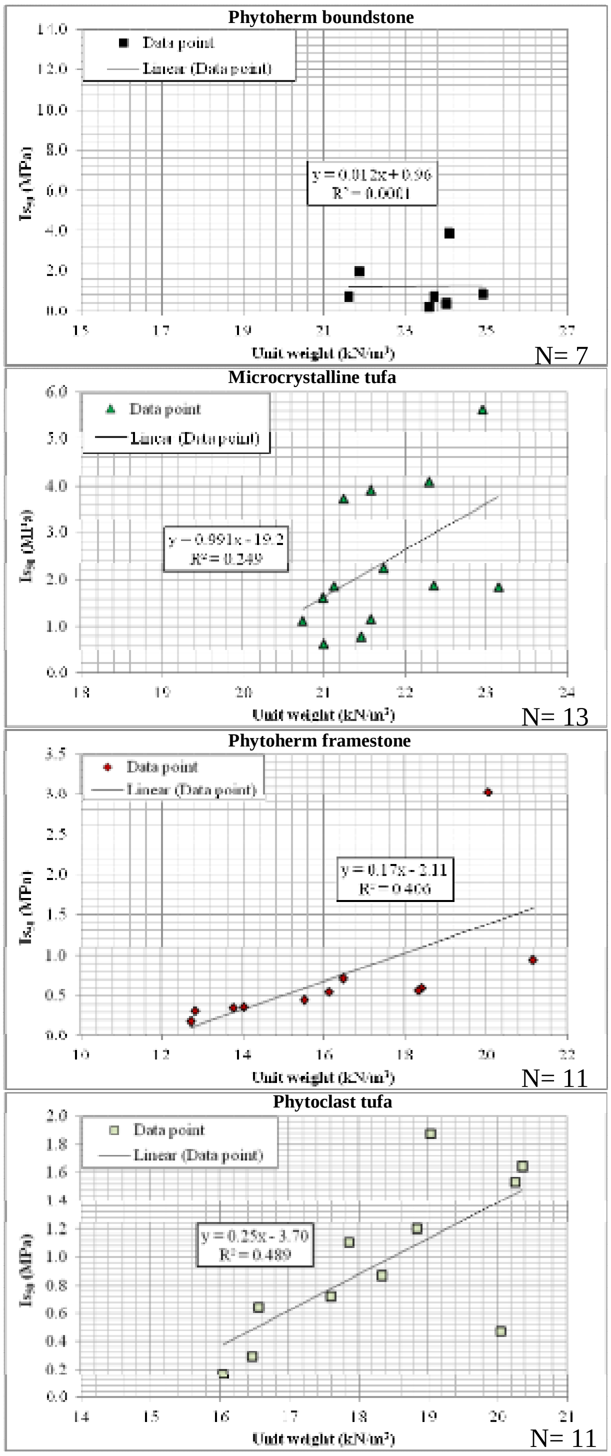

Figure 115 (cont'd.). Regression plots of point load strength index (Is_{50}) vs. unit weight (γ) for the Antalya tufa rock mass and tufa rock types.

2. Point load strength index and porosity of the Antalya tufa rock mass

Correlation between the point load strength index (Is_{50}) and porosity (n) of the Antalya tufa rock mass is given by Figure 116.

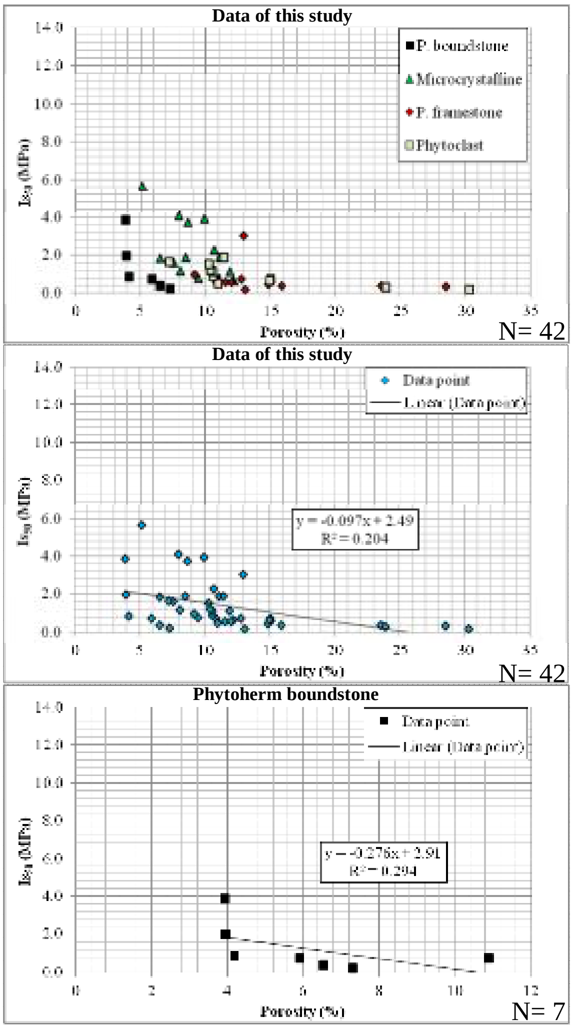

Figure 116. Regression plots of point load strength index (Is_{50}) vs. porosity (n) for the Antalya tufa rock mass and tufa rock types.

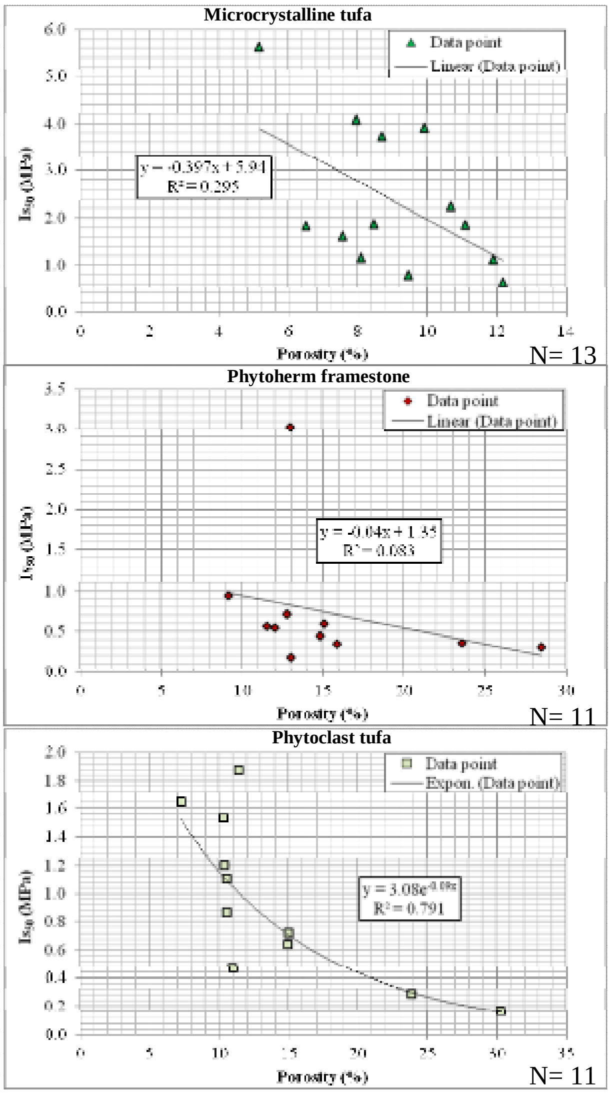

Figure 116 (cont'd.). Regression plots of point load strength index (Is_{50}) vs. porosity (n) for the Antalya tufa rock mass and tufa rock types.

3. Point load strength index and seismic wave velocity correlations of the Antalya tufa rock mass

Correlations between the point load strength index (Is_{50}) and seismic wave velocities (Vp and Vs) of the Antalya tufa rock mass is illustrated by Figures 117 and 118.

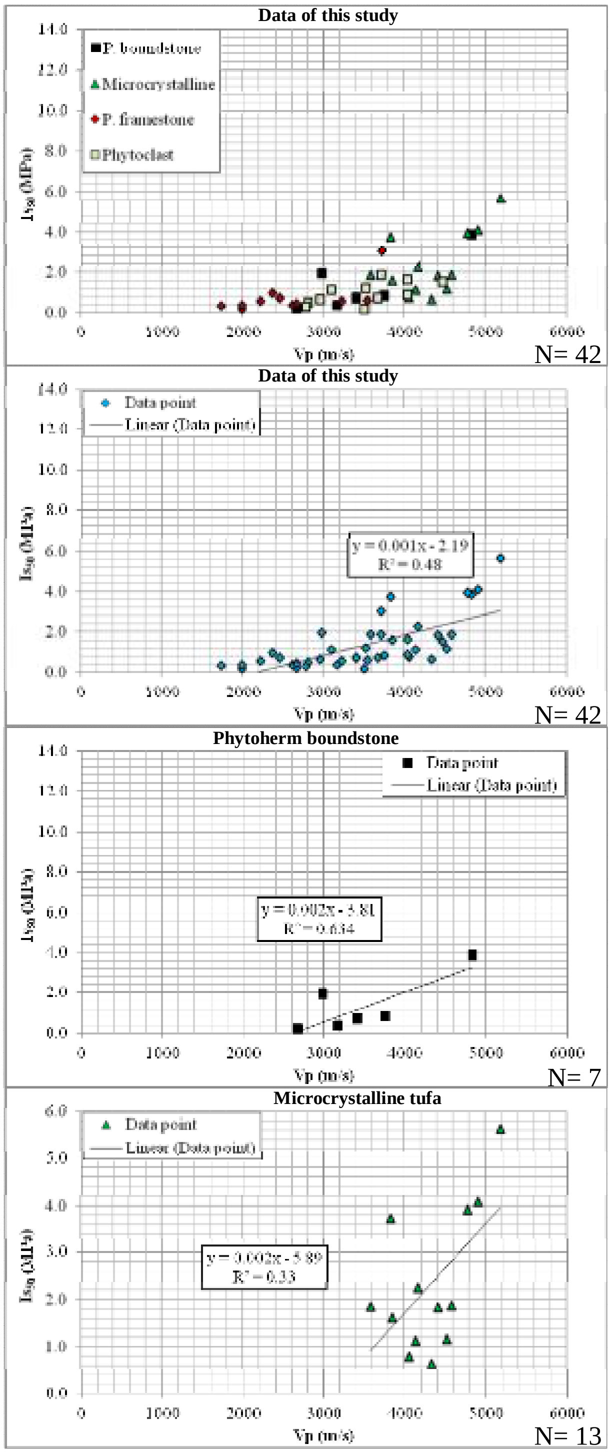

Figure 117. Regression plots of point load strength index (Is_{50}) vs. seismic wave velocity (Vp) for the Antalya tufa rock mass and tufa rock types.

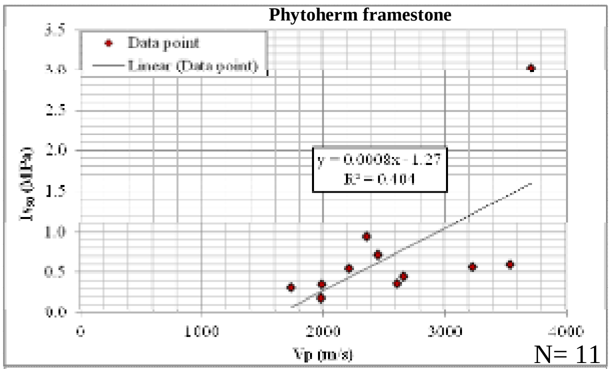

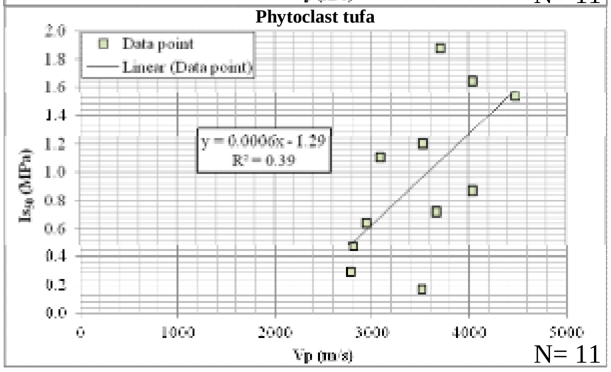

Figure 117 (cont'd.). Regression plots of point load strength index (Is_{50}) vs. seismic wave velocity (Vp) for the Antalya tufa rock mass and tufa rock types.

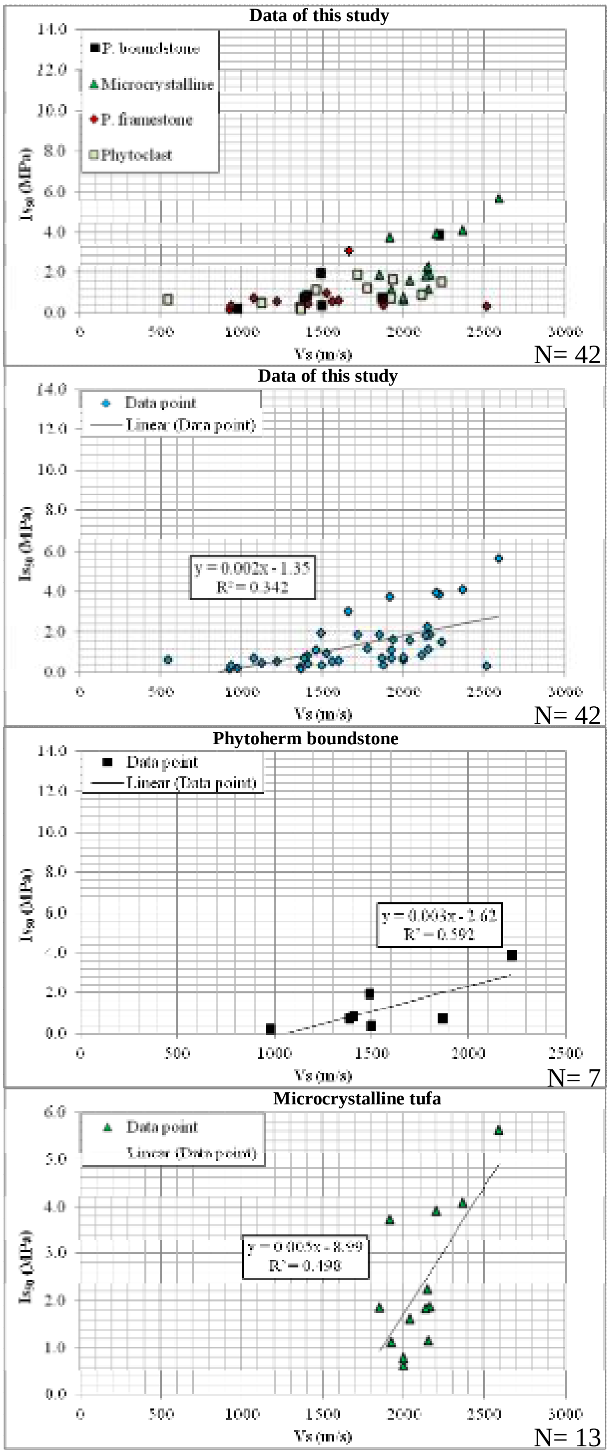

Figure 118. Regression plots of point load strength index (Is_{50}) vs. seismic wave velocity (Vs) for the Antalya tufa rock mass and tufa rock types.

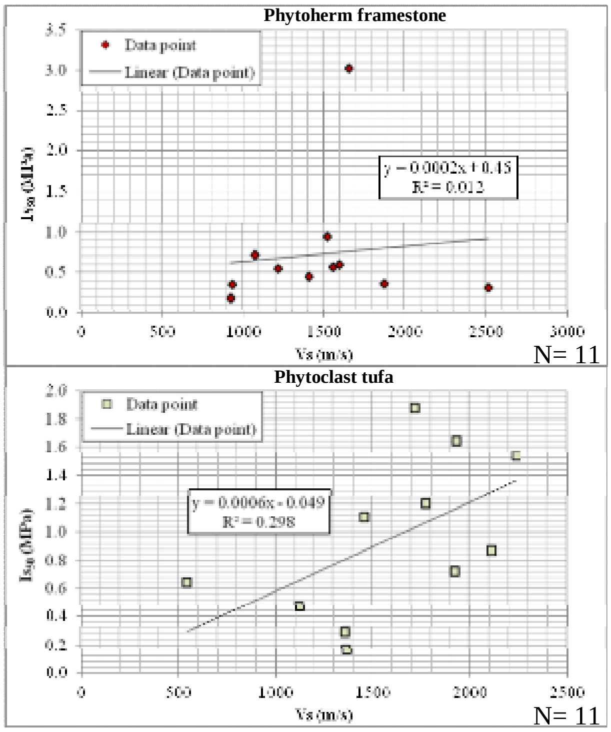

Figure 118 (cont'd.). Regression plots of point load strength index (Is_{50}) vs. seismic wave velocity (Vs) for the Antalya tufa rock mass and tufa rock types.

4. Point load strength index and slake durability correlations of the Antalya tufa rock mass

Correlation between the point load strength index (Is_{50}) and slake durability index (Id_2) of the Antalya tufa rock mass is given by Figure 119.

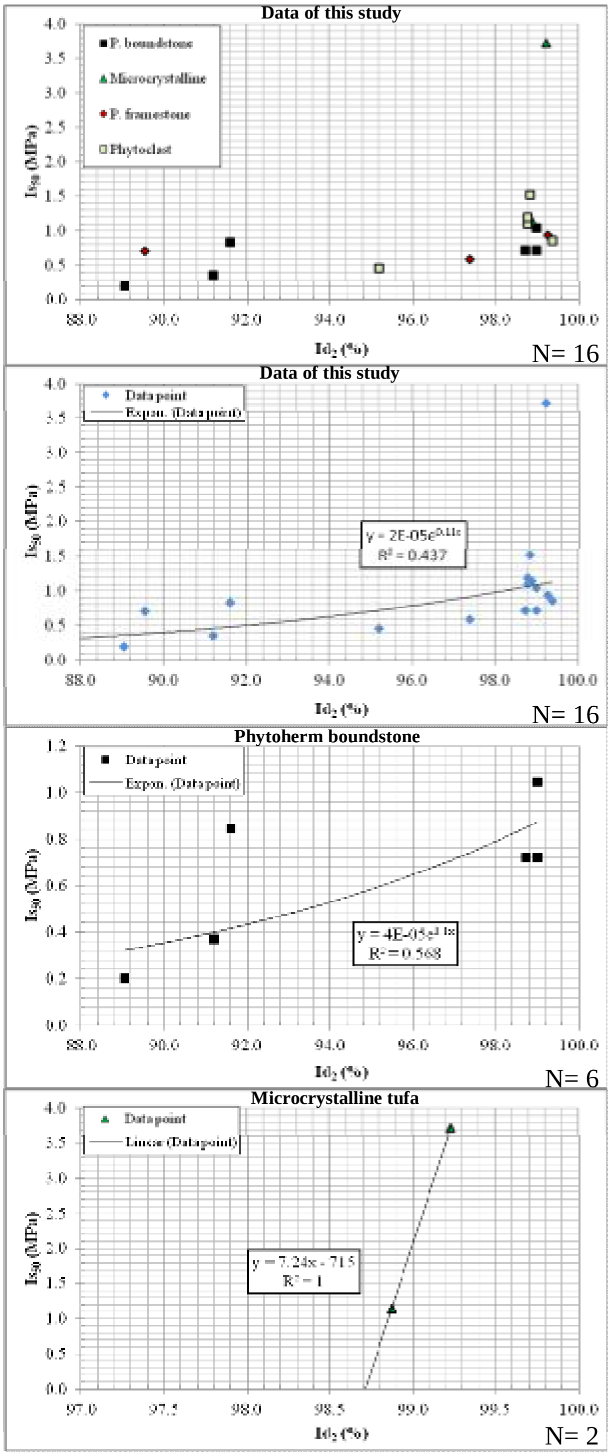

Figure 119. Regression plots of point load strength index (Is_{50}) vs. slake durability index (Id_2) for the Antalya tufa rock mass and tufa rock types.

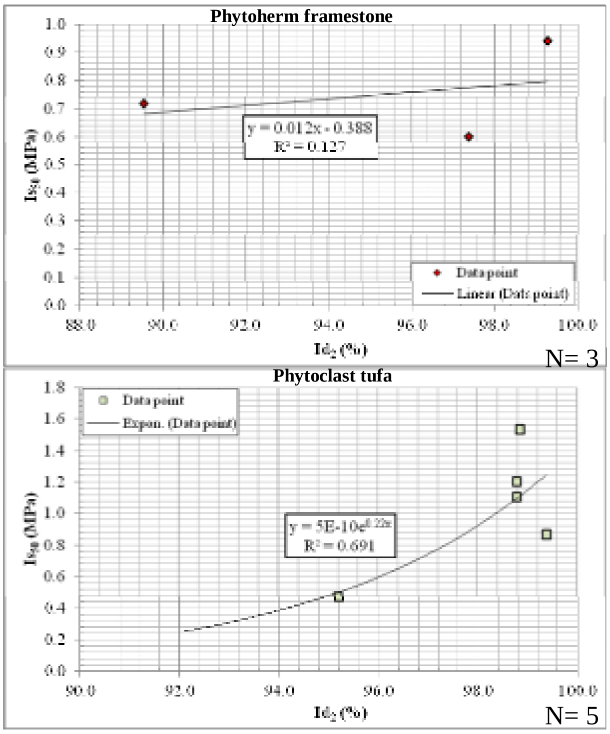

Figure 119 (cont'd.). Regression plots of point load strength index (Is_{50}) vs. slake durability index (Id_2) for the Antalya tufa rock mass and tufa rock types.

VII.3.5 Correlations between seismic wave velocity (Vp, Vs) and other parameters of the Antalya tufa rock mass

Since correlations between seismic wave velocity (Vp, Vs) and uniaxial compressive strength (UCS), between seismic wave velocity (Vp, Vs) and Elasticity modulus (E), between seismic wave velocity (Vp, Vs) and tensile strength (σ_t), between the seismic wave velocity Vp, Vs and point load strength index (Is_{50}) of the Antalya tufa rock mass have been presented in the previous sections, correlation between seismic wave velocity (Vp, Vs) and other strength parameters will be given in this section.

<u>*1. Seismic wave velocity and unit weight of the Antalya tufa rock mass*</u>

Correlation between seismic wave velocity (Vp and Vs) and unit weight (γ) of the Antalya tufa rock mass is given by Figures 120 and 121, respectively.

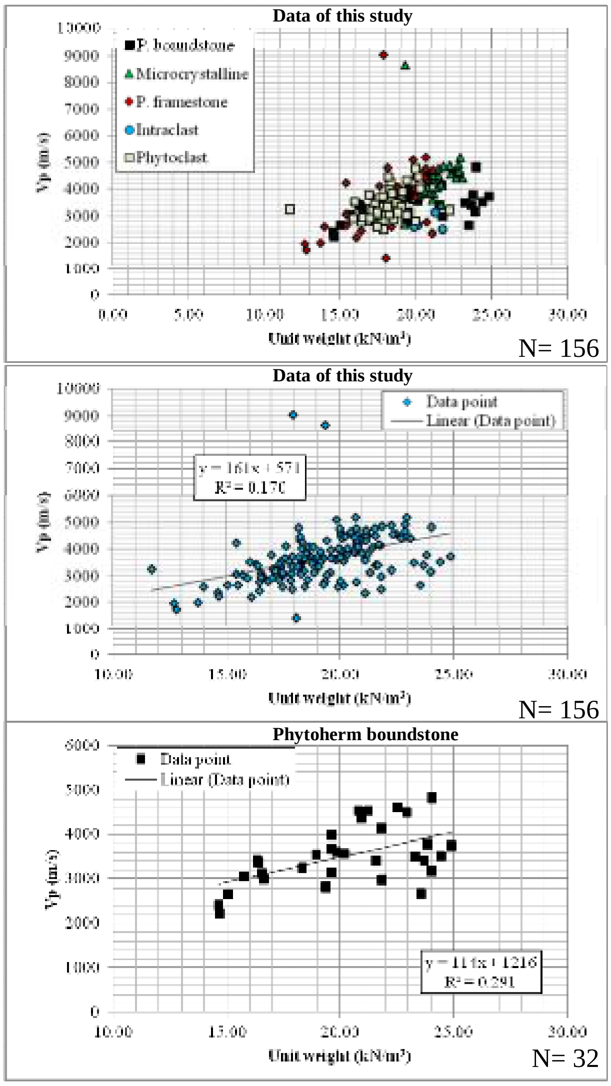

Figure 120. Regression plots of seismic wave velocity (Vp) vs. unit weight (γ) for the Antalya tufa rock mass and tufa rock types.

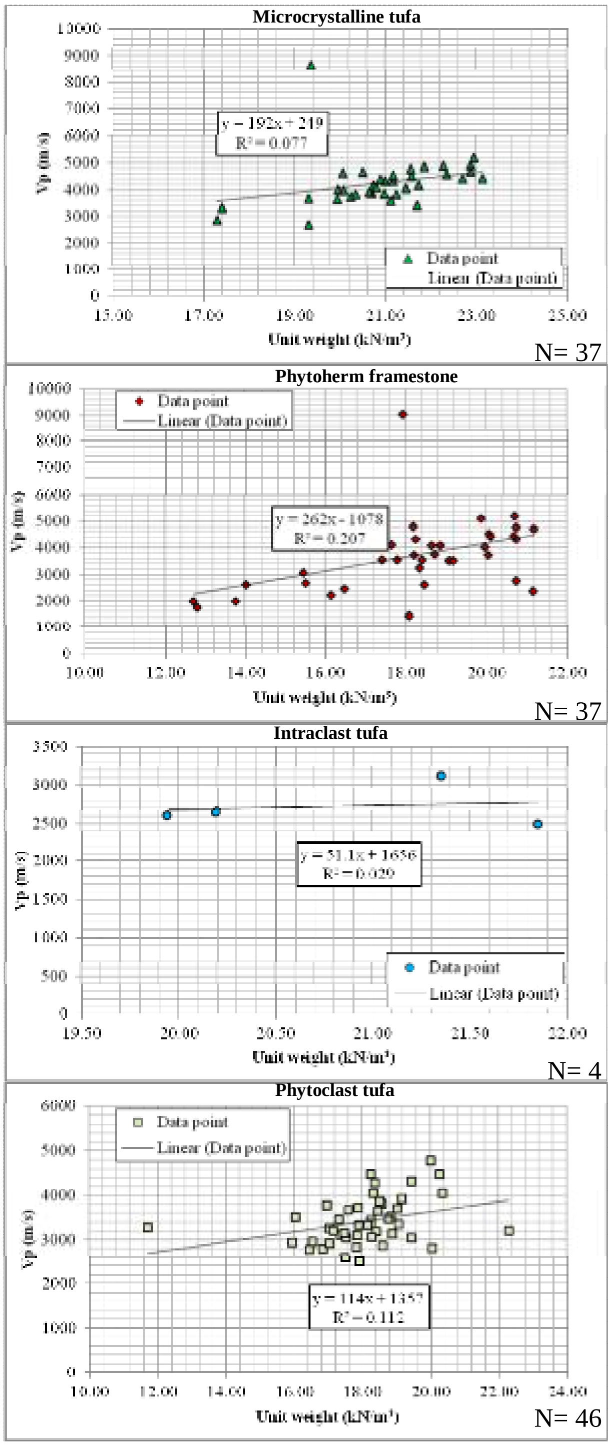

Figure 120 (cont'd.). Regression plots of seismic wave velocity (Vp) vs. unit weight (γ) for the Antalya tufa rock mass and tufa rock types.

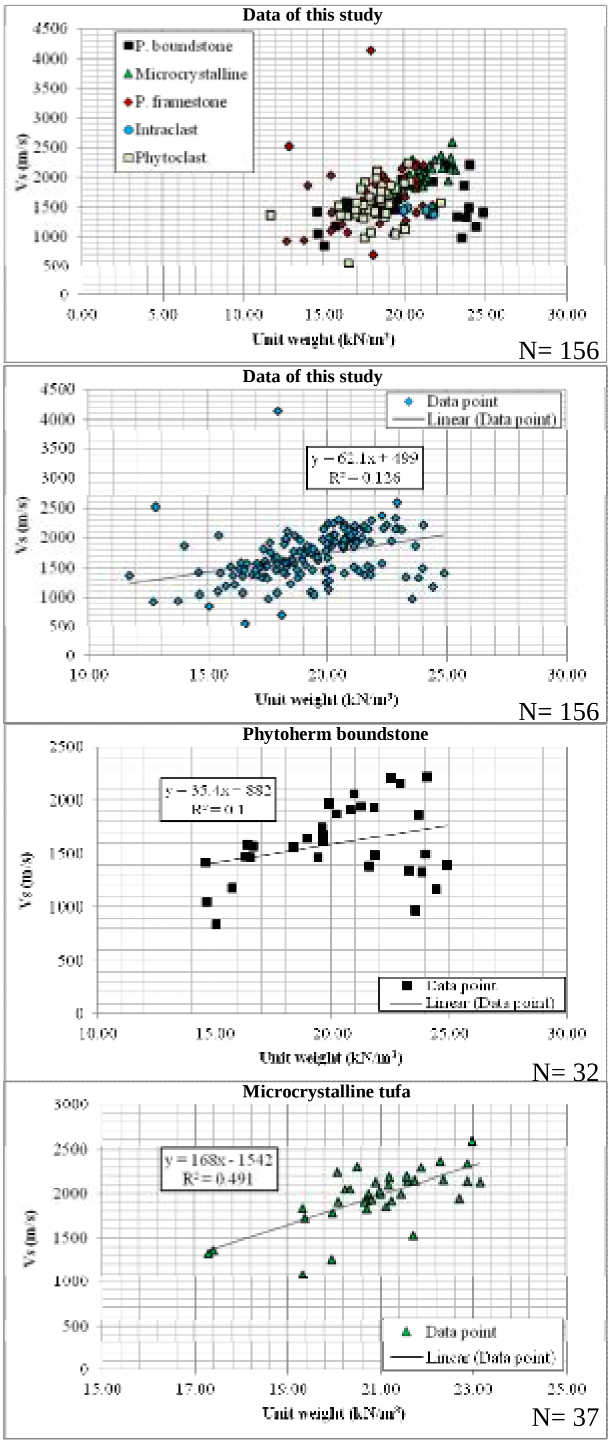

Figure 121. Regression plots of seismic wave velocity (Vs) vs. unit weight (γ) for the Antalya tufa rock mass and tufa rock types.

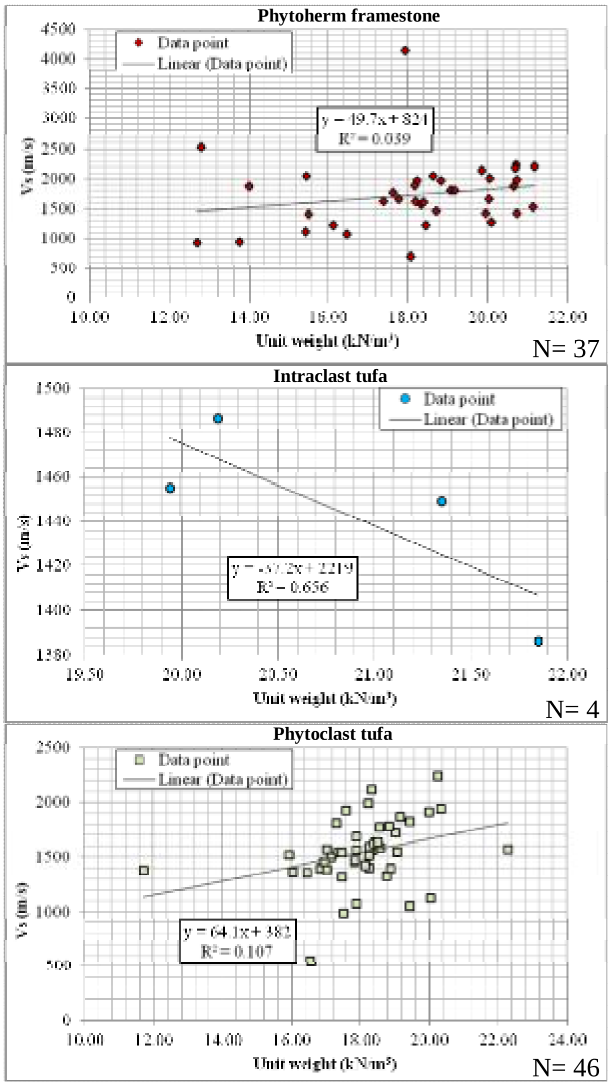

Figure 121 (cont'd.). Regression plots of seismic wave velocity (Vs) vs. unit weight (γ) for the Antalya tufa rock mass and tufa rock types.

2. Seismic wave velocity and porosity of the Antalya tufa rock mass

Correlation between seismic wave velocity (Vp and Vs) and porosity (n) of the Antalya tufa rock mass is given by Figures 122 and 123.

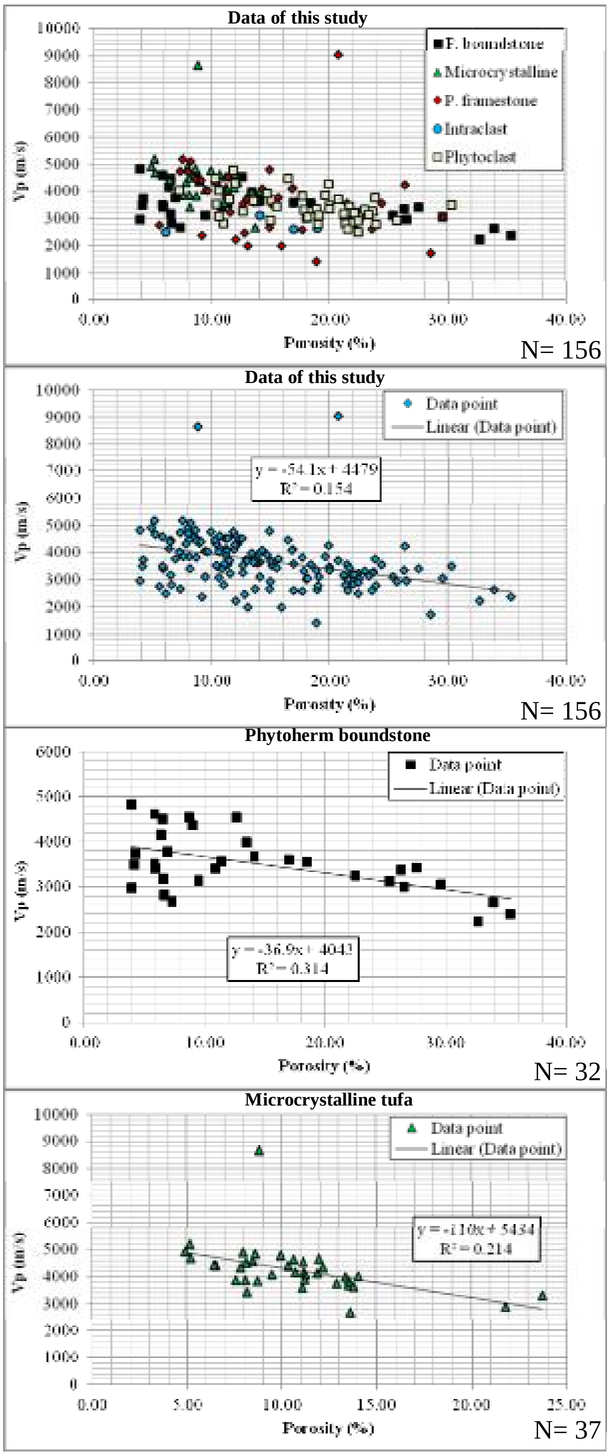

Figure 122. Regression plots of seismic wave velocity (Vp) vs. porosity (n) for the Antalya tufa rock mass and tufa rock types.

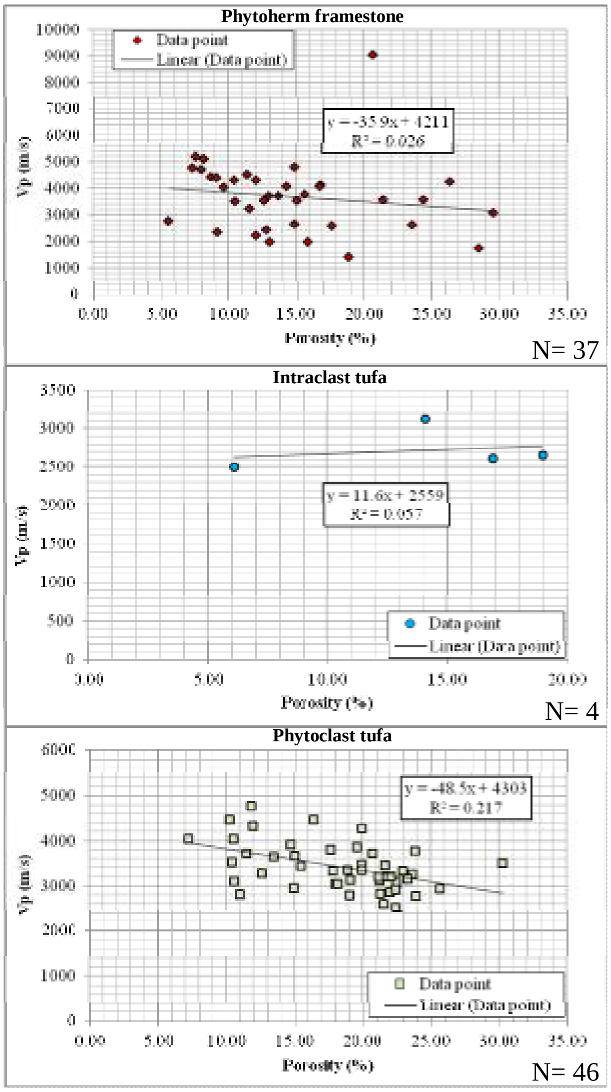

Figure 122 (cont'd.). Regression plots of seismic wave velocity (Vp) vs. porosity (n) for the Antalya tufa rock mass and tufa rock types.

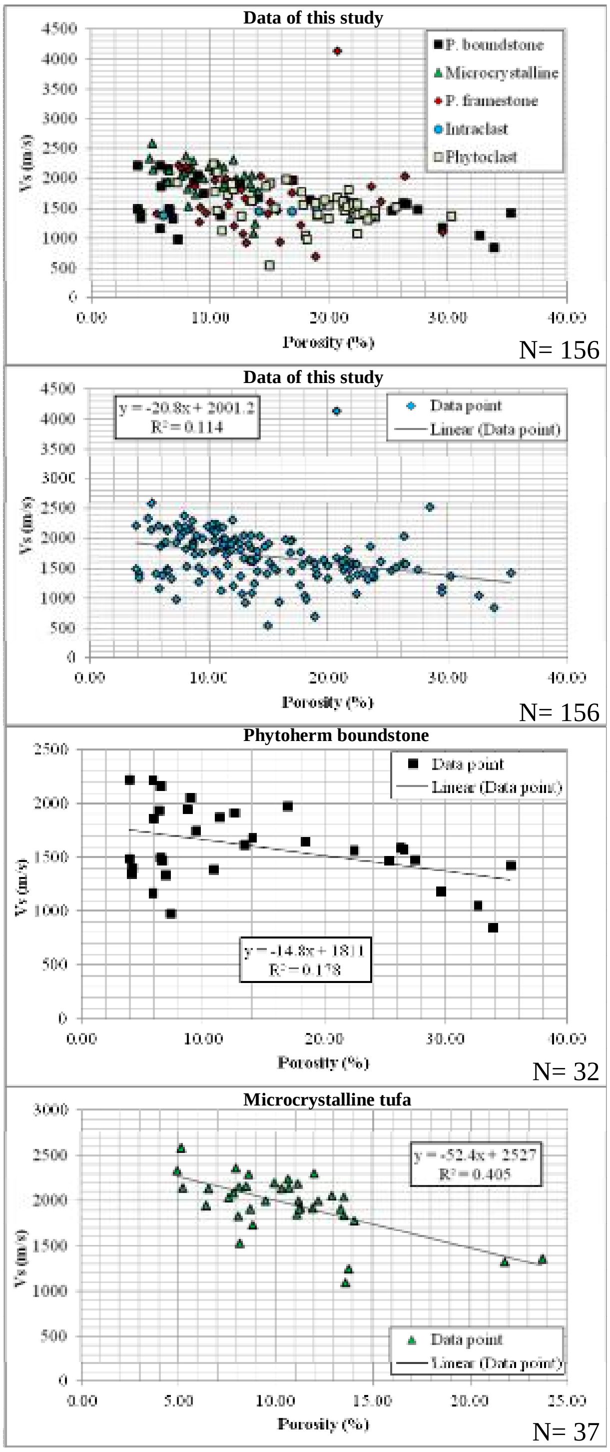

Figure 123. Regression plots of seismic wave velocity (Vs) vs. porosity (n) for the Antalya tufa rock mass and tufa rock types.

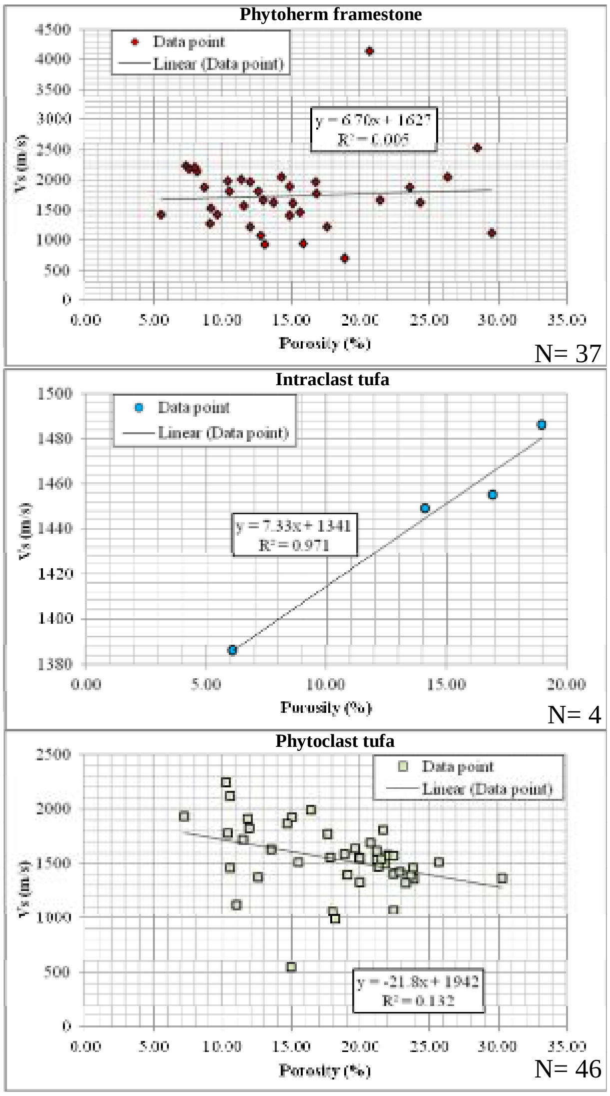

Figure 123 (cont'd.). Regression plots of seismic wave velocity (Vs) vs. porosity (n) for the Antalya tufa rock mass and tufa rock types.

3. Seismic wave velocity and slake durability correlations of the Antalya tufa rock mass

Correlation between seismic wave velocity (Vp, Vs) and slake durability index (Id_2) of the Antalya tufa rock mass is given by Figures 124 and 125, respectively.

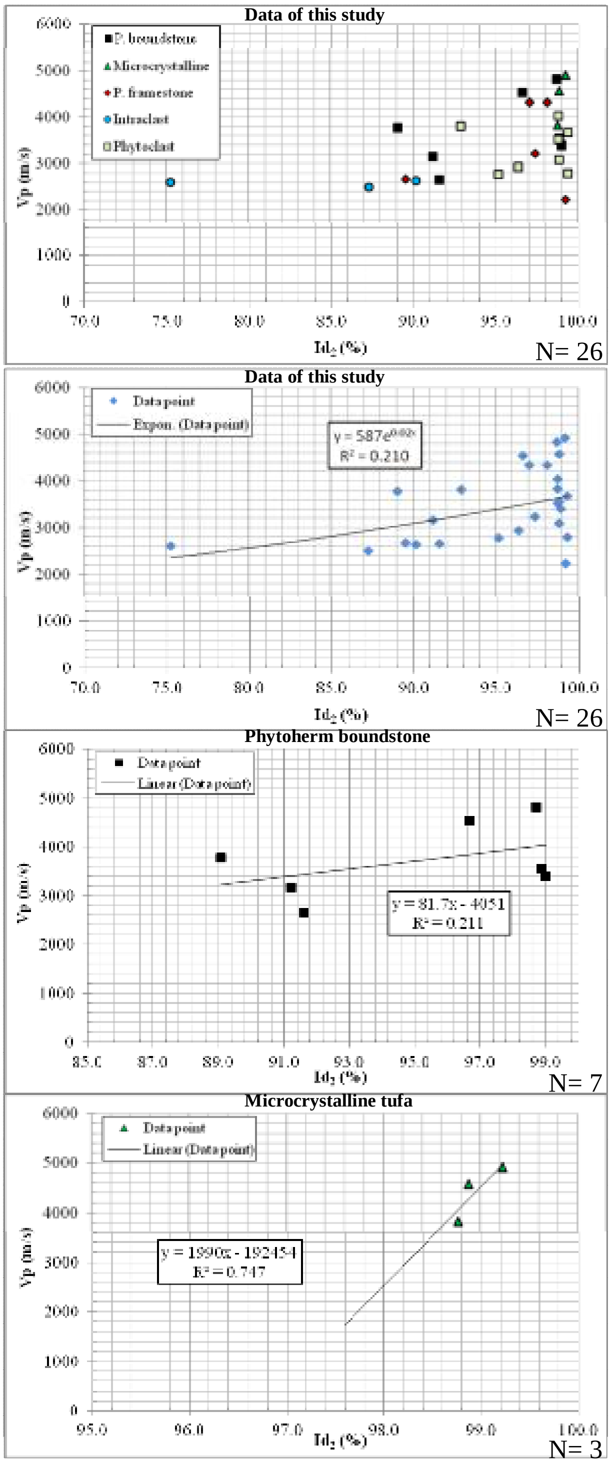

Figure 124. Regression plots of seismic wave velocity (Vp) vs. slake durability index (Id_2) for the Antalya tufa rock mass and tufa rock types.

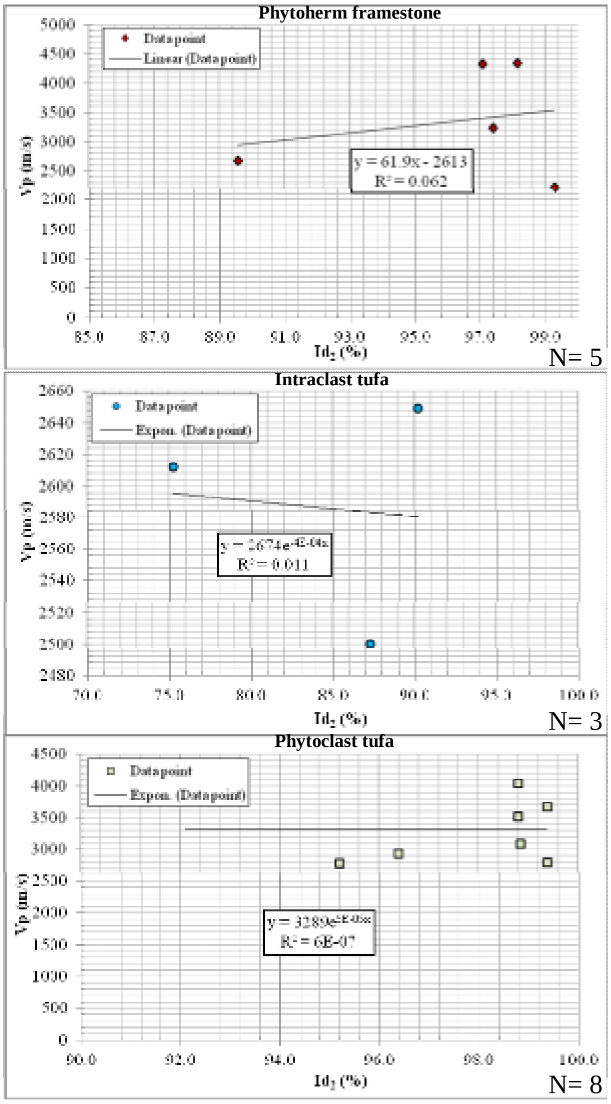

Figure 124 (cont'd.). Regression plots of seismic wave velocity (Vp) vs. slake durability index (Id_2) for the Antalya tufa rock mass and tufa rock types.

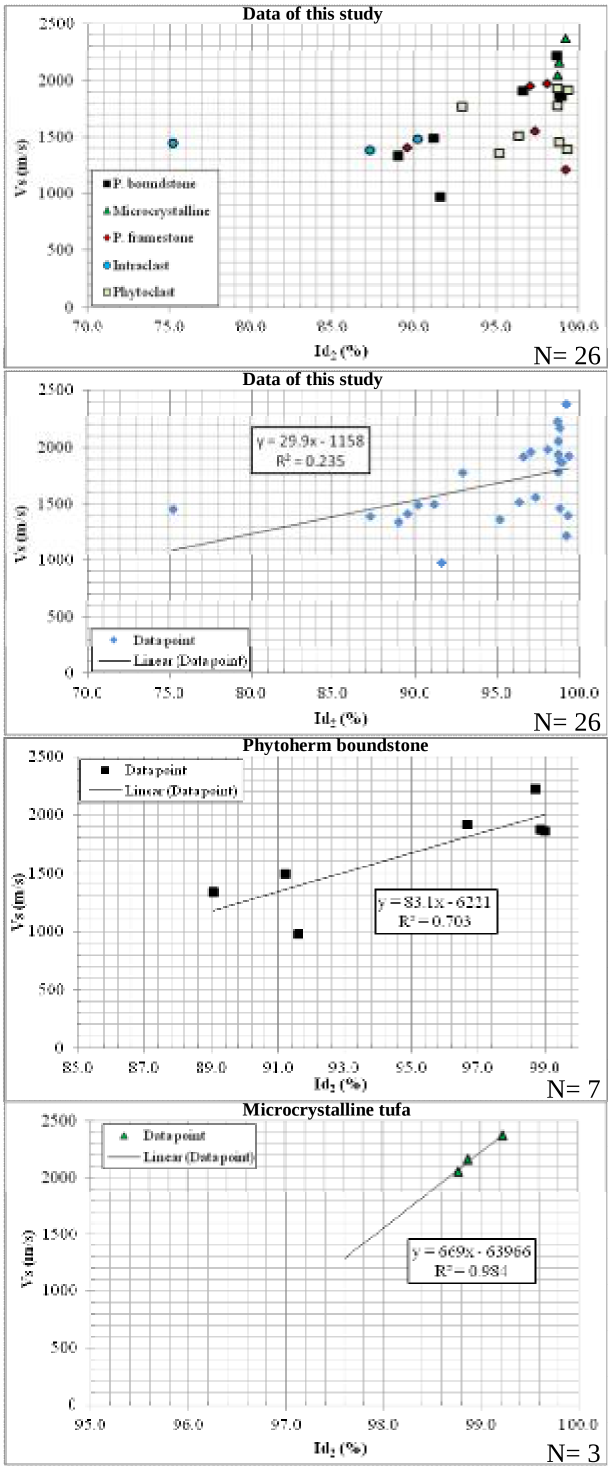

Figure 125. Regression plots of seismic wave velocity (Vs) vs. slake durability index (Id$_2$) for the Antalya tufa rock mass and tufa rock types.

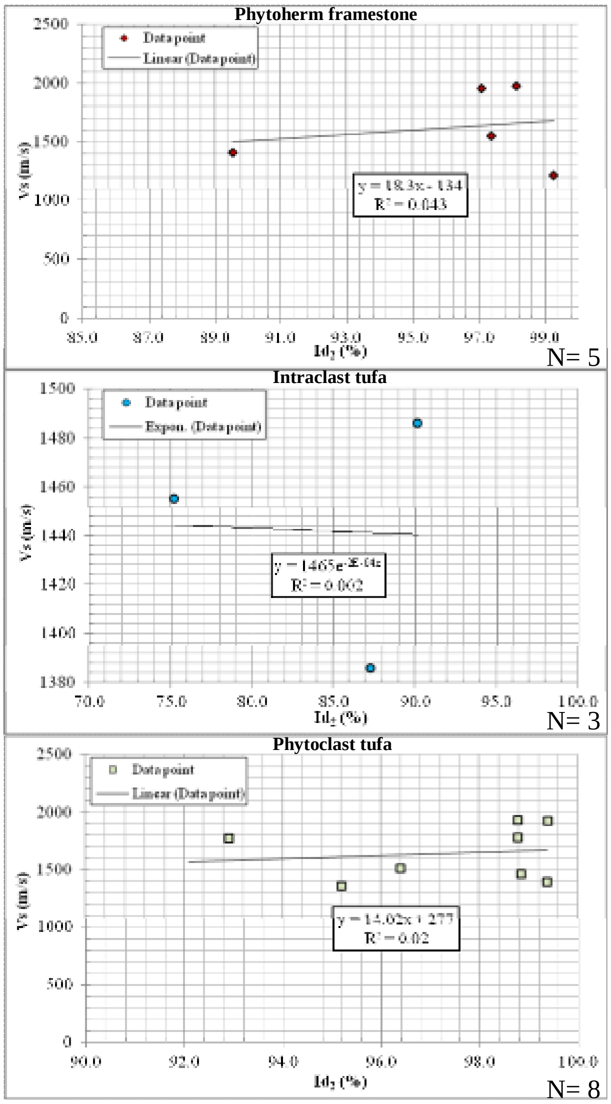

Figure 125 (cont'd.). Regression plots of seismic wave velocity (Vs) vs. slake durability index (Id_2) for the Antalya tufa rock mass and tufa rock types.

VII.3.6 Correlations between slake durability index and other parameters of the Antalya tufa rock mass

Since correlations between slake durability index (Id_2) and uniaxial compressive strength (UCS), between slake durability index and Elasticity modulus (E), between slake durability index and tensile strength (σ_t), between the slake durability index and point load strength index (Is_{50}), between slake durability index and seismic wave velocity (Vp, Vs) of the Antalya tufa rock mass have been presented in the previous sections, correlation between slake durability index and other strength parameters will be given in this section.

1. Slake durability index and unit weight of the Antalya tufa rock mass

Correlation between slake durability index (Id_2) and unit weight (γ) of the Antalya tufa rock mass is given by Figure 126.

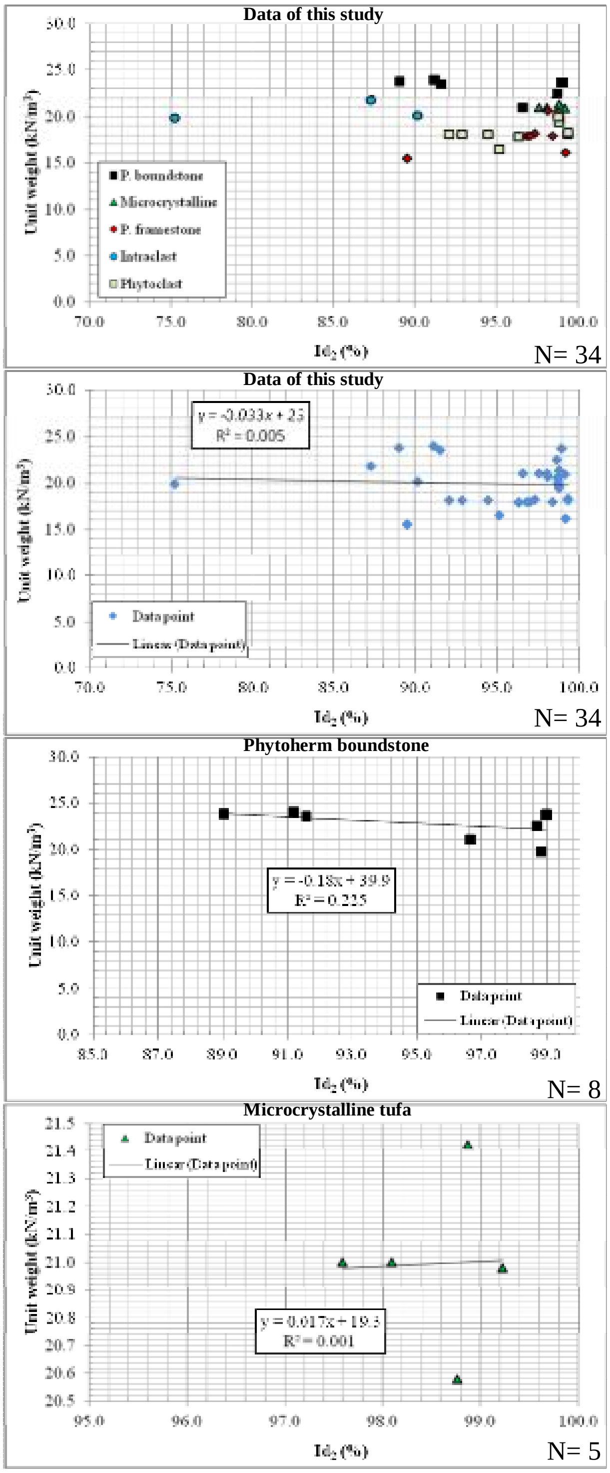

Figure 126. Regression plots of slake durability index (Id_2) vs. unit weight (γ) for the Antalya tufa rock mass and tufa rock types.

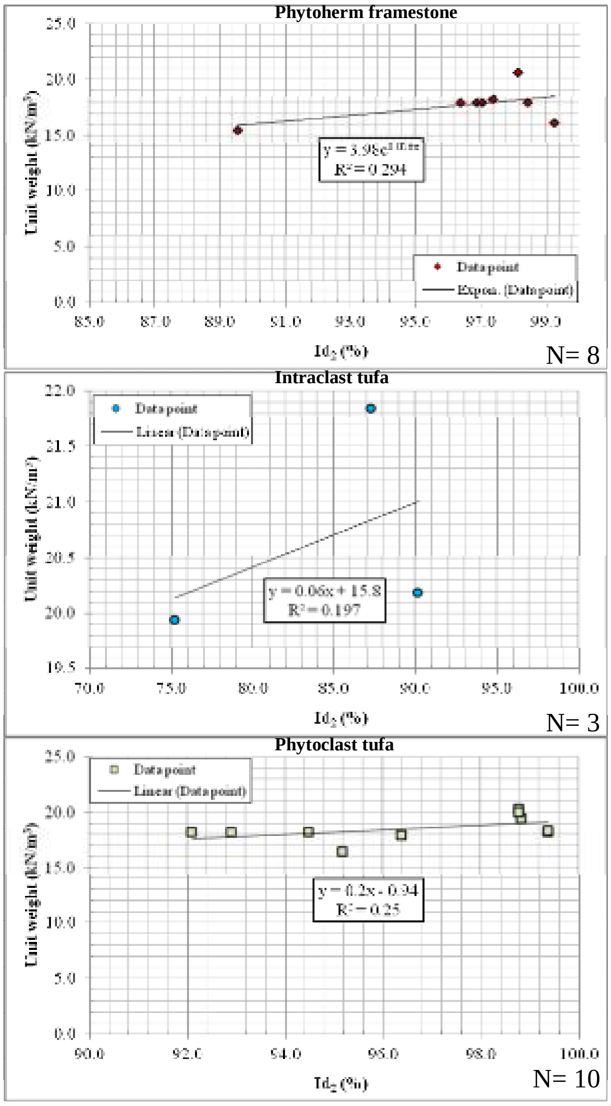

Figure 126 (cont'd.). Regression plots of slake durability index (Id_2) vs. unit weight (γ) for the Antalya tufa rock mass and tufa rock types.

2. Slake durability index and porosity of the Antalya tufa rock mass

Correlation between slake durability index (Id_2) and porosity (n) of the Antalya tufa rock mass is given by Figure 127.

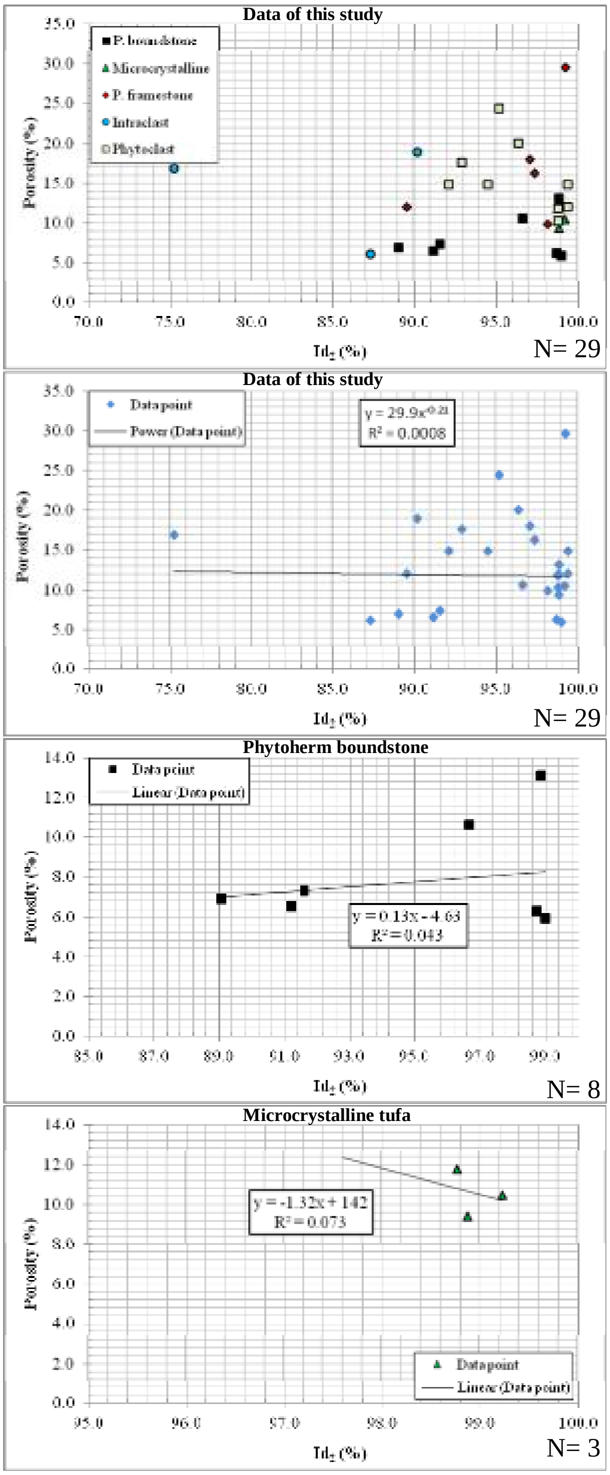

Figure 127. Regression plots of slake durability index (Id_2) vs. porosity (n) for the Antalya tufa rock mass and tufa rock types.

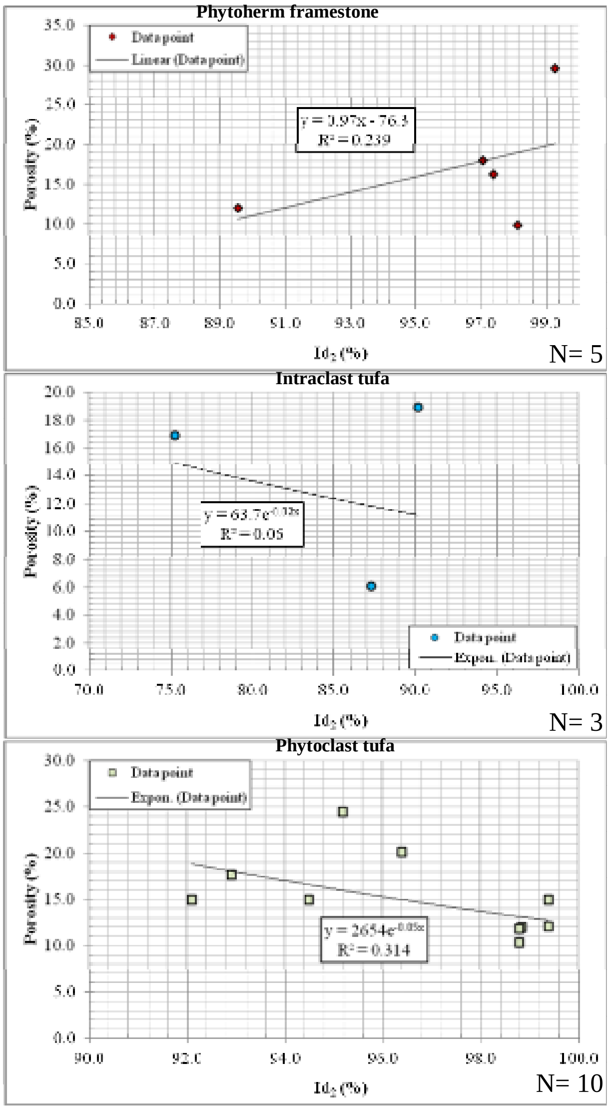

Figure 127 (cont'd.). Regression plots of slake durability index (Id_2) vs. porosity (n) for the Antalya tufa rock mass and tufa rock types.

VII.4 Discussion of the correlations obtained between the geotechnical parameters of the Antalya tufa rock mass

After relating the individual geotechnical parameters of the Antalya tufa rock mass, a number of good correlations ($R^2 \geq 0.75$) were obtained for the tufa rock types and for the tufa rock mass in general. Table 28, in which cells with good correlations are highlighted in gray, summarizes the results of the regression studies of the Antalya tufa rock types and rock mass, respectively. The regressions which obeyed linear, exponential or power laws are indicated by different numbers in Table 28.

When the regression results of the geomechanical parameters tested for the Antalya tufa rock mass are to be studied, it is recognized that the Antalya tufa rock mass could be characterized better by using strength parameters, namely, uniaxial compressive and tensile strength, together with index parameters, namely, unit weight and porosity. Higher coefficient of determination values obtained for these parameters in Table 28 reveal this situation. Elaborate statistical evaluation of these geomechanical parameters will be performed in the next chapter.

The Antalya tufa rock mass possesses higher coefficient of determination values between UCS and E, between UCS and σ_t, between n and γ, and between Vs and Vp, respectively. These correlations were all determined to be linear. Further correlations between the other geomechanical parameters of the Antalya tufa rock mass, such as between UCS and Vs, between UCS and Is_{50}, between E and Vp, have resulted in fair ($0.5 < R^2 < 0.75$) coefficient of determination values. Slake durability index values of the Antalya tufa rock mass have been observed to lead to poor correlations with the other geomechanical parameters. However, it has been determined to be a fairly well representative parameter for the assessment of the durability of the weaker tufa types against weathering and water reaction.

Among the types of the Antalya tufa rock mass, intraclast tufa has been poorly characterized since very limited number of samples has been recovered due to its fragile and weak structure. Only 4 core samples were able to be recovered for laboratory tests, therefore, the coefficient of determination values determined for the correlation of geomechanical parameters of intraclast tufa need to be verified by a larger data set. On the other hand, in order to give an idea for the range of the geomechanical parameters of intraclast tufa, all the laboratory test results of intraclast tufa type have been presented by figures and tables.

Table 28. Summary of the results of the regression (R^2) studies of the geomechanical parameters of the Antalya tufa rock mass.

TUFA ROCK MASS (ENTIRE DATA)

	UCS	γ	n	E	σ_t	Is_{50}	Vp	Vs	Id_2
UCS	-	0.508	0.340	*0.909*	*0.768*	0.711	0.551	0.643	*0.102*
γ		-	*0.769*	0.476	0.384	*0.231*	*0.169*	*0.126*	*0.005*
n			-	0.462	0.262	*0.204*	*0.154*	*0.114*	0.0008
E				-	0.273	0.565	0.725	0.685	0.412
σ_t					-	0.319	*0.248*	0.083	0.253
Is_{50}						-	*0.480*	*0.342*	0.437
Vp							-	*0.812*	0.210
Vs								-	*0.235*
Id_2									-

PHYTOHERM BOUNDSTONE

	UCS	γ	n	E	σ_t	Is_{50}	Vp	Vs	Id_2
UCS	-	0.919	0.941	0.918	*0.600*	*0.722*	0.583	0.389	*0.350*
γ		-	*0.887*	0.982	*0.033*	*0.0001*	*0.291*	*0.099*	*0.225*
n			-	*0.931*	*0.024*	*0.294*	*0.314*	*0.178*	*0.043*
E				-	0.681	0.803	0.523	0.149	*0.078*
σ_t					-	0.138	0.113	0.024	0.530
Is_{50}						-	*0.634*	*0.592*	0.570
Vp							-	*0.691*	*0.210*
Vs								-	*0.700*
Id_2									-

MICROCRYSTALLINE

	UCS	γ	n	E	σ_t	Is_{50}	Vp	Vs	Id_2
UCS	-	*0.62*	*0.387*	*0.882*	*0.915*	*0.802*	*0.571*	*0.644*	*0.99*
γ		-	*0.803*	*0.502*	*0.813*	*0.249*	*0.077*	*0.491*	*0.001*
n			-	*0.212*	0.778	*0.295*	*0.214*	*0.405*	*0.073*
E				-	*0.349*	*0.934*	0.884	*0.902*	*1.000*
σ_t					-	*0.128*	0.476	*0.284*	0.39
Is_{50}						-	*0.330*	*0.498*	*1.000*
Vp							-	*0.775*	*0.75*
Vs								-	*0.98*
Id_2									-

Linear, exponential and power laws of correlations are indicated by italic, regular and underlined numbers, respectively.

Table 28 (cont'd.). Summary of the results of the regression (R^2) studies of the geomechanical parameters of the Antalya tufa rock mass.

PHYTOHERM FRAMESTONE

	UCS	γ	n	E	σ_t	Is_{50}	Vp	Vs	Id_2
UCS	-	0.345	*0.140*	*0.674*	*0.581*	*0.802*	0.841	0.755	*0.644*
γ		-	*0.718*	*0.649*	*0.623*	*0.406*	*0.207*	*0.039*	0.294
n			-	*0.968*	*0.480*	*0.083*	*0.026*	*0.005*	*0.239*
E				-	-	*0.860*	*0.809*	*0.796*	*1.000*
σ_t					-	0.032	*0.500*	*0.315*	0.698
Is_{50}						-	*0.404*	*0.012*	*0.127*
Vp							-	*0.885*	*0.062*
Vs								-	*0.043*
Id_2									-

INTRACLAST

	UCS	γ	n	E	σ_t	Is_{50}	Vp	Vs	Id_2
UCS	-	0.255	0.072	0.189	-	-	0.128	0.174	*0.914*
γ		-	*0.789*	*0.875*	-	-	*0.029*	*0.656*	*0.197*
n			-	*0.992*	-	-	*0.057*	*0.971*	0.060
E				-	-	-	*1.000*	*0.996*	0.739
σ_t					-	-	-	-	-
Is_{50}						-	-	-	-
Vp							-	*0.094*	0.011
Vs								-	0.002
Id_2									-

PHYTOCLAST

	UCS	γ	n	E	σ_t	Is_{50}	Vp	Vs	Id_2
UCS	-	0.007	0.141	*0.155*	*0.056*	*0.910*	*0.078*	*0.354*	*0.716*
γ		-	*0.609*	*0.170*	*0.264*	*0.489*	*0.112*	*0.107*	*0.250*
n			-	*0.100*	*0.149*	0.791	*0.217*	*0.132*	0.314
E				-	*0.198*	*0.032*	*0.277*	*0.921*	0.429
σ_t					-	*0.764*	*0.399*	*0.209*	*0.116*
Is_{50}						-	*0.393*	*0.292*	0.691
Vp							-	*0.557*	0.000
Vs								-	*0.019*
Id_2									-

Linear, exponential and power laws of correlations are indicated by italic, regular and underlined numbers, respectively.

Conflicting trends i.e., between UCS and Vs (Figure 100), between UCS and Vp (Figure 101), between E and Vp (Figure 104), between E and Vs (Figure 105), between Vs and γ (Figure 121), between Vp and n (Figure 122), between n and Vs (Figure 123), between Id_2 and Vp (Figure 124), and between Id_2 and Vs (Figure 125) have been observed for intraclast tufa. Ultrasonic wave velocity values determined for intraclast tufa had no correlation with most of the other geomechanical parameters tested. The medium porous structure and possible clay minerals along the rims of pore spaces might have had a significant effect on the varying ultrasonic wave velocity measurements, which could have decreased the degree of correlation (Figure 57).

Similar to the intraclast tufa type, the phytoclast tufa type is one of the weak rock types of the Antalya tufa rock mass. The coefficient of determination values given for phytoclast tufa in Table 28 have shown that a few good correlations between geomechanical parameters could be used for the characterization purposes. The point load strength index has been found to be in good correlation with UCS, n and σ_t. The point load strength index of a rock sample is easy to determine both in the field and in the laboratory due to its flexibility for sample geometry requirements. Hence, its correlations with other strength parameters might be very useful in cases of scarce data. Furthermore, a good linear correlation between Vs and E has been observed for phytoclast tufa. Besides, conflicting trends, i.e., between UCS and σ_t (Figure 97) and between E and Is_{50} (Figure 106) have been observed for phytoclast tufa. Although the coefficient of determination values of these conflicting trends was very low, the existence of such relationships has illustrated the variability of the geomechanical properties of the phytoclast tufa.

Phytoherm boundstone type has been observed to be characterized better by UCS, n, E and γ as also observed for the Antalya tufa rock mass. Most of the correlations for these geomechanical parameters have been linear, only the correlations between n and γ, and between n and E have been exponential. Conflicting trends, i.e., between E and Id_2 (Figure 107), between σ_t and Is_{50} (Figure 111), and between γ and Id_2 (Figure 126) have been observed for phytoherm boundstone tufa.

Vp, Vs, UCS, E and n parameters of phytoherm framestone type have been observed to be in good correlation with each other. Most of the correlations have been linear. Only the correlation between UCS and ultrasonic wave velocity has been determined to be exponential. Conflicting trends, i.e., between σ_t and Is_{50} (Figure 111), between σ_t and Vs (Figure 113), and between Vs and n (Figure 123) have been observed for phytoherm framestone tufa.

Microcrystalline tufa, which has been observed to be stronger and massive as compared to the other tufa types of the Antalya tufa rock mass, has been successfully characterized as far as most of the geomechanical parameters tested are concerned. For the characterization purposes, it would be better to use E, UCS, n, γ and σ_t parameters with high R^2 values, which is also the situation for the Antalya tufa rock mass.

CHAPTER VIII

STATISTICAL ANALYSES OF THE GEOTECHNICAL PARAMETERS OF THE ANTALYA TUFA

VIII.1 Introduction

This chapter covers the statistical analyses of the geotechnical parameters, whose variances have been observed to be large during the interpretation of the laboratory test results of the Antalya tufa rock mass. All the statistical analyses have been carried out by the IBM SPSS software version 19.

Prior to the statistical analyses of the geotechnical parameters, which will be named in the following sections as the variables of the Antalya tufa rock mass, the entire raw data set formed by the ten variables have been evaluated to check whether they are normally distributed or not. Upon the completion of normal distribution analyses of the variables, principal component analysis (PCA) of the data set was performed to reveal the internal structure of the data set. Finally, multiple linear regression analyses (MLRA) of the variables was performed to obtain the relationships between the variables.

Since the data set of this study is not large and mathematical relationships between variables are required, an artificial neural network method has not been attempted. As it is well known, input values of the variables are processed through a hidden or unknown algorithm to predict real output values during artificial neural network analysis. At the end of this analysis, only the accuracy of the predictions without mathematical relationships can be shown as the result of analysis.

VIII.2 The normal distribution analysis, Shapiro-Wilk W test

The normal probability density, usually referred to simply as the normal distribution, is considered the most important probability distribution since it is very tractable analytically. In other words, a large number of results involving this distribution can be derived in explicit form and it arises as the outcome of the central limit theorem, which states that under mild conditions the sum of a large number of random variables is distributed approximately normally (Casella and Berger, 2001).

In order to test whether the entire data is normally distributed or not, first the kurtosis and the skewness of the data have been examined (Table 29). The skewness simply refers to the "lean" of a distribution - a positive skew indicates a longer tail to the right than to the left, and a negative skew indicates a longer tail to the left than to the right. The kurtosis simply refers to how "flat" a distribution is. In general, if kurtosis and skewness are not between -2 and +2, the data is too far away from a normal distribution and needs to be corrected before applying tests that have assumptions of normality. Accordingly, unit weight, porosity and the point load strength index have been found to be normally distributed (Table 29).

A more rigorous test of normality applicable to data sets of approximately two thousand elements or less is offered by the Shapiro-Wilk W test. If the significance value of the Shapiro-Wilk test is greater than 0.05 then the data is normal. If it is below 0.05 then the data significantly deviates from a normal distribution.

According to the results of the Sahpiro-Wilk test presented in Table 30, the only variable having normal probability distribution is the unit weight. In order to normalize the other variables, the logarithm of the other variables have been taken and tested. After data transformation through normalization process by taking the logarithm of the variables, the other parameters, namely, UCS, E, σ_t and Is_{50} have been observed to have a normal probability distribution (Table 31).

Table 29. Skewness and kurtosis values of the experimental data

Case Processing Summary								
Geotechnical parameters or variables	Cases						Skewness	Kurtosis
	Valid		Missing		Total			
	N	Percent	N	Percent	N	Percent		
Unit weight (kN/m^3)	149	95.5%	7	4.5%	156	100.0%	-0.83	-0.59
n (%)	149	95.5%	7	4.5%	156	100.0%	0.659	-0.234
LOI (%)	22	14.1%	134	85.9%	156	100.0%	-1.918	2.158
V_s (m/s)	148	94.9%	8	5.1%	156	100.0%	1.242	7.180
V_p (m/s)	148	94.9%	8	5.1%	156	100.0%	1.438	8.645
UCS (MPa)	41	26.3%	115	73.7%	156	100.0%	3.190	12.639
E (MPa)	24	15.4%	132	84.6%	156	100.0%	2.098	4.095
σ_t (MPa)	46	29.5%	110	70.5%	156	100.0%	1.617	3.606
Id_2 (%)	26	16.7%	130	83.3%	156	100.0%	-2.085	5.372
Is_{50} (MPa)	42	26.9%	114	73.1%	156	100.0%	1.377	1.363

Table 30. The results of normality test of the experiment data

Geotechnical parameters or variables	Shapiro-Wilk		
	Statistic	df	Sig.
Unit weight (kN/m^3)	.996	149	.936
n (%)	.950	149	.000
LOI (%)	.549	22	.000
V_s (m/s)	.917	148	.000
V_p (m/s)	.910	148	.000
UCS (MPa)	.652	41	.000
E (MPa)	.722	24	.000
σ_t (MPa)	.869	46	.000
Id_2 (%)	.736	26	.000
Is_{50} (MPa)	.835	42	.000

Table 31. The results of normality test of the transformed experiment data.

Geotechnical parameters or variables	Shapiro-Wilk		
	Statistic	df	Sig.
Unit weight (kN/m^3)	.996	149	.936
Log n (%)	.981	149	.038
Log LOI (%)	.528	22	.000
Log V_s (m/s)	.961	148	.000
Log V_p (m/s)	.965	148	.001
Log UCS (MPa)	.954	41	.100
Log E (MPa)	.973	24	.740
Log σ_t (MPa)	.976	46	.437
Log Id_2 (%)	.710	26	.000
Log Is_{50} (MPa)	.971	42	.353

VIII.3 Principal component analysis (PCA)

The idea behind the principal component analysis (PCA) can be simply explained as the reduction of the dimensionality of a data set comprising of interrelated variables, while retaining as much as possible of the variance present in the data set. This is achieved by transforming to a new set of variables, the principal components (PCs), which are uncorrelated, and which are ordered so that the first few retain most of the variation present in all of the original variables (Jolliffe, 2002).

Principal component analysis requires that there be correlations greater than 0.30 between the variables included in the analysis. However, the data consisting of the geotechnical parameters of Antalya tufa rock mass have some missing values for some variables. In other words, not all of the samples in the data set have been able to be tested for each geotechnical parameter. Hence, the number of correlations has not been as much as the number of the samples. Also, not all of the parameters have been included in the analysis. The available data allow including the unit weight, porosity, seismic velocities, uniaxial compressive strength and Young's modulus in PCA. For this set of variables, there are 14 correlations in the matrix greater than 0.30, satisfying this requirement (Table 32).

Table 32. The correlation matrix of the analyzed data.

Geotechnical parameters or variables	Unit weight (kN/m^3)	n (%)	V_s (m/s)	V_p (m/s)	UCS (MPa)	E (MPa)
Unit weight (kN/m^3)	1.000	-	-	-	-	-
n (%)	-.849	1.000	-	-	-	-
V_s (m/s)	.554	-.444	1.000	-	-	-
V_p (m/s)	.474	-.456	.939	1.000	-	-
UCS (MPa)	.568	-.447	.774	.625	1.000	-
E (MPa)	.563	-.466	.776	.648	.955	1.000

The PCA requires also that the Kaiser-Meyer-Olkin measure of sampling adequacy (MSA) be greater than 0.50 for each individual variable as well as the set of variables. Moreover, the probability associated with Bartlett's test of sphericity should be less than the level of significance. The probability associated with the Bartlett test is <0.001, which satisfies this requirement (Table 33).

Table 33. Kaiser-Meyer-Olkin measure of sampling adequacy (MSA) and Bartlett's test results of the analyzed data

Kaiser-Meyer-Olkin measure of sampling adequacy		0.667
Bartlett's test of sphericity	Approx. Chi-Square	148.693
	df	15
	Sig.	0.000

After the first iteration, the MSA for all of the individual variables included in the analysis was greater than 0.5, supporting their retention in the analysis (Table 34).

Table 34. Anti-image matrices of the analyzed data

		Unit weight (kN/m^3)	n (%)	V_s (m/s)	V_p (m/s)	UCS (MPa)	E (MPa)
Anti-image covariance	Unit weight (kN/m^3)	.190	.169	-.041	.048	-.004	.008
	n (%)	.169	.214	-.045	.057	-3.018E-6	.014
	V_s (m/s)	-.041	-.045	.048	-.055	-.019	-.002
	V_p (m/s)	.048	.057	-.055	.072	.021	-.003
	UCS (MPa)	-.004	-3.018E-6	-.019	.021	.076	-.068
	E (MPa)	.008	.014	-.002	-.003	-.068	.083
Anti-image correlation	Unit weight (kN/m^3)	.641[a]	.839	-.431	.409	-.036	.062
	n (%)	.839	.580[a]	-.438	.459	-2.357E-5	.106
	V_s (m/s)	-.431	-.438	.658[a]	-.932	-.314	-.025
	V_p (m/s)	.409	.459	-.932	.615[a]	.281	-.045
	UCS (MPa)	-.036	-2.357E-5	-.314	.281	.726[a]	-.857
	E (MPa)	.062	.106	-.025	-.045	-.857	.766[a]

a. Measures of sampling adequacy(MSA)

According to the output of the first iteration, there were two Eigen values greater than 1.0 (Table 35). The latent root criterion for a number of factors to derive would indicate that there were two components to be extracted for these variables. In addition, the cumulative proportion of variance criteria can be met with two components to satisfy the criterion of explaining 60% or more of the total variance. The solution with two components would explain 86.995% of the total variance.

Table 35. Total variance explained by the principal components of the experimental data

Component	Initial Eigen values			Extraction sums of squared loadings		
	Total	% of Variance	Cumulative %	Total	% of Variance	Cumulative %
1	4.204	70.061	70.061	4.204	70.061	70.061
2	1.016	16.935	86.995	1.016	16.935	86.995
3	0.557	9.288	96.284			
4	0.152	2.530	98.814			
5	0.045	0.745	99.559			
6	0.026	0.441	100.000			

Since the SPSS default is to extract the number of components indicated by the latent root criterion, the initial factor solution was based on the extraction of two components.

Communalities represent the proportion of the variance in the original variables that is accounted for by the factor solution. The factor solution should explain at least half of each original variable's variance, so the communality value for each variable should be 0.50 or higher (Table 36).

The pattern of factor loadings has been examined to identify variables that have complex structure: Complex structure occurs when one variable has high loadings or correlations (0.40 or greater) on more than one component (Table 37). If a variable has a complex structure, it should be removed from the analysis. Variables are only checked for complex structure if there is more than one component in the solution. Variables that load on only one component are described as having simple structure.

None of the variables demonstrated complex structure. Hence, it was deemed not necessary to remove any additional variables because of complex structure.

Table 36. Communulaties of the variables.

Geotechnical parameter	Initial	Extraction
Unit weight (kN/m^3)	1.000	0.923
n (%)	1.000	0.933
V_s (m/s)	1.000	0.912
V_p (m/s)	1.000	0.770
UCS (MPa)	1.000	0.836
E (MPa)	1.000	0.847

Table 37. Rotated component matrix (rotation converged in 3 iterations) of the variables.

Geotechnical parameter	Component	
	1	2
Unit weight (kN/m^3)	0.896	0.345
n (%)	-0.939	-0.226
V_s (m/s)	0.249	0.922
V_p (m/s)	0.232	0.846
UCS (MPa)	0.293	0.866
E (MPa)	0.300	0.870

The information in six of the variables can be represented by two components:

- component 1 includes the variables unit weight γ and the porosity (n),
- component 2 includes the variables seismic velocities (V_s, V_p), uniaxial compressive strength (UCS) and Young's modulus (E).

The two components explain 86.995% of the total variance in the variables which are included in the components.

VIII.4 Multiple linear regression analysis (MLRA)

Regression analyses, in general, are used for the estimation of the linear relationship between a dependent variable and one or more independent variables or covariates. The purpose in applying linear regression for the data of the Antalya tufa rock mass is to express one variable or geotechnical parameter in terms of other variables or parameters with a reasonable accuracy. For the purpose of MLRA, each type of tufa rock has been tested and documented as follows, noting that the intraclast tufa type has been disregarded during MLRA since a few samples, which were statistically insignificant, were available.

VIII.4.1 Phytoherm boundstone

The Young's modulus and uniaxial compressive strength of the phytoherm boundstone has been expressed as a function of unit weight and porosity by Eqs. (8) and (9), respectively. The coefficient of determinations (R^2) for linear regressions has been determined as 0.992 and 0.941, respectively (Tables 38 and 39).

The tensile strength of the phytoherm boundstone, which has been disregarded during PCA, has been expressed as a function of unit weight, seismic velocity and porosity by Eq. (10). The coefficient of determinations for this linear regression has been determined as R^2=0.32 (Table 40).

Table 38. Multiple linear regression analysis result for Young's modulus of phytoherm boundstone tufa.

Dependent variable: E (MPa)		Mean	Std. deviation	N
		3794.000	1842.8995	5

Source	Type III Sum of squares	F	Sig.
Corrected model	13471646.672[a]	118.727	0.008
Intercept	456138.241	8.040	0.105
Unit weight (kN/m^3)	821219.921	14.475	0.063
n (%)	182389.428	3.215	0.215
Error	113467.328		
Total	85557294.000		
Corrected total	13585114.000		

a. R^2= 0.992

Parameter	B	Std. error	t	Sig.
Intercept	-16709.561	5893.011	-2.835	0.105
Unit weight (kN/m^3)	886.107	232.904	3.805	0.063
n (%)	128.617	71.733	1.793	0.215

$$E\ (MPa) = 886.107\gamma + 128.617n - 16709.561,\ R^2 = 0.992 \qquad \text{Eq. (8)}$$

Table 39. Multiple linear regression analysis result for uniaxial compressive strength of phytoherm boundstone tufa.

Dependent variable: Log (UCS) (MPa)	Mean	Std. deviation	N
	0.6967	0.53756	7

Source	Type III Sum of squares	F	Sig.
Corrected model	1.631[a]	31.726	0.004
Intercept	0.005	0.182	0.692
Unit weight (kN/m^3)	3.501E-5	0.001	0.972
n (%)	0.037	1.437	0.297
Error	0.103		
Total	5.132		
Corrected total	1.734		

a. R^2= 0.941

Parameter	B	Std. error	t	Sig.
Intercept	1.211	2.840	0.426	0.692
Unit weight (kN/m^3)	0.004	0.113	0.037	0.972
n (%)	-0.042	0.035	-1.199	0.297

$$Log\ \sigma_c\ (MPa) = 0.004\gamma - 0.042n + 1.211,\ R^2 = 0.941 \qquad \text{Eq. (9)}$$

Table 40. Multiple linear regression analysis result for tensile strength of phytoherm boundstone tufa.

Dependent variable: Log σ_t (MPa)	Mean	Std. deviation	N
	0 .1068	0.35980	11

Source	Type III Sum of squares	F	Sig.
Corrected model	0.414^a	1.096	0.412
Intercept	0.354	2.817	0.137
log n (%)	0.097	0.771	0.409
Unit weight (kN/m^3)	0.177	1.405	0.275
Log Vs (m/s)	0.254	2.016	0.199
Error	0.881		
Total	1.420		
Corrected total	1.295		

a. R^2= .320

Parameter	B	Std. error	t	Sig.
Intercept	-8.259	4.920	-1.679	0.137
Log n (%)	0.616	0.702	0.878	0.409
Unit weight (kN/m^3)	0.091	0.077	1.185	0.275
Log Vs (m/s)	1.866	1.315	1.420	0.199

$$Log\sigma_t\ (MPa) = 1.866 LogV_s + 0.616 Logn + 0.091\gamma - 8.259,\ R^2 = 0.320 \quad \text{Eq. (10)}$$

VIII.4.2 Microcrystalline tufa

The Young's modulus and uniaxial compressive strength of the microcrystalline tufa has been expressed as a function of unit weight and porosity by Eqs. (11) and (12), respectively. The coefficient of determinations (R^2) for linear regressions has been determined as 0.502 and 0.667, respectively (Tables 41 and 42).

The tensile strength of the microcrystalline tufa, which has been disregarded during PCA, has been expressed as a function of unit weight and porosity by Eq. (13). The coefficient of determination (R^2) for this linear regression has been determined as 0.843 (Table 43).

Table 41. Multiple linear regression analysis result for Young's modulus of microcrystalline tufa.

Dependent variable: E (MPa)	Mean	Std. deviation	N
	13252.20000	7469.803358	5

Source	Type III Sum of squares	F	Sig.
Corrected model	1.121E8	1.010	0.498
Intercept	42010154.639	0.757	0.476
Unit weight (kN/m^3)	64745922.762	1.166	0.393
n (%)	3946.728	0.000	0.994
Error	1.111E8		
Total	1.101E9		
Corrected total	2.232E8		

a. R^2= 0.502

Parameter	B	Std. error	t	Sig.
Intercept	-113449.904	130432.943	-0.870	0.476
Unit weight (kN/m^3)	5775.503	5348.647	1.080	0.393
n (%)	19.554	2319.373	0.008	0.994

$$E\ (MPa) = 5775.503\gamma + 19.554n - 113449.904,\ R^2 = 0.502 \qquad \text{Eq. (11)}$$

Table 42. Multiple linear regression analysis result for uniaxial compressive strength of microcrystalline tufa.

Dependent variable: log (UCS) (MPa)	Mean	Std. deviation	N
	1.3366	0.29716	10

Source	Type III Sum of squares	F	Sig.
Corrected model	0.530[a]	7.023	0.021
Intercept	0.226	5.991	0.044
Unit weight (kN/m^3)	0.364	9.631	0.017
n (%)	0.052	1.389	0.277
Error	0.264		
Total	18.660		
Corrected total	0.795		

a. R^2= 0.667

Parameter	B	Std. error	t	Sig.
Intercept	-7.140	2.917	-2.448	0.044
Unit weight (kN/m^3)	0.373	0.120	3.103	0.017
n (%)	0.051	0.043	1.179	0.277

$$Log\ \sigma_c(MPa) = 0.373\gamma + 0.051n - 7.140,\ R^2 = 0.667 \quad \text{Eq. (12)}$$

Table 43. Multiple linear regression analysis result for tensile strength of microcrystalline tufa.

Dependent variable: log σ_t (MPa)		Mean	Std. deviation	N
		0.4398	0.23223	11

Source	Type III Sum of squares	F	Sig.
Corrected model	0.455[a]	21.559	0.001
Intercept	0.050	4.768	0.061
Unit weight (kN/m^3)	0.084	7.991	0.022
Log n (%)	0.022	2.068	0.188
Error	0.084		
Total	2.667		
Corrected total	0.539		

a. R^2= 0.843

Parameter	B	Std. error	t	Sig.
Intercept	-5.177	2.371	-2.184	0.061
Unit weight (kN/m^3)	0.218	0.077	2.827	0.022
Log n (%)	1.100	0.765	1.438	0.188

$$Log\ \sigma_t\ (MPa) = 0.218\gamma + 1.1Logn - 5.177,\ R^2 = 0.843 \quad \text{Eq. (13)}$$

VIII.4.3 Phytoherm framestone

The Young's modulus and uniaxial compressive strength of the phytoherm framestone has been expressed as a function of unit weight and porosity by Eqs. (14) and (15), respectively. The coefficient of determinations (R^2) for linear regressions has been determined as 0.898 and 0.664, respectively (Tables 44 and 45).

The tensile strength of the phytoherm framestone, which has been disregarded during PCA, has been expressed as a function of unit weight and porosity by Eq. (16). The coefficient of determinations (R^2) for this linear regression has been determined as 0.763 (Table 46).

Table 44. Multiple linear regression analysis result for Young's modulus of phytoherm framestone tufa.

Dependent variable: E (MPa)	Mean	Std. deviation	N
	4405.20000	2987.777217	5

Source	Type III Sum of squares	F	Sig.
Corrected model	32071284.945[a]	8.821	0.102
Intercept	277749.017	0.153	0.734
Unit weight (kN/m^3)	2449599.741	1.347	0.366
n (%)	8670589.042	4.769	0.161
Error	3635965.855		
Total	1.327E8		
Corrected total	35707250.800		

a. R^2= 0.898

Parameter	B	Std. error	t	Sig.
Intercept	-6642.192	16993.392	-0.391	0.734
Unit weight (kN/m^3)	880.144	758.231	1.161	0.366
n (%)	-562.711	257.665	-2.184	0.161

$$E\ (MPa) = 880.144\gamma - 562.711n - 6642.192,\ R^2 = 0.898 \quad \text{Eq. (14)}$$

Table 45. Multiple linear regression analysis result for uniaxial compressive strength of phytoherm framestone tufa.

Dependent variable: UCS (MPa)		Mean	Std. deviation	N
		7.76026	5.347884	12

Source	Type III Sum of squares	F	Sig.
Corrected model	209.005[a]	8.907	0.007
Intercept	58.871	5.018	0.052
Unit weight (kN/m^3)	20.692	1.764	0.217
Log n (%)	132.385	11.283	0.008
Error	105.594		
Total	1037.259		
Corrected total	314.598		

a. R^2= 0.664

Parameter	B	Std. error	t	Sig.
Intercept	80.612	35.987	2.240	0.052
Unit weight (kN/m^3)	-1.781	1.341	-1.328	0.217
Log n (%)	-36.089	10.744	-3.359	0.008

$$\sigma_c\ (MPa) = -1.781\gamma - 36.089Logn + 80.612,\ R^2 = 0.664 \quad \text{Eq. (15)}$$

Table 46. Multiple linear regression analysis result for tensile strength of phytoherm framestone tufa.

Dependent variable: log σ_t (MPa)	Mean	Std. deviation	N
	-0.0060	0.44108	11

Source	Type III Sum of squares	F	Sig.
Corrected model	1.187[a]	9.636	0.013
Intercept	0.526	8.549	0.027
Unit weight (kN/m^3)	0.838	13.605	0.010
Log n (%)	0.203	3.303	0.119
Error	0.370		
Total	1.557		
Corrected total	1.556		

a. R^2= 0.763

Parameter	B	Std. error	t	Sig.
Intercept	-5.853	2.002	-2.924	0.027
Unit weight (kN/m^3)	0.234	0.064	3.688	0.010
Log n (%)	1.439	0.792	1.817	0.119

$$Log\ \sigma_t(MPa) = 0.234\gamma + 1.439Logn - 5.853,\ R^2 = 0.763 \quad \text{Eq. (16)}$$

VIII.4.4 Phytoclast tufa

The Young's modulus and uniaxial compressive strength of the phytoclast tufa has been expressed as a function of unit weight and seismic velocity by Eqs. (17) and (18), respectively. The coefficient of determinations for linear regressions has been determined as 0.338 and 0.605, respectively (Tables 47 and 48).

The tensile strength of the phytoclast tufa, which has been disregarded during PCA, has been expressed as a function of unit weight and seismic velocity by Eq. (19). The coefficient of determinations (R^2) for this linear regression has been determined as 0.527 (Table 49).

Table 47. Multiple linear regression analysis result for Young's modulus of phytoclast tufa.

Dependent variable: E (MPa)	Mean	Std. deviation	N
	2182.50000	543.771183	5

Source	Type III Sum of squares	F	Sig.
Corrected model	499562.908[a]	0.766	0.539
Intercept	155530.374	0.477	0.540
Unit weight (kN/m^3)	131050.043	0.402	0.571
Log Vs (m/s)	215647.544	0.661	0.476
Error	978872.592		
Total	30058273.000		
Corrected total	1478435.500		

a. R^2= 0.338

Parameter	B	Std. error	t	Sig.
Intercept	-3432.993	4972.420	-0.690	0.540
Unit weight (kN/m^3)	170.263	268.660	0.634	0.571
Log Vs (m/s)	1.369	1.684	0.813	0.476

$$E\ (MPa) = 170.263\gamma + 1.369 LogV_s - 3432.993,\ R^2 = 0.338 \quad \text{Eq. (17)}$$

Table 48. Multiple linear regression analysis result for uniaxial compressive strength of phytoclast tufa.

Dependent variable: UCS (MPa)	Mean	Std. deviation	N
	5.48529	1.935555	8

Source	Type III Sum of squares	F	Sig.
Corrected model	15.871[a]	3.832	0.098
Intercept	1.562	0.754	0.425
Unit weight (kN/m^3)	7.794	3.764	0.110
v_s (m/s)	3.539	1.709	0.248
Error	10.354		
Total	266.932		
Corrected total	26.225		

a. R^2= 0.605

Parameter	B	Std. error	t	Sig.
Intercept	-10.643	12.256	-0.868	0.425
Unit weight (kN/m^3)	1.108	0.571	1.940	0.110
V_s (m/s)	-0.003	0.002	-1.307	0.248

$$\sigma_c\ (MPa) = 1.108\gamma - 0.003V_s - 10.643,\ R^2 = 0.605 \qquad \text{Eq. (18)}$$

Table 49. Multiple linear regression analysis result for tensile strength of phytoclast tufa.

Dependent variable: Log σ_t (MPa)	Mean	Std. deviation	N
	0.0249	0.25295	13

Source	Type III Sum of squares	F	Sig.
Corrected model	0.404[a]	5.562	0.024
Intercept	0.327	8.987	0.013
Unit weight (kN/m^3)	0.401	11.019	0.008
Vs (m/s)	0.149	4.104	0.070
Error	0.363		
Total	0.776		
Corrected total	0.768		

a. R^2= 0.527

Parameter	B	Std. error	t	Sig.
Intercept	-2.649	0.884	-2.998	0.013
Unit weight (kN/m^3)	0.187	0.056	3.319	0.008
Vs (m/s)	-4.53E-4	0.000	-2.026	0.070

$$Log\sigma_t(MPa) = 0.187\gamma - (4.53 \times 10^{-4})V_s - 2.649, \; R^2 = 0.527 \quad \text{Eq. (19)}$$

VIII.4.5 Antalya tufa rock mass

The Young’s modulus and uniaxial compressive strength of the Antalya tufa rock mass has been expressed as a function of unit weight, porosity, uniaxial compressive strength and seismic velocity by Eqs. (20), (21) and (22), respectively. The coefficient of determinations for linear regressions has been determined as 0.913, 0.601 and 0.603, respectively (Tables 50 and 51).

The tensile strength of the Antalya tufa rock mass has been expressed as a function of unit weight and seismic velocity by Eq. (23). The coefficient of determinations (R^2) for this linear regression has been determined as 0.469 (Table 52).

Table 50. Multiple linear regression analysis result for Young's modulus of the Antalya tufa rock mass.

Dependent variable:E (MP)a	Mean	Std. deviation	N
	5752.05	5892.544	20

Source	Type III Sum of squares	F	Sig.
Corrected model	6.024E8	89.301	0.000
Intercept	474.521	0.000	0.991
UCS (MPa)	2.119E8	62.821	0.000
Vs (m/s)	488699.224	0.145	0.708
Error	57337228.007		
Total	1.321E9		
Corrected total	6.597E8		

a. R^2= 0.913

Parameter	B	Std. error	T	Sig.
Intercept	-44.216	3727.724	-0.012	0.991
UCS (MPa)	292.981	36.965	7.926	0.000
Vs (m/s)	0.835	2.194	0.381	0.708

$$E\ (MPa) = 292.981\sigma_c + 0.835V_s - 44.216,\ R^2 = 0.913 \qquad \text{Eq. (20)}$$

Dependent variable:Log E (MP)a	Mean	Std. deviation	N
	3.5936	0.37966	20

Source	Type III Sum of squares	F	Sig.
Corrected model	1.733a	13.563	0.000
Intercept	0.112	1.746	0.203
UCS (MPa)	0.012	0.185	0.672
Vs (m/s)	0.323	5.053	0.037
Error	1.150		
Total	274.079		
Corrected total	2.883		

a. R^2= 0.601

Table 50 (cont'd.). Multiple linear regression analysis result for Young's modulus of the Antalya tufa rock mass

Parameter	B	Std. error	T	Sig.
Intercept	1.504	1.138	1.321	0.203
n (%)	-0.007	0.016	-0.430	0.672
γ (kN/m^3)	0.107	0.048	2.248	0.037

$$LogE\ (MPa) = 0.107\gamma - 0.007n + 1.504,\ R^2 = 0.601 \qquad \text{Eq. (21)}$$

Table 51. Multiple linear regression analysis result for uniaxial compressive strength of the Antalya tufa rock mass.

Dependent variable:Log (UCS) (MP)a	Mean	Std. deviation	N
	0.9090	0.41203	37

Source	Type III Sum of squares	F	Sig.
Corrected model	3.686a	25.836	0.000
Intercept	0.315	4.421	0.043
Log γ (kN/m^3)	0.592	8.303	0.007
Log n (%)	0.014	0.196	0.661
Error	2.425		
Total	36.681		
Corrected total	6.112		

a. R^2= 0.603

Parameter	B	Std. error	T	Sig.
Intercept	-6.672	3.173	-2.103	0.043
Log γ (kN/m^3)	6.008	2.085	2.882	0.007
Log n (%)	-0.215	0.485	-0.443	0.661

$$Log\sigma_c\ (MPa) = 6.008Log\gamma - 0.215Logn - 6.672,\ R^2 = 0.603 \qquad \text{Eq. (22)}$$

Table 52. Multiple linear regression analysis result for tensile strength of the Antalya tufa rock mass.

Dependent variable:Log (σ_t) (MP)a	Mean	Std. deviation	N
	0.1412	0.35043	46

Source	Type III Sum of squares	F	Sig.
Corrected model	2.593a	19.005	0.000
Intercept	1.505	22.056	0.000
Log n (%)	0.513	7.513	0.009
Log γ (kN/m^3)	1.769	25.939	0.000
Error	2.933		
Total	6.443		
Corrected total	5.526		

a. R^2= 0.469

Parameter	B	Std. error	T	Sig.
Intercept	-9.493	2.021	-4.696	0.000
Log n (%)	0.886	0.323	2.741	0.009
Log γ (kN/m^3)	6.741	1.324	5.093	0.000

$$Log\sigma_t = 6.741Log\gamma + 0.886Logn - 9.493, \; R^2 = 0.469 \qquad \text{Eq. (23)}$$

VIII.5 Discussion of the results of the statistical analyses of the geotechnical parameters of the Antalya tufa rock mass

Only three geotechnical parameters, namely, porosity, unit weight and point load strength index, of the Antalya tufa rock mass have been determined to be normally distributed from the data of this study. Standard deviation values greater than the mean values of the other geotechnical parameters have leaded to such a situation. However, transformations such as taking the logarithm ($\log_{10}$) of the data have yielded more geotechnical parameters, namely, seismic wave velocity, uniaxial compressive strength and Young's modulus of the Antalya tufa rock mass to be normally distributed. Hence, they have been subjected to multiple linear regression analyses with their transformed forms.

Principal component analysis (PCA) of the data that was demonstrated to be normally distributed has resulted in two main components, one which involves porosity and unit weight. The other component includes members such as seismic wave velocity, uniaxial compressive strength and Young's modulus.

According to the texture or physical appearance of the Antalya tufa rock mass, porosity, which is inversely proportional with unit weight, has been expected to be one of the parameters that might control the strength of the tufa rock mass. Also, other geotechnical parameters determined for component 2 have been observed to be in strong relation with the compressive strength of the Antalya rock mass. Hence, it is possible to say that the results of PCA have been conformable with these expectations.

A number of geotechnical parameters of the Antalya tufa rock mass have been reduced via PCA in order to involve only interrelated parameters in the multiple linear regression analyses (MLRA). The Antalya tufa rock mass and rock types have been analyzed separately (Tables 53, 54 and 55). Reasonable relationships in terms of porosity (n) and unit weight (γ) have been determined for Young's modulus (E), tensile strength (σ_t) and uniaxial compressive strength (σ_c) of phytoherm boundstone, phytoherm framestone and microcrystalline tufa. E, σ_t and σ_c of phytoclast tufa and the Antalya tufa rock mass, however, have been expressed as a function of Vs, n, σ_c and γ.
It is useful to express the strength parameters of the Antalya tufa rock mass as a function of index properties, namely, n and γ that possessed reasonably high coefficient of determinations since index properties could be obtained easier in order to estimate the strength parameters of the Antalya tufa rock mass and rock types.

Table 53. Results of MLRA for Young's modulus of the Antalya tufa rock mass and rock types.

Tufa type	Result of MLRA	R^2	N
Phytoherm Boundstone	$E\ (MPa) = 886.107\gamma + 128.617n - 16710$	0.992	5
Microcrystalline tufa	$E\ (MPa) = 5775.503\gamma + 19.554n - 113450$	0.502	5
Phytoherm framestone	$E\ (MPa) = 880.144\gamma - 562.711n - 6642$	0.898	5
Phytoclast tufa	$E\ (MPa) = 170.263\gamma + 1.369LogV_s - 3433$	0.338	5
Antalya tufa rock mass	$E\ (MPa) = 292.981\sigma_c + 0.835V_s - 440$	0.913	20
	$LogE\ (MPa) = 0.107\gamma - 0.007n + 1.504$	0.601	20

Table 54. Results of MLRA for uniaxial compressive strength of the Antalya tufa rock mass and rock types.

Tufa type	Result of MLRA	R^2	N
Phytoherm boundstone	$Log\ \sigma_c\ (MPa) = 0.004\gamma - 0.042n + 1.21$	0.941	7
Microcrystalline tufa	$Log\ \sigma_c(MPa) = 0.373\gamma + 0.051n - 7.14$	0.660	10
Phytoherm framestone	$\sigma_c\ (MPa) = -1.781\gamma - 36.089Logn + 80.6$	0.664	12
Phytoclast tufa	$\sigma_c\ (MPa) = 1.108\gamma - 0.003V_s - 10.6$	0.605	8
Antalya tufa rock mass	$Log\sigma_c\ (MPa) = 6.008Log\gamma - 0.215Logn - 6.67$	0.603	37

Table 55. Results of MLRA for tensile strength of the Antalya tufa rock mass and rock types.

Tufa type	Result of MLRA	R^2	N
Phytoherm boundstone	$Log\sigma_t\ (MPa) = 1.87LogV_s + 0.62Logn + 0.091\gamma - 8.26$	0.320	11
Microcrystalline tufa	$Log\ \sigma_t\ (MPa) = 0.218\gamma + 1.1Logn - 5.177$	0.843	11
Phytoherm framestone	$Log\ \sigma_t(MPa) = 0.234\gamma + 1.439Logn - 5.85$	0.763	11
Phytoclast tufa	$Log\sigma_t(MPa) = 0.187\gamma - (4.53 \times 10^{-4})V_s - 2.65$	0.527	13
Antalya tufa rock mass	$Log\sigma_t = 6.741Log\gamma + 0.886Logn - 9.493$	0.469	46

For the application purposes, index properties, namely, porosity and unit weight together with uniaxial compressive strength (σ_c) and Young's modulus (E) parameters of the Antalya tufa rock mass have been arranged in the forms of curves according to the results of MLRA given in Tables 53, 54 and 55 (Figures 128, 129 and 130). The uniaxial compressive strength and Young's modulus of the Antalya tufa rock mass could be predicted relatively easily via the known index properties in these curves. ıt should be noted that these estimation curves are open to modifications with further data that might be available in the future.

In addition to estimation charts, a sensitivity study has been carried out in order to determine the effect of porosity on the strength or on the Young's modulus of the Antalya tufa rock mass (Figure 131). The curves of the sensitivity analysis have shown that the effect of porosity could be felt more, i.e., curves start to deviate further, when the unit weight of the rock sample is greater than 19 kN/m^3.

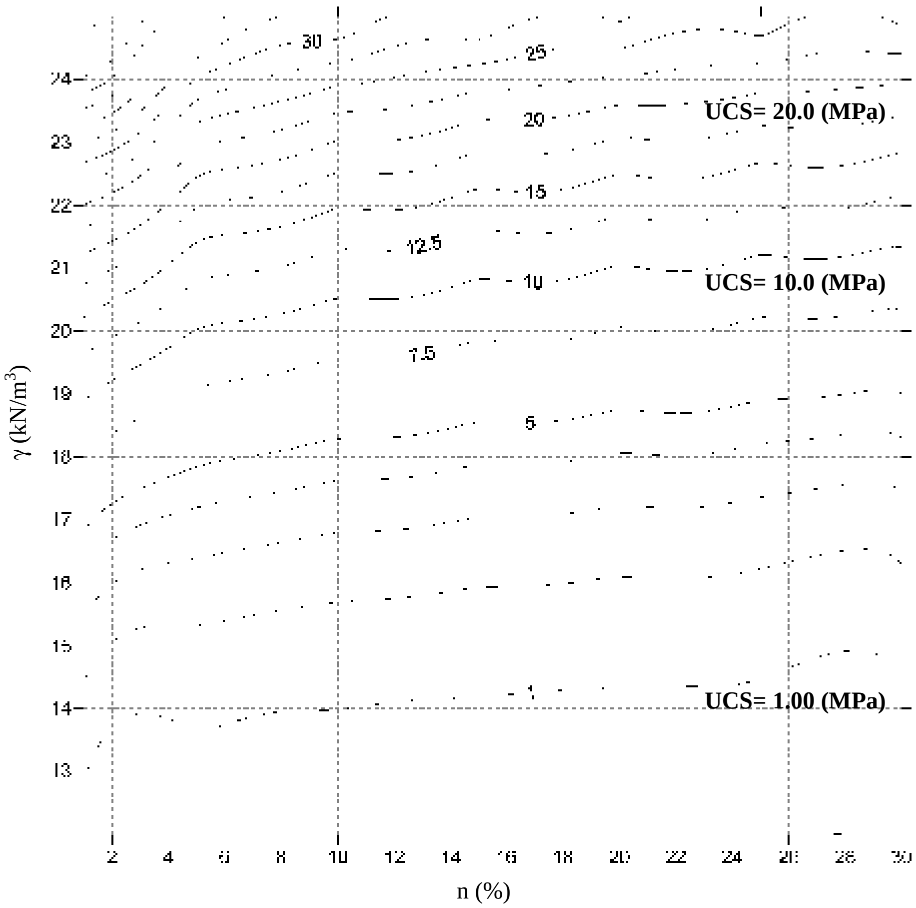

Figure 128. Estimation curves for uniaxial compressive strength (UCS) of the Antalya tufa rock mass as a function of porosity (n) and unit weight (γ).

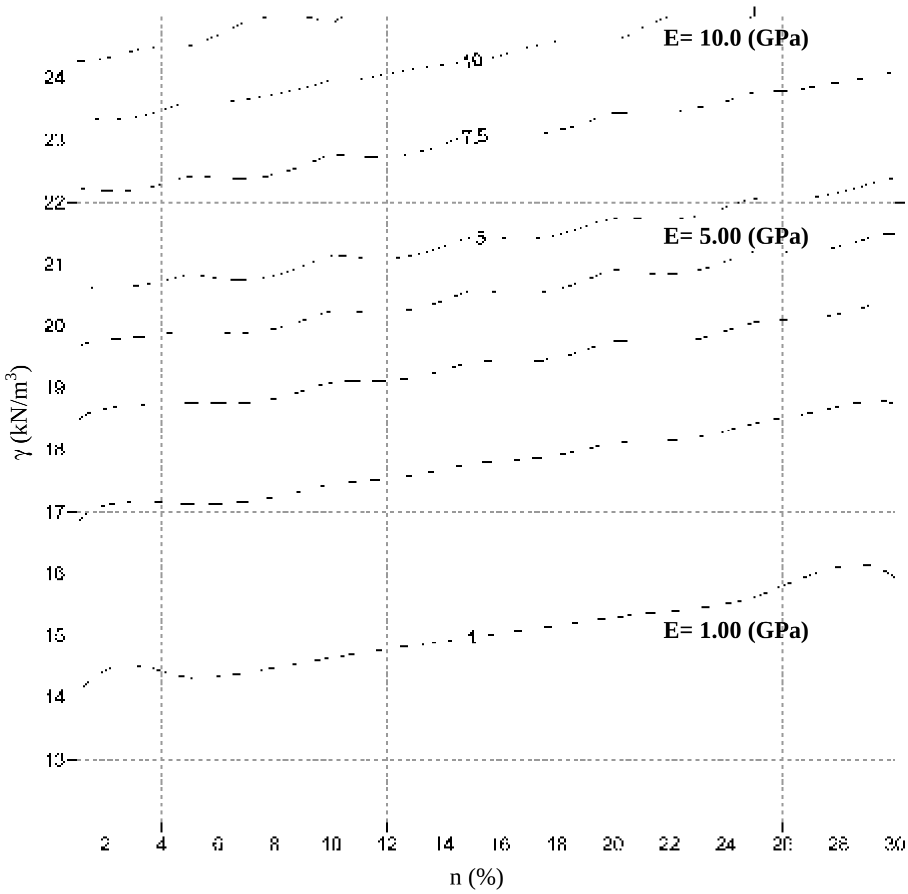

Figure 129. Estimation curves for Young's modulus (E) of the Antalya tufa rock mass as a function of porosity (n) and unit weight (γ).

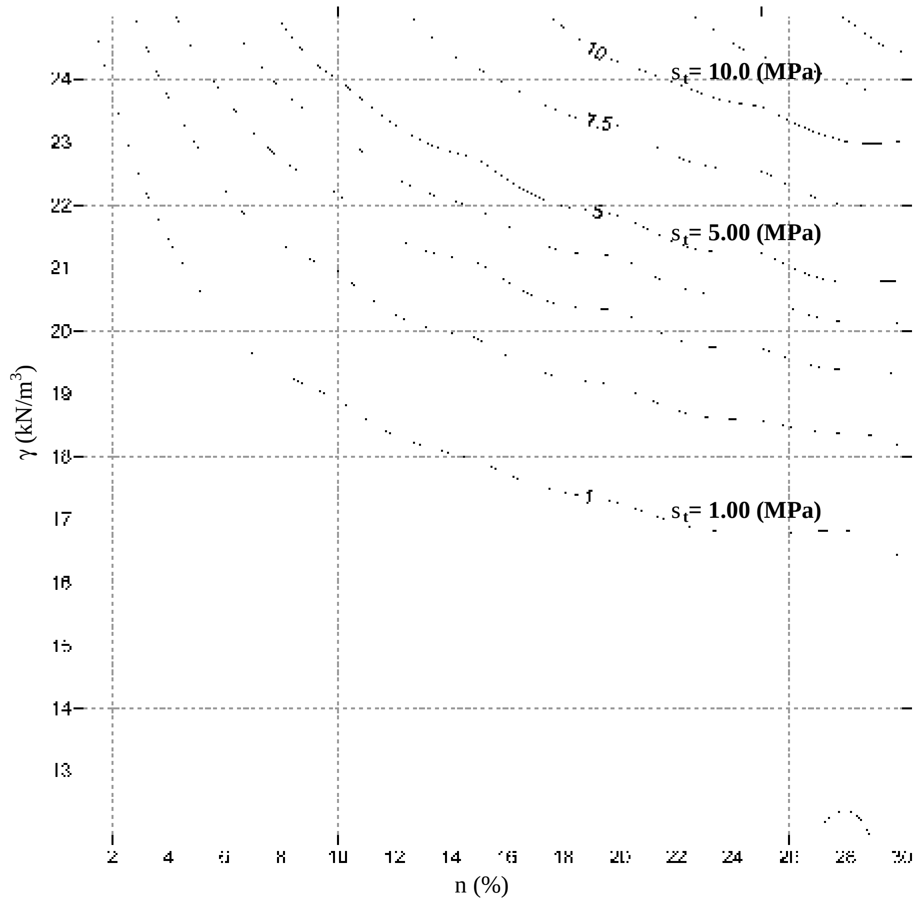

Figure 130. Estimation curves for tensile strength (σ_t) of the Antalya tufa rock mass as a function of porosity (n) and unit weight (γ).

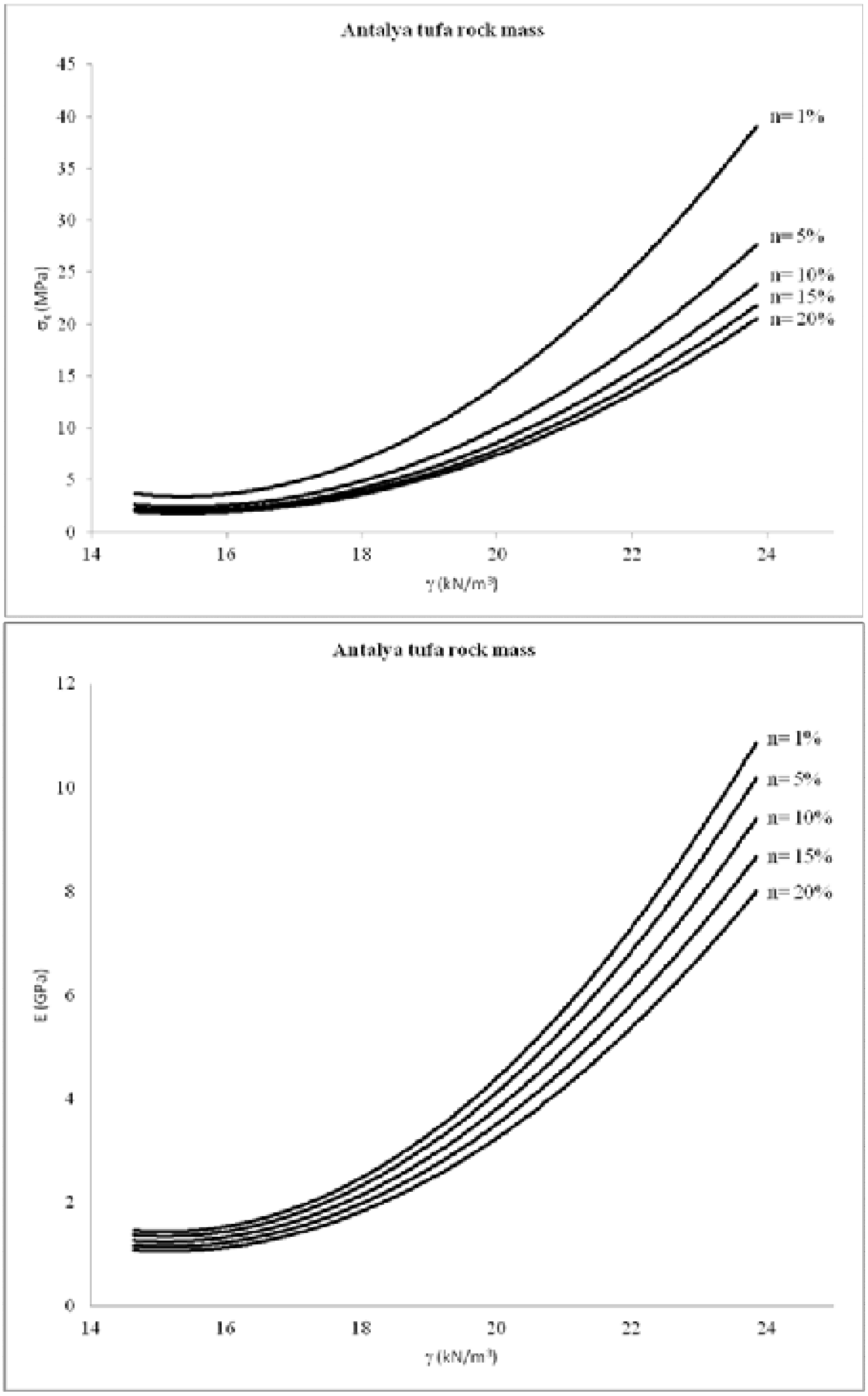

Figure 131. The curves of the sensitivity analysis illustrating effect of porosity (n) and unit weight (γ) on the compressive strength (σ_c), Young's modulus (E) and tensile strength (σ_t) of the Antalya tufa rock mass.

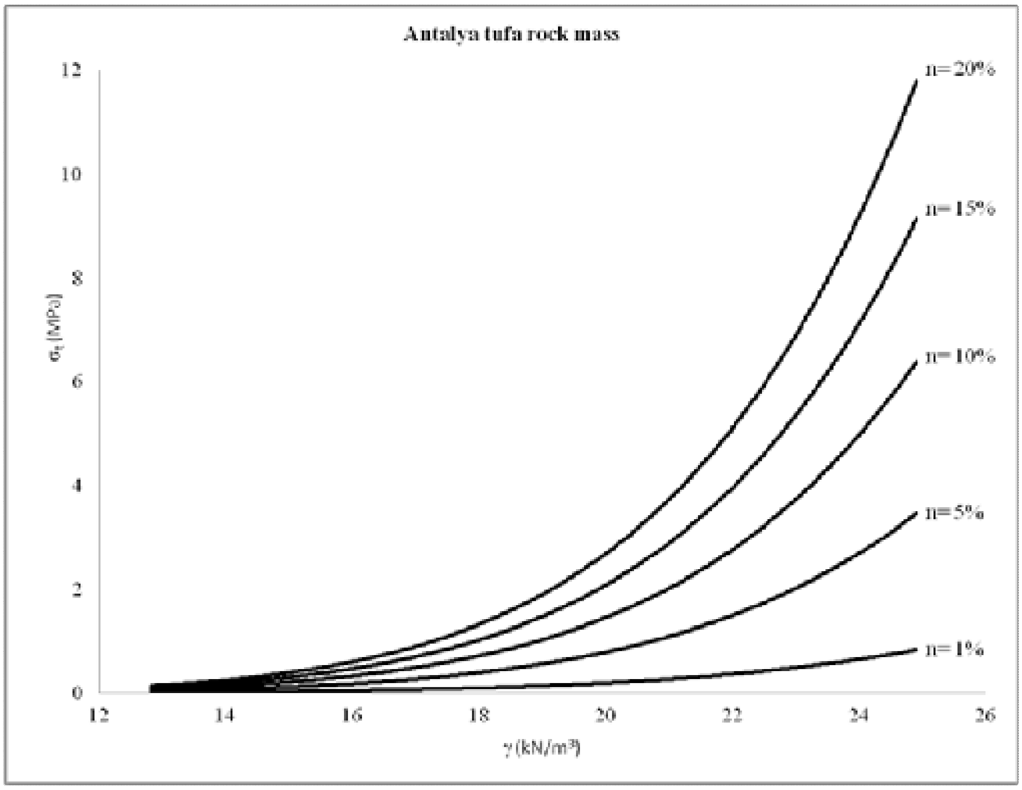

Figure 131 (cont'd.). The curves of the sensitivity analysis illustrating effect of porosity (n) and unit weight (γ) on the compressive strength (σ_c), Young's modulus (E) and tensile strength (σ_t) of the Antalya tufa rock mass.

CHAPTER IX

STRENGTH CRITERIA AND ROCK MASS CLASSIFICATION OF THE ANTALYA TUFA

IX.1 Strength criteria of the Antalya tufa rock mass

IX.1.1 Introduction

The strength criterion that best represents the failure of the Antalya tufa rock mass has been attempted to be determined in this chapter. This attempt involved unconstrained non-linear regression analyses to identify the strength criterion and material constants in terms of fitting an equation and parameters. Before the attempt, the fitting of the laboratory data to the failure criteria defined by Coulomb (1776), Bieniawski (1974) and Hoek and Brown (1980) has been carried out by means of constrained regression analyses. For the regression analyses, the results of the uniaxial and triaxial compressive strength tests and Brazilian tensile strength tests (Tables 15, 17 and 19) have been used as mentioned previously. The analysis has been carried out in two stages: first, the results of the uniaxial and triaxial compressive strength tests have been included in the regression analyses; second, the results of the uniaxial, triaxial compressive strength tests and Brazilian tensile strength tests have been included in the analyses (Table 56). For the Brazilian test results, the minor principal stress was accepted to be equal to the tensile strength of the rock sample and the major principal stress was compressive and equaled three times the tensile strength calculated at the center of the disk sample where the failure has initiated (Jaeger and Cook, 1979). In all of these analyses, the tufa rock samples were assumed to be isotropic.

Table 56. Experimental data developed from uniaxial and triaxial compressive strength test and the Brazilian test results for regression analyses

No	Sample No.	σ_c (MPa)	σ_1 (MPa)	σ_3 (MPa)	σ_1/σ_c	σ_3/σ_c
1	B1	7.36	7.36	0.00	1.00	0.00
2	B1	7.36	18.4	1.00	2.50	0.14
3	B2	12.1	12.1	0.00	1.00	0.00
4	B3	8.61	8.61	0.00	1.00	0.00
5*	B3	8.61	2.55	0.85	0.30	0.10
6*	B3	8.61	2.46	0.82	0.29	0.09
7*	B3	8.61	4.05	1.35	0.47	0.16
8	B3	8.61	10.8	0.50	1.26	0.06
9	B6	17.2	18.2	1.00	1.06	0.06
10	B6	17.2	29.6	3.00	1.72	0.17
11*	B6	17.2	4.53	1.51	0.26	0.09
12*	B6	17.2	21.2	7.08	1.23	0.41
13*	B6	17.2	6.72	2.24	0.39	0.13
14	B78	0.57	1.41	0.00	2.48	0.00
15	B78	0.57	2.64	1.00	4.63	1.75
16	B78	0.57	4.19	2.00	7.34	3.51
17*	B78	0.57	1.02	0.34	1.79	0.59
18	M1	26.2	26.2	0.00	1.00	0.00
19	M1	26.2	19.2	0.50	0.73	0.02
20	M1	26.2	28.0	1.00	1.07	0.04
21	M1	26.2	8.77	0.00	0.33	0.00
22	M1	26.2	17.6	1.00	0.67	0.04
23	M1	26.2	27.5	2.00	1.05	0.08
24†	M1	26.2	14.7	4.91	0.56	0.19
25†	M1	26.2	9.87	3.29	0.38	0.13
26	M3	41.2	44.9	0.00	1.09	0.00
27	M3	41.2	29.9	0.50	0.73	0.01
28	M3	41.2	13.1	1.00	0.32	0.02
29	M3	41.2	13.4	0.00	0.33	0.00
30	M3	41.2	16.9	1.00	0.41	0.02
31	M3	41.2	32.6	2.00	0.79	0.05
32*	M3	41.2	8.85	2.95	0.22	0.07
33†	M3	41.2	11.0	3.67	0.27	0.09
34*	M3	41.2	3.87	1.29	0.09	0.03
35	M4	8.91	8.91	0.00	1.00	0.00

Table 56 (cont'd.). Experimental data developed from uniaxial and triaxial compressive strength test and the Brazilian test results for regression analyses.

No	Sample No.	σ_c (MPa)	σ_1 (MPa)	σ_3 (MPa)	σ_1/σ_c	σ_3/σ_c
36	M4	8.91	7.62	0.50	0.86	0.06
37	M4	8.91	15.4	1.00	1.73	0.11
38†	M4	8.91	11.2	3.74	1.26	0.42
39†	M4	8.91	9.00	3.00	1.01	0.34
40	M5	20.8	24.9	0.00	1.20	0.00
41	M5	20.8	38.4	1.00	1.85	0.05
42	M5	20.8	59.9	2.00	2.88	0.09
43*	M5	20.8	2.49	0.83	0.12	0.04
44†	M5	20.8	11.0	3.67	0.53	0.18
45†	M5	20.8	12.3	4.09	0.59	0.19
46†	M5	20.8	6.54	2.18	0.32	0.11
47	P1	3.55	4.15	0.00	1.17	0.00
48	P1	3.55	7.88	2.00	2.22	0.56
49	P1	3.55	6.22	3.00	1.75	0.85
50*	P1	3.55	1.47	0.49	0.41	0.14
51	P3	0.28	0.28	0.00	0.99	0.00
52	P3	0.28	1.06	1.00	3.79	3.57
53	P3	0.28	2.19	2.00	7.82	7.14
54*	P3	0.28	1.50	0.50	5.36	1.79
55*	P3	0.28	0.33	0.11	1.18	0.39
56	P6	6.36	6.36	0.00	1.00	0.00
57	P6	6.36	21.9	2.00	3.45	0.31
58	P6	6.36	11.9	4.00	1.87	0.63
59	P8	6.50	5.52	0.00	0.85	0.00
60	P8	6.50	10.4	1.00	1.59	0.15
61	P8	6.50	11.7	2.00	1.79	0.31
62*	P8	6.50	5.19	1.73	0.79	0.27
63*	P8	6.50	5.64	1.88	0.87	0.29
64*	P8	6.50	6.21	2.07	0.96	0.32
65*	P8	6.50	3.45	1.15	0.53	0.18
66	P9	18.9	18.9	0.00	1.00	0.00
67	P9	18.9	30.9	0.50	1.63	0.03
68	P9	18.9	24.4	1.00	1.29	0.05
69*	P9	18.9	5.25	1.75	0.28	0.09
70*	P9	18.9	7.29	2.43	0.39	0.13
71	PF3	9.36	3.93	0.50	0.42	0.05

Table 56 (cont'd.). Experimental data developed from uniaxial and triaxial compressive strength test and the Brazilian test results for regression analyses.

No	Sample No.	σ_c (MPa)	σ_1 (MPa)	σ_3 (MPa)	σ_1/σ_c	σ_3/σ_c
72	PF3	9.36	14.1	1.00	1.50	0.11
73*	PF3	9.36	1.50	0.50	0.16	0.05
74	PF4	6.23	5.76	0.00	0.93	0.00
75*	PF4	6.23	7.17	2.39	1.15	0.38
76*	PF4	6.23	5.40	1.80	0.87	0.29
77	PF5	3.23	3.23	0.00	1.00	0.00
78	PF5	3.23	8.06	0.50	2.49	0.16
79	PF5	3.23	5.39	1.00	1.67	0.31
80*	PF5	3.23	2.19	0.73	0.68	0.23
81*	PF5	3.23	5.43	1.81	1.68	0.56
82*	PF5	3.23	2.82	0.94	0.87	0.29
83	PF6	4.54	5.41	0.00	1.19	0.00
84	PF6	4.54	12.9	1.00	2.86	0.22
85	PF6	4.54	9.34	2.00	2.06	0.44
86*	PF6	4.54	2.46	0.82	0.54	0.18
87*	PF6	4.54	3.99	1.33	0.88	0.29
88*	PF6	4.54	3.63	1.21	0.80	0.27
89*	PF6	4.54	6.63	2.21	1.46	0.49
90*	PF7	4.35	4.20	1.40	0.97	0.32

*Brazilian test results
†Outlier data neglected during analyses.
B: Phytoherm boundstone. M: Microcrystalline. P: Pyhtoherm framestone. PF: Phytoclast tufa

IX.1.2 Coulomb's failure criterion

Coulomb (1776) has expressed the shear strengths of the rocks in two parts – a constant cohesion component and stress-dependent frictional component. This criterion can also be expressed in terms of principal stresses at failure as follows (Eqs. 24 and 25):

$$\sigma_1 = \sigma_c + \sigma_3 tan\varphi \qquad \text{Eq. (24)}$$

where,

σ_1, σ_3 = major and minor principal stresses

σ_c = uniaxial compressive strength = $\dfrac{2c\cos\emptyset}{1 - \sin\emptyset}$

$$tan\varphi = \frac{1+\sin\emptyset}{1-\sin\emptyset} \qquad \text{Eq. (25)}$$

$\emptyset$ = internal friction angle

Linear regression analysis by least squares fitting of the triaxial compressive strength test results of the Antalya tufa rock mass has yielded the following relations with the related coefficient of determinations (Tables 57 and 58, Figures 132 and 133):

Table 57. Coulomb's criterion developed from uniaxial and triaxial compressive strength test results.

Antalya tufa rock mass (N= 52)	$\frac{\sigma_1}{\sigma_c} = 1.14\frac{\sigma_3}{\sigma_c} + 1$	$R^2 = 0.71$
Phytoherm boundstone (N= 10)	$\frac{\sigma_1}{\sigma_c} = 1.88\frac{\sigma_3}{\sigma_c} + 1$	$R^2 = 0.89$
Microcrystalline tufa (N= 18)	$\frac{\sigma_1}{\sigma_c} = 6.01\frac{\sigma_3}{\sigma_c} + 1$	$R^2 = 0.21$
Phytoherm framestone (N= 15)	$\frac{\sigma_1}{\sigma_c} = 0.94\frac{\sigma_3}{\sigma_c} + 1$	$R^2 = 0.86$
Phytoclast tufa (N= 9)	$\frac{\sigma_1}{\sigma_c} = 3.55\frac{\sigma_3}{\sigma_c} + 1$	$R^2 = 0.37$

Table 58. Coulomb’s criterion developed from uniaxial, triaxial compressive strength tests and Brazilian test results.

Antalya tufa rock mass (N= 82)	$\frac{\sigma_1}{\sigma_c} = 1.15\frac{\sigma_3}{\sigma_c} + 1$	$R^2 = 0.67$
Phytoherm boundstone (N= 17)	$\frac{\sigma_1}{\sigma_c} = 1.82\frac{\sigma_3}{\sigma_c} + 1$	$R^2 = 0.85$
Microcrystalline tufa (N=21)	$\frac{\sigma_1}{\sigma_c} = 2.54\frac{\sigma_3}{\sigma_c} + 1$	$R^2 = 0.00$
Phytoherm framestone (N= 24)	$\frac{\sigma_1}{\sigma_c} = 1.00\frac{\sigma_3}{\sigma_c} + 1$	$R^2 = 0.77$
Phytoclast tufa (N= 20)	$\frac{\sigma_1}{\sigma_c} = 1.02\frac{\sigma_3}{\sigma_c} + 1$	$R^2 = 0.09$

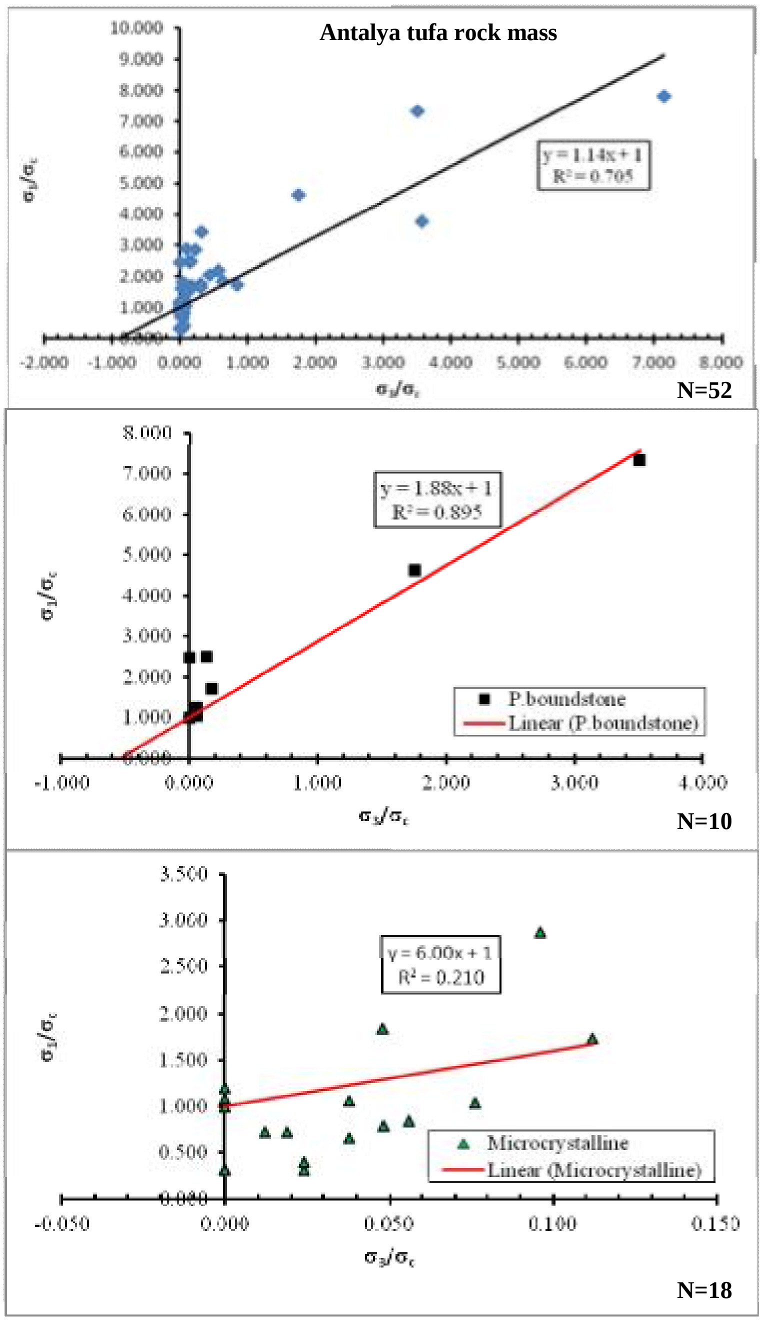

Figure 132. Coulomb's criterion: curve fitting of the Antalya tufa rock mass as obtained from the uniaxial and triaxial compressive strength test results.

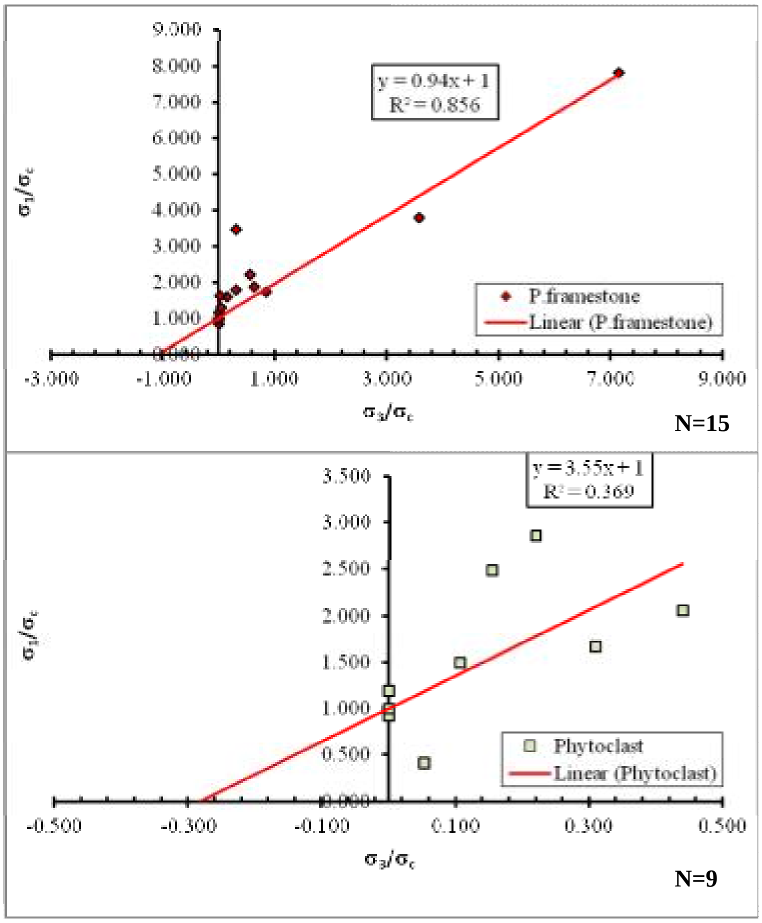

Figure 132 (cont'd.). Coulomb's criterion: curve fitting of the Antalya tufa rock mass as obtained from the uniaxial and triaxial compressive strength test results.

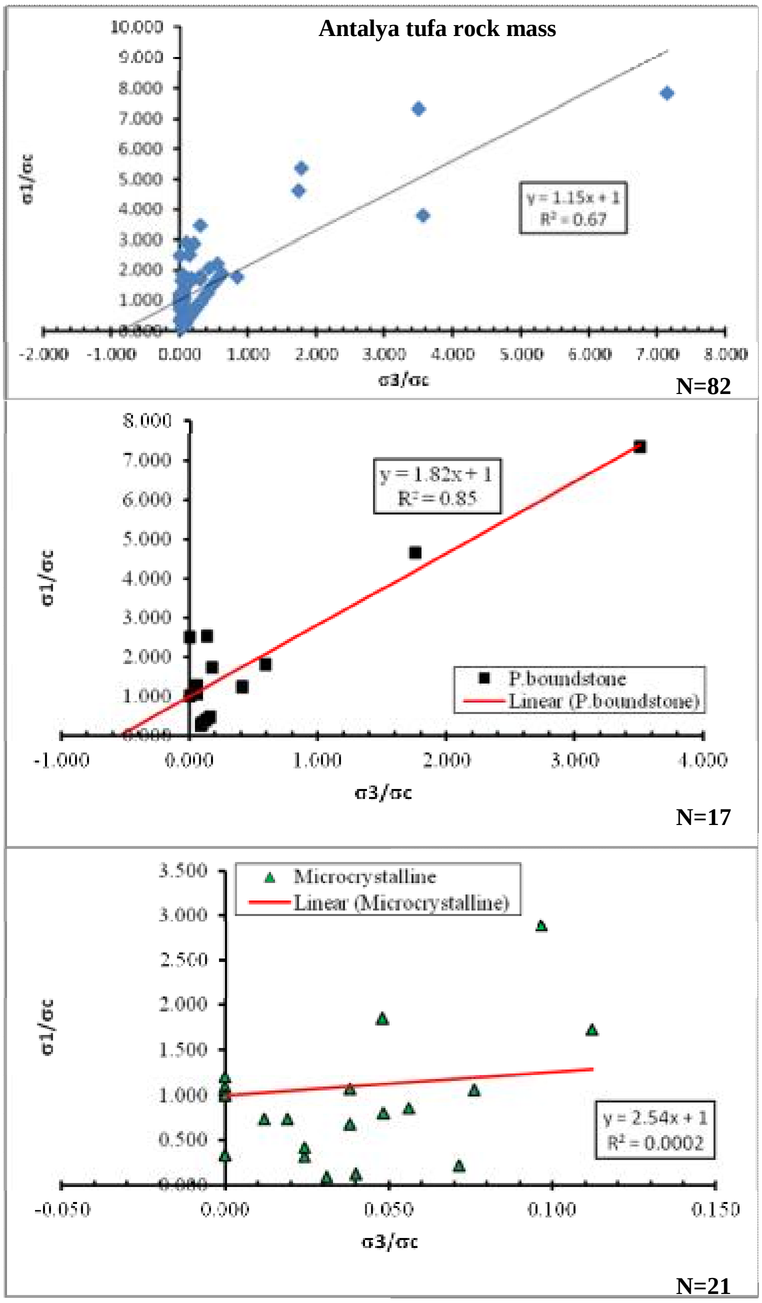

Figure 133. Coulomb's criterion: curve fitting of the Antalya tufa rock mass as obtained from the uniaxial, triaxial compressive strength tests and Brazilian test results.

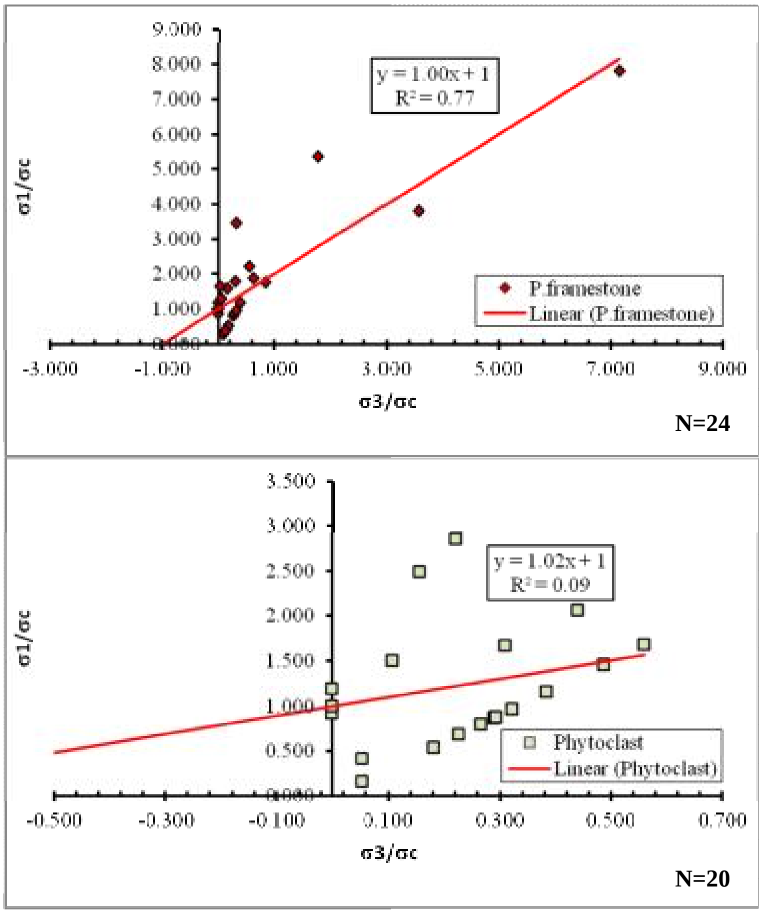

Figure 133 (cont'd.). Coulomb's criterion: curve fitting of the Antalya tufa rock mass as obtained from the uniaxial, triaxial compressive strength tests and Brazilian test results.

IX.1.3 Bieniawski's failure criterion

Bieniawski (1974) has proposed an empirical failure criterion which is in the form of a power law representing σ_1 vs. σ_3 and τ vs. σ_n envelops in concave downwards shape observed during strength tests on rock cores. Accordingly, the peak triaxial strengths of various rock types can be well expressed by the criterion (Eqs. 26, 27 and 28):

$$\frac{\sigma_1}{\sigma_c} = 1 + A\left(\frac{\sigma_3}{\sigma_c}\right)^k \qquad \text{Eq. (26)}$$

or

$$\frac{\tau_m}{\sigma_c} = 0{,}1 + B\left(\frac{\sigma_m}{\sigma_c}\right)^C \qquad \text{Eq. (27)}$$

$$\tau_m = \frac{1}{2}(\sigma_1 - \sigma_3)\ and\ \sigma_m = \frac{1}{2}(\sigma_1 + \sigma_3) \qquad \text{Eq. (28)}$$

where,

A, B, C, k are empirical constants.

Non-linear regression analysis of the triaxial compressive strength test results of the Antalya tufa rock mass, which has been performed by IBM SPSS software, has yielded the following relations with related coefficient of determinations (Tables 59 and 60, Figures 134 and 135):

Table 59. Bieniawski's criterion developed from uniaxial and triaxial compressive strength test results.

Antalya tufa rock mass (N= 52)	$\frac{\sigma_1}{\sigma_c} = 1 + 2.08\left(\frac{\sigma_3}{\sigma_c}\right)^{0.612}$	$R^2 = 0.79$
Phytoherm boundstone (N= 10)	$\frac{\sigma_1}{\sigma_c} = 1 + 2.68\left(\frac{\sigma_3}{\sigma_c}\right)^{0.669}$	$R^2 = 0.92$
Microcrystalline tufa (N= 18)	$\frac{\sigma_1}{\sigma_c} = 1 + 534\left(\frac{\sigma_3}{\sigma_c}\right)^{2.770}$	$R^2 = 0.36$
Phytoherm framestone (N= 15)	$\frac{\sigma_1}{\sigma_c} = 1 + 1.55\left(\frac{\sigma_3}{\sigma_c}\right)^{0.711}$	$R^2 = 0.88$
Phytoclast tufa (N= 9)	$\frac{\sigma_1}{\sigma_c} = 1 + 2.15\left(\frac{\sigma_3}{\sigma_c}\right)^{0.554}$	$R^2 = 0.45$

Table 60. Bieniawski's criterion developed from uniaxial, triaxial compressive strength tests and Brazilian test results.

Antalya tufa rock mass (N= 82)	$\frac{\sigma_1}{\sigma_c} = 1 + 1.33\left(\frac{\sigma_3}{\sigma_c}\right)^{0.898}$	$R^2 = 0.67$
Phytoherm boundstone (N= 17)	$\frac{\sigma_1}{\sigma_c} = 1 + 1.59\left(\frac{\sigma_3}{\sigma_c}\right)^{1.129}$	$R^2 = 0.85$
Microcrystalline tufa (N=21)	$\frac{\sigma_1}{\sigma_c} = 1 - 0.03\left(\frac{\sigma_3}{\sigma_c}\right)^{-0.646}$	$R^2 = 0.04$
Phytoherm framestone (N= 24)	$\frac{\sigma_1}{\sigma_c} = 1 + 1.37\left(\frac{\sigma_3}{\sigma_c}\right)^{0.811}$	$R^2 = 0.79$
Phytoclast tufa (N= 20)	$\frac{\sigma_1}{\sigma_c} = 1 + 1.42\left(\frac{\sigma_3}{\sigma_c}\right)^{1.336}$	$R^2 = 0.09$

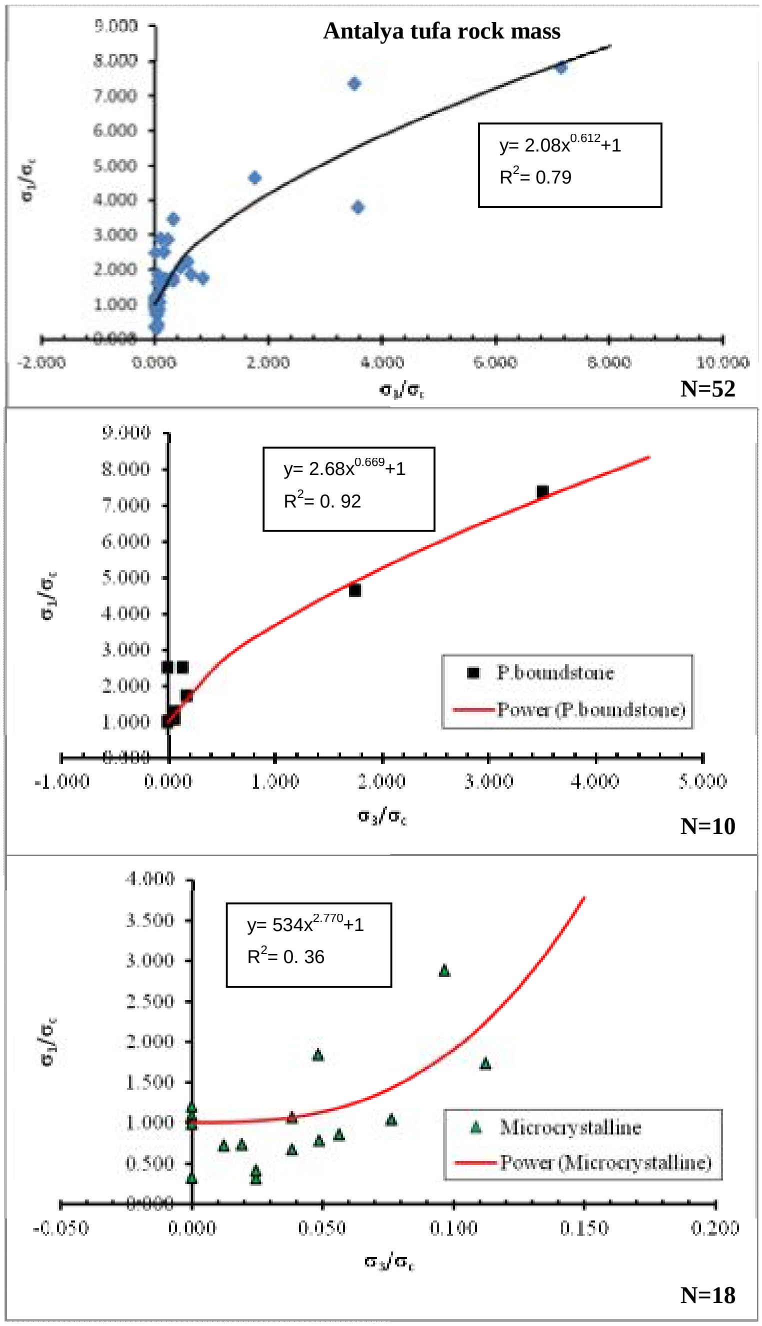

Figure 134. Bieniawski's criterion: curve fitting for the Antalya tufa rock mass and rock types.

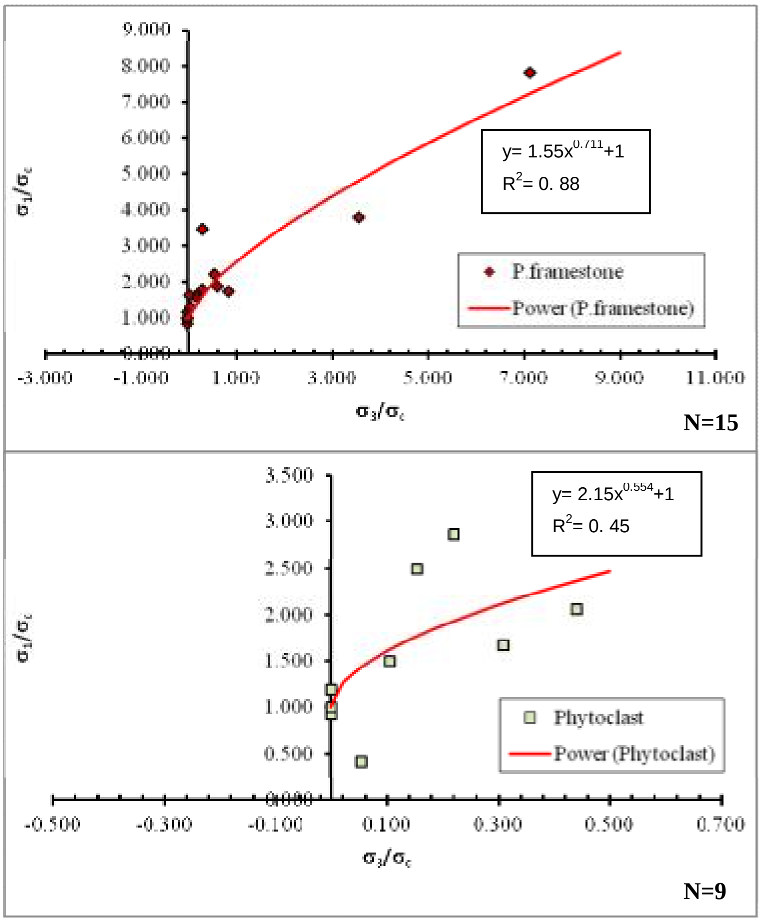

Figure 134 (cont'd.). Bieniawski's criterion: curve fitting for the Antalya tufa rock mass and rock types.

Antalya tufa rock mass

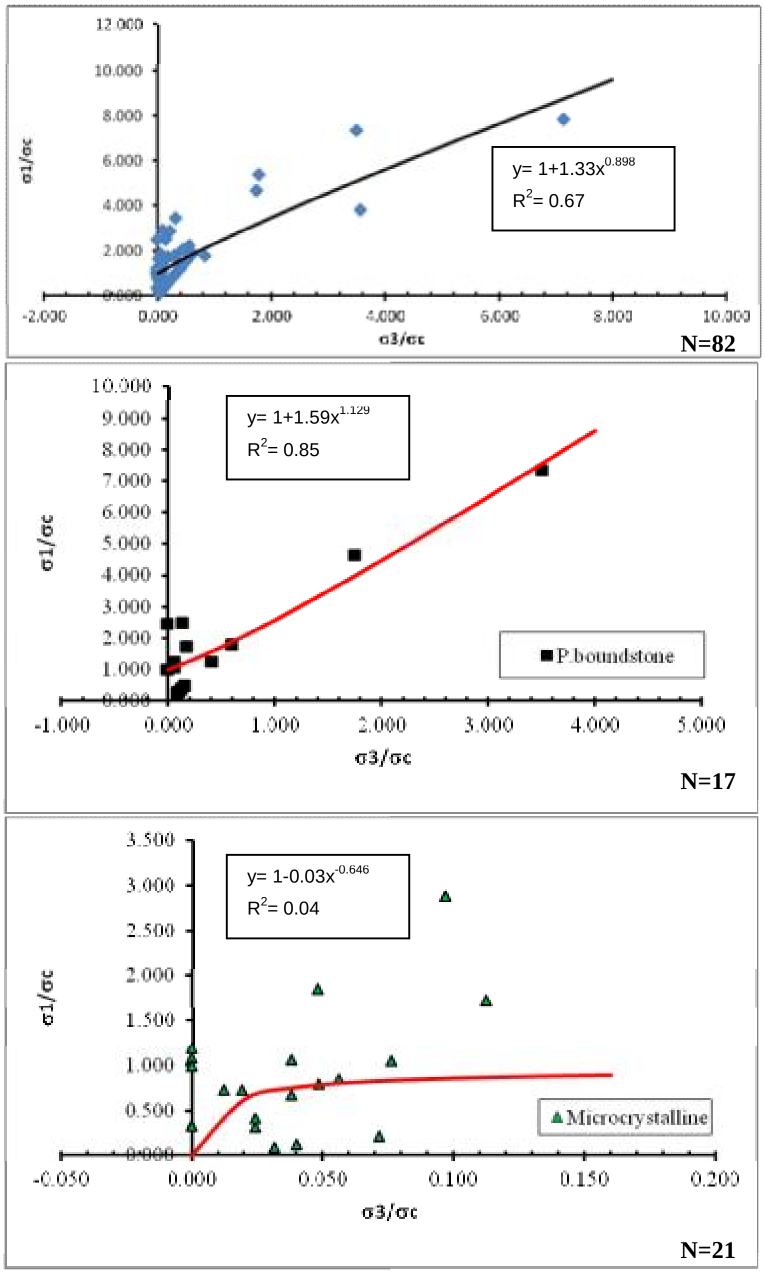

Figure 135. Bieniawski's criterion: curve fitting of the Antalya tufa rock mass as obtained from the uniaxial, triaxial compressive strength tests and Brazilian test results.

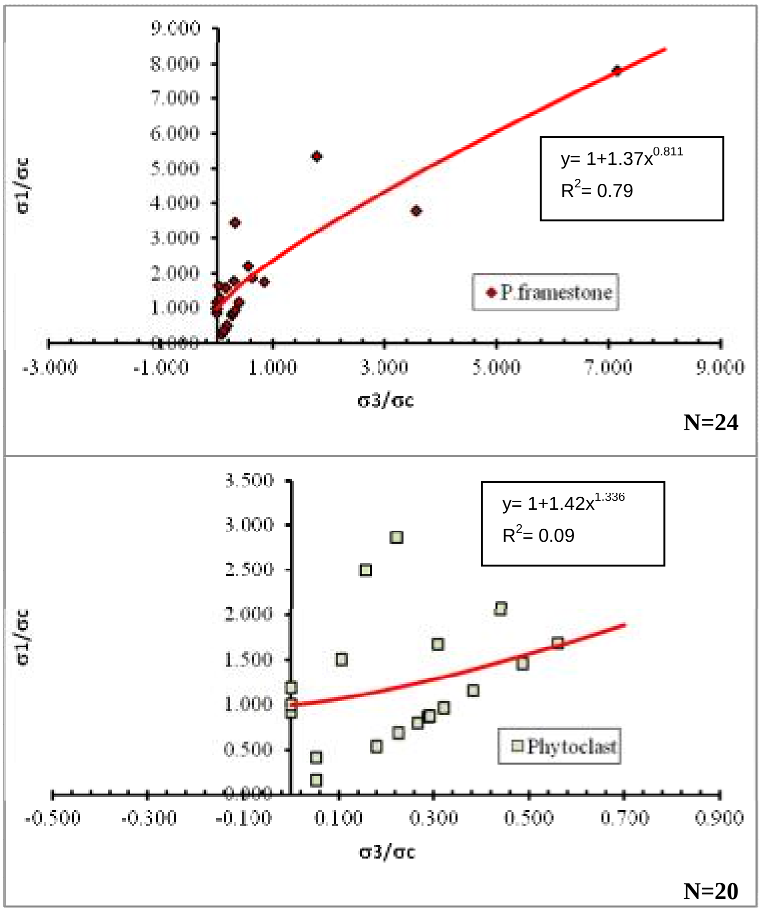

Figure 135 (cont'd.). Bieniawski's criterion: curve fitting of the Antalya tufa rock mass as obtained from the uniaxial, triaxial compressive strength tests and Brazilian test results.

IX.1.4 Hoek and Brown failure criterion

Hoek and Brown (1980) have proposed the following empirical relationship between the major and minor principal stresses associated with the failure of rock (Eq. 29):

$$\sigma_1 = \sigma_3 + (m\sigma_c\sigma_3 + s\sigma_c^2)^{1/2} \quad or \quad \frac{\sigma_1}{\sigma_c} = \frac{\sigma_3}{\sigma_c} + \left(m\frac{\sigma_3}{\sigma_c} + s\right)^{1/2} \qquad \text{Eq. (29)}$$

where,

$\sigma_1, \sigma_3 = major\ and\ minor\ principal\ stresses$

$\sigma_c = uniaxial\ compressive\ strength$

$m, s = empirical\ constants\ (s = 1\ for\ intact\ rock)$

Non-linear regression analysis of the triaxial compressive strength test results of the Antalya tufa rock mass, which has been performed by IBM SPSS software with sequential quadratic programming estimation method, has yielded the following relations with related coefficient of determinations (Tables 61 and 62, Figures 136 and 137):

Table 61. Hoek and Brown criterion developed from uniaxial and triaxial compressive strength test results (rock mass parameter s=1).

Antalya tufa rock mass (N= 52)	$\frac{\sigma_1}{\sigma_c} = \frac{\sigma_3}{\sigma_c} + \left(\frac{\sigma_3}{\sigma_c} + 1\right)^{1/2}$	$R^2 = 0.71$
Phytoherm boundstone (N= 10)	$\frac{\sigma_1}{\sigma_c} = \frac{\sigma_3}{\sigma_c} + \left(4.24\frac{\sigma_3}{\sigma_c} + 1\right)^{1/2}$	$R^2 = 0.91$
Microcrystalline tufa (N= 18)	$\frac{\sigma_1}{\sigma_c} = \frac{\sigma_3}{\sigma_c} + \left(10.4\frac{\sigma_3}{\sigma_c} + 1\right)^{1/2}$	$R^2 = 0.19$
Phytoherm framestone (N= 15)	$\frac{\sigma_1}{\sigma_c} = \frac{\sigma_3}{\sigma_c} + \left(\frac{\sigma_3}{\sigma_c} + 1\right)^{1/2}$	$R^2 = 0.70$
Phytoclast tufa (N= 9)	$\frac{\sigma_1}{\sigma_c} = \frac{\sigma_3}{\sigma_c} + \left(7.87\frac{\sigma_3}{\sigma_c} + 1\right)^{1/2}$	$R^2 = 0.42$

Table 62. Hoek and Brown criterion developed from uniaxial, triaxial compressive strength test and Brazilian test results (rock mass parameter s=1).

Antalya tufa rock mass (N= 82)	$\frac{\sigma_1}{\sigma_c} = \frac{\sigma_3}{\sigma_c} + \left(\frac{\sigma_3}{\sigma_c} + 1\right)^{1/2}$	$R^2 = 0.66$
Phytoherm boundstone (N= 17)	$\frac{\sigma_1}{\sigma_c} = \frac{\sigma_3}{\sigma_c} + \left(3.09\frac{\sigma_3}{\sigma_c} + 1\right)^{1/2}$	$R^2 = 0.83$
Microcrystalline tufa (N=21)	$\frac{\sigma_1}{\sigma_c} = \frac{\sigma_3}{\sigma_c} + \left(\frac{\sigma_3}{\sigma_c} + 1\right)^{1/2}$	No correlation
Phytoherm framestone (N= 24)	$\frac{\sigma_1}{\sigma_c} = \frac{\sigma_3}{\sigma_c} + \left(\frac{\sigma_3}{\sigma_c} + 1\right)^{1/2}$	$R^2 = 0.71$
Phytoclast tufa (N= 20)	$\frac{\sigma_1}{\sigma_c} = \frac{\sigma_3}{\sigma_c} + \left(\frac{\sigma_3}{\sigma_c} + 1\right)^{1/2}$	$R^2 = 0.05$

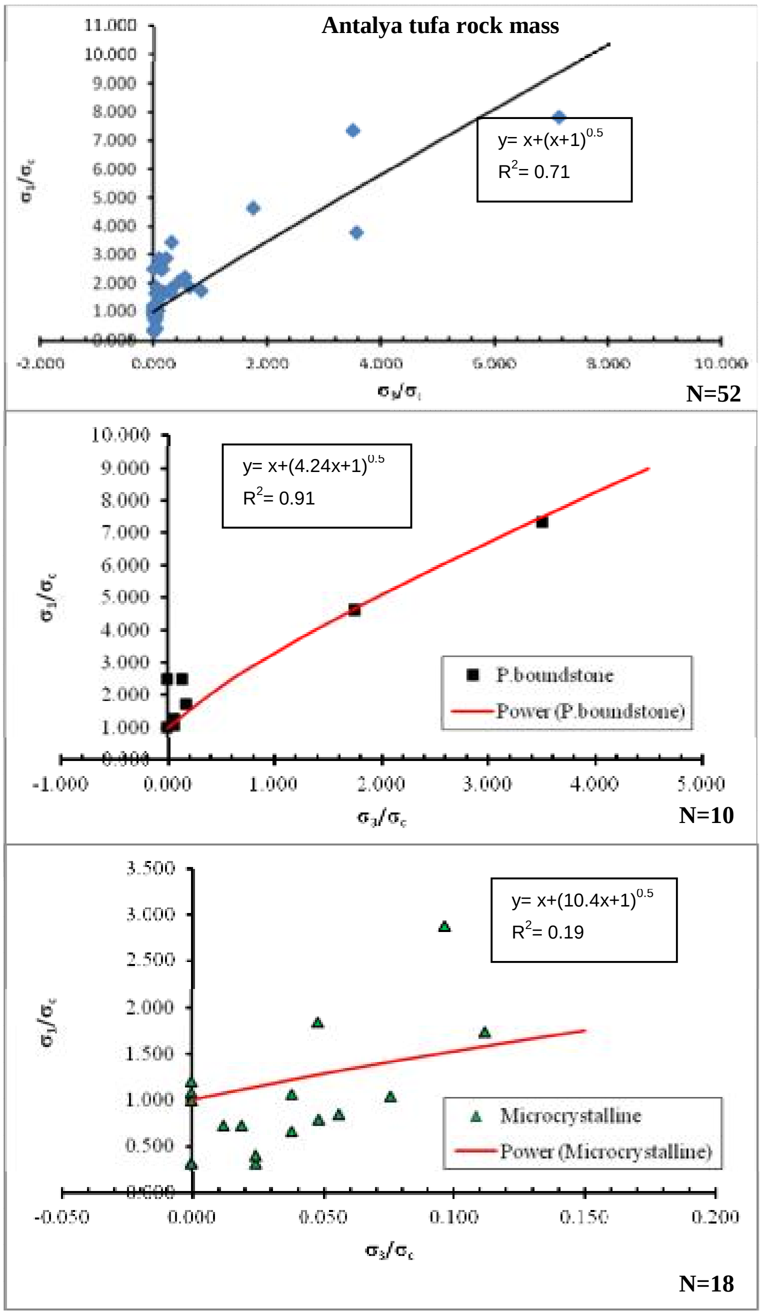

Figure 136. Hoek and Brown criterion: curve fitting for the Antalya tufa rock mass (rock mass parameter s=1).

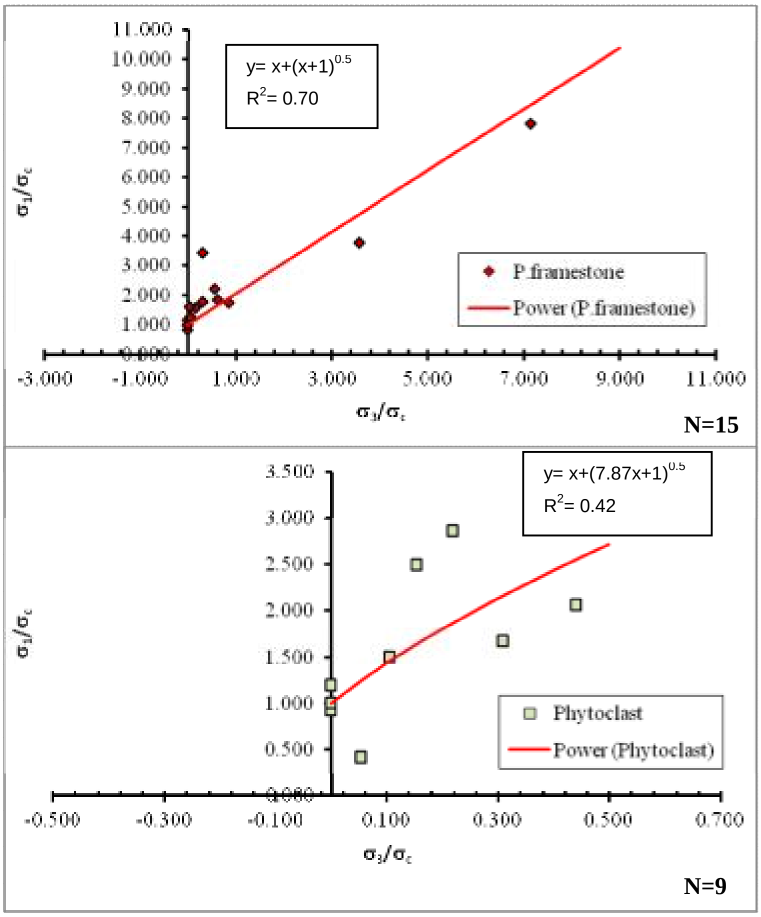

Figure 136 (cont'd.). Hoek and Brown criterion: curve fitting for the Antalya tufa rock mass (rock mass parameter s=1).

Antalya tufa rock mass

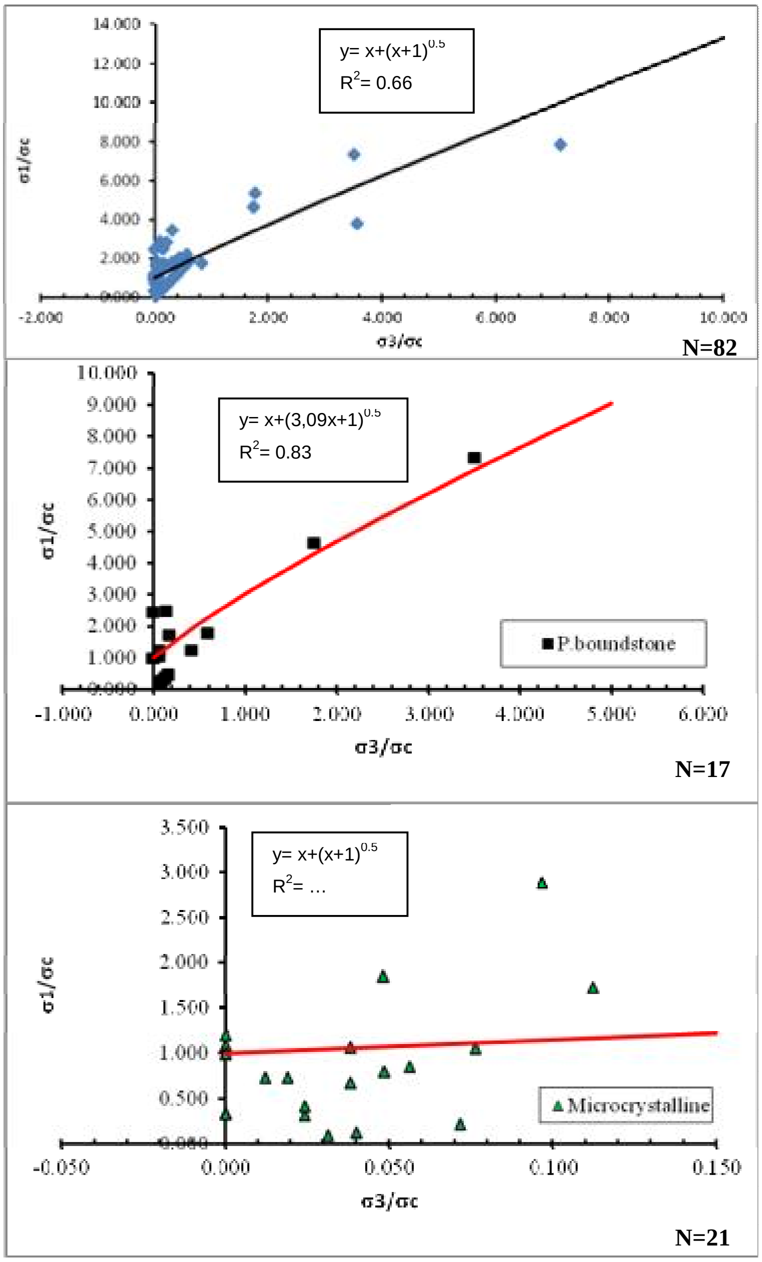

Figure 137. Hoek and Brown criterion: curve fitting for the Antalya tufa rock mass as obtained from the uniaxial, triaxial compressive strength tests and Brazilian test results.

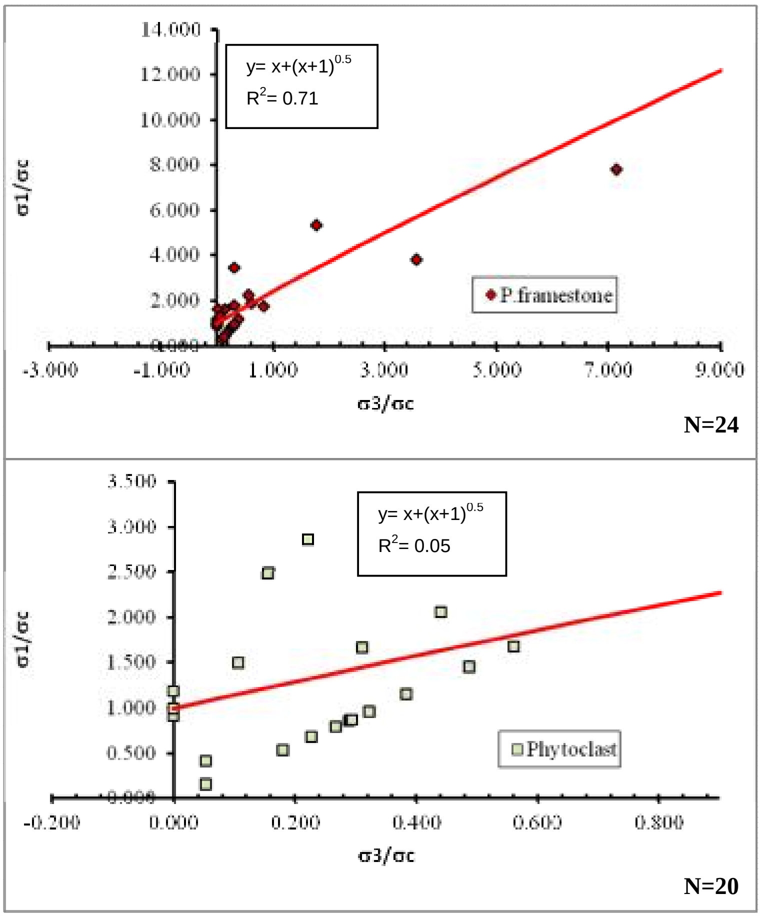

Figure 137 (cont'd.). Hoek and Brown criterion: curve fitting for the Antalya tufa rock mass as obtained from the uniaxial, triaxial compressive strength tests and Brazilian test results.

Non-linear regression analysis of the triaxial compressive strength test results of the Antalya tufa rock mass, which has been performed by the RocData software with Levenberg-Marquardt estimation method, has yielded the following results (Tables 63 and 64, Figures 138 and 139):

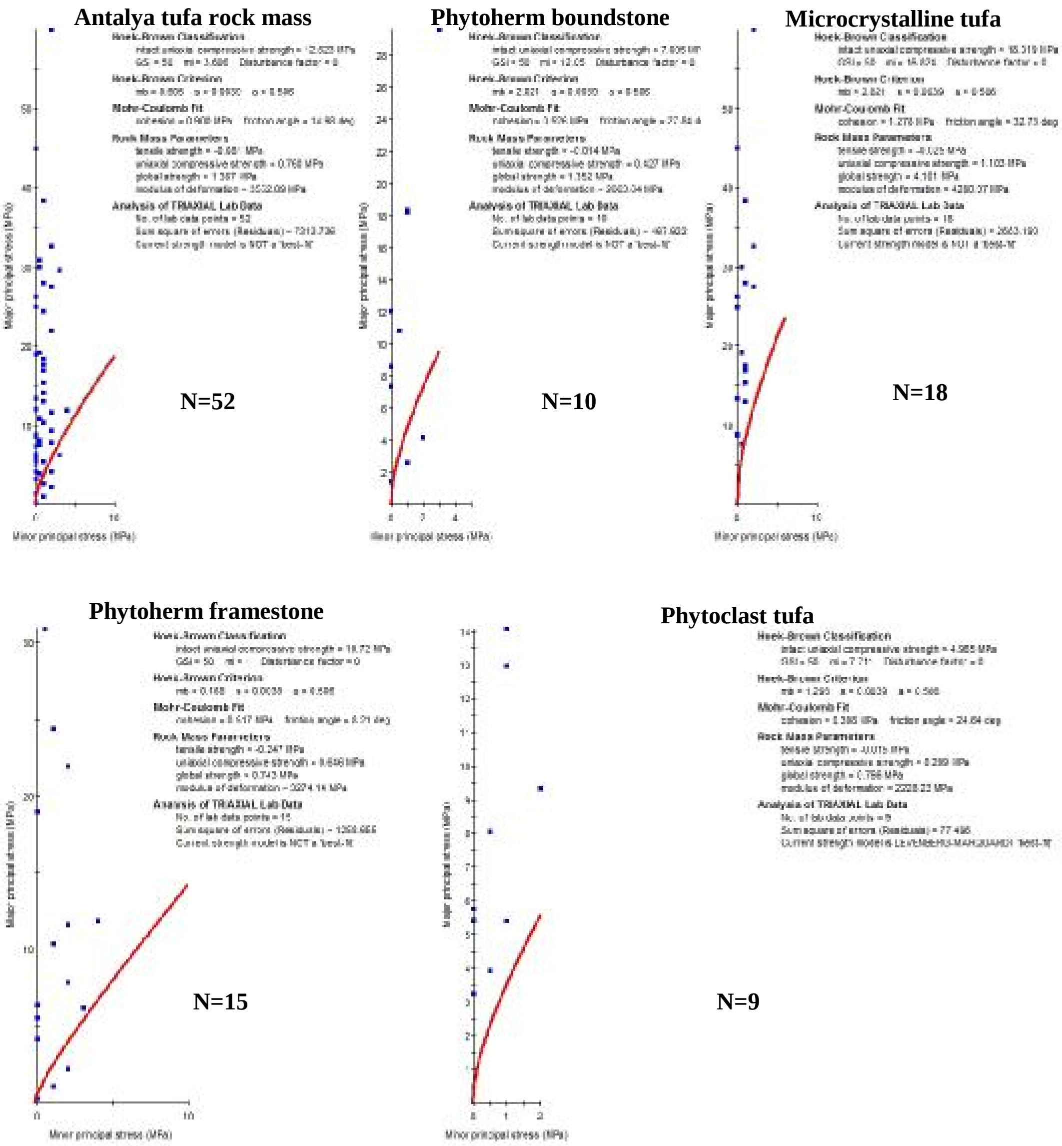

Figure 138. Hoek and Brown criterion: rocdata curve fitting of the Antalya tufa rock mass and rock types (rock material parameter s=1).

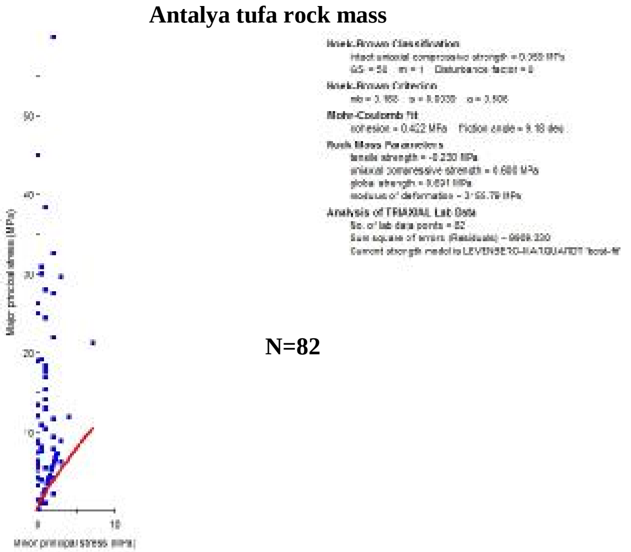

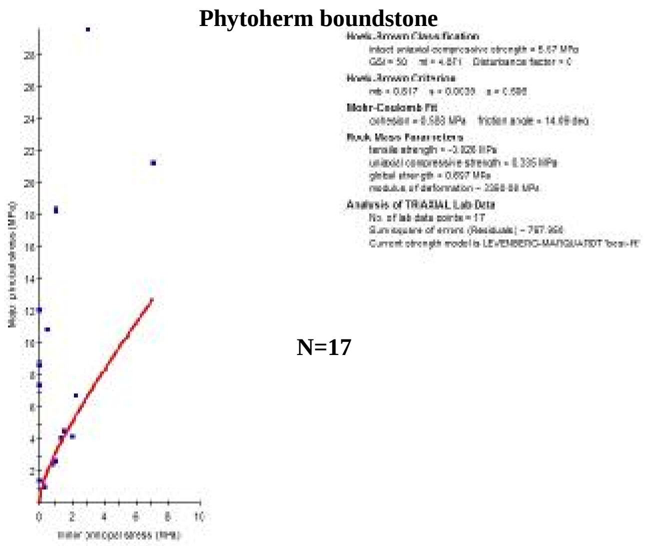

Figure 139. Hoek and Brown criterion: rocdata curve fitting of the Antalya tufa rock mass and rock types (rock material parameter s=1).

Microcrystalline tufa

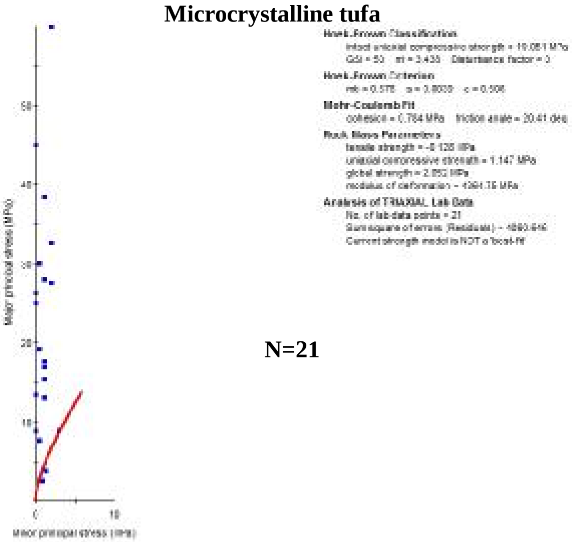

Phytoherm framestone

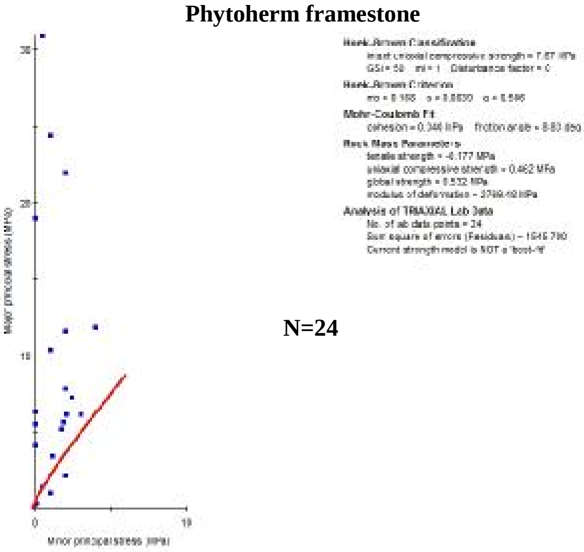

Figure 139 (cont'd.) Hoek and Brown criterion: rocdata curve fitting of the Antalya tufa rock mass and rock types (rock material parameter s=1).

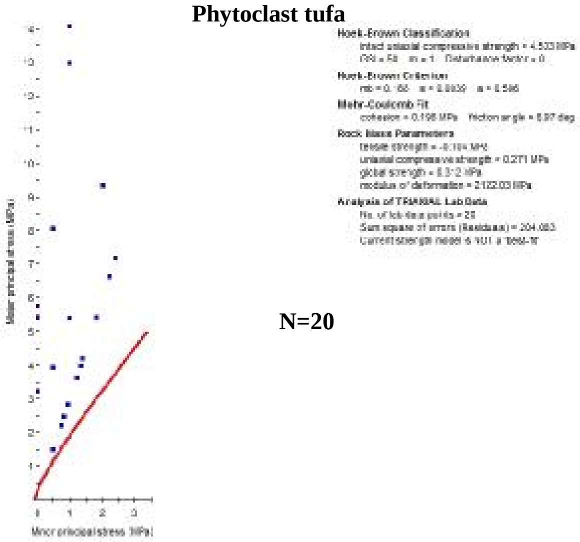

Figure 139 (cont'd.) Hoek and Brown criterion: rocdata curve fitting of the Antalya tufa rock mass and rock types (rock material parameter s=1).

Table 63. Hoek and Brown criterion: A comparison of the results of two different non-linear regression methods of triaxial compressive strength test results.

Method / Tufa type	Non-linear regression by IBM SPSS (Semi quadratic programming)			Non-linear regression by Rocdata (Levenberg-Marquardt)	
	Intact rock			Intact rock	
	m_i	s_i	R^2	m_i	σ_{ci} (MPa)
Tufa in general (N= 52)	1.00	1.00	0.71	3.61	12.6
Microcrystalline tufa (N= 18)	10.4	1.00	0.19	16.3	18.3
P. boundstone (N= 10)	4.24	1.00	0.91	12.1	7.09
P. framestone (N= 15)	1.00	1.00	0.70	1.0	10.7
Phytoclast tufa (N= 9)	7.87	1.00	0.42	7.71	4.97

Table 64. Hoek and Brown's criterion: A comparison table for the results of two different non-linear regression methods of triaxial compressive strength test results.

Method / Tufa type	Non-linear regression by IBM SPSS (Semi quadratic programming)			Non-linear regression by Rocdata (Levenberg-Marquardt)	
	Intact rock			Intact rock	
	m_i	s_i	R^2	m_i	σ_{ci} (MPa)
Tufa in general (N= 82)	1.00	1.00	0.66	1.00	10.2
P. boundstone (N= 17)	3.09	1.00	0.83	4.87	5.57
Microcrystalline tufa (N= 21)	1.00	1.00	No correlation	1.00	21.7
P. framestone (N= 24)	1.00	1.00	0.71	1.00	7.67
Phytoclast tufa (N= 20)	1.00	1.00	0.05	1.00	4.50

IX.1.5 Comparison of failure criteria fits

According to the two-stage curve fitting studies performed through linear and non-linear regression analyses of the experimental data, it has been determined that the strength characteristics of the Antalya tufa rock mass show a better fit with the Bieniawski's failure criterion as far as the data of the uniaxial and triaxial compressive strength tests are concerned (Table 65).

Table 65. Coefficient of determination (R^2) values for the different failure criteria fits utilized by excluding the Brazilian test results.

Tufa type	Coulomb's fit	Bieniawski's fit	Hoek and Brown's fit
Tufa in general (N= 52)	0.71	0.79	0.71
P.boundstone (N= 10)	0.89	0.92	0.91
Microcrystalline tufa (N= 18)	0.21	0.36	0.19
P.framestone (N= 15)	0.86	0.88	0.70
Phytoclast tufa (N= 9)	0.36	0.45	0.42

When the number of data included in the analyses is expanded from 52 to 82 with the addition of the Brazilian test results, the values of the coefficient of determination have been mostly observed to be reduced (Table 66).

Table 66. Coefficient of determination (R^2) values for the different failure criteria fits utilized by including the Brazilian test results.

Tufa type	Coulomb's fit	Bieniawski's fit	Hoek and Brown's fit
Tufa in general (N= 82)	0.66	0.67	0.66
P.boundstone (N= 17)	0.85	0.85	0.83
Microcrystalline tufa (N= 21)	No correlation	0.04	No correlation
P.framestone (N= 24)	0.77	0.79	0.71
Phytoclast tufa (N=20)	0.09	0.09	0.05

The general reduction of the coefficient of determination (R^2) with the addition of the Brazilian test results could be explained by the variable mechanical behavior of the Antalya tufa rock mass even within the differentiated individual tufa rock types. During the geotechnical characterization attempts, individual tufa rock types have been observed to have a wide range of geotechnical parameters. Hence, the variance could be further increased with the inclusion of the Brazilian test results (Jaeger and Cook, 1979).

The coefficient of determination values obtained from each failure criterion for the individual tufa rock types have been observed to be close. In other words, the strength characteristics of the Antalya tufa rock types and of the tufa rock mass fitted reasonably well to all of the failure criteria that were considered herein.

IX.1.6 The strength criterion of Antalya tufa rock masses (unconstrained non-linear regression analysis)

In this section, a compressive failure criterion for the Antalya tufa rock mass has been attempted to be proposed on the basis of the results of the triaxial compressive strength tests, uniaxial compressive strength tests and Brazilian tensile strength tests. What is needed is a non-linear failure envelope that fits the test data with a reasonably well relationship. The non-linearity, which is expected over an extended interval far from the origin, of the criterion brings the necessity of minor principal stress values other than zero, otherwise a non-linear fit as of power regression would not be possible to be obtained. Hence, this situation is overcome by normalization of the data via plotting $(\sigma_1-\sigma_3)/\sigma_c$ against $(\sigma_1+\sigma_3)/\sigma_c$ (Pariseau, 2007). The power regression analysis of the data has resulted in the following compressive strength criterion for the Antalya tufa rock mass with a coefficient of determination (R^2) of 0.88 (Figure 140, Eq. 30).

$$\frac{\sigma_1-\sigma_3}{\sigma_c} = 0.89\left(\frac{\sigma_1+\sigma_3}{\sigma_c}\right)^{0.76},\ R^2 = 0.88 \qquad \text{Eq. (30)}$$

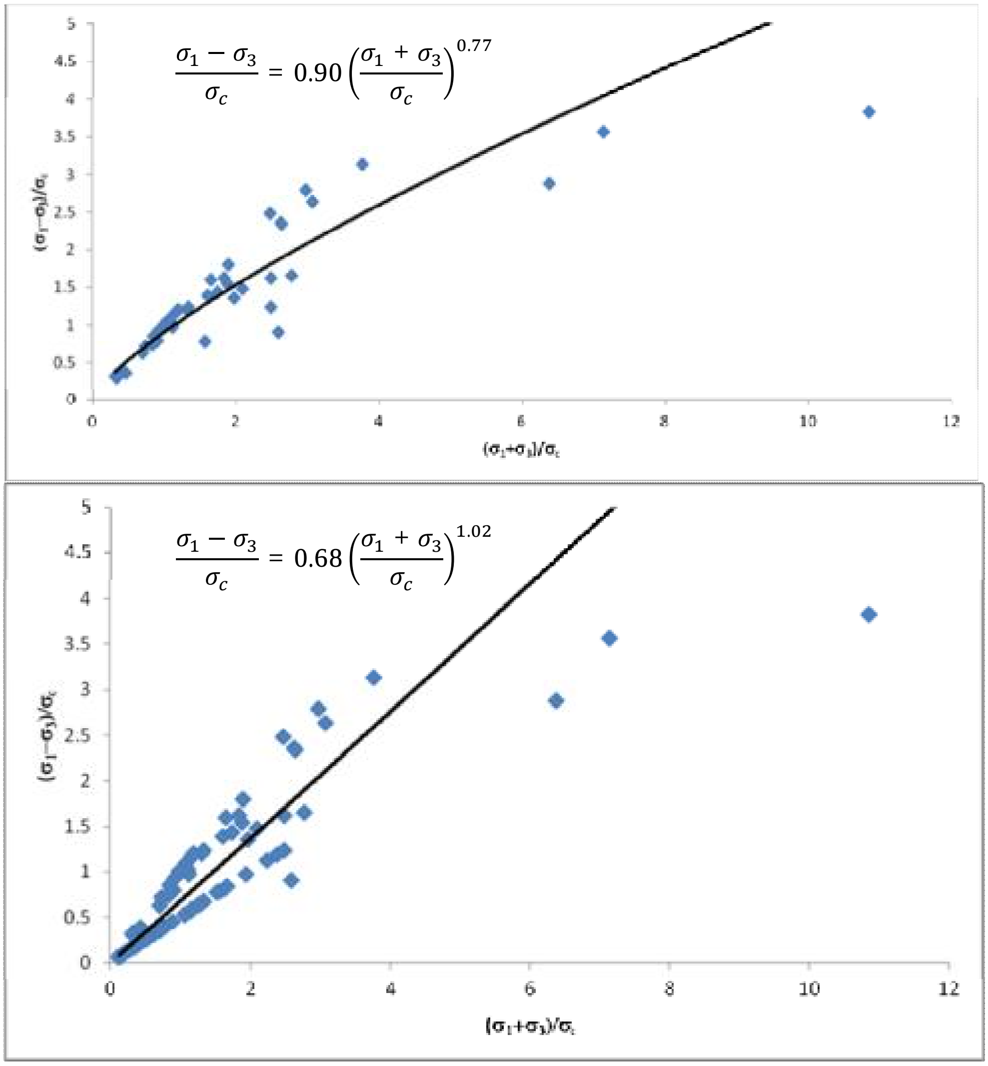

Figure 140. Proposed compressive strength failure criterion a. N=52 b. N=82

As it is seen from Figure 140, the (R^2) values are very close and reasonably high in both of the data sets possessing different number of samples. The tensile strength values, which are small and close to the origin, were interpreted to be the reason for this phenomenon.

In addition to the strength criterion, stress paths that were drawn by plotting the maximum shear stress, p= $(\sigma_1-\sigma_3)/2$ against the mean normal stress q= $(\sigma_1+\sigma_3)/2$ for the same data sets have resulted in the following equation with a coefficient of determination (R^2) of 0.97 (Figure 141, Eq. 31).

$$\tau_m = 0.89\sigma_m + 0.18,\ R^2 = 0.97 \qquad \text{Eq. (31)}$$

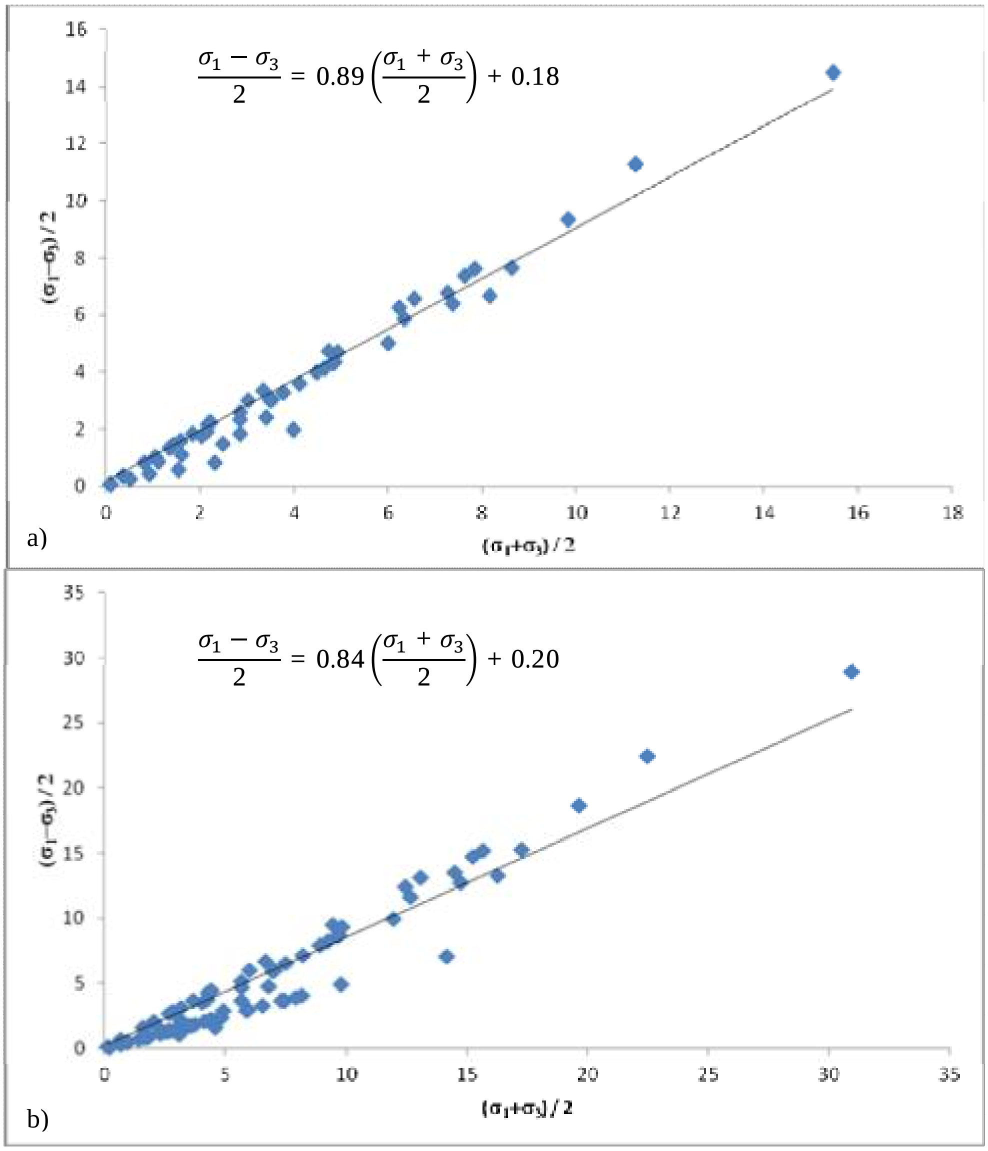

Figure 141. Maximum shear stress versus mean normal stress plots a) N=52. b) N=82.

Instead of drawing Mohr's circles, stress paths as shown in Figure 141 can be drawn to obtain related shear strength parameters (Day, 2005). The relationship of the shear strength parameters with the Mohr's circle and the basis of the p-q plot are given in Figure 142.

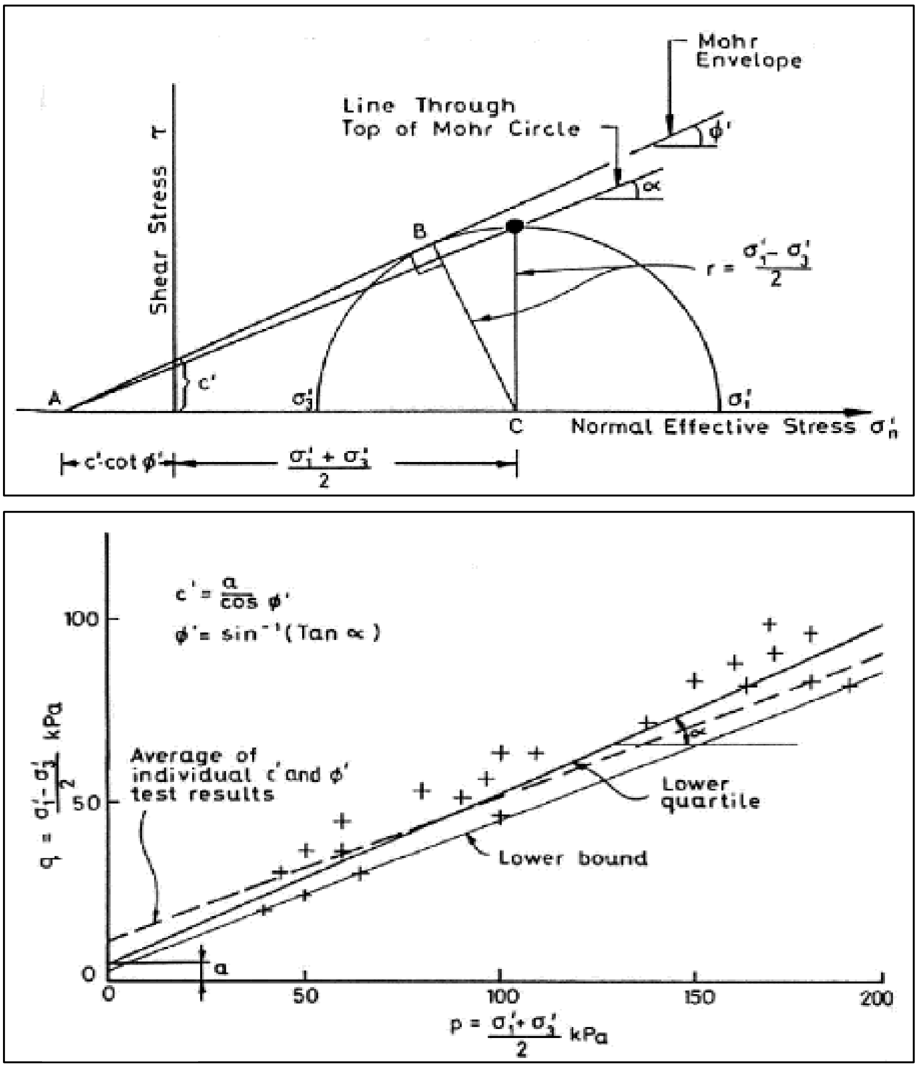

Figure 142. The relationship between Mohr's circle and p-q plot (Fell et al., 1992).

The cohesion and internal friction angle of the Antalya tufa rock mass have been calculated from Figure 141 (a) and Figure 141 (b) as c= 0.39 MPa, ϕ= 62,87° and c= 0.37 MPa, ϕ= 57.14°, respectively.

According to the p-q plots of the intact rock samples of the the Antalya tufa rock types, cohesion and internal friction angle values of the Antalya tufa rock types range from 0.0 to 0.39 MPa and 57.14° to 70.44°, respectively (Figure 143).

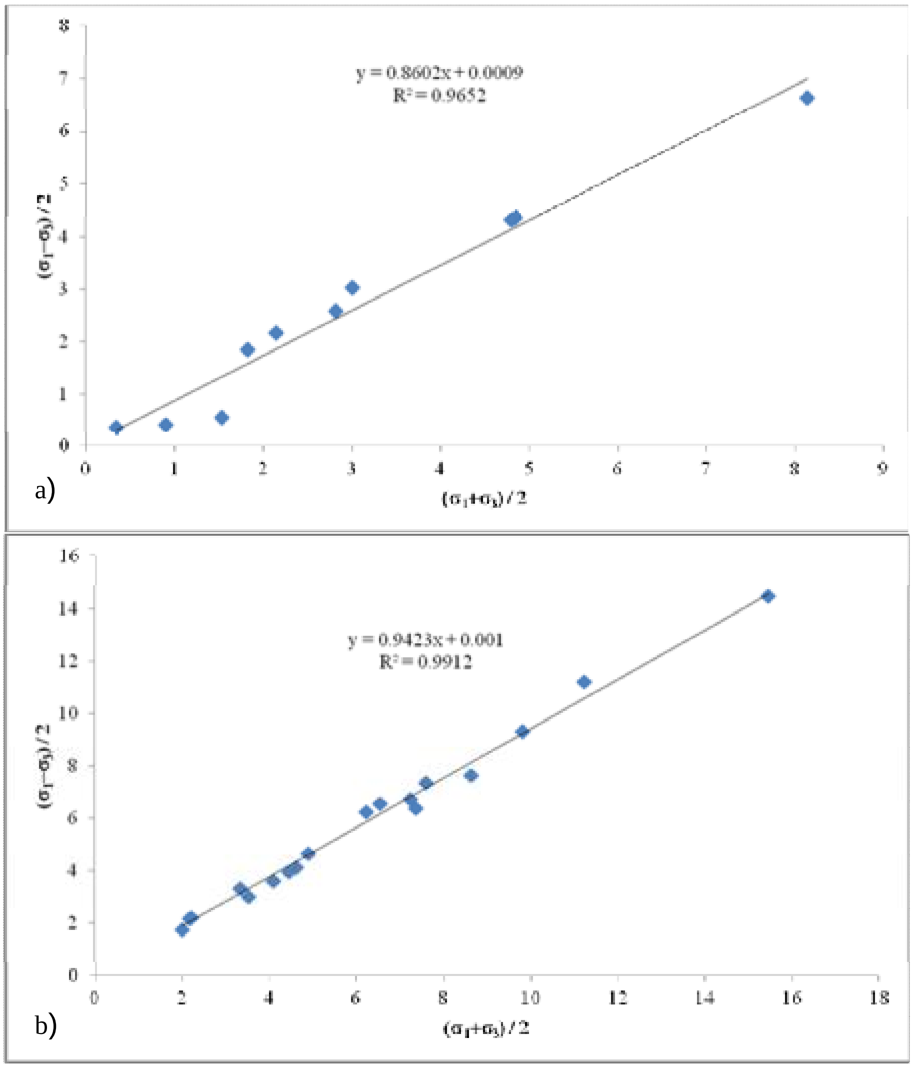

Figure 143. P-q plots of the Antalya tufa rock types. a) Phytoherm boundstone b) Microcrystalline tufa c) Phytoherm framestone d) Phytoclast tufa.

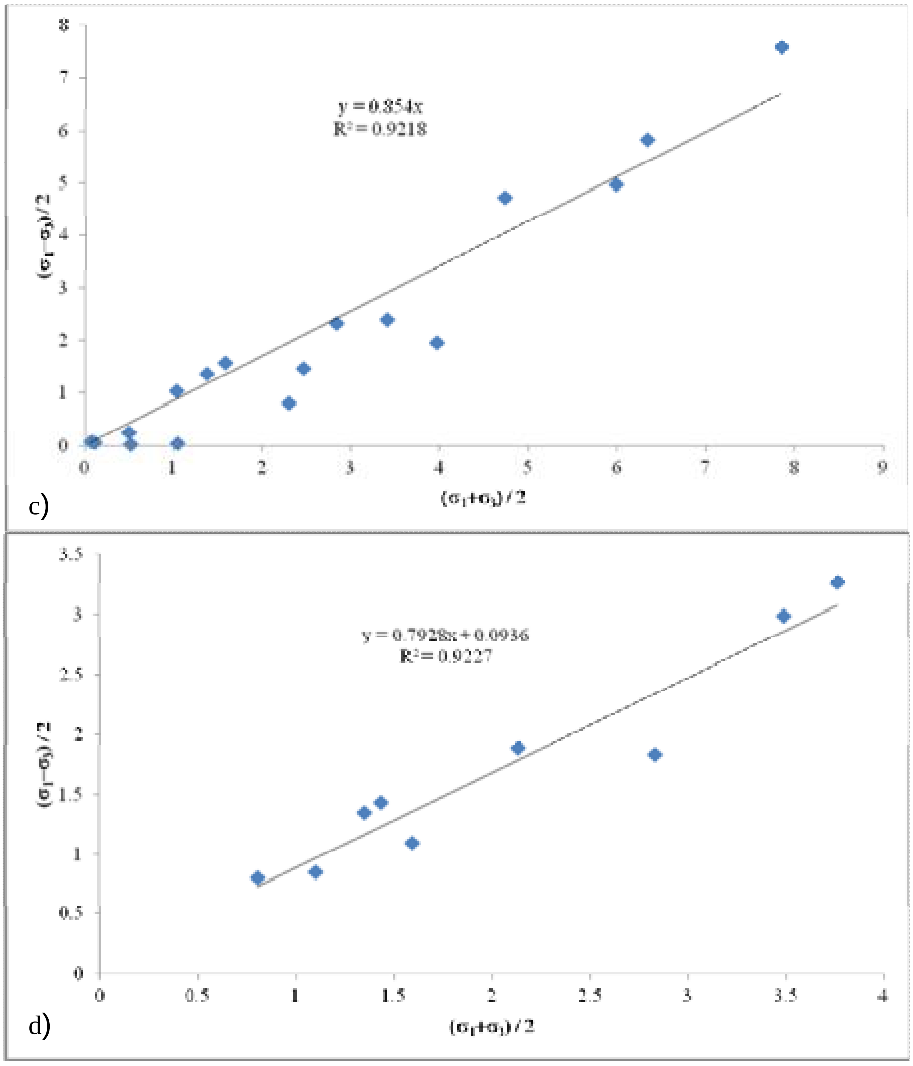

Figure 143 (cont'd.). P-q plots of the Antalya tufa rock types. a) Phytoherm boundstone b) Microcrystalline tufa c) Phytoherm framestone d) Phytoclast tufa.

IX.1.7 Proposed failure criterion for the anisotropic Antalya tufa rock mass

IX.1.7.1 Background

The most widely used failure criteria that describe ultimate strength in rock mechanics are named as Mohr and Coulomb, Hoek and Brown, Bieniawski, and Drucker and Prager.

Sometimes, they are also referred to as yield functions. The principal assumption for all strength criteria mentioned above is that the rock material is assumed to be homogeneous and isotropic.

The Drucker and Prager criterion, which is expressed as a function of principal stresses, is different from Mohr and Coulomb or Hoek and Brown by the inclusion of the intermediate principal stress. The criterion is a cone centered on the space diagonal in principal stress space as illustrated by Figure 144 (Pariseau, 2007).

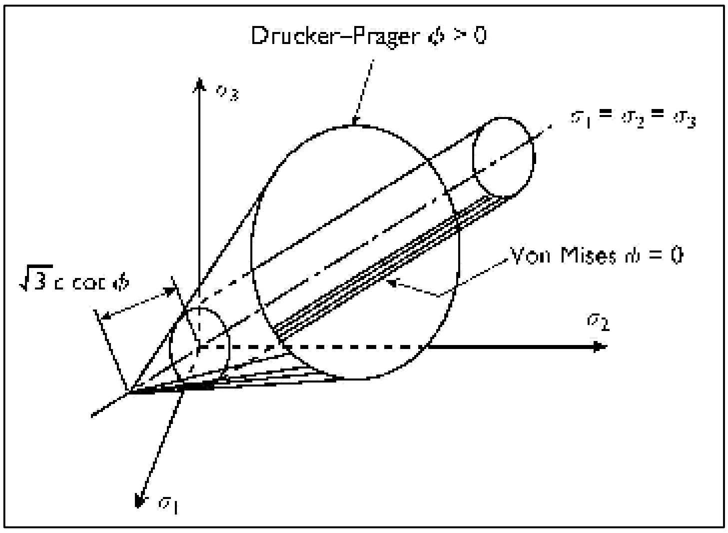

Figure 144 Drucker and Prager failure criterion in principal stress space (after Zienkiewicz, 1977)

The Drucker and Prager failure criterion defined in terms of principal stresses is given by (Eq. 32) as follows:

$$\left(\sqrt{\frac{2}{3}}\right)\left[\left(\frac{\sigma_1-\sigma_2}{2}\right)^2 + \left(\frac{\sigma_2-\sigma_3}{2}\right)^2 + \left(\frac{\sigma_3-\sigma_1}{2}\right)^2\right]^{1/2} = A(\sigma_1 + \sigma_2 + \sigma_3) + B \qquad \text{Eq. (32)}$$

where,

A and B are the strength properties of the material.

The Drucker and Prager strength criterion is often written in short form given by (Eq. 33) as follows:

$$J_2^{1/2} = AI_1 + B \qquad \text{Eq. (33)}$$

where,

J_2= the second principal invariant of deviatoric stress,

I_1= the first principal invariant of total stress.

IX.1.7.2 General formulation of the proposed failure criterion

An empirical approach to develop a compressive failure criterion for the heterogeneous Antalya tufa rock mass is presented in this section. The triaxial stress analyses are affected by the heterogeneity of the rock sample, loading rate, sample size and sample shape. In this investigation, the heterogeneity affect, has assumed to be represented by the unit weight and porosity of the tufa rock sample. These two parameters have resulted in the largest variances as compared to the other parameters as was identified in Chapter VIII.3. The affect of the loading rate, sample size and sample shape has been assumed to be constant for all the tufa samples tested, whose length to diameter (L/D) ratios were mostly 2 and shapes were cylindrical. Hence, the general expression of the proposed failure criterion by means of the second invariant of stress deviation [$(J_2)^{1/2}$] at failure should include the first invariant of stress (I_1), porosity of the rock (n) and unit weight of the rock as follows (Eq. 34) (Fuenkajorn and Daemen, 1992).

$$(J_2)^{1/2} = f\{I_1, n, \gamma\} \qquad \text{Eq. (34)}$$

where,

$$J_2 = \frac{1}{6}[(\sigma_1 - \sigma_2)^2 + (\sigma_2 - \sigma_3)^2 + (\sigma_3 - \sigma_1)^2]$$

$$I_1 = \sigma_1 + \sigma_2 + \sigma_3$$

n= porosity of the rock sample

γ= unit weight of the rock sample.

This formulation assumes that homogeneity is relative and depends on porosity, which was assessed to be a key parameter that controls the homogeneity of the tufa rock mass. It should also be noted that the effect of unit weight and porosity on the strength for each tufa sample or type may not be the same.

The proposed failure criterion considers principal stresses at failure though the effect of σ_2 which has not been analyzed due to lack of data.

In order to have an unbiased proposal for the intact rock failure criterion, multiple linear and non-linear regression analyses have been performed for the experimental data of the Antalya tufa rock mass.

According to the results of multiple linear regression analysis of the data of this study, assuming an identical set of test parameters where the first stress invariant, unit weight and porosity control the variation in rock strength, [$(J_2)^{1/2}$] at failure may be represented by (Eq. 35):

$$J_2^{1/2} = 0.493I_1 - 0.034n + 0.296\gamma - 5.673,\ R^2 = 0.959,\ N = 46 \qquad \text{Eq. (35)}$$

Similarly, assuming an identical set of test parameters where the first stress invariant and porosity or the first stress invariant and unit weight control the variation in rock strength, [$(J_2)^{1/2}$] at failure may be represented by (Eq. 36) and (Eq. 37), respectively:

$$J_2^{1/2} = 1588I_1 + 15.1n + 4.014,\ R^2 = 0.955,\ N = 46 \qquad \text{Eq. (36)}$$

$$J_2^{1/2} = 1433I_1 + 24\gamma + 28.7,\ R^2 = 0.959,\ N = 46 \qquad \text{Eq. (37)}$$

According to the results of multiple non-linear regression analyses, $[(J_2)^{1/2}]$ at failure in terms of the first stress invariant and porosity or the first stress invariant and unit weight may be represented by (Eq. 38) and (Eq. 39), respectively:

$$J_2^{1/2} = 0.514I_1 - 0.211e^{0.083n},\ R^2 = 0.952,\ N = 46 \qquad \text{Eq. (38)}$$

$$J_2^{1/2} = 0.511I_1 - 103.121e^{-0.267\gamma},\ R^2 = 0.956,\ N = 46 \qquad \text{Eq. (39)}$$

IX.1.7.3 Failure envelopes of the proposed failure criterion

Failure envelopes for the Antalya tufa rock mass could be drawn from Eq. (35), Eq. (38) and Eq. (39). Figure 145 displays the variation of $J_2^{1/2}$ as a function of I_1 for mean unit weight (γ) value of 19 of the Antalya tufa rock mass. Similarly, Figure 146 and Figure 147 show the variation of $J_2^{1/2}$ as a function of I_1 and porosity (n) and as a function of I_1 and unit weight (γ)of the Antalya tufa rock mass, respectively.

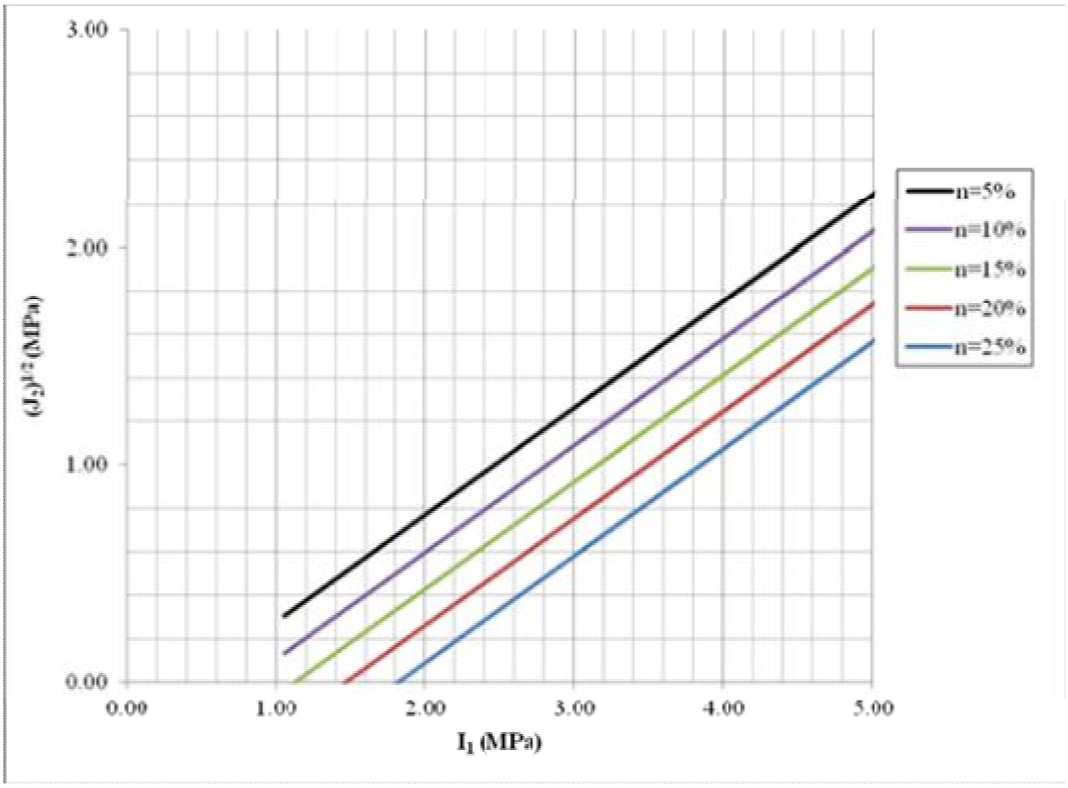

Figure 145. Failure envelopes for the samples of the Antalya tufa rock mass with a mean unit weight (γ) value of 19 kN/m^3 (Eq. 35).

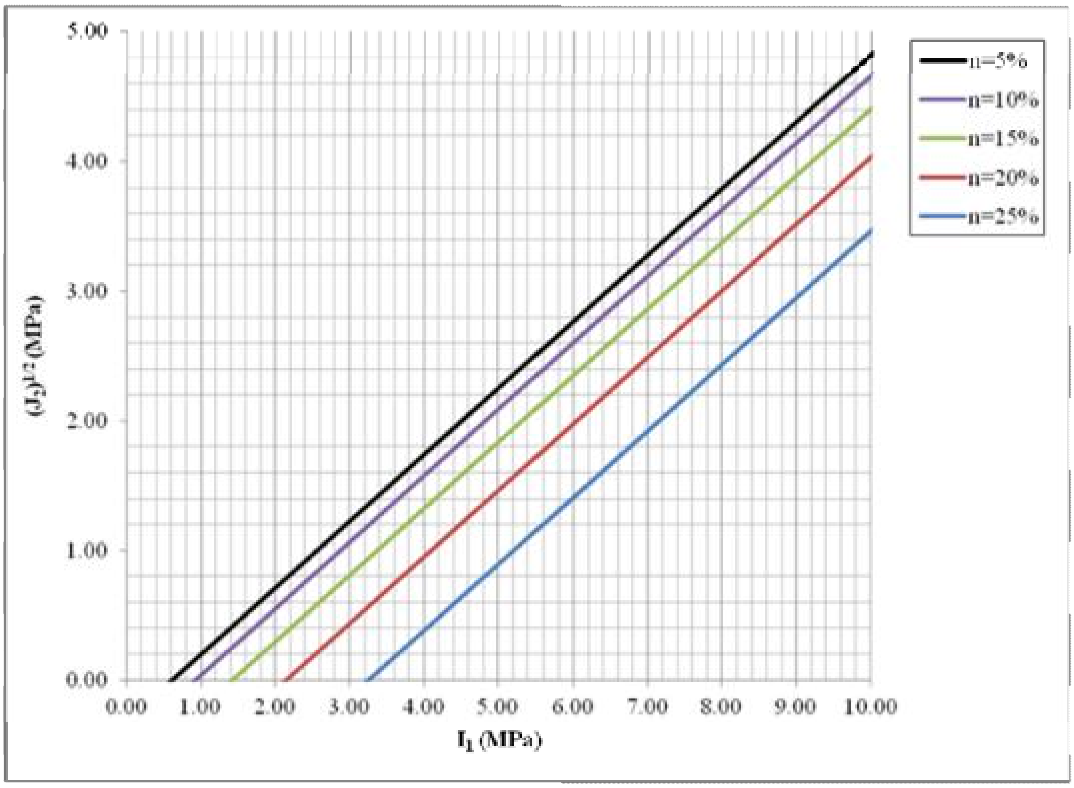

Figure 146. Failure envelopes for the variation of $J_2^{1/2}$ as a function of I_1 and porosity (n) of the Antalya tufa rock mass (Eq. 38)..

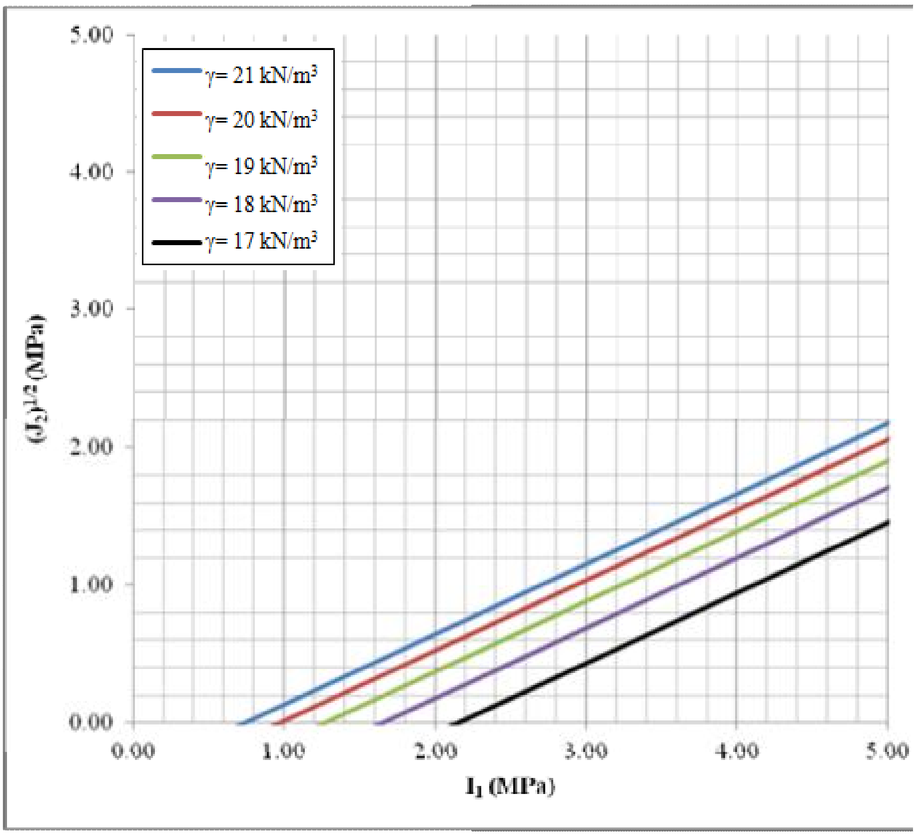

Figure 147. Failure envelopes for the variation of $J_2^{1/2}$ as a function of I_1 and unit weight (γ)of the Antalya tufa rock mass (Eq. 39).

Figure 145 reveals that the the proposed failure criterion (Eq. 35) is more reliable for the selected porosity range when I1 $\geq$ 2 MPa. Similarly, the failure envelopes given by Figure 144 and Figre 145 are more reliable for the selected range of the parameters when I1 $\geq$ 3 MPa and I1 $\geq$ 2.50 MPa, respectively. .

The failure envelopes given in Figures 145, 146 and 147 could be re-drawn for different values of the porosity and unit weight of the Antalya tufa rock mass. However, the results of failure predictions are not affected as long as the same values are used consistently throughout the derivation and predictions.

IX.1.7.4 Predictive capability of the proposed failure criterion

In order to assess the predictive capability of the proposed failure criterion, theoretical and predicted strengths ($J_2^{1/2}$) calculated from the results of triaxial compressive strength tests and predicted through proposed failure criteria, respectively have been compared in Figure 148. The comparison between theoretical and predicted strengths ($J_2^{1/2}$) calculated from Eq. (35), Eq. (38) and Eq. (39) are presented in Table 67. The ratio of theoretical to predicted strength given in Table 67 reveals that some of the strength predictions are less while others are larger than the theoretical strength values of the Antalya tufa rock types. However, particularly the non-linear equations, namely Eq. (38) and Eq. (39), which are believed to represent better the natural variability of the Antalya tufa rock mass, have estimated strength values less than the theoretical strength in total average. Hence, it is recommended to use Eq. (38) and Eq. (39) for the strength prediction.

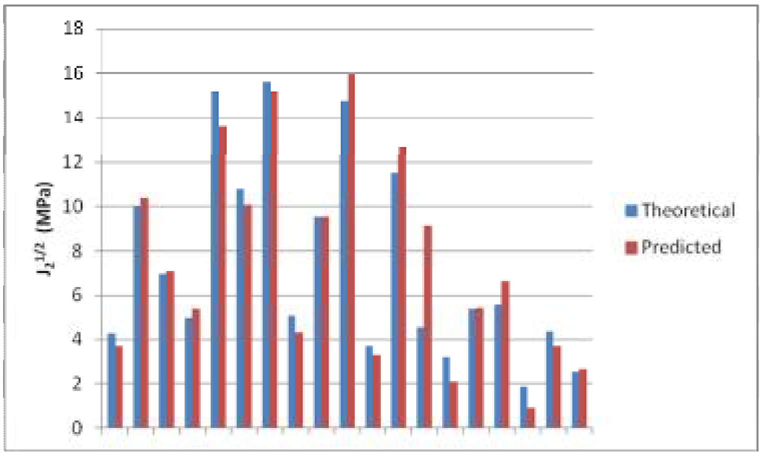

a)

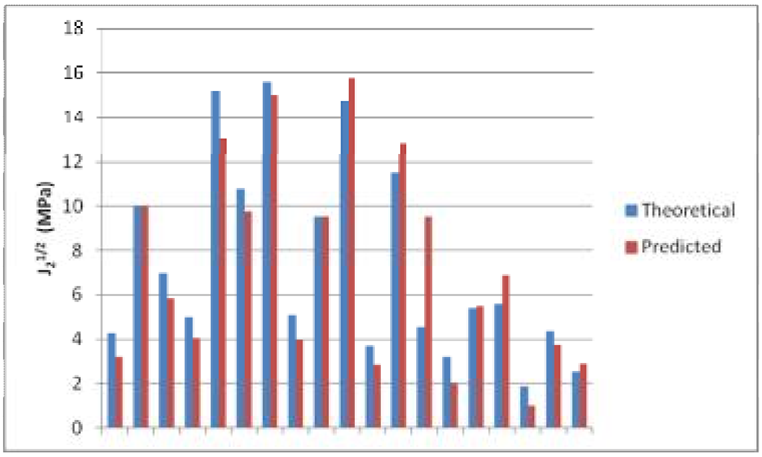

b)

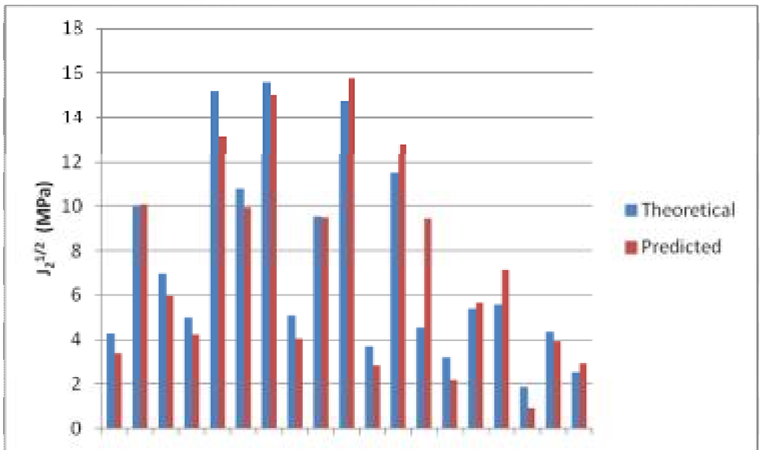

c)

Figure 148. Comparison between theoretical and predicted strengths ($J_2^{1/2}$) of the Antalya tufa rock mass. a) $J_2^{1/2}$ predicted by Eq. 35. b) $J_2^{1/2}$ predicted by Eq. 38. c) $J_2^{1/2}$ predicted by Eq. 39.

Table 67. Comparison of theoretical and predicted strengths ($J_2^{1/2}$) of the Antalya tufa rock types.

Tufa type	[1] Theoretical values of $J_2^{1/2}$	[2] Predicted values of $J_2^{1/2}$ (Eq. 35)	[1]/[2]	[3] Predicted values of $J_2^{1/2}$ (Eq. 38)	[1]/[2]	[4] Predicted values of $J_2^{1/2}$ (Eq. 39)	[1]/[2]
Phytoherm boundstone	4.25	3.69	1.15	3.18	1.33	3.36	1.26
	10.05	10.39	0.97	10.06	1.00	10.08	1.00
	6.96	7.08	0.98	5.85	1.19	5.97	1.16
	4.97	5.40	0.92	4.05	1.23	4.22	1.18
Average	6.56	6.64	0.99	5.79	1.13	5.91	1.11
Micro-crystalline	15.14	13.59	1.11	13.06	1.16	13.14	1.15
	10.79	10.08	1.07	9.79	1.10	9.94	1.09
	15.61	15.16	1.03	14.97	1.04	15.01	1.04
	5.06	4.31	1.17	3.93	1.29	4.05	1.25
	9.56	9.55	1.00	9.55	1.00	9.51	1.01
	14.72	15.97	0.92	15.78	0.93	15.77	0.93
Average	11.81	11.45	1.03	11.18	1.06	11.24	1.05
Phytoherm framestone	3.67	3.29	1.12	2.84	1.30	2.84	1.29
	11.53	12.68	0.91	12.80	0.90	12.78	0.90
	4.56	9.17	0.50	9.53	0.48	9.46	0.48
	3.19	2.06	1.55	1.98	1.60	2.15	1.48
	5.40	5.43	0.99	5.50	0.98	5.64	0.96
	5.57	6.65	0.84	6.86	0.81	7.14	0.78
Average	5.65	6.55	0.86	6.59	0.86	6.67	0.85
Phytoclast	1.86	0.93	2.01	1.01	1.84	0.91	2.06
	4.36	3.69	1.18	3.74	1.17	3.91	1.12
	2.54	2.67	0.95	2.87	0.88	2.91	0.87
Average	2.92	2.43	1.20	2.54	1.15	2.58	1.13
Total average	7.36	7.46	0.99	7.23	1.02	7.30	1.01

The comparison results given in Table 67 reveal that the strength values of the Antalya tufa rock types predicted through regressions are slightly (almost 1 %) smaller than the theoretical strength values in average.

IX.2 Rock mass classification of theAntalya tufa

IX.2.1 General

Rock is a complex material, which is an assemblage of intact rock blocks (rock material) separated by geological structures, namely, discontinuities. Hence, the characteristics of both intact rock (rock material) and discontinuities must be considered. Though the properties of the rock material are overshadowed by the properties of the discontinuities in the rock mass, they should not be disregarded when considering the rock mass behavior.

The oldest major classification in rock engineering history was proposed over 60 years ago for tunneling with steel supports (Terzaghi, 1946). Today, rock mass classification forms the backbone in empirical design methods. It is not a substitute for engineering design, yet a powerful tool when it is applied appropriately in conjunction with observational and analytical studies. Therefore, the main objectives of the rock classification are (Singh and Goel, 2011):

1. Identification of the most significant parameters governing rock mass behavior
2. Dividing the rock mass into groups of similar characteristics
3. Providing a basis to comprehend the characteristics of each rock mass group
4. Generating quantitative data for engineering design
5. Establishing a common basis for communication between engineers from different disciplines.

Several empirical rock mass classification systems have been developed during 66 years. Among them, quantitative rock mass classification systems, namely, Rock Mass Rating (RMR) by Bieniawski (1989), Rock Mass Quality (Q) by Barton et al. (1974, 2002) and Rock Mass Index (RMi) by Palmstrom (1995) have been mostly used in engineering designs. These classification systems provide a transition from intact rock or material properties to rock mass properties.

Each rock mass classification system has its own case histories through which they have been evolved. Each has its advantages and disadvantages in estimating rock mass strength and each provides support measures or recommendations for excavations. Rock mass classification systems inevitably have been modified and revised as feedbacks have been available from both field and laboratory studies.

The key or common rock mass structure in all quantitative rock mass classification systems is the discontinuity of the rock mass. All of them have attempted to describe rock discontinuity conditions such as volume or density, weathering, infilling, roughness, strength, stress, aperture and spacing in order to estimate rock mass strength.

Lastly, Hoek and Brown (1997) developed a qualitative Geological Strength Index (GSI) classification, which offers a rock mass classification by visual inspection through a simple chart. Six main groups of rock, namely, intact or massive, blocky, very blocky, blocky/folded, crushed and laminated/sheared have been adopted from Terzaghi's classification (Singh and Goel, 2011). Further, surface conditions similar to joint conditions have been classified into 5 groups in order to form a matrix of 6 x 5 through which the corresponding GSI is determined. By using GSI values and triaxial test results on rock cores, Hoek (1994) and Hoek and Brown (1997) have proposed rock mass parameters m and s from the back analysis of instrumented openings and slopes. Then, these rock mass parameters have been utilized in the calculation of rock mass strength parameters.

IX.2.2 Rock mass characteristics of the Antalya tufa

The Antalya tufa rock mass, which has not been studied in such detail before, has varying rock mass characteristics due to its mode of occurrence from a geological point of view. Different types of tufa with different structures exist in the Antalya tufa rock mass as mentioned previously and as summarized in Figure 149.

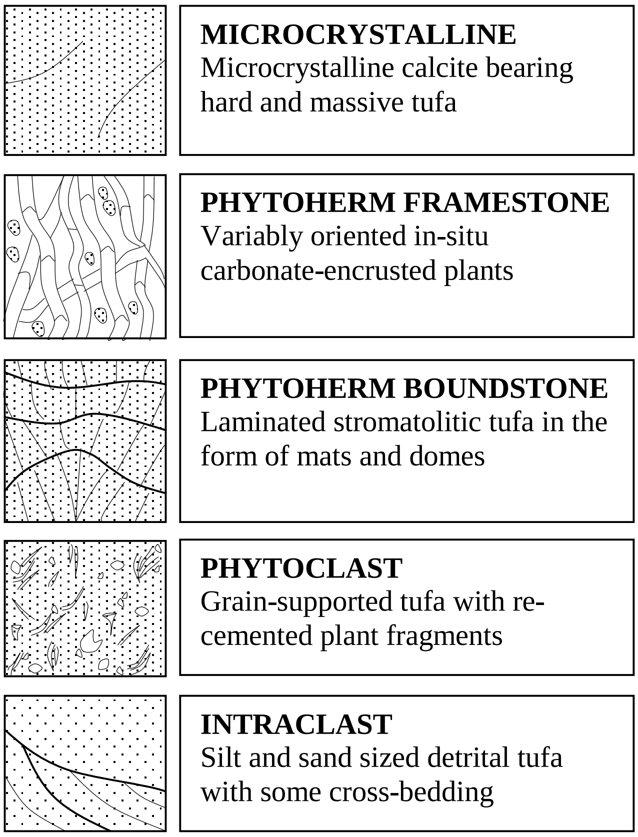

Figure 149. Structural characteristics of different tufa types observed in the Antalya tufa rock mass.

The Antalya tufa rock mass is unique that it has generally no distinct discontinuity surfaces, which are key structures for almost all rock mass classification systems. No bedding planes or systematical joint systems have been observed for the Antalya tufa rock mass during field observations (Figure 150). However, few banding structures have been observed particularly for the phytoherm boundstone type. Regarding the rock mass structure, which is free of discontinuities, laboratory samples of the Antalya tufa rock mass could be interpreted as a representative symbolic (miniature) model of the rock mass.

Figure 150. Views from several outcrops of the Antalya tufa rock mass.

Although the Antalya tufa rock mass could be considered to be a homogeneous material, which is almost entirely composed of the calcium mineral, it is anisotropic. The main source of anisotropy in the Antalya tufa rock mass is porosity, which arises from mostly karstic dissolutions and primary pores developed during carbonate encrustation of plants. It is difficult to characterize the dimensions and distribution of the pores within the tufa rock mass. The pore spaces, particularly the ones developed in the form of dissolution cavities, may be partially or entirely filled up with sediments. These sediments could be terra-rossa type red clay or calcium carbonate precipitation or any other detrital fillings (Figure 151).

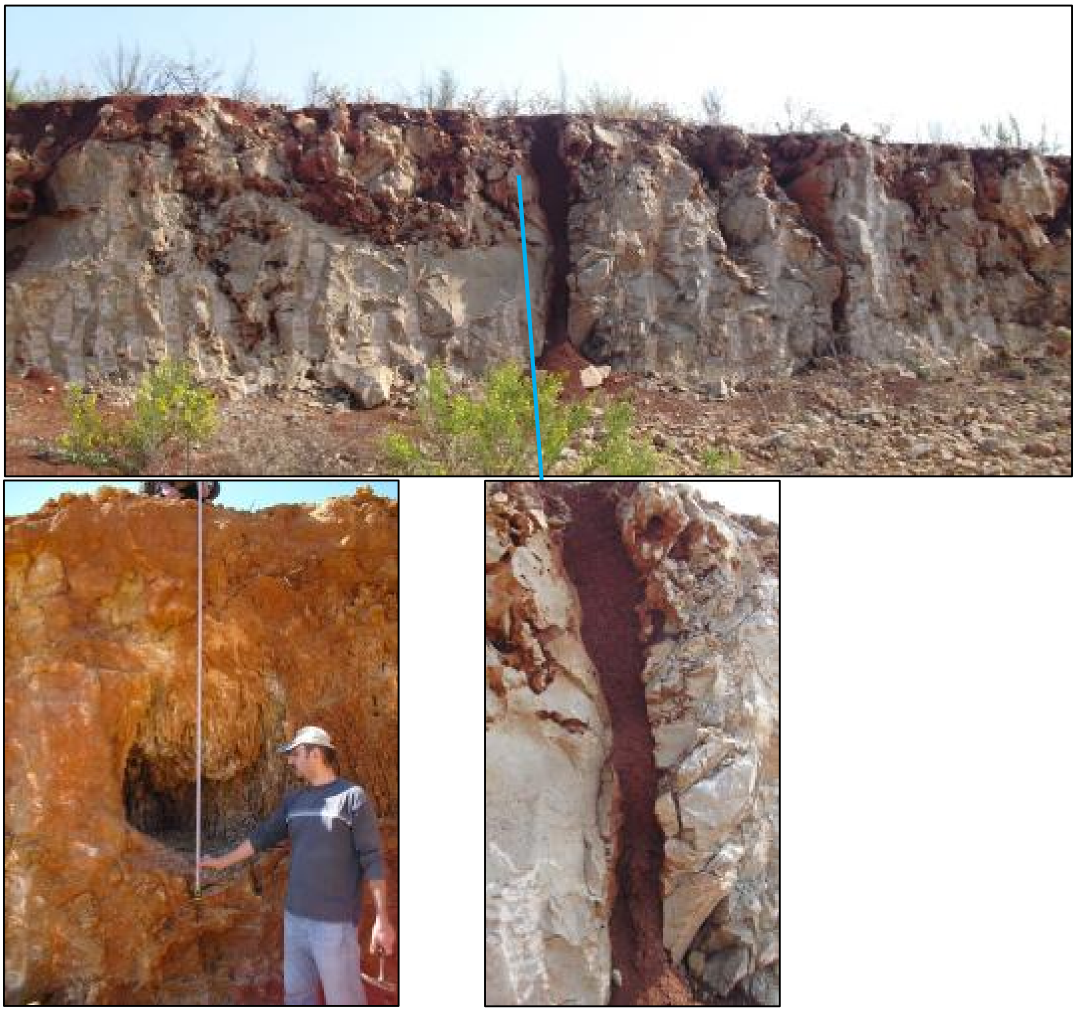

Figure 151. Views of dissolution cavities filled with terra rossa and calcium carbonate.

Carbonate-bonding or cementation, which could be loosened by water that is unsaturated with calcium carbonate, is believed to be another key parameter that governs the tufa rock mass strength. Depending on the climatic conditions in the region, groundwater can play an effective role in dissolving carbonate rocks and decreasing the strength. The same weakening effect could also be caused by the urban sewe (waste water) released into the underground tufa rock mass.

The Antalya tufa rock mass includes various tufa rock types as discussed before. These tufa rock types show lateral and vertical transitions/variations between each other over short distances. Hence, since the range of the values of the geomechanical properties for each tufa type overlaps most of the time, it is generally hard to make a clear distinction between tufa types from a geomechanical parameter point of view.

In order to determine the strength parameters of the Antalya tufa rock mass for engineers who are going to construct underground or infra structures within tufa, rock mass classification system is a powerful tool. Therefore, in the following sections, the applicability of the existing rock mass classification systems for the Antalya tufa rock mass is discussed.

IX.2.3 Geomechanics Classification (Rock Mass Rating System)

The RMR system is very simple to use and applicable to many different situations. The RMR System was developed by Bieniawski during 1972-1973 and modified over the years. It simply includes six parameters to classify a rock mass.

1. Uniaxial compressive strength (UCS) of rock material
2. Rock quality designation (RQD)
3. Spacing of discontinuities
4. Condition of discontinuities
5. Groundwater conditions
6. Orientation of discontinuities.

It is preferably used for jointed rock masses to provide selection of a rock support for tunnels, in-situ deformability of rock mass and rock mass shear strength parameters.

However, the application of the RMR System to the Antalya tufa rock mass is not deemed to be possible. Although the first two parameters of the RMR System can be determined from laboratory rock mechanics tests and drillings, the other three parameters related with discontinuities cannot be determined since the Antalya tufa rock mass has no well-developed discontinuity sets or systems.

IX.2.4 Q-system

Barton et al. (1974) considered six parameters to classify rock masses via the Q-system. These six parameters were utilized in the following equation to give the overall rock mass quality Q as follows (Eq. 40):

$$Q = \frac{RQD}{J_n} \times \frac{J_r}{J_a} \times \frac{J_w}{SRF} \qquad \text{Eq 40}$$

where,

RQD= Rock quality designation

Jn= joint set number

Jr= joint roughness number

Ja= joint alteration number

Jw= joint water reduction number

SRF= stress reduction factor.

The Q value is related to tunnel support requirements by defining equivalent dimension, which is the ratio of the excavation size (span or height) to excavation support ratio (ESR). Furthermore, length of bolts, maximum unsupported span and permanent support pressure can be calculated from the Q-system rating.

However, the application of the Q-system to the Antalya tufa rock mass is not deemed to be possible. The Jr and Ja parameters are all related to the discontinuities present within the rock mass. Since the Antalya tufa rock mass has no well-developed discontinuity systems or sets, the rock mass quality (Q) could not be determined. Only some assumptions, such as minimum Jr/Ja ratio, could be made but the justification of this assumption is not possible. Therefore, it is not possible to calculate a Q value for the Antalya tufa rock mass.

Barton (2002) presented a new Q-value correlation (Q_c) for the parameters needed for design. The results of seismic refraction measurements in terms of P-wave velocity have been integrated into the Q-System (Eqs. 41, 42, 43, 44, 45 and 46):

$$Q_C = Q \times \frac{\sigma_C}{100} = \frac{RQD}{J_n} \times \frac{J_r}{J_a} \times \frac{J_w}{SRF} \times \frac{\sigma_c}{100} \qquad \text{Eq. (41)}$$

$$Q_c \cong 10^{(V_p - 3.5)} \qquad \text{Eq. (42)}$$

$$\text{Cohesive component, c} \cong \left(\frac{\mathrm{RQD}}{\mathrm{J_n}} \times \frac{1}{\mathrm{SRF}} \times \frac{\sigma_C}{100}\right) \qquad \text{Eq. (43)}$$

$$\text{Frictional component, } \emptyset \cong tan^{-1}\left(\frac{J_r}{J_a} \times \frac{J_W}{1}\right) \qquad \text{Eq. (44)}$$

$$RQD = \left(\frac{V_F}{V_L}\right)^2 \times 100 \qquad \text{Eq. (45)}$$

$$E_{mass} = 10{Q_c}^{1/3} \qquad \text{Eq. (46)}$$

However, the data set of the new Q-value correlation has been obtained from cases of “hard rock” tunneling in several countries. Therefore, these new Q-value correlations are not expected to be applicable to the Antalya tufa rock mass, which tends to be a relatively weak rock mass.

IX.2.5 Geological Strength Index (GSI)

Hoek et al. (1995) proposed the Geological Strength Index (GSI) for rock masses. A simple chart with six main qualitative rock classes provides the estimation of the GSI value. Discontinuities are classified into five surface conditions in this chart. The same authors have established relationships between the GSI value and rock mass strength parameters, m_b, s and a of the Hoek-Brown failure criterion (1980). These relationships have been modified over the years by several authors. Lately, Hoek et al. (2002) proposed the following equations for the rock mass parameters of the Hoek-Brown failure criterion (Eqs. 47, 48 and 49):

$$m_b = m_i \exp\left(\frac{GSI-100}{28-14D}\right) \qquad \text{Eq. (47)}$$

$$s = \exp\left(\frac{GSI-100}{9-3D}\right) \qquad \text{Eq. (48)}$$

$$a = \frac{1}{2} + \frac{1}{6}\left(e^{-\frac{GSI}{15}} + e^{-\frac{20}{3}}\right) \qquad \text{Eq. (49)}$$

m_i, which is involved in Eq. (47), is calculated from triaxial testing of intact rock as a curve fitting parameter as demonstrated by Eq. (50) (Hoek and Brown, 1988).

$$m_i = \left(\frac{1}{\sigma_{ci}}\right) \times \left[\frac{\left(\sum x.y - \frac{\sum x.\sum y}{n}\right)}{\left(\sum x^2 - {(\sum x)^2}/{n}\right)}\right] \qquad \text{Eq. (50)}$$

where,

$x = \sigma_3$

$y = (\sigma_1 - \sigma_3)^2$

n = number of tests

σ_{ci} = uniaxial compressive strength.

Eberhardt (2012) stated that for practicing engineers, the Hoek–Brown and GSI procedures mentioned above provide an estimation of isotropic rock mass properties.

However, the decision of whether the rock mass can be represented with an equivalent continuum or not must be made. The criterion should be used when the rock mass is moderately to heavily jointed and the rock mass strength is approximately isotropic. Rock mass failure and failure kinematics should not be influenced by discontinuities.

When the rock mass characteristics of the Antalya tufa rock mass are considered, the GSI method seems to be a favorable rock mass classification method for the Antalya tufa rock mass as compared to the others. Antalya tufa rock mass can be considered as massive, free of discontinuities, and can be assumed to be isotropic by neglecting the porosity effect in rock core size scale.

m_i and E_i (intact rock modulus) for the Antalya tufa rock mass can be calculated from the results of the triaxial and uniaxial compressive strength tests. According to the triaxial test data of this study, m_i values for each Antalya tufa rock type and the Antalya tufa rock mass have been proposed as follows (Table 68):

Table 68. Proposed m_i values for the Antalya tufa rock mass.

Tufa type	m_i	n (number of tests)
Microcrystalline	15 ± 14	3
Phytoherm framestone	6 ± 5	3
Phytoherm boundstone	10 ± 9	3
Phytoclast	9 ± 8	3
Tufa rock mass	10 ± 9	12

As it can be noticed, the proposed m_i values, which were calculated by Roc Lab V.1.032, are slightly different from the ones stated in Table 18, since m_i values of 50 have been excluded from the database. An m_i value of 50 was determined by Dr. Evert Hoek as a threshold value, where he points out that, higher m_i values indicate a very narrow range range of confining stress in triaxial testing. The typical range of m_i values is from about 5, for soft ductile rocks, to 35 for very hard brittle rocks (RocLab 1.0 manual). Furthermore, the standard deviations of m_i values obtained from triaxial tests have resulted in values larger than the mean m_i values, which indicate the highly variable nature of the Antalya tufa rock types and rock mass. Nevertheless, some modifications, such as neglecting the maximum and minimum values have been made in an attempt to reduce the standard deviation values as given in Table 68.

Table 69 presents the, GSI values proposed for the Antalya tufarock types and rock mass, where a GSI value of 75±5 for microcrystalline tufa, 40±5 for phytoherm framestone, 30±5 for phytoherm boundstone and 20±5 for phytoclast tufa have been proposed. Intraclast tufa, which was not been able to be tested for triaxial compressive strength, was assumed to have very similar properties with that of phytoclast tufa. Hence, it was suggested that the same GSI and m_i values of phytoclast tufa were also valid for intraclast tufa.

Utilizing the above proposed mi values and calculated UCS values, the GSI rock mass classification parameters that have been proposed for the Antalya tufa rock mass is presented by Table 70. It should be noted that the Hoek-Brown and deformation parameters of the Antalya tufa rock mass and rock types have been evaluated by the RocLab software version 1.032.

Table 69. Proposed GSI intervals for the Antalya tufa rock mass types.

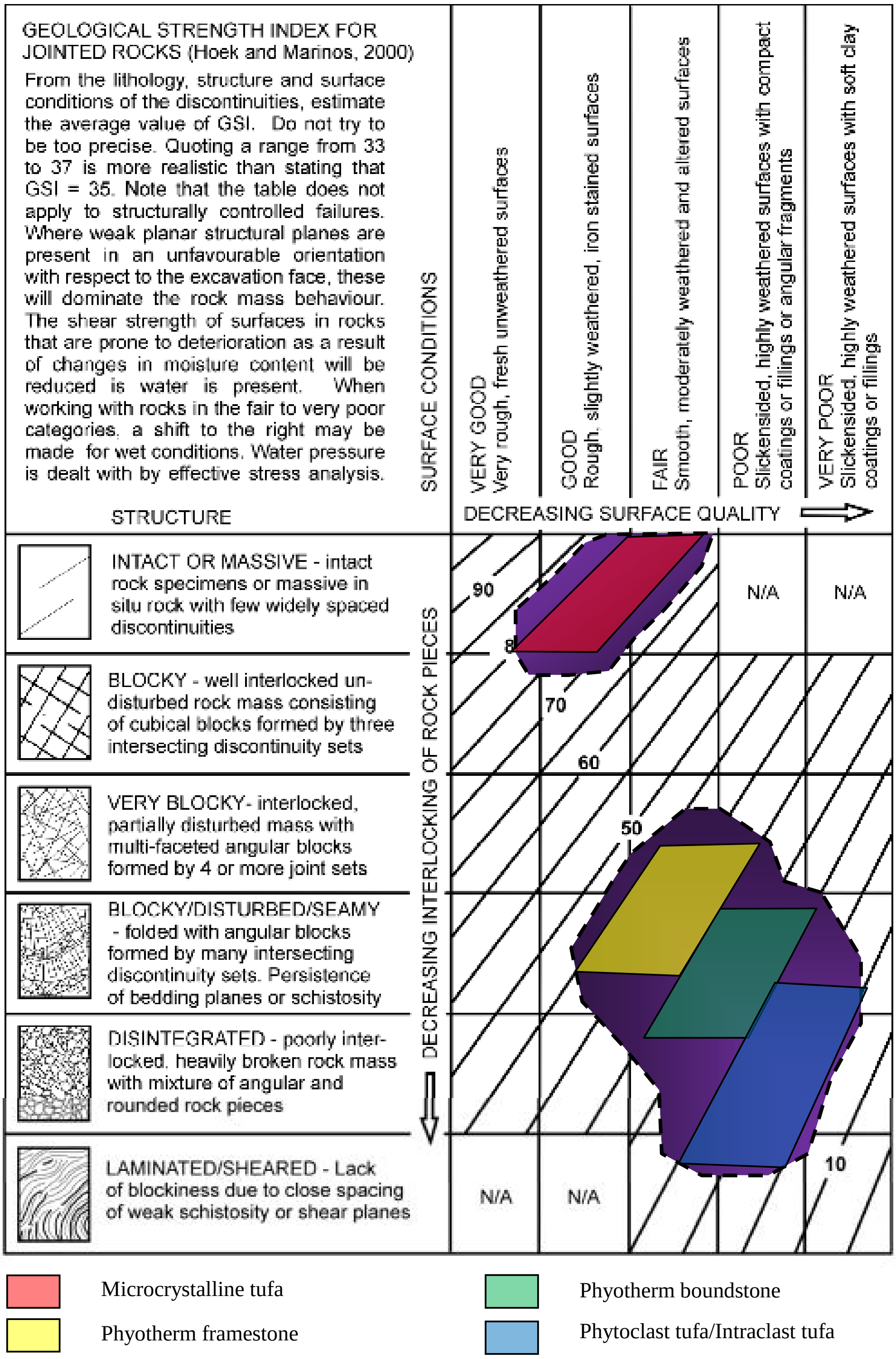

Table 70. Suggessted Hoek-Brown constants for the Antalya tufa rock mass and rock types.

Antalya tufa rock mass

Intact rock strength (MPa):	11.8	Hoek-Brown constant, mb:	1.173
Hoek-Brown constant, m_i:	10	Hoek-Brown constant, s:	0.0013
Geological Strength Index:	40±5	Constant, a:	0.511
Intact rock modulus (GPa):	5.35	Deformation modulus (GPa):	0.85

Microcrystalline tufa

Intact rock strength (MPa):	27	Hoek-Brown constant, mb:	6.142
Hoek-Brown constant, m_i:	15	Hoek-Brown constant, s:	0.0622
Geological Strength Index:	75±5	Constant, a:	0.501
Intact rock modulus (GPa):	13.3	Deformation modulus (GPa):	10.9

Phytoherm framestone

Intact rock strength (MPa):	7.18	Hoek-Brown constant, mb:	0.704
Hoek-Brown constant, m_i:	6	Hoek-Brown constant, s:	0.0013
Geological Strength Index:	40±5	Constant:	0.511
Intact rock modulus (GPa):	4.41	Deformation modulus (GPa):	0.70

Phytoherm boundstone

Intact rock strength (MPa):	7.76	Hoek-Brown constant, mb:	0.821
Hoek-Brown constant, m_i:	10	Hoek-Brown constant, s:	0.0004
Geological Strength Index:	30±5	Constant, a:	0.522
Intact rock modulus (GPa):	3.79	Deformation modulus (GPa):	0.31

Phytoclast tufa

Intact rock strength (MPa):	5.49	Hoek-Brown constant, mb:	0.517
Hoek-Brown constant, m_i:	9	Hoek-Brown constant, s:	0.0001
Geological Strength Index:	20±5	Constant, a:	0.544
Intact rock modulus (GPa):	2.26	Deformation modulus (GPa):	0.10

CHAPTER X

SUMMARY AND DISCUSSIONS

The results of more than ten different geotechnical characterization methods, which were carried out in both field and laboratory, have shown large variations inhibiting ideal identification and characterization of the Antalya tufa rock types and of the Antalya tufa rock mass. In fact, such large variations were expected due to the nature and mode of occurrence of the Antalya tufa rock mass, or rock in general. In addition to the natural variability, other factors such as sampling, testing, etc., might be other sources of variability in this study. In the following paragraphs, a brief discussion has been provided on possible sources of variations and difficulties in geomechanical characterization of the Antalya tufa rock mass.

Tufa is a living system depending on several parameters such as water chemistry, climate, terrain slope, organisms, etc., as mentioned in Chapter IV. Many different tufa rock types are formed as even one of these parameters changes slightly in time. The spatial extent of this variability of tufa rock mass is hard to estimate. It might change so often in short intervals as in the case of the Antalya tufa rock mass. The differences that might be in form or structure of the rock mass will definately have an effect on the strength or deformability of the rock mass.

Characterization and classification of the rock in terms of strength or strength related (i.e., deformation) parameters is very useful in engineering design. However, it is not an easy task since several features might affect the strength or deformability of the rock. One of the most common and controlling features is the discontinuity of the rock mass. However, the Antalya tufa rock mass has been observed to be free of discontinuity, which is the key structure in describing “rock mass” and “rock material (intact rock)”. So, as an answer to the question “what is (are) the factor(s) controlling the rock mass strength or behavior of the Antalya tufa rock?”, porosity has been observed to be most probable candidate responsible for variations. Pore spaces in tufa might be formed during either tufa formation or dissolution after the formation. Spatial and dimensional variation as well as the shape and filling condition of the pore spaces are very difficult to estimate.

The results of in-situ geophysical tests, namely, seismic refraction tomography (SRT) and vertical electrical sounding (VES) have been partially successful in the prediction of possible cavity location underground during this study. A delay in the arrival time of the wave velocity and lower earth resistivity values obtained during SRT and VES measurements, respectively, have been assessed and verified as an indication of cavity. Therefore, these two methods can be applied together for detection of cavities in the Antalya tufa rock mass.

From a geomechanical characterization and rock mass classification of the Antalya tufa rock mass point of view, dimensioning rather than locating a cavity or a pore space and determination of the pore size distribution are more useful. However, most of the time it is impossible to figure out the dimensions of cavities or pore size distribution of the rock even roughly in the field. In pore size distribution point of view, in the literature, some analytical methods, namely, the homogenization method and the microstructure method have been recommended for the evaluation of the overall behavior of the porous media (Tokashiki et al., 1993). Nevertheless, these methods are complex and not practical to be applied in the field. Therefore, the effect of pore size distribution on the strength of the Antalya tufa rock mass was not considered in this study. The pore sizes larger than a rock core sample with a diameter (D) of 54 mm and a minimum length (L) of about 108 mm have not been taken into consideration during geomechanical characterization and rock mass classification. It has been assumed that such cavity or pore space size that might cause anisotropy as compared to the scale of the engineering structure concerned has been disregarded during geomechanical characterization and rock mass classification of the Antalya tufa rock mass. In such circumstances where large pore spaces are encountered within the ground, the interaction between a cavity and an engineering structure concerned is recommended to be evaluated on a scale base. In other words, tufa rock mass including dimensional and spatial charactersitics of the cavity should be modeled together with the engineering structure for design consideration.

According to the results of the porosity measurements of tufa rock cores, a mean porosity of 14.7±7.1% has been determined for the Antalya tufa rock mass. It is included between "medium porous" and "high porous" class according to FAO, 2006. Microcrystalline tufa, which has been observed mostly in massive appearance during site visits, has been determined to possess the lowest porosity while phytoclast tufa, which was the only allochtohonous type, possessed the highest porosity. Porosity values of tufa rock core samples have been simply determined as the difference between submerged and air-dried weights. The isolated pore spaces within the rock core samples have not been calculated. However, it is possible to take into account these pore spaces by using mercury or nitrogen injection porosimeters, which are expensive and require more effort in sample preparation.

Being inversely proportional with porosity, the unit weight of the Antalya tufa rock mass has been determined to possess a mean value of 19.5±2.1 kN/m^3. As expected, microcrystalline tufa possessed the highest unit weight while phytoclast tufa possessed the lowest unit weight.

The results of SRT and VES measurements have shown variations indicated by large standard deviation values. These variations might be primarily attributed to spatial variability of tufa types, which is related with the porous structure, and accuracy of the testing method. Though in-situ SRT and VES measurements have been applied on specific tufa rock types from the ground surface, sometimes different tufa rock types might be present below the ground surface at the location of in-situ test. So, the results of the measurements might belong to the other tufa rock type which was not able to be identified at each specific location. Furthermore, most of the in-situ geophysical tests have been carried out at unoccupied sites between housings in different parts of the Antalya city. Environmental factors such as traffic load, underground structures, groundwater, etc. might have had a significant effect on the results of the measurements. Though utmost attention has been given to have noise free test locations, some test records might have been affected inevitably. According to the results of the SRT measurements, mean shear wave velocity (Vs) of 1.23 km/s ±0.3 (Vp= 2.23 km/s ±0.44) has been determined for microcrystalline tufa, which is followed by phytoherm framestone with mean shear wave velocity (Vs) of 0.93 km/s ±0.07 (Vp= 2.35 km/s ±0.44). Phytoclast tufa had the lowest mean shear wave velocity (Vs) of 0.62 km/s ±0.2 (Vp= 1.71 km/s ±0.61). It should be noted that the wave velocity of the rocks might increase with depth in the earth's crust due to closing of pores by higher confining pressure. The depth effect on the wave velocity might be felt more for porous rocks as they are buried by denser rocks.

The results of the ultrasonic velocity measurements carried out in the laboratory have been conformable with the results of the in-situ SRT measurements. In other words, mean shear wave velocity (Vs) of 1.97 km/s ±0.32 (Vp= 4.26 km/s ±0.93) has been determined for microcrystalline tufa, which was followed by phytoherm framestone with a mean shear wave velocity (Vs) of 1.73 km/s ±0.58 (Vp= 3.69 km/s ±1.34). Intraclast tufa had the lowest mean shear wave velocity (Vs) of 1.44 km/s ±0.04 (Vp= 2.72 km/s ±0.28). The range of the wave velocities of the common rocks and the Antalya tufa rock mass are given in Figure 152.

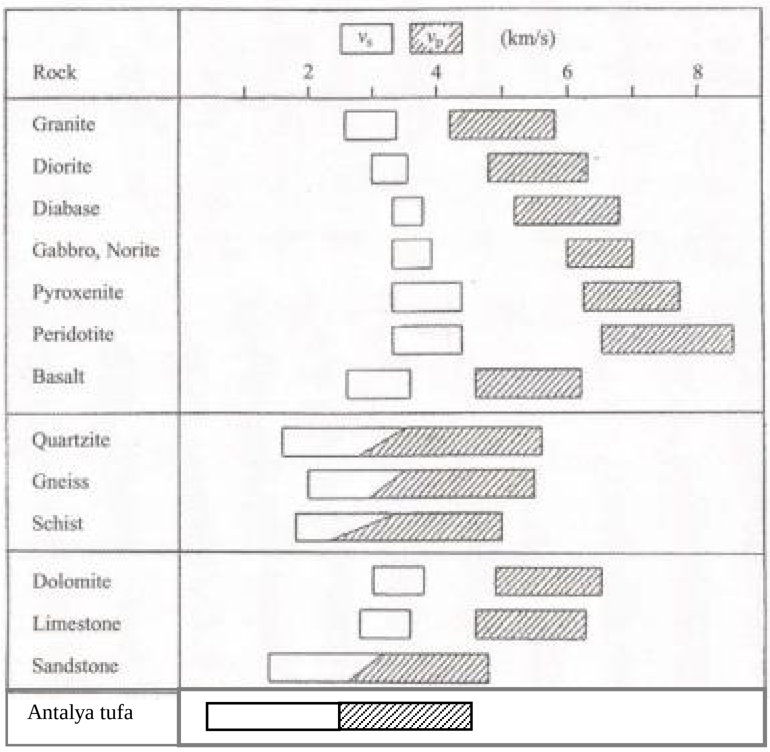

Figure 152. Range of wave velocities for different rocks (from Schön, 1996).

Among the five Antalya tufa rock types, mainly three categories with different strengths have been determined according to the results of the uniaxial compressive strength tests. Accordingly, microcrystalline tufa forms “medium strong (15-50 MPa)” category while phytoherm framestone and phytoherm boundstone form “weak (5-15 MPa)” category. Phytoclast tufa and intraclast tufa form “very weak (1-5 MPa)” category. The uniaxial strength (σ_c) for the entire tufa rock core samples (Antalya tufa rock mass) with an L/D ratio of 2 has been determined to be 11.8 MPa. All the samples have been tested in ambient laboratory conditions. The mean value of the Young’s modulus and Poisson’s ratio measured between 30% and 80% of the failure load of the intact tufa rock samples were 5.35 GPa and 0.09, respectively. A circumferential extensometer has been used during the measurement of the deformability parameters due to the porous and irregular surface of the tufa rock core samples that prevented strain gage installation. However, some of the results of Poisson’s ratio measurement of the porous Antalya tufa rock types might have been miscalculated when a number of rollers of the circumferential extensometer are failed to provide a full contact with the surface of rock core sample. During the UCS testing of phytoherm framestone tufa type, which is one of the hardest and porous types, intermediate failure stages associated with the pre-faiulre closure of pore spaces have been observed prior to the final failure load. The overall strength of the rock might have been affected somehow depending on the pore size and spatial distribution. The deformability characteristics of the the Antalya tufa rock mass might mostly resemble those of sedimentary rocks, namely, shale and sandstone (Table 71).

The Brazilian tensile strength (σ_t) measured from 54 mm diameter disk samples led to a mean tensile strength of 1.84 ± 1.36 MPa where all of the samples have been tested in ambient laboratory conditions. No correlation existed between L/D ratio of the disk specimen and tensile strength. The popular correlation, which is given as $\sigma_t = -\sigma_c/10$, between UCS and tensile strength of the intact rock in the literature did not prove to be valid for the Antalya tufa rock mass. Instead, the results of the laboratory tests led to a correlation of $\sigma_t = -\sigma_c/4.5$ in regards to the tensile strength prediction of the Antalya tufa rock mass. The Brazilian tensile strength of the Antalya tufa rock mass has been determined to be appreciably lower than the tensile strength of the other rock types mentioned in the literature (Table 72).

Table 71. Range of Young's modulus and Poisson's ratio of intact rocks (after AASHTO, 1989).

Rock type	No. of values	No. of rock types	Elastic modulus (GPa) Mean	Elastic modulus (GPa) St. dev.	Poisson's ratio Mean	Poisson's ratio St. dev.
Granite	26 (22)	26 (22)	52.7	24.5	0.20	0.08
Diorite	3	3	51.4	42.7	-	-
Gabbro	3 (3)	3 (3)	75.8	6.69	0.18	0.02
Diabase	7 (6)	7 (6)	88.3	12.3	0.29	0.06
Basalt	12 (11)	12 (11)	56.1	17.9	0.23	0.05
Quartzite	7 (6)	7 (6)	66.1	16.0	0.14	0.05
Marble	14 (5)	13 (5)	42.6	17.2	0.28	0.08
Gneiss	13 (11)	13 (11)	61.1	15.9	0.22	0.09
Slate	11	2	9.58	6.62	-	-
Schist	13 (12)	12 (11)	34.3	21.9	0.12	0.08
Phyllite	3	3	11.8	3.93	-	-
Sandstone	27 (12)	19 (9)	14.7	8.21	0.20	0.11
Siltstone	5 (3)	5 (3)	16.5	11.4	0.18	0.06
Shale	30 (3)	14 (3)	9.79	10.0	0.09	0.06
Limestone	30 (19)	30 (19)	39.3	25.7	0.23	0.06
Dolostone	17 (5)	16 (5)	29.1	23.7	0.08	0.08
Antalya tufa	23 (21)	5 (5)	5.35	5.62	0.09	0.09

Numbers in parantheses refer to number of rock samples tested for Poisson's ratio determination.

Table 72. Brazilian tensile strengths of various rocks (after Singh, 1989)

	Tensile strength (MPa)	
Rock type	Mean	St. dev.
Dolomite	8.87	3.3
Granite	13.8	2.1
Limestone (Bedford)	7.5	3.6
Limestone (Indiana)	9.1	3.8
Magnetite silica	12.5	1.7
Phyolite porphyry	14.4	1.8
Sandstone	7.7	1.8
Sandstone (Berea)	7.1	5.2
Sandstone (Berea)	10.2	5.7
Shale	10.1	1.9
Antalya tufa	1.84	1.36

Point load strength index ($I_{s(50)}$) tests have resulted in a mean strength of 1.34 ±1.24 MPa for the Antalya tufa rock mass. It is mentioned that the results of the point load tests on rocks with UCS below 25 MPa are likely to be highly ambiguous (Marinos and Hoek, 2001). In such cases qualitative description for the field estimation of strength is recommended as follows (Table 73):

Table 73. Field estimates of uniaxial compressive strength of intact rock (Marinos and Hoek, 2001).

Grade*	Term	Uniaxial Comp. Strength (MPa)	Point Load Index (MPa)	Field estimate of strength	Examples
R6	Extremely Strong	> 250	>10	Specimen can only be chipped with a geological hammer	Fresh basalt, chert, diabase, gneiss, granite, quartzite
R5	Very strong	100 - 250	4 - 10	Specimen requires many blows of a geological hammer to fracture it	Amphibolite, sandstone, basalt, gabbro, gneiss, granodiorite, peridotite, rhyolite, tuff
R4	Strong	50 - 100	2 - 4	Specimen requires more than one blow of a geological hammer to fracture it	Limestone, marble, sandstone, schist
R3 Antalya tufa	Medium strong	25 - 50	1 - 2	Cannot be scraped or peeled with a pocket knife, specimen can be fractured with a single blow from a geological hammer	Concrete, phyllite, schist, siltstone
R2	Weak	5 - 25	**	Can be peeled with a pocket knife with difficulty, shallow indentation made by firm blow with point of a geological hammer	Chalk, claystone, potash, marl, siltstone, shale, rocksalt,
R1	Very weak	1 - 5	**	Crumbles under firm blows with point of a geological hammer, can be peeled by a pocket knife	Highly weathered or altered rock, shale
R0	Extremely weak	0.25 - 1	**	Indented by thumbnail	Stiff fault gouge

* Grade according to Brown (1981).
** Point load tests on rocks with a uniaxial compressive strength below 25 MPa are likely to yield highly ambiguous results.

The results of the slake durability index tests have revealed that the majority of the Antalya tufa rock types were very highly durable (Id_2= 90-95%) to extremely high durable (Id_2=95-100%) according to the durability classification proposed by Franklin and Chandra (1972). It is obvious for carbonate rocks such as tufa that the chemical composition of the slaking fluid has a significant effect on the slaking durability. During this study tap water, whose chemical composition determined at the inlet of waste water treatment plant (WWTP) in Ankara, was very similar to that of water at the inlet of Antalya WWTP (Table 74). However, other properties of water such as partial pressure of CO_2 and pH, may significantly affect the durability of tufa rock mass.

Table 74. Comparison of water compositions between water used as a slaking fluid and water at the inlet of Antalya WWTP.

Elements	Antalya WWTP inlet*	Ankara Çubuk WWTP inlet**
Biological oxygen content (mg/L)	~400	~250
Chemical oxygen content (mg/L)	~550-600	~400
Solid particles in suspension (mg/L)	~300-400	~200
Azot (mg/L)	~60	~30
Phosphor (mg/L)	~12	~6
pH	~7-8	-

*Antalya Metropolitan Municipality. **http://www.aski.gov.tr

The majority of the Antalya tufa rock types failed in a brittle mode according to Mogi's criterion proposed for the transition between brittle to ductile behavior. Triaxial compressive strength tests, where low confining pressures have been preferred for the simulation of shallow foundation conditions, have resulted in average Hoek-Brown constant (m_i) of 10.

After relating the individual geotechnical parameters of the Antalya tufa rock mass, a number of good correlations ($R^2 \geq 0.75$) were obtained for the tufa rock types and for the tufa rock mass in general. The regressions have been determined to obey linear, exponential or power laws in general. Some conflicting trends have been encountered during regression studies. Possible reasons for such trends have been interpreted as high intrinsic variability of the rock, inadequacy of samples and accuracy of testing. Similar studies interrelating rock index properties with strength or deformability parameters have been carried out for different rocks in the literature (Table 75).

Table 75. Correlations suggested for E, σ_t and σ_c for various rock types.

Rock type	$E\ (GPa)$	R^2	Authors
Dolomite, marble, limestone	$10.67V_p - 18.71$	0.86	Yaşar and Erdoğan (2004)
Artificial porous rock	$10.10 - 0.109n$	0.74	Leite and Ferland (2001)
Mudstone, claystone, siltstone	$37.9e^{-0.863n}$	0.68	Lashkaripour (2002)
Antalya tufa	$0.0128e^{0.276\gamma}$	0.467	This study
Antalya tufa	$10.35e^{-0.088n}$	0.462	This study

Rock type	$\sigma_c\ (MPa)$	R^2	Authors
Granitic rocks	$183 - 16.55n$	0.69	Tuğrul and Zarif (1999)
Granitic rocks	$0.566\gamma - 1347$	0.67	Tuğrul and Zarif (1999)
Chalk	$273e^{-0.076n}$	0.87	Palchik and Hatzor (2004)
Chalk	$0.0116e^{3.58\gamma}$	-	Bowden et al. (2002)
Antalya tufa	$25e^{-0.09n}$	0.34	This study
Antalya tufa	$0.018e^{0.31\gamma}$	0.67	This study

Rock type	$\sigma_t\ (MPa)$	R^2	Authors
-	$0.5\sigma_c[m_i - (m_i^2 + 4)^{0.5}]$	-	Hoek-Brown (1981)
*	$TP_a\left[\frac{\sigma_c}{P_a}\right]^t$	-	Lade (1993)
Antalya tufa	$5 \times 10^{-5}\gamma^{3.46}$	0.38	This study
Antalya tufa	$3.18e^{-0.053n}$	0.26	This study

*Pa=atmospheric pressure in the same units as those of σ_t and σ_c.

Igneous rocks:	T=-.0435,	t=0.740
Metamorphic rocks:	T=-0.0518	t=1.017
Sedimentary rocks:	T=-0.316	t=0.770
All rocks:	T=-0.219	t=0.825

PCA and MLRA studies have resulted in useful charts for the estimation of strength and deformability characteristics of the Antalya tufa rock mass. Accuracy and reliability of the proposed charts depend on the range of parameters utilized in rock characterization testing. Predictions suggested by these charts have been derived for rock material (intact rock). All geomechanical parameters were calculated in ambient laboratory conditions.

These estimation curves are open to modifications with further data that might be available in the future. The effect of the porosity on strength and on the deformability of the Antalya tufa rock mass has been observed to be more when the unit weight of the rock sample was greater than 19 kN/m^3.

According to the two-stage curve fitting studies performed through linear and non-linear regression analyses of the experimental data, it has been determined that the strength characteristics of the Antalya tufa rock mass show a better fit with the Bieniawski's failure criterion as far as the data of the uniaxial and triaxial compressive strength tests of this study are concerned.

According to the results of the power regression analysis of the strength data of this study, compressive strength criterion and shear strength equation for the Antalya tufa rock mass has been suggested. According to the p-q plots of the intact rock samples of the Antalya tufa rock types, cohesion and internal friction angle values of the Antalya tufa rock types range 0.0 to 0.4 MPa and 57° to 70°, respectively.

Regarding the rock mass characteristics of the Antalya tufa, the GSI method has been selected to be the favorable rock mass classification method for use. The m_i and E_i (intact rock modulus) for the Antalya tufa rock mass have been computed by RocLab software version 1.032 to obtain rock mass constants of Hoek-Brown and rock mass deformation modulus. GSI value in the range of 20-50 has been suggested for the majority of the Antalya tufa rock types, except for microcrystalline type whose GSI value has been recommended as 75±5. Hoek-Brown rock mass constants (mb, s, a) for the Antalya tufa rock mass have been suggested as 1.173, 0.0013 and 0.511, respectively. Rock mass deformation modulus of the Antalya tufa rock mass has been determined to vary between 0.1 and 11 GPa.

CHAPTER XI

CONCLUSIONS

This dissertation that was carried out for the geotechnical characterization and rock mass classification of the Antalya karstic rock masses reached the following conclusions:

According to the results of the porosity measurements of the tufa rock cores, a mean porosity of 14.7±7.1% has been determined for the Antalya tufa rock mass. Being inversely proportional with porosity, the unit weight of the Antalya tufa rock mass has been determined to possess a mean value of 19.5±2.1 kN/m^3.

According to the results of the SRT measurements, mean shear wave velocity (Vs) of 1.23 km/s ±0.3 (Vp= 2.23 km/s ±0.44) has been determined for microcrystalline tufa, which is followed by phytoherm framestone with mean shear wave velocity (Vs) of 0.93 km/s ±0.07 (Vp= 2.35 km/s ±0.44). Phytoclast tufa had the lowest mean shear wave velocity (Vs) of 0.62 km/s ±0.2 (Vp= 1.71 km/s ±0.61). The results of the ultrasonic velocity measurements carried out in the laboratory have been conformable with the results of the in-situ SRT measurements. In other words, mean shear wave velocity (Vs) of 1.97 km/s ±0.32 (Vp= 4.26 km/s ±0.93) has been determined for microcrystalline tufa, which was followed by phytoherm framestone with a mean shear wave velocity (Vs) of 1.73 km/s ±0.58 (Vp= 3.69 km/s ±1.34). Intraclast tufa had the lowest mean shear wave velocity (Vs) of 1.44 km/s ±0.04 (Vp= 2.72 km/s ±0.28).

The uniaxial strength (σ_c) for the entire tufa rock core samples (Antalya tufa rock mass) with an L/D ratio of 2 has been determined to be 11.8 MPa.

The uniaxial strength (σ_c) for the entire tufa rock core samples (Antalya tufa rock mass) with an L/D ratio of 2 has been determined to be 11.8 MPa.

The mean value of the Young's modulus and Poisson's ratio measured between 30% and 80% of the failure load of the intact tufa rock samples were 5.35 GPa and 0.09, respectively.

The Brazilian tensile strength (σ_t) measured from 54 mm diameter disk samples led to a mean tensile strength of 1.84 ± 1.36 MPa. The results of the laboratory tests led to a correlation of $\sigma_t = -\sigma_c/4.5$ in regards to the tensile strength prediction of the Antalya tufa rock mass.

Point load strength index ($I_{s(50)}$) tests have resulted in a mean strength of 1.34 ±1.24 MPa for the Antalya tufa rock mass.

The mean values of the modulus of subgrade reaction of the Antalya tufa rock types have been determined to be ranging between 11 000 t/m^3 and 79 000 t/m^3.

The results of the slake durability index tests have revealed that the majority of the Antalya tufa rock types were very highly durable (Id_2= 90-95%) to extremely high durable (Id_2=95-100%) according to the durability classification proposed by Franklin and Chandra (1972).

The majority of the Antalya tufa rock types failed in a brittle mode according to Mogi's criterion proposed for the transition between brittle to ductile behavior. Triaxial compressive strength tests, where low confining pressures have been preferred for the simulation of shallow foundation conditions, have resulted in average Hoek-Brown constant (m_i) of 10.

After relating the individual geotechnical parameters of the Antalya tufa rock mass, a number of good correlations ($R^2 \geq 0.75$) were obtained for the tufa rock types and for the tufa rock mass in general. The regressions have been determined to obey linear, exponential or power laws in general.

PCA and MLRA studies have resulted in useful charts for the estimation of strength and deformability characteristics of the Antalya tufa rock mass.

According to the two-stage curve fitting studies performed through linear and non-linear regression analyses of the experimental data, it has been determined that the strength characteristics of the Antalya tufa rock mass show a better fit with the Bieniawski's failure criterion.

According to the p-q plots of the intact rock samples of the Antalya tufa rock types, cohesion and internal friction angle values of the Antalya tufa rock types range from 0.0 to 0.4 MPa and 57° to 70°, respectively.

Regarding the rock mass characteristics of the Antalya tufa, the GSI method has been selected to be the favorable rock mass classification method for use. GSI value in the range of 20-50 has been suggested for the majority of the Antalya tufa rock types, except for microcrystalline type whose GSI value has been recommended as 75±5. Hoek-Brown rock mass constants (mb, s, a) for the Antalya tufa rock mass have been suggested as 1.173, 0.0013 and 0.511, respectively. Rock mass deformation modulus of the Antalya tufa rock mass has been determined to vary between 0.1 and 11 GPa.

CHAPTER XII

RECOMMENDATIONS FOR FUTURE RESEARCH

The results of this study are not recommended to be used beyond the range of parameters utilized in rock characterization testing.

In order to determine the effects of pore size, pore size distribution and water on the mechanical properties of the Antalya tufa rock mass, and to improve the represenativeness of the experimental results, additional test parameters and test methods are recommended. Larger rock core or rock block samples with different dimensions should be tested to determine size or volume effect on the strength and deformability of the tufa rock.

Porosity assessments are suggested to be extended by the inclusion of effective porosity concept and the use of improved porosimeters such as nitrogen or mercury intrusion porosimeters.

The strength and durability of the Antalya tufa rock mass are recommended to be explored in terms of environmental factors such as climate and water chemistry in the Antalya region. Possible effects of urban waste water characteristics, namely, pH, temperature and partial pressure of CO_2, on durability and dissolution of the tufa rock mass need to be investigated.

Field or laboratory applications of the relations proposed for the predition of strength and deformability properties of the Antalya tufa rock mass are essential for the verification of the suggested methods. So, these relations need to be checked and verified during engineering design projects.

Large scale in-situ or laboratory testing methods such as large scale triaxial testing and large scale flat jack technique are suggested to investigate rock mass properties since most of the time it was hard to obtain rock core samples that satisfied ASTM or ISRM standards from various tufa rock types due to either highly fragile or highly porous nature. Non-destructive testing or exploration methods may produce useful information but, they need to be verified or supplemented by other methods. Ground penetrating radar (GPR) method, for example, is recommended for the exploration of larger pore spaces, even caves.

By the inclusion of the future geomechanics data on the Antalya tufa rock mass, the database of this study should be extended and re-evaluated in order to verify the relations proposed in this study.

Investigation of pore properties in terms of micro-scale interconnection, microcracks and deterioriation are suggested for future researches on tufa rocks.

REFERENCES

Akay, E., Uysal, S., Poisson, A., Cravatte, J. and Muller, C., 1985. Stratigraphy of the Antalya Neogene Basin. Geological Society of Turkey Bulletin 28, 105–119.

Antalya Varsak Municipality, 2004. Geological and geotechnical report for regulatory land use map study.

Arıkan, A., Ekmekçi, M., 1985. A multi dimensional approach to rainfall – streamflow relationship in Manavgat river basin. Proceedings of the Karst water Resources, eds: G. Günay, A.I. Johnson, IAHS Publication No. 161, p. 57-66.

ASSHTO, 1989. Standard specifications for highway bridges. 14th edition, American Association of State Highway and Transport Officials, Washington DC.

ASTM, 1999.Standard Guide for Selecting Surface Geophysical Methods, Designation D-6429, Philadelphia, PA.

ASTM C25. Standard test methods for chemical analysis of limestone, quicklime, and hydrated lime.

ASTM D1196. Standard test method for nonrepetitive static plate poad tests of soils and flexible pavement components, for use in evaluation and design of airport and highway pavements.

ASTM D 6429. Standard guide for selecting surface geophysical methods.

ASTM D 2845. Standard test method for laboratory determination of pulse velocities and ultrasonic elastic constants of rock.

ASTM D 2938. Standard test method for unconfined compressive strength of intact rock core specimens.

ASTM D 4644. Standard test method for slake durability of shales and similar weak rocks.

ASTM D 4719. Standard test methods for prebored pressuremeter testing in soils.

ASTM D 7012. Standard test method for compressive strength and elastic moduli of intact rock core specimens under varying states of stress and temperatures.

ASTM E 494. Standard practice for measuring ultrasonic velocity in materials.

Barton, N., 2002. Some new Q value correlations to assist in site characterization and tunnel design. Int. J. Rock Mech. Min. Scie. and Abstr., 39, 185-216.

Barton, N., Lien, R. and Lunde, J., 1974. Engineering classification of rock masses for the design of tunnel support. Rock Mech., 6, 189-236 .

Bieniawski, Z.T., 1989. Engineering rock mass classifications. John Wiley, Rotterdam.

Buccino G., D'Argenio B., Ferreri V., Brancaccio L., Ferreri M., Panichi C., Stanzione D., 1978. I Travertini della bassa valle del Tanagro (Campania). Studio Geomorphologico, Sedimentologico e Geochimico. Bolletino Societa Geologica Italiana 97: 617–646.

Bowden, A.J., Spink, T.W. and Mortmore, R.N., 2002. Engineering description of chalk: Its strength, hardness and density. Q. J. Engrg. Geol. Hydrogeol., 35,355-361.

Chafetz H.S., Folk R.L., 1984. Travertines: depositional morphology and their bacterially constructed constituents. Journal of Sedimentary Petrology 54: 289–316.

Çiner A., Karabıyıkoğlu M., Monod O., Deynoux M. and Tuzcu S., 2008. Late Cenozoic Sedimentary Evolution of the Antalya Basin, Southern Turkey, Turkish Journal of Earth Sciences (Turkish J. Earth Sci.), Vol. 17, 2008, pp. 1–41.

Day, W. Robert, 2006. Foundation engineering handbook: Design and construction with the 2006 international building code. McGraw-Hill Professional (2005-11-21) | ISBN: 0071447695.

Değirmenci, M., 1989. Köprüçay havzası ve yakın dolayının karst hidrojeolojisi incelemesi, Doktora Tezi, Hacettepe Üniversitesi, Mühendislik Fakültesi, 372 s., (yayınlanmamış).

Denizman, C., 1989. Kırkgöz kaynakları ve Antalya traverten platosunun hidrojeolojik etüdü, Yük. Müh. Tezi, Hacettepe Üniversitesi, Mühendislik Fakültesi, 146 s.

Deynoux, M., Çiner, A., Monod, O., Karabıyıkoğlu, M., Manatschal, G. and Tuzcu, S., 2005. Facies architecture and depositional evolution of alluvial fan to fan delta complexes in the tectonically active Miocene Koprüçay Basin, Isparta Angle, Turkey. In: Kelling, G., Robertson, A.H.F. & Van Buchem, F. (eds), Cenozoic Sedimentary Basins of South Central Turkey. Sedimentary Geology 173, 315–343.

Dipova, N., 2002, Collapse Mechanism of Antalya Tufa Deposits, Ph. D. Thesis, Middle East Technical University, Geological Engineering Department.

Dipova N., Cangir B., 2008. Antalya tufasının fiziksel ve indeks özelliklerinin belirlenmesi, 11. Ulusal Kaya Mekaniği Kongresi, İzmir, Bildiriler Kitabı.

Dipova N., 2011, The engineering properties of tufa in the Antalya area, SW Turkey, Quarterly Journal of Engineering Geology and Hydrogeology, February 2011; 44: 123 – 134.

Dumont, J.F. and Kerey, E., 1975. L'accident de Kırkkavak, un decrochement majeur dans le Taurus occidental. Bulletin Societe Geologique de France 17, 1071–1073.

Ekmekçi, M., 1987. Beyşehir gölünün komşu havza akımlarına olan etkilerinin araştırılması, Yüksek Lisans Tezi, Hacettepe Üniversitesi, Mühendislik Fakültesi, 101 s., (yayınlanmamış).

Emay International Engineering Services Ltd. Şti, 2004. Site investigation report for 100. Yıl boulevard and Güllük street under-pass.

Fell, R., Mc Gregor, P. and Stapledon, D., 1992. Geotechnical engineering of embankment dams, A. A. Balkema, 1992.

Flecker, R., 1995. Miocene basin evolution of the Isparta angle, southern Turkey. PhD Thesis, Edinburg University [unpublished].

Flecker, R., Robertson, A.H.F., Poisson, A. and Muller, C., 1995. Facies and tectonic significance of two contrasting Miocene basins in south coastal Turkey. Terra Nova 7, 221–232.

Flecker, R., Ellam, R.M., Muller, C., Poisson, A., Robertson, A.H.F. and Turner, J., 1998. Application of Sr isotope stratigraphy and sedimentary analysis to the origin and evolution of the Neogene basins in the Isparta Angle, southern Turkey. Tectonophysics 298, 83–101.

Food and agriculture organization (FAO) of the United Nations, 2006. Guidelines for soil description. Fourth edition, Rome 2006.

Gretel F., Mario, P., Emanuela, M., Stefano, G., Davide T., 2009. Comparison of loss on ignition and thermal analysis stepwise methods for determination of sedimentary organic matter. Aquatic Conser*v*: Mar. Freshw. Ecosyst. 19: 24–33

Fuenkajorn, K. and Daemen, J.J.K., 1992. An empirical strength criterion for heterogenous tuff, Engineering Geology, V.32, pp. 209-223.

Glover C., 1995. Plio-Quaternary Sediments and Neotectonics of the Isparta Angle, S.W. Turkey. PhD thesis, University of Edinburgh, UK.

Glover C., Robertson A.H.F., 1998. Role of regional extensional and uplift in the Plio-Pleistocene evolution of the Aksu Basin, SW Turkey. Journal of the Geological Society, London 15: 365–388.

Glover, C., Roberston, A.H.F., 2003. Origin of tufa (cool-water carbonate) and related terraces in the Antalya area, SW Turkey, Geological Journal, V.38, p.329-358.

Golubic, S., 1969. Cyclic and non-cyclic mechanisms in the formation of travertine. Verhandlungen der Internationalen Vereinigung fur Theoretische und Angewandte Limnologie 17: 956–961.

Günay, G., 1981. Manavgat havzası ve dolayının karst hidrojeolojisi incelemesi, Doçentlik Tezi, Hacettepe Üniversitesi, Mühendislik Fakültesi, Ankara, 185 s.

Gürer,İ., Arıkan, A., Ultu, L., 1980. Beyşehir-Antalya karst alanının hidrometeorolojik girdilerinin analizi, Yerbilimleri, Hacettepe Üniversitesi, Ankara, vol. 6, s. 48-60.

Harzem Mühendislik Ltd. Şti., 2008. Antalya 100. Yıl sport saloon site investigation report.

Hoek, E. and Brown, E.T., 1988. The Hoek-Brown criterion – a 1988 update. Proc. 15th Can. Rock Mech. Symp., University of Toronto, Canada, 31-38.

ISO, 2008. EN ISO 22476-4 Geotechnical investigation and testing – Field testing – Ménard pressuremeter test.

ISRM, 1981. ISRM suggested methods for rock characterization, testing and monitoring.

İnan, N., 1985. Antalya travertenlerinin oluşumu ve özellikleri, Jeoloji Mühendisliği Dergisi, Temmuz 1985.

Julia, R., 1983. edited by Scholle, Peter A., Bebout, Dan G., Moore, Clyde H., Travertines: Carbonate depositional environments, [AAPG memoir 33]: Tulsa, Oklahoma. p. 64-72.

Karabıyıkoğlu, M., Çiner, A., Monod, O., Deynoux, M., Tuzcu, S., Orcen, S., 2000. Tectonosedimentary evolution of the Miocene Manavgat Basin, Western Taurids, Turkey. In: Bozkurt, E., Winchester, J.A. & Pıper, J.D.A. (eds), Tectonics and Magmatism in Turkey and the Surrounding Area. Geological Society, London, Special Publications 173, 475–498.

Karabıyıkoğlu, M., Çiner, A., Deynoux, M., Monod, O., Tuzcu, S., Manatschal, G. 2004. Miocene tectonosedimentary evolution of the Late Cenozoic Antalya Basin. Mineral Research and Exploration Institute (MTA) of Turkey–CNRS (France)–The Scientific and Technological Research Council of Turkey (TUBİTAK) Co-Project Report [unpublished].

Karabıyıkoğlu, M., Tuzcu, S., Çiner, A., Deynoux, M., Orcen., S., Hakyemez, A., 2005. Facies and environmental setting of the Miocene coral reefs in the late-orogenic fill of the Antalya Basin, Western Taurids, Turkey. In: Kelling, G., Robertson, A.H.F. & Van Buchem, F. (eds), Cenozoic Sedimentary Basins of South Central Turkey. Sedimentary Geology 173, 345–371.

Kılıç, R., Yavuz, Ş., 1994. Relationship between geotechnical properties of the Antalya (Turkey) travertine. Bull. of IAEG, 50, pp. 43-50, Paris.

Koşun E., Sarıgül A., Varol, B., 2005. Antalya tufalarının litofasiyes özellikleri, MTA Dergisi 130, p. 57-70.

Koçkar, M.K., Akgün, H., 2003a. Methodology for Tunnel and Portal Support Design in Mixed Limestone, Schist and Phyllite Conditions: A Case Study in Turkey, International Journal of Rock Mechanics and Mining Sciences, V.40, 2, p.173-196.

Koçkar, M.K., Akgün, H., 2003b. Engineering Geological Investigations along the Ilıksu Tunnels, Alanya, Southern Turkey, Engineering Geology, Vol. 6, 3-4, p.141-158.

Koyuncu, H., 2003. Batı Toroslar karst sistemi hidrojeolojik özelliklerinin uydu görüntülerinin sayısal analizleri ile irdelenmesi, Doktora Tezi, Hacettepe Üniversitesi, Mühendislik Fakültesi.

Lade, P.V., 1993. Rock strength criteria: The theories and the evidence. Comprehensive Rock Engineering-Principle, practice and projects. Ed: J.A. Hudson, Pergamon, Oxford, UK, 1, 255-284.

Lashkaripour, G.R., 2002. Predicting mechanical properties of mudrock from index parameters. Bull. Engrg. Geol. Envir., 61, 73-77.

Leite, M.H. and Ferland, F., 2001. Dtermination of unconfined compressive strength and Young’s modulus of porous materials by indentation tests. Engineering Geology, 59, 267-280.

Marinos, P. and Hoek, E., 2001. Estimating the eotechnical properties of heterogeneous rock masses such as flysch. Bull. Engrg. Geol. Env., 60, 85-92.

Ordonez, S., Garcia del Cura, M.A., 1983. Recent and Tertiary fluvial carbonates in central Spain. In Modern and Ancient Fluvial Systems, Collinson JD, Lewin J (Eds). Special Publication 6. International Association of Sedimentologists: 485–497.

Özüş, A.S., 1992. Antalya traverten platosunun jeolojik, hidrolojik hidrojeolojik ve hidrokimyasal özelliklerinin incelenmesi, Doktora Tezi, Çukurova Üniversitesi, Mühendislik Fakültesi.

Palchik, V. and Hatzor., Y.H., 2004. Influence of porosity on tensile and compressive strength of porous chalks. Rock. Mech. And Rock Engrg., 37, 331-341.

Palmström, A., 1995. RMi-A system for characterizing rock mass strength for use in rock engineering. J. oj Rock Mech. and Tunneling Tech., India, 1, 69-108.

Pariseau, W.G., 2007. Fitting failure criteria to laboratory strength test. Int. J. of Rock Mech. and Min. Science, 44: 637-646.

Pedley, H.M., 1990. Classification and environmental models of cool freshwater tufas: Sedimentary Geology, v. 68, p. 143-154.

Pedley, H.M., Carannante, G. (Eds) 2006. Cool-water carbonates. Depositional systems and palaeo-environmental controls. Geological Society Special Publication no. 255. vi + 373 pp. London.

Pentecost, A., 2005. Travertine, 445 pp. Berlin, Heidelberg, New York: Springer-Verlag.

Planhol X., 1956. Contribution a` l’e´tude ge´omorphologique de Taurus Occidental et de plaines bordie`res. Revue de Ge´ographie Alpine 44: 609–685.

Poisson, A., 1977. Recherches geologiques dans les Taurides occidentales (Turquie). PhD Thesis, Universite Paris Sud-Orsay [unpublished].

Poisson, A., Yağmurlu, F., Bozcu, M., Şentürk, M., 2003. New insights on the tectonic setting and evolution around the apex of the Isparta Angle (SW Turkey). Geological Journal 38, 257–282.

Schön, J.H., 1996. Physical properties of rocks – Fundamentals and principles of petrophysics. Pergamon, Oxford, UK.

Sheehan, J. R., Doll, W. E., Watson, D. B., and Mandell, W. A., 2005. Application of seismic refraction tomography to karst cavities, in Kuniansky, E.L., ed., U.S. Geological Survey Karst Interest Group Proceedings, Rapid City, South Dakota, September 12 -15, 2005, U.S. Geological Survey Scientific Investigations Report 2005-5160.

Sheehan, J. R., Doll, W. E. Watson, D. B., and Mandell, W. A., 2005. Detecting cavities with seismic refraction tomography: Can it be done?. Proc. 2005 Symposium on the application of geophysics to environmental and engineering problems, p. 989-1003.

Singh, M.M., 1989. Strength of rock. In: Physical Properties of Rocks and Minerals (Y.S. Touloukian, W.R., Judd and R.F., Roy, eds.) Hemisphere Publishing Corp. pp. 83-121.

Singh, B. and Goel, R. K., 2011. Engineering rock mass classification: Tunneling, foundations and landslides. Elsevier, Oxford, UK.

Sipahi, H.M., 1985. Karst hydrogeology of the Aksu river basin, Antalya. Proceedings of the Karst Water Resources Conference, eds: G. Günay, A.I. Johmson, IAHS Publication No. 161, p. 417-430.

Sowers G.F., 1996. Buildings on sinkholes: Design and construction of foundations in Karst terrain, ASCE Press, New York, N.Y.

Temelsu Uluslararası Mühendislik Hizmetleri A.Ş., 1997. Asarkayası Tüneli Kesin Proje Raporu, Cilt 1, T.C Bayındırlık ve İskan Bakanlığı Karayolları Genel Müdürlüğü, p. 15.

Terzaghi, K., 1946. Rock defects and loads on tunnel support. Rock tunneling with steel supports, ed. R.V. Proctor and T. White, Commercial Shearing Co., Youngstown, OH.

Tokashiki, N., Aydan Ö., Kyoya T., Ichikawa, Y., 1993. Mechanical properties and failure of porous rocks. Proc. Int. Symp. on Assessment and Prevention of Failure Phenomena in Rock Engineering, 101-106, İstanbul.

Thomas, L. and Dobecki, S., 2006. Geophysical applications to detect sinkholes and ground subsidence. The leading edge, March.

Toker Drilling and Construction Co. Ltd. Şti., 2010. Site investigation report for Antalya airport taxi road.

Toros Geotechnical Engineering Ltd. Şti, 2006. Site investigation report for Kepez municipality lot 1242.

Toros Geotechnical Engineering Ltd. Şti, 2007. Site investigation report for Kızıllı municipal solid waste landfill.

Toros Geotechnical Engineering Ltd. Şti, 2007. Site investigation report for Minicity project.

Tuğrul, A. and Zarif, I.H., 1999. Correlation of mineralogical and textural characteristics with engineering properties of selected granitic rocks from Turkey. Engrg. Geol., 51, 303-317.

UNDP, 1983. Strengthening DSİ groundwater investigative capability, Phase II, Turkey. Technical report: Karst waters of Southern Turkey, DP/UN/TUR-77-015/1.

Walter, E.D., Jr., 1974. Determination of carbonate and organic matter in calcareous sediments and sedimentary rocks by loss on ignition: comparison with other methods. Journal of sedimentary petrology, Vol. 44, no. 1, p. 242-248.

Waltham A.C., Fookes P.G., 2005. Engineering classification of karst ground conditions Speleogenesis and Evolution of Karst Aquifers 3 (1), 20 pages, re-published from Quarterly Journal of Engineering Geology and Hydrogeology, 2003, vol. 36, pp. 101-118.

Waltham, T., Bell, F., Culshaw, M., 2005. Sinkholes and subsidence, karst and cavernous rocks in engineering and construction, Praxis Publishing, UK, ISBN 3-540-20725-2.

Yağız S., Akyol E., 2005. Geomechanical assessment of travertine in Antalya Region. In: Proceedings of 1st International Symposium on Travertine. Özkul M, vd. (Eds), 235-239. September 21-25, 2005. Denizli, Turkey, 2005.

Yaşar, E. and Erdoğan, Y., 2004. Correlating sound velocity with the density, compressive strength and Young's modulus of carbonate rocks. Int. J. Rock Mech. Min. Sci., 41, 871-875.

Yüksel Proje Uluslararası A.Ş., 2000a. Ilıksu tunelleri kesin proje raporu, Cilt 1, T.C. Bayındırlık ve İskan Bakanlığı Karayolları Genel Müdürlüğü, p. 65.

Yüksel Proje Uluslararası A.Ş., 2000b. Ilıksu tunelleri ön proje jeoteknik raporu, Cilt 1, T.C. Bayındırlık ve İskan Bakanlığı Karayolları Genel Müdürlüğü, p. 55.

Yüksel Proje Uluslararası A.Ş., 2000c. Ilıksu tunelleri portal kesin proje raporu, Cilt 1, T.C. Bayındırlık ve İskan Bakanlığı Karayolları Genel Müdürlüğü, p. 36.

Yüksel Proje Uluslararası A.Ş., 2006. Antalya first stage light railway transportation project, geological and geotechnical investigation report.

Zemartem Ltd. Şti., 2002. Site investigation report for Yaşankent cooperative housing society.

CURRICULUM VITAE

PERSONAL INFORMATION

Surname, Name: Sopacı, Evrim

Nationality: Turkish (TC)

Date and Place of Birth: 7 August 1978, Ankara

Marital Status: Single

Phone: +90 312 250 67 92

Fax: +90 312 438 52 14

e-mail: evrimsopaci@gmail.com

EDUCATION

Degree	**Institution**	**Year of Graduation**
MS	METU Geological Engineering	2003
BS	METU Geological Engineering	2000
High School	Balıkesir High School	1995

WORK EXPERIENCE

Year	**Place**	**Enrollment**
2000-Present	Temelsu International Eng. Serv. Inc.	Geological Engineer

PUBLICATIONS

1. Sopacı, E. and Akgün, H., 2009. Portal slope stability assessment of a proposed highway tunnel in northeastern Turkey. ISRM-Sponsored International Symposium on Rock Mechanics: “Rock Characterisation, Modelling and Engineering Design Methods”, SINOROCK 2009, pp. 48-53, Hong Kong.

2. Sopacı, E. and Akgün, H., 2008. Engineering geological investigations and the preliminary support design for the proposed Ordu Peripheral Highway Tunnel, Ordu, Turkey. Engineering Geology, v. 96, issues 1-2, 7 January 2008, Pages 43-61.

3. Sopacı, E. and Akgün, H., 2008. Engineering Geological Investigations and Tunnel Support Design for the Tunnels of Ordu Peripheral Highway, IXth Regional Rock Mechanics Symposium, İzmir-Türkiye.

4. Sopacı, E., Akgün, H. and Akıncı, M., 2005. Rock Mass Characterization and Primary Support Design for the Boztepe Tunnel, Turkey. Proceedings of the 31st ITA-AITES World Tunnel Congress, 7-12 May 2005, İstanbul-Turkey.

HOBBIES

Computers, literature search in geology, books, traveling, sports, amateur sailing and yachting.